

Alma Mater Studiorum – Università di Bologna

Facoltà di Scienze Matematiche Fisiche e Naturali
Scuola di Dottorato in Scienze Biologiche, Biomediche e Biotecnologiche

DOTTORATO DI RICERCA

**IN BIOLOGIA FUNZIONALE DEI SISTEMI CELLULARI E
MOLECOLARI**

Ciclo XXI

Settore scientifico disciplinare di afferenza: BIO10

**Intrinsic uncoupling in the ATP synthase of
Escherichia coli. Studies on WT and ϵ -truncated
mutants.**

PhD student Dott.ssa Manuela D'Alessandro

PhD Coordinator

Tutor

**Chiar.mo Prof.
Vincenzo Scarlato**

**Chiar.mo Prof.
Bruno Andrea Melandri**

Esame finale anno 2009

Science knows no country,
because knowledge belongs to humanity,
and is the torch which illuminates the world.

Louis Pasteur

I am among those who think that science has great beauty.
A scientist in his laboratory is not only a technician:
he is also a child placed before natural phenomena
which impress him like a fairy tale.

Marie Curie

Table of contents

Chapter 1	1
Introduction	1
1.1 <i>Escherichia coli</i>	1
1.1.1 <i>E. coli</i> metabolism.....	2
1.1.2 Respiratory chain of <i>E. coli</i>	3
1.1.3 Chemiosmosis.....	4
1.2 F_0F_1 ATP synthase.....	5
1.2.1 Structural features: F_1 domain.....	6
1.2.2 Structural features: F_0 domain.....	10
1.3 Catalytic models.....	12
1.3.1 The catalytic mechanism of F_1 : the binding change mechanism proposed by Boyer	12
1.3.2 The binding change mechanism in the presence of saturating concentration of ATP	14
1.3.3 The rotation of the γ subunit.....	15
1.3.4 Hypothesis on the catalytic mechanism of the F_0 portion.....	16
1.4 Regulation of the ATP synthase.....	19
1.4.1 Inhibition of <i>E. coli</i> ATP synthase activity by ADP and P_i	19
1.5 Structural changes of the ϵ subunit and their relevance to the catalytic and regulatory processes of the enzyme.....	19
1.5.1 Up- and down-state of the ϵ subunit.....	20
1.5.2 Role of the C-terminal helices of the ϵ subunit.....	22
1.6 Intrinsic uncoupling.....	23
1.6.1 Intrinsic uncoupling in the complexes of the mitochondrial oxidative phosphorylation.....	23
1.6.2 Intrinsic uncoupling elicited by lowering the [ADP] and [P_i] concentrations in the ATP synthase from <i>Rb. capsulatus</i>	24
1.7 Aim of the present work.....	26
Chapter 2	27
Materials and methods	27
2.1 <i>E. coli</i> membrane preparation.....	27
2.1.1 <i>E. coli</i> membrane preparation according to Mosher et al., 1985.....	27
2.1.2 <i>E. coli</i> membrane preparation according to Elliot Hertzberg & Peter Hinkle (1974)	27
2.2 ATP hydrolysis.....	28

2.2.1 Phenol Red Assay	28
2.2.2 Piruvate Kinase-ADP trap Assay	29
2.2.3 Malachite Green Assay	30
2.2.3.1 Measurement of the inorganic phosphate in PhosphoEnolPyruvate solution.	31
2.3 Dicyclohexylcarbodiimide (DCCD) assay	31
2.4 Measurement of pyruvate kinase activity	31
2.5 9-Amino-6-chloro-2-methoxyacridine (ACMA) assay	32
2.6 Plasmid construction and mutagenesis	32
2.6.1 Development of a low copy number expression vector carrying extra copy of mutated <i>uncC</i>	32
2.6.2 Transformation of <i>E. coli</i> cell with plasmids	33
2.6.3 Transformation of <i>E. coli</i> competent cells	33
2.6.4 Transformation of strains with plasmids	33
2.6.5 Induction and analysis of protein from plasmid	34
2.7 Purification of <i>E. coli</i> ATP synthase and its reconstitution into liposomes	34
2.7.1 <i>E. coli</i> and growth conditions	34
2.7.2 Preparation of membrane vesicles and isolation of ATP synthase	34
2.7.3 Preparation of liposomes	35
2.7.4 Reconstitution of EF ₀ F ₁ into liposomes	35
2.7.5 SDS polyacrylamide gel electrophoresis	36
2.8 Measurement of ATP synthesis	37
2.9 ACMA calibration	37
2.10 Measurement of protein concentration	39
2.10.1 Bradford method	39
2.10.2 Lowry method	39
2.11 Measurement of the ADP content in the ATP solution	39
2.12 Western Blot	40
Chapter 3.....	41
Results	41
3.1 Intrinsic uncoupling in the ATP synthase of <i>E. coli</i>	41
3.2 Effect of P _i on ATP hydrolysis and proton pumping	41
3.3 Evaluation of the ACMA response in the <i>E. coli</i> membrane system	46
3.4 Effect of ADP depletion on the P _i inhibited ATP hydrolysis	48
3.5 Effect of ADP depletion on proton pumping	49
3.6 Effect of ADP depletion on proton pumping as a function of P _i concentration	51
3.7 Discussion	54

Chapter 4	57
Results	57
4.1 Purity and concentration of the ATP synthase	57
4.2 Proton pumping, ATP hydrolysis rate and ATP synthesis rate in the presence of different protein-to-lipid ratios during the reconstitution	58
4.2.1 Proton pumping	59
4.2.2 ATP hydrolysis rate.....	61
4.2.3 ATP synthesis	62
4.3 ATP hydrolysis and synthesis as a function of the average number of ATP synthases per liposome	64
4.4 Poisson distribution of ATP synthases/vesicle	65
4.5 Calibration of the ACMA response in proteoliposomes	66
4.5.1 Calibration of the quenching of ACMA fluorescence in terms of ΔpH 's of known extents	67
4.6 Discussion	70
Chapter 5	71
Results	71
5.1 Functional studies in the isolated and reconstituted EF_0F_1	71
5.2 Effect of P_i on ATP hydrolysis and proton pumping	71
5.2.1 Conversion of the quenching values into ΔpH and $[\text{H}^+]_{\text{in}}$ values.....	74
5.2.2 Quantitative evaluation on the uncoupling degree induced by P_i depletion.....	76
5.3 Evaluation of the ACMA response in proteoliposomes during ATP hydrolysis.....	77
5.4 Effect of ADP depletion on ATP hydrolysis and proton pumping.....	79
5.4.1 Calculation of the ADP concentrations present at the different PK activities	82
5.4.1.1 Measurement of the apparent K_M^{ADP}	84
5.4.1.2 Measurement of competitive inhibition by ATP	85
5.4.2 Quantitative evaluation of the uncoupling degree induced by ADP depletion	86
5.5 Effect of added ADP on ATP hydrolysis and proton pumping.....	86
5.6 Effect of P_i on ATP hydrolysis and proton pumping in the presence of $1\mu\text{M}$ ADP and of 25U/ml PK.....	88
5.7 Discussion	90
Chapter 6	95
Results	95
6.1 Functional studies on ϵ truncation mutants	95
6.2 Plasmid construction and <i>E. coli</i> DK8 cells double transformation.....	96
6.2.1 Development of a low copy number expression vector carrying extra copy of WT or mutated <i>uncC</i>	96

6.2.2 Transformation of DK8 <i>E. coli</i> strains with plasmids.....	100
6.2.3 Western Blot analysis of expressed ϵ mutants and WT	101
6.3 Comparison of ATPase activity and ATP dependent proton pumping in membrane vesicles from the four <i>E. coli</i> strains at different P_i concentrations.....	102
6.4 Effect of P_i on ATP hydrolysis and proton pumping	104
6.4.1 ATP hydrolysis in WT and in $\epsilon_{88\text{-stop}}$ mutant as a function of P_i concentration	104
6.4.2 Proton pumping in WT and in $\epsilon_{88\text{-stop}}$ mutant as a function of P_i concentration	106
6.4.3 Effect of P_i on ATP hydrolysis and proton pumping in WT and in $\epsilon_{88\text{-stop}}$ mutant in the presence of 1 μ M ADP, pre-incubated for an undefined time interval	108
6.5 ADP concentration dependence of the proton pumping in WT and in $\epsilon_{88\text{-stop}}$ mutant	110
6.6 Dependence of ATP hydrolysis and proton pumping on the pre-incubation time in the presence of ADP, in WT and in $\epsilon_{88\text{-stop}}$ mutant	111
6.7 Dependence of ATP hydrolysis and proton pumping in WT and in $\epsilon_{88\text{-stop}}$ mutant on the ADP concentration during preincubation.....	115
6.8 Effect of P_i on ATP hydrolysis and proton pumping in WT and in $\epsilon_{88\text{-stop}}$ mutant, after preincubation in the presence of ADP	120
6.8.1 ATP hydrolysis and proton pumping as a function of P_i , after 30min of preincubation in the presence of 1 and 0.1 μ M ADP.....	120
6.8.2 ATP hydrolysis and proton pumping as a function of P_i , after 30min of preincubation in the presence of 1 nM ADP	125
6.9 Effect of PK on ATP hydrolysis and proton pumping in WT and in $\epsilon_{88\text{-stop}}$ mutant.....	128
6.10 Discussion	130
Chapter 7.....	133
Conclusions	133
References	135

Abbreviations

ACMA, 9-amino-6-chloro-2-methoxyacridine

AM, ammonium molybdate

APS, ammonium persulfate

BD, bidistilled water

DCCD, dicyclohexylcarbodiimide

DMSO, dimethyl-sulfoxide

EF₁, hydrophilic subcomplex of the ATP synthase of *E. coli*

EF₁F₀, ATP synthase of *E. coli*

KCN, potassium cyanide

LDAO, lauryldimethylamine oxide

LDH, lactic dehydrogenase

MG, malachite green

NADH, nicotinamide- dinucleotide

PEP, phospho(enol)pyruvic acid

Phenol Red, 4,4'-(3H-2,1-benzoxathiol-3-ylidene) bis-phenol, S,S-dioxide

PK, pyruvate kinase

Pmf, protonmotive force

PVDF, polyvinylidene difluoride

ROS, oxygen free radicals

Tricine, N-[2-Hydroxy-1,1-bis(hydroxymethyl)ethyl] glycine

Tris, tris(hydroxymethyl)aminomethane

TMAO, trimethylamine-N-oxide

Tw, Tween

ΔpH , transmembrane difference of pH

$\Delta\psi$, bulk-to-bulk transmembrane electrical potential difference

$\Delta\tilde{\mu}_{\text{H}^+}$, transmembrane difference of electrochemical potential of protons

Acknowledgements

First I would like to thank my parents for their moral and financial support. A special thank is to my mother for helping me in drawing the pictures of the plasmid. Many thanks to the people who mainly contribute in forming my scientific personality: Prof. B.A. Melandri and Paola Turina. They taught me the importance of complexity and how to reduce and study this complexity. A particular thank to Paola for accurately reviewing my thesis work.

A special thank to Prof, S.D. Dunn not only for welcoming in his lab and introducing me to the biomolecular techniques but also for making easier my adaptation in Canada (I will be missing the nice morning walk to school, the tomatillos and the terrific maple syrup!). A special thank to Yumin Bi for her fundamental help in the lab work, especially for the quantitative Western blots reported in this thesis.

Many thank to my colleagues in Italy, Manu and Lisa (for their scientific advise and for sharing with me the nice and the bad sides of the research work and of crude life), Alby, Francesco, and Titti-Martina-Sara (the coffee break trio); and many thanks to my colleagues in Canada, Lee Ann and in particular Paul for teaching me all tricks in the lab work and...for the funny break, during my thesis writing, with the racoon videos. And many thanks for scientific conversations, useful advises and the witty cues to all the Professors and researchers I met during the Bioenergetics congresses (among the others, M. Forgac, W. Frasch, D. Bald, M. Boersch and W. Junge).

I also want to thank all the nice international people I met during my stay in Canada for teaching me to see research life under different point of views: the French group, in particular Benjamin for his French to English adaptations, the Japanese and Latin group and the Little Italy community (Simo for the support during my stay in London and during the writing of my thesis, Samuel, Marco and Paolo for the help in the English translations and for the nice Italian dinners), and a special thank to JB for his stories. A final thank to my brother Marco for simplify the layout procedure of my thesis and for his strong support.

Chapter 1.

INTRODUCTION

All organisms need a continuous contribution of free energy in order to accomplish three main functions:

- production of mechanic work for cellular motion;
- active transport of molecules and ions;
- synthesis of macromolecules starting from precursors.

The free energy required for these processes comes from the environment and prevents organisms from reaching a thermodynamic equilibrium. Chemotrophic organisms attain this energy by the oxidation of chemical compound present in the environment; phototrophic ones by the radiant energy trapped by their pigments. Part of this free energy, obtained by the oxidation of chemical compounds or by light, is transformed in a form more easily available to cells. In most endoergonic processes, this special transporter of intracellular energy is adenosine triphosphate (ATP), which is considered the universal transporter of energy in all biological system.

1.1. *Escherichia coli*.

E. coli is a facultative anaerobe (Fig. 1.1.1. A and B). It is characterized by a rapid growth rate (it reproduces by binary fission roughly every 20 minutes), simple nutritional requirements and can produce several final metabolites by fermentation. It contains a single circular chromosome with 4,639,221 base pairs and 4288 protein-coding genes. It is commonly used as host cell for cloning segments of genomic DNA and for plasmid transformation. Because of all those characteristics, *E. coli* has become a model organism for studying many of life's essential processes.

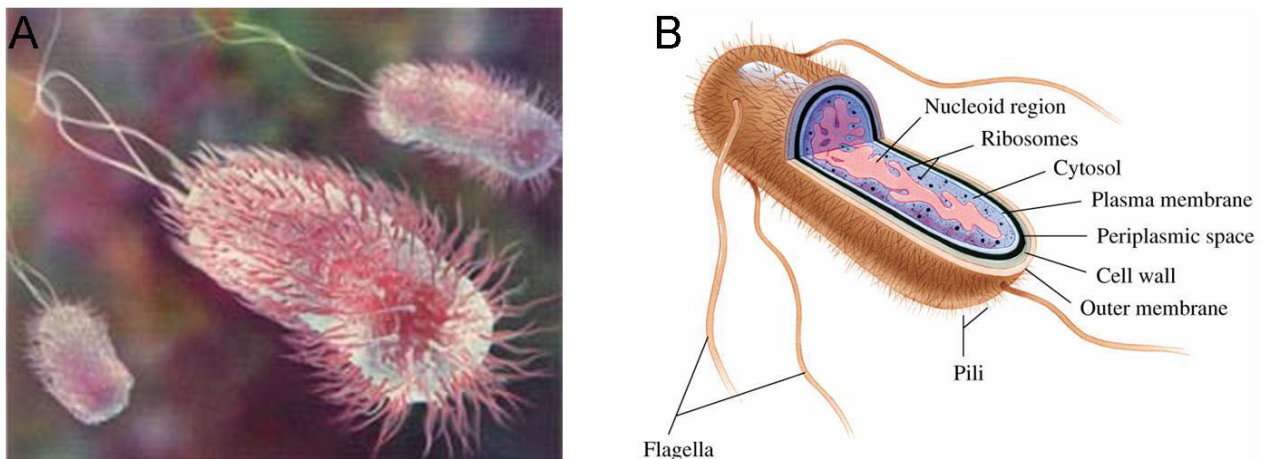


Fig. 1.1.1. Photograph and schematic representation of *Escherichia coli*.

1.1.1. *E. coli* metabolism

E. coli produces ATP by two general mechanisms based on oxidoreductive reactions:

- respiration: in this process the organic or inorganic substrate is totally oxidized under either aerobic or anaerobic conditions;
- fermentation: this process does not involve an electron transport chain and results in a partial oxidation of the organic substrate.

In the respiratory chain, the electron transporters have a well-defined orientation across the membrane in order to work vectorially. In this way the electron transfer is accompanied by a proton translocation from the cytoplasm to the periplasm, which leads to the establishment of a proton gradient, since the membrane is largely impermeable to protons. The energy associated with this gradient can be utilized by different processes like active transport or ATP synthesis (see §1.1.3 for the chemiosmotic model of ATP formation). The exergonic going back of proton across the membrane portion of the ATP synthase energizes the phosphorylation of ADP to ATP.

E. coli can use different enzymes of the respiratory chain based on the environmental conditions, the presence/absence of oxygen and the kind of available substrates. Under aerobic conditions, *E. coli* synthesizes two different cytochrome oxidases, cytochrome oxidase **bo** and **bd** (Anraku & Gennis, 1987; Poole & Ingledew, 1984; Lin & Kuritzkes, 1987), whereas under anaerobic conditions up to five terminal oxidoreductases can be present in its respiratory chain. These enzymes employ, as final acceptors, nitrate, dimethyl-sulfoxide (DMSO), or fumarate. In both the oxygenic and anoxygenic respiratory chain, a quinone couples the NADH oxidation (via NADH-dehydrogenase) to the reduction of the final acceptor operated by the terminal oxidoreductases. Cytochrome oxidase **bo** is prevalent under aerobic conditions, but if the oxygen concentration decreases the concentration of cytochrome oxidase **bd** starts to increase. Under anoxygenic conditions the cell synthesizes enzymes involved in the anaerobic respiration, enabling the cell to keep living on respiratory metabolism, more efficient than the fermentative one. The synthesis of anaerobic oxidoreductases is nitrate dependent, and nitrate is the preferential electron acceptor (Fig.1.1.2.). Only when nitrate is in short supply, the synthesis of alternative reductases (DMSO/TMAO reductase and fumarate reductase) will increase. The regulation of the synthesis of the enzymes involved in the respiration enables the cell to make an optimized use of the space available on the membrane.

In the absence of the different substrates for the oxidoreductases, the cell switches to fermentation.

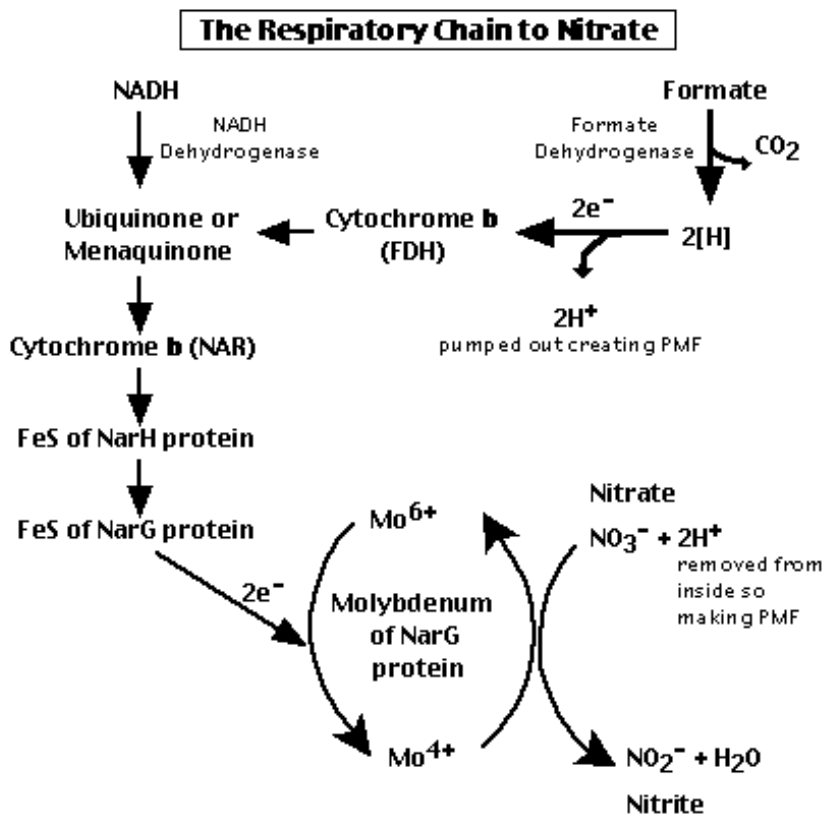


Fig.1.1.2. *E. coli* respiratory chain. Formate-nitrate reductase system (taken from <http://www.micro.siu.edu/micr425/425Notes/07-Respire.html>).

1.1.2. Respiratory chain of *E. coli*.

If *E. coli* grows under aerobic conditions, the components of its respiratory chain are different from the ones present in mitochondria. Concerning the first step of the electron transfer (quinone reduction) *E. coli* can use two different NADH- dehydrogenases (Matsushita K., 1987):

- NADH dhI –dehydrogenase which reacts with deamino-NADH and NADH. Its turnover contributes to the formation of an electrochemical proton gradient. This dehydrogenase is not strictly related to complex I of mitochondria;
- NADH dhII –dehydrogenase which reacts with NADH; its turnover does not determine an electrochemical proton gradient.

E. coli employs both enzymes but the amount of these enzyme present on the membranes depends on growth conditions and on O₂ concentration. Moreover alternative dehydrogenases have been identified, which oxidize L-lactate, D-lactate, malate and glycerol-3-phosphate.

The organization and the distribution of the complexes downstream ubiquinone do not respect the linear scheme of the mitochondrial respiratory chain; indeed different oxidases can be present at the same time, giving rise to branched respiratory chains. In particular, as already mentioned, two different cytochrome oxidases can oxidize ubiquinone, cytochrome oxidase **bo** and **bd**. The most part of the electron flux is channeled to cytochrome oxidase **bo**, since cytochrome oxidase **bd** is less efficient (Calohoun et al., 1993). Nevertheless, cytochrome oxidase **bd** has a higher affinity for

oxygen and is synthesized under low O_2 concentrations. It is possible to hypothesize that the lowered stoichiometry of proton translocation allows a high rate of electron transportation when there is no need of a high proton motive force. This is what happens in the absence of a proton back pressure generated by the proton motive force. It is clear that the *E. coli* respiratory chain is truncated and branched and has $q^+/2e^-$ and $H^+/2e^-$ ratios which are lower with respect to those observed in mitochondria. If the H^+/ATP ratio for the ATPase is the same as that observed in other organisms, the maximum P/O ratio per reduced O_2 (starting from the oxidation of a molecule of ubiquinole) is even lower (0.67 and 1.33 for the electron flux to cytochrome **bd** and **bo** respectively, instead of the theoretical values of 2 and 1.5, which are observed in submitochondrial particles and mitochondria respectively).

The electron transport system in *E. coli* shows that an organism will not always try to reach the highest possible stoichiometry of ATP production. The *E. coli* habitat might abound with substrates that it can metabolize, which is why it does not need to maximize the production of ATP. Moreover the branched respiratory chain enables *E. coli* to adapt its metabolism to different environmental conditions.

1.1.3. Chemiosmosis.

Among the models suggested to explain how the reaction involved in the redox chain could promote ATP synthesis, the Mitchell's chemiosmotic theory implied a totally different and innovative model based on an energy coupling mechanism (Mitchell, 1966). The idea postulated by Mitchell have been extensively demonstrated during the past years and now his theory is universally accepted and considered the mechanism of energy transfer most largely adopted by living organisms. The principal statements of the chemiosmotic theory can be summarized as follows:

- 1) the membranes involved in processes of energy transduction are vesicular and largely impermeable to protons except for the H^+ translocation pathway catalyzed by redox reaction or proteins;
- 2) the energy is stored in the form of a transmembrane electrochemical proton gradient:

$$\Delta\tilde{\mu}_{H^+} = F\Delta\psi - 2.3 RT \Delta pH;$$
- 3) a crucial point is the vectorial organization of the membrane complexes and the alternation of electron transporter and proton carrier;
- 4) the enzymatic complexes of the oxidoreductive chain can translocate H^+ and contribute to the generation of a transmembrane $\Delta\tilde{\mu}_{H^+}$;
- 5) a single enzyme, present on the coupling membrane, couples the proton translocation to ATP synthesis;
- 6) the ATP synthesis is coupled to an exergonic flux of H^+ , driven by the $\Delta\tilde{\mu}_{H^+}$. The opposite reaction of ATP hydrolysis, by energizing an H^+ transport in the opposite direction, determines the generation of a transmembrane $\Delta\tilde{\mu}_{H^+}$;
- 7) the uncouplers (e.g. protonofors) abolish the proton gradient and uncouple electron transfer from phosphorylation.

1.2. F₀F₁ ATP synthase.

As mentioned, all living organisms need a continuous contribution of free energy to carry out their vital functions. The nucleotide adenosine triphosphate (ATP) is the most important energy vector in all cells. This molecule consists of a purine base (adenine) attached to the 1' carbon atom of a pentose sugar (ribose). Three phosphate groups are attached at the 5' carbon atom of the pentose sugar. ATP is a high-energy molecule, since it contains two phosphoanhydride bonds which have a high Gibbs free energy of hydrolysis:

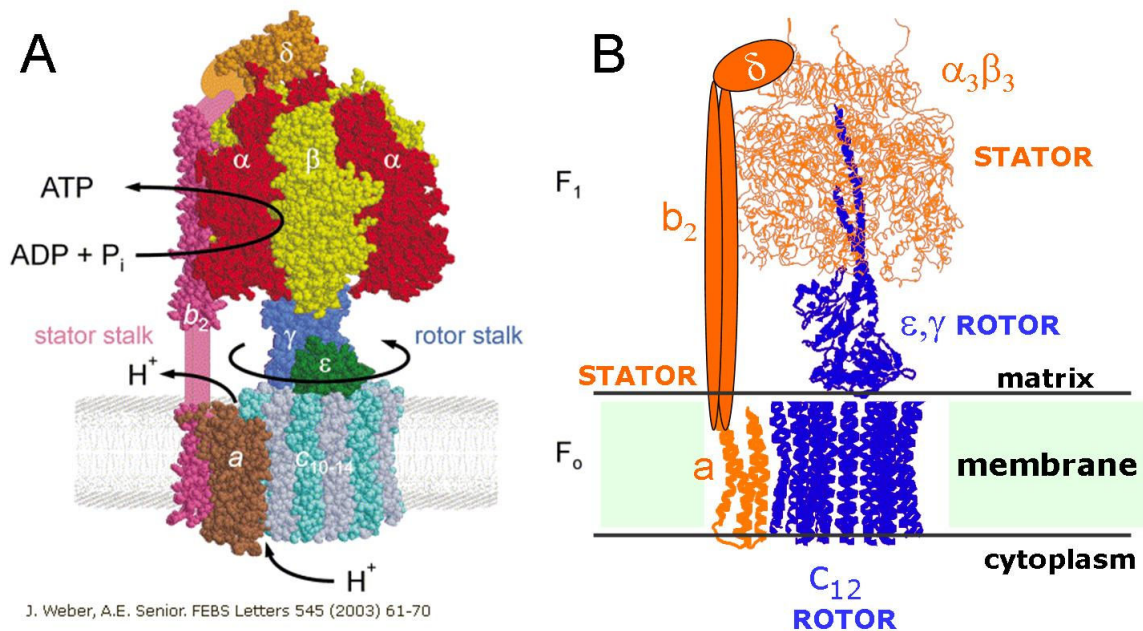
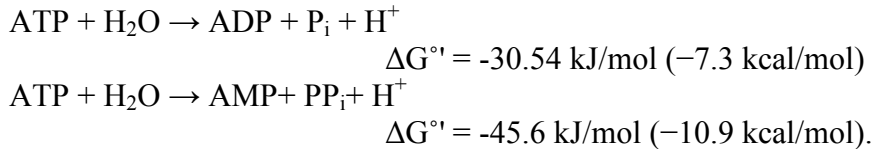


Fig.1.2.1. Schematic models of the ATP synthase.

Panel A., Secondary structure of the enzyme (from Weber &Senior, 2003);

Panel B., Stator (in orange) and rotor (in blue) parts of the ATP synthase.

The ATP synthase is a transmembrane enzymatic complex able to couple a chemical reaction, the ATP synthesis/hydrolysis, with an osmotic process, the proton translocation across the membrane (Fig.1.2.1.A).

F₀ F₁-ATPases or ATP synthases can be found in bacteria, mitochondria and chloroplasts (Boyer 1997, Fillingame et al. 2000, Yoshida et al. 2001, Capaldi & Aggeler 2002, Wilkens 2005). These highly conserved enzymes catalyze ATP synthesis at the expense of a transmembrane electrochemical potential difference of protons (or Na⁺ ions in some species) but can also work in the ATP hydrolysis direction, in this way building up a proton (or Na⁺) electrochemical potential difference. They are composed of a membrane embedded hydrophobic sector, F₀, which is involved in proton translocation across the membrane, and in its simplest form contains 3 subunits in

stoichiometry $\mathbf{ab}_2\mathbf{c}_{10-15}$, and of a hydrophilic extrinsic sector, F_1 , which in its simplest form contains 5 subunits in stoichiometry $\alpha_3\beta_3\gamma\delta\epsilon$ and the catalytic sites. These two parts are structurally linked by an external stalk represented by the \mathbf{b} and δ subunits and a central stalk formed by the γ and ϵ subunits (Fig.1.2.1.A,B). In 1994 the first crystal structure of the bovine mitochondrial F_1 was reported by Abrahams et al.. Following this achievement, further high resolution structural information for the soluble part has continued to appear, but a high resolution structure of the whole complex is still lacking.

The F_0 portion can be pulled apart from F_1 , upon which F_1 can hydrolyze but not synthesize ATP, and protons can be transported passively across F_0 . The number of subunits in the holoenzyme changes in different organisms (8 subunits in aerobic bacteria, 9 in photosynthetic bacteria and up to 16 in mitochondria). However the tertiary and quaternary structures of the enzymes are highly conserved even in species which are evolutionarily far apart.

1.2.1. Structural features: F_1 domain.

The F_1 portion has a globular structure, 80 Å high and 160Å wide. It is made of 5 different polypeptidic chains, some of them present in multicopy, with stoichiometry $\alpha_3\beta_3\gamma\delta\epsilon$. Much structural information at high resolution is available about the F_1 portion. In J.Walker laboratory, more than 85% of the aminoacid residues of α , β , and ϵ subunit of the bovine heart mitochondrial F_1 -ATPase have been identified by x-ray crystallography (Abrahamas et al., 1994). In the same laboratory, the entire structure of the γ subunit and of the δ subunit, which is homologous to the bacterial ϵ subunit, have been solved (Gibbon et al., 2000). The crystal structure of the complex $\gamma\epsilon$ from *E. coli* ATPase is also available at a resolution of 2.1Å (Rodgers & Wilce, 2000). In addition, incomplete F_1 structures from *E. coli* and chloroplasts have been published (Hausrath et al., 1999; Groth & Pool, 2001). Based on these information the F_1 domain consists of a trimer of heterodimers α - β , alternatively laid around a central cavity, which hosts two coiled coil α -helices of the γ subunit.

α/β subunit

The α and β subunits share a sequence homology of 20%, mainly clustered in the nucleotides/Pi binding domain. Both of them consist of three domains (Fig.1.2.2.):

- a N- terminal β barrel domain of 6 strands, ;
- a central α/β domain, which hosts the nucleotide binding site;
- a C-terminal domain made of 6 α -helices (7 in the α subunit).

The N- terminal β barrel domains are linked and form an apical crown, which seems to stabilize the entire F_1 structure. The tertiary structures of the α and β subunits have a similar folding, but the aminoacids constituting the nucleotide binding sites, present at the interface between the α and β subunits, are significantly different. This is a structural evidence that the three nucleotide binding sites in the subunit α are not catalytic; it is possible that they have a structural and/or regulatory function. Indeed the three catalytic sites are on the β subunit, in particular at the interface of the α/β heterodimers. From the x-ray structure (Fig.1.2.2.) it appears that the catalytic sites have different affinities for their substrates, since they can adopt, in the same enzyme, three different conformations:

- β_{TP} , with an AMP-PNP bound (adenylyl-imidodiphosphate, a non-hydrolysable analogous of ATP);
- β_{DP} , with an ADP bound;
- β_E , without any bound nucleotide.

A fourth conformation (β_{HC}) has been seen under different crystallization conditions, (determined from crystals grown in the presence of ADP and fluoroaluminate) (Menz et al., 2001):

- β_{HC} , is intermediate between the closed and open state, it has bound ADP and sulfate (mimicking Pi). This structure probably represents the posthydrolysis pre-product release step on the catalytic pathway (see §1.3.2.).

In the β_{TP} and β_{DP} conformations, the active sites are closed and strongly hydrophobic, in the β_E and β_{HC} conformations they are open and half closed respectively. The catalytic sites asymmetry gives support to the binding change mechanism proposed by Boyer; this model states that the three catalytic sites are not equivalent and undergo a transition among three different functional states (§1.3.1.). The three α are all in the same conformations.

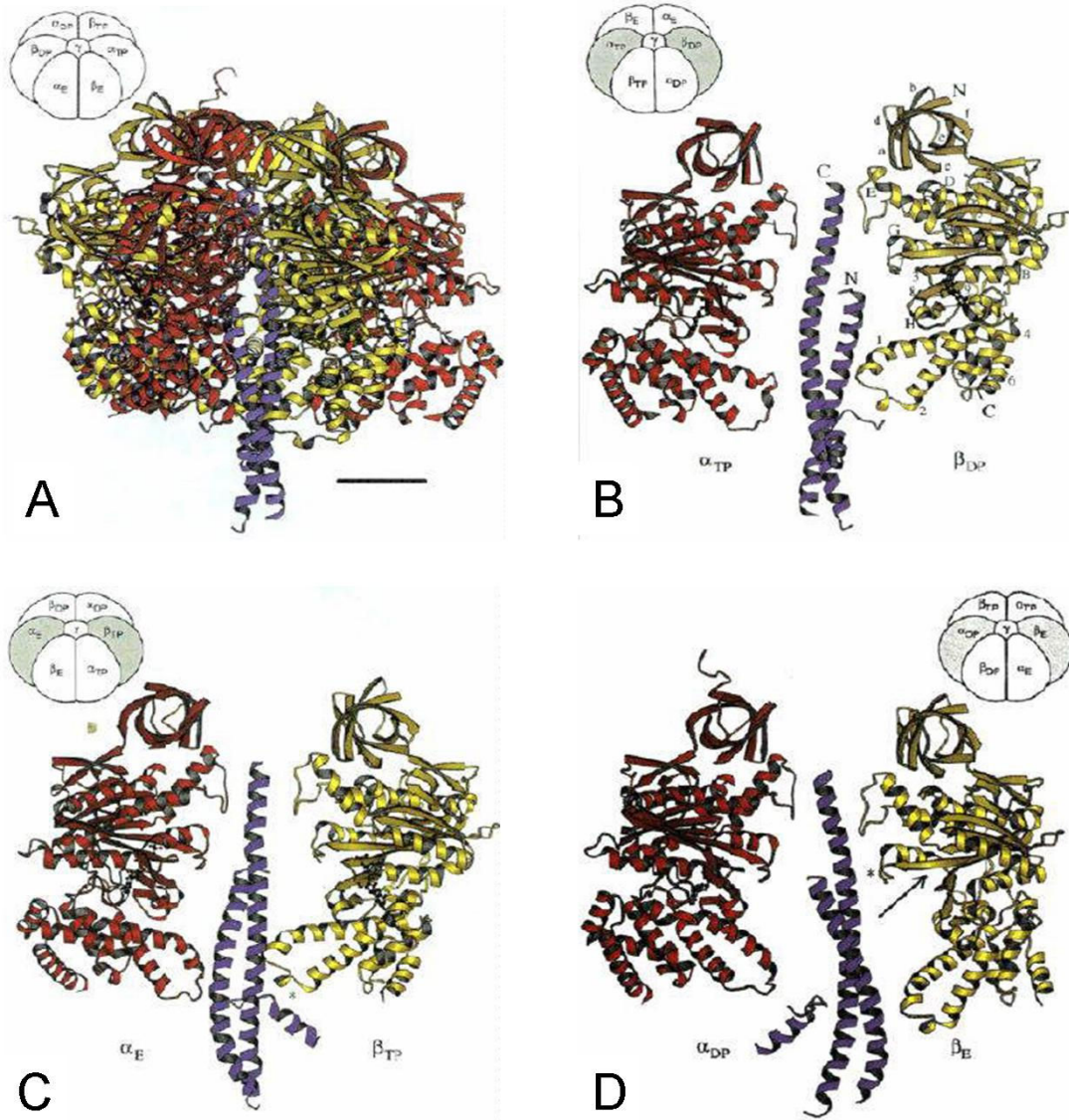


Fig.1.2.2. Walkers's three-dimensional structure of F₁ solved by X-rays crystallography. The α subunits are in red and the β subunits in yellow. Panel A., assembly; Panel B-C-D, different interactions of γ with the α/β pairs (from Abrahamas et al., 1994).

γ subunit

The γ is constituted by:

- a left-handed coiled coil domain, formed by two α -helices, one, which is 90Å long, at the C-terminus and the other one at the N-terminus. These two coil-coiled helices are hosted into the cavity formed by the assembly of the $\alpha_3\beta_3$ subunits.
- a central domain, mainly formed by an α/β motif with 5 β strands, with the shortest strand (residues 179-183, γ - β 5) antiparallel to the others. The β strands alternate with two α -helices (residues 91-108 (γ - α 3) and 150-161 (γ - α 5)), (Fig.1.2.3.A). A short α -helix (residues 120-124 (γ - α 4) links strands 2 and 3.

Of the two coiled-coil α -helices, the top of the C-terminal helix reaches the small dimple, 15Å deep, found in the upper part of the α_3/β_3 hexamer, whereas the N-terminal helix extends through the first half of the central body of the α_3/β_3 complex. This asymmetric structure, located within the cavity of the hexamer, enables the γ subunit to interact in a differential way with each of the three β subunits. The prevalent working hypothesis in the field is that the different conformations of the β subunits are induced by these different modes of γ/β interaction (Fig.1.2.2.).

The structure of the γ subunit has been solved by X-ray crystallography of bovine heart mitochondrial F_1 -ATPase (Gibbons et al., 2000), moreover the structure of the γ/ϵ complex of *E. coli* ATPase has been published (Rodgers & Wilce, 2000). The two structures are compared in Fig.1.2.3.A-B..

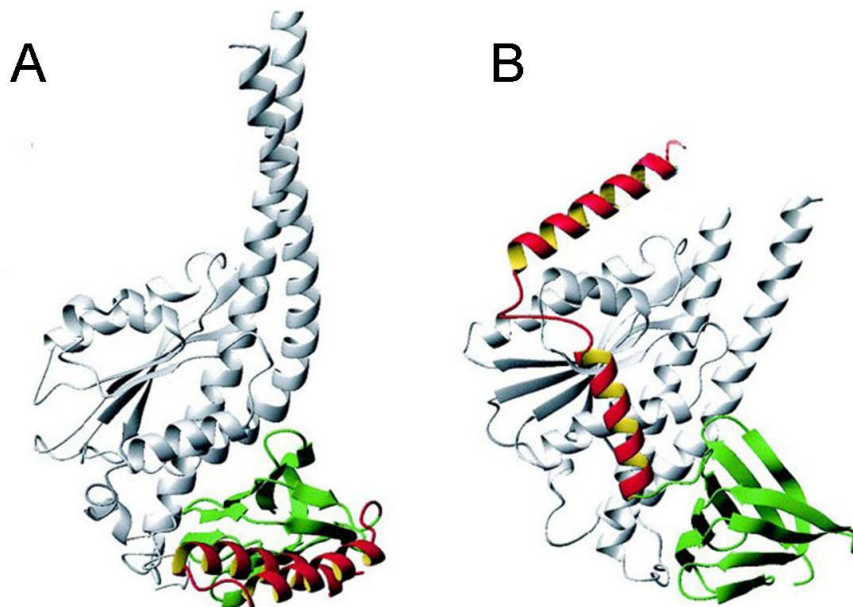


Fig.1.2.3. γ/ϵ solved by X-rays crystallography.

The subunit γ is in gray, the ϵ subunit in red (C-terminus domain) and green (N-terminus domain), (adapted from Suzuki et al., 2003).

Panel A., γ/δ crystal complex from bovine heart mitochondrial F_1 -ATPase

(δ subunit is homologous to the ϵ subunit in *E. coli*), (Gibbons et al., 2000);

Panel B., γ/ϵ crystal complex from *E. coli* F_1 -ATPase, (Rodgers & Wilce, 2000).

ϵ subunit

The structure of the ϵ subunit has been solved by NMR spectroscopy (Wilkens et al., 1995). The subunit is constituted by two domains (Fig.1.2.4.):

- a N-terminus domain, represented by a β barrel of 10 strands (residues 1-86);
- a C-terminus domain, represented by an helix-loop-helix motif (residues 88-103 ($\epsilon\alpha_1$) and 115-138 ($\epsilon\alpha_2$)).

Cross-linking data have shown that the β barrel domain of ϵ has contacts with the membrane and with the upper part of F_0 (subunit **c**); whereas the helix-loop-helix motif forms an hairpin which comes in contact with the bottom of the $\alpha_3\beta_3$ hexamer. The structure of ϵ in the ATP synthase complex has been controversial since two different conformations of ϵ , the “up conformation” (Rodgers & Wilce, 2000; Hausrath et al., 2001; Hausrath et al., 1999) and the “down conformation” (Gibbons et al., 2000), have been seen in crystal structures. A crystal of the up conformation has been published by Rogers et al. in 2000. The crystal structures of the down conformation of ϵ are from bovine heart mitochondria and yeast $F_0 F_1$ (Gibbons et al, 2000; Stock et al, 1999). However in these organisms an additional subunit of the ATP synthase prevents the ϵ up conformation. The N-domain is essentially located in the same position in both conformations, though in a different orientation, but in the up conformation the helices of the C-domain are extended and partially wrapped around γ to make contact with $\alpha_3\beta_3$, whereas in the down conformation the two α -helices fold on themselves and lie next to the N-domain on top of the c_{10} oligomer (compare Fig.1.2.3.B and Fig.1.2.4.). Moreover cross-linking data seem to confirm that the helix-loop-helix motif has a marked mobility (Ganti & Vik, 2007), even in the holoenzyme, depending on the presence of different substrates. It is possible to hypothesize that this mobility of the C-terminus of ϵ may have a defined functional role (§1.5.1.).

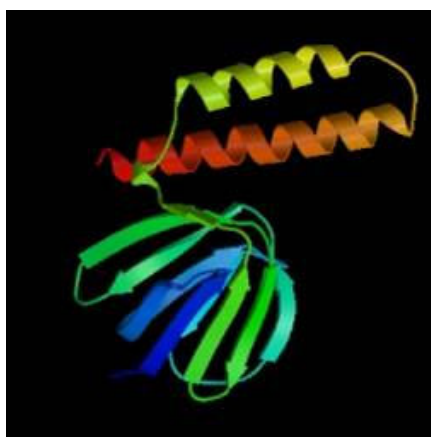


Fig. 1.2.4. Structure of the ϵ subunit of *E. coli* obtained by NMR spectroscopy.
(Wilkens et al., 1995)

 δ subunit

Up to now 134 residues over 176 of δ subunit have been solved by NMR spectroscopy. This part is characterized by a bunch of α helices. Crosslinking studies between the δ and **b** subunits have shown that δ is located peripherally to the $\alpha_3\beta_3$ hexamer (Ogilvie et al., 1998).

As already mentioned, the δ subunit is part of the external stalk, which links F_1 and F_0 (§1.2.); in *E. coli* this stalk includes the δ subunit and a dimer of **b** subunits. By immunoelectronmicroscopy studies the δ subunit has been shown to be docked to the upper part of F_1 (Wilkens et al., 2000).

1.2.2. Structural features: F_O domain.

The F_O domain represents the transmembrane component of the ATP synthase and acts as a proton channel. The proton flux is driven across such domain by the transmembrane $\Delta\tilde{\mu}_H^+$. A general structural model of the F_O domain has been developed by electron microscopy (Birkenhafer et al., 1995) and atomic force microscopy (Singh et al., 1996; Seelert et al., 2000) studies. According to this model, the **a/b**₂ complex is located externally to the oligomer of **c** subunits (**c**-ring).

c subunit

The structure of the **c** subunit has been solved by NMR spectroscopy (Girvin et al., 1998). This subunit is the smallest of the complex and is represented by a hairpin of two trans-membrane α -helices (residues 10-31 and 54-76). The two helices are linked by a short polar loop, which sticks out from the cytoplasmatic side of the membrane (Fig.1.2.5.). This loop hosts three conserved residues: Arg41, Glu42 and Pro43 (*E. coli* numeration), which interact with the ϵ subunit (from crosslinking studies). The two helices are tightly leaned one against the other along their length and they are made entirely of hydrophobic residues except for Asp61. These charged residues are located in the middle of the C-terminal α -helix and determine a partial interruption of its secondary structure. The carboxylic group in position 61 is universally conserved either as Asp or Glu. The protonation/deprotonation of this residue could have a key role in the proton translocation across F_O. This hypothesis has been confirmed by mutagenesis and DCCD inhibition studies. The individual monomer of **c** subunit interacts to form a ring (**c**-ring), (Seelert et al., 2000). The two α -helices of every subunit are arranged in the oligomer so as to form two concentric rings, an internal ring formed by the N-terminus α -helices and an external ring constituted by the C-terminus α -helices. The **c**-oligomer on the whole appears like a cylinder with an external diameter of 55-60Å and an internal one of 11-12Å. The stoichiometry of the **c** subunit in the ring changes according to the organism: 10 copies have been found in the yeast mitochondrial ATP synthase (Stock et al., 1999), 14 in chloroplasts (Seelert et al., 2000), 11 in *I. tartaricus* (Dimroth et al., 2000) and between 10 and 12 in *E. coli* (Fillingame et al., 1998).

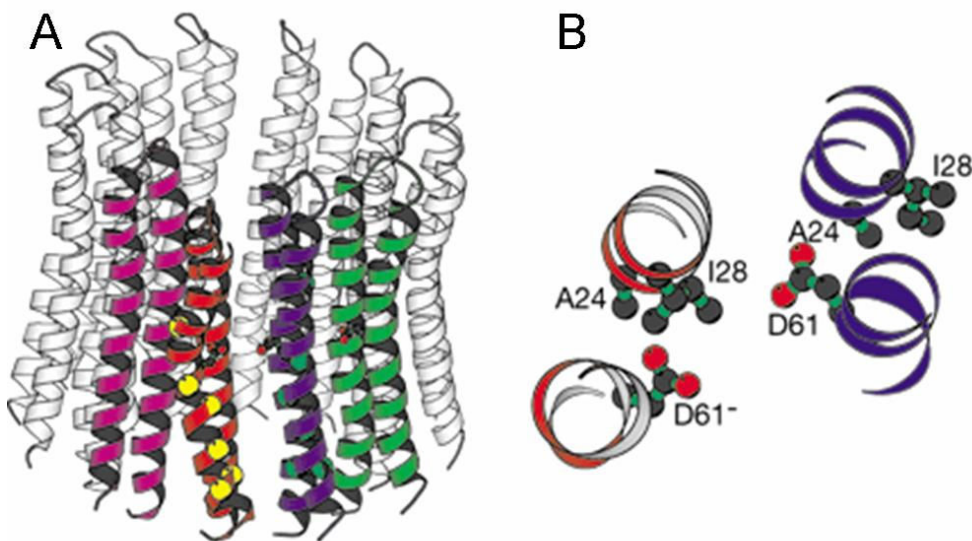


Fig.1.2.5. Secondary structure of the c-ring.

Panel A., lateral view of the **c**-ring; Panel B., section of a **c** monomer interfaced with a section of the α -helices of the **a** subunit (adapted from Rastogi & Girvin, 1998).

b subunit

The structural data of the **b** subunit are incomplete. This subunit is made of two portions:

- an hydrophobic transmembrane N-terminal portion;
- an hydrophilic C-terminal portion. This part is mainly represented by an α -helix which sticks out from the cytoplasmatic side of the membrane.

Analytical ultracentrifugation studies have indicated that the **b** subunit is present as a dimer; in particular residues 55-122 are involved in the dimerization (Dunn et al., 2000). The homodimer can be divided into four functional sub-domains: the subunit δ binding domain, the dimerization domain, the linkage domain and the membrane domain.

a subunit

The **a** subunit has a high percentage of hydrophobic aminoacids; the secondary structure is represented by 5 transmembrane α -helices (Fig.1.2.6.).

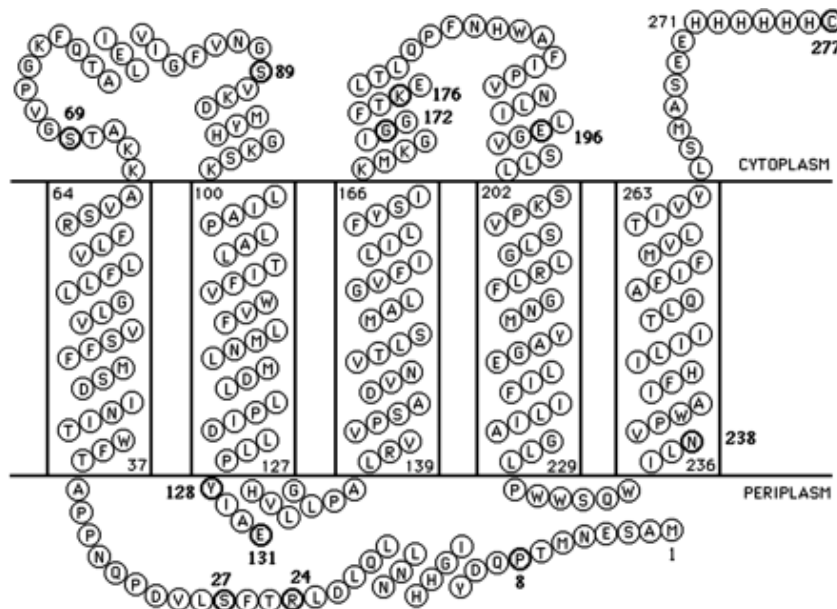


Fig.1.2.6. Topologic model of the a subunit. (Fillingame et al., 2000).

At the C-terminus several residues are highly conserved; experiments with mutants have established that:

- the mutation of Arg210 (*E. coli* numeration) determines the blockage of the enzyme activity. Therefore, a specific catalytic role of Arg210 can be hypothesized; it has been suggested that a transient salt bridge between Arg210 and Asp61 (of the **c** subunit) is established at every catalytic cycle;
- mutations of Gly218 and His245 partially impair the proper working of the enzyme.

Experiments with deletion mutants have shown that the N-terminal portion is involved in the incorporation of the **a** subunit into the membrane.

In 1999, Girvin and Rastogi have proposed a structural model that explains how the **a** subunit can interact with the **c**-ring. According to this model (Rastogi & Girgin, 1999),

the side chain of Arg210 is located at a peripheral position in the **a** subunit and interacts with the **c** subunits, in particular with Asp61, which is located at the same height of Arg210 relative to membrane thickness (Fig.1.2.7.).

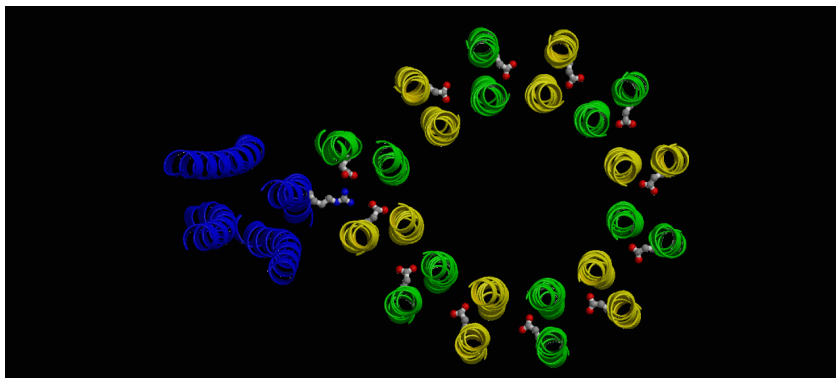


Fig. 1.2.7. Theoretical model of the a-c subunit interaction.

The **a-c**₁₂ complex is shown in cross-section. The subunit **a** is blue. The **c**-ring monomers are yellow and green (adapted from <http://www.bioc.aecom.yu.edu/labs/girvlab/ATPase/ATPase.html>).

1.3. Catalytic models.

As already described (§1.2.) the ATP synthase has a complicated structure and is composed of a

membrane-embedded portion, F_0 , the central and side stalks, and a large portion sticking out from the membrane, F_1 . The central portion ($F_1\gamma\varepsilon-F_0c_{10-14}$) rotates with respect to the surrounding portion ($F_1\alpha_3\beta_3\delta-F_0ab_2$); analogously to the functioning of a motor the former part can be considered the ‘rotor’ and the latter the ‘stator’, although the rotor/stator relationship is relative. When the magnitude of $\Delta\tilde{\mu}_H^+$, generated by the respiratory/photosynthetic chain, is large, the downhill proton flow through F_0 causes rotation of the F_0 rotor and, hence, rotation of the $\gamma\varepsilon$ -subunits of F_1 . The rotary motion of the γ alternates the conformations of the β -subunit so that ATP is synthesized. In the reverse reaction, ATP hydrolysis in F_1 induces the rotation of γ and, hence, of the F_0 rotor in the reverse direction. This then drives proton pumping.

In either case, the side stalk connecting the stator of F_0 and that of F_1 prevents them from being dragged by the central rotor. It is therefore possible to define the ATP synthase as a complex of two motors — an ATP driven F_1 motor and a proton-driven F_0 motor. They are connected by a common rotary shaft and their directions of rotation are opposite. The motor motions have been visualized for F_1 (Noji et al., 1997), but this has yet to be done for F_0 .

During the past years, a number of models have been developed to explain how the rotation of the different components of the ATP synthase can be coupled to its catalytic activity and how the mechanism of rotational catalysis can work on a molecular basis.

In the following, a summary of the most important proposed models is presented.

1.3.1. The catalytic mechanism of F_1 : the binding change mechanism proposed by Boyer.

At the beginning of the ‘70s, Boyer and coworkers, based on the statistic distribution of ^{18}O isotopomers within all the products generated during the catalytic activity of the ATP synthase, proposed that the energy of the proton gradient was mainly required for the release of ATP from the enzyme and not for its synthesis. Moreover they deduced that the three catalytic sites, on the β subunits, were equivalent from a biochemical point

of view and interacted cooperatively. Indeed the binding of ADP and P_i to one site determined the release of ATP from one other site. According to these considerations, they developed the “binding change mechanism”. This model predicts that the catalytic sites on the β subunit cyclically adopt, during the turnover, three interchangeable conformations, with different ligand affinities (Fig.1.3.1.).

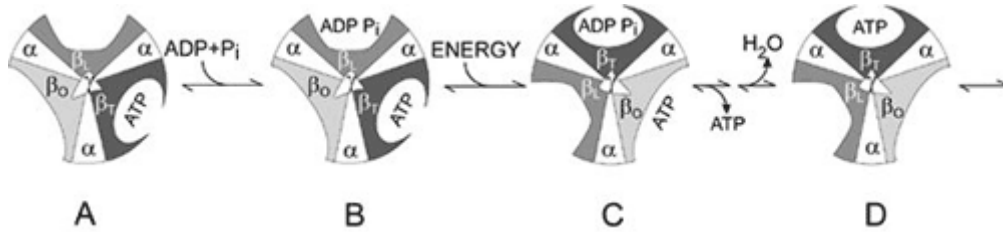


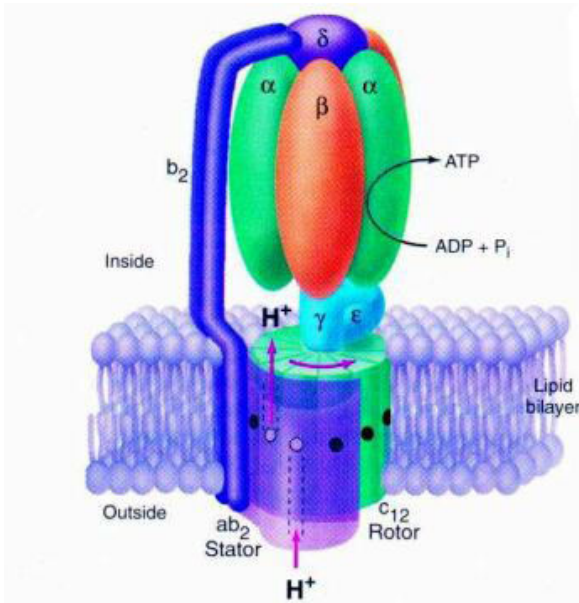
Fig.1.3.1. Boyer's "Binding Change Mechanism.

(from http://nobelprize.org/nobel_prizes/chemistry/laureates/1997/press.html)

The proton flux through the ATP synthase would promote the interconversion of the three sites; in this model the three β subunits would be, at any time, not functionally equivalent. According to this model, in any moment, a catalytic site is in an open conformation (O site) and has a low affinity for the substrates; a second site is in a loose conformation (L site) which is inactive and binds the substrates weakly; a third site is in a tight conformation (T site) which is catalytically active and binds the ligands tightly. If we assume that ATP is bound to the T site and ADP and P_i to the L site, the proton flux across the enzyme energizes the conversion of the T site into the O site, the L site into the T one and the O site into the L one. These structural changes determine the release of ATP from the new low affinity O site and the synthesis of ATP from the ADP and P_i present in the new T site (L site before the rotation). According to this model, the enzyme cyclically undergoes a concerted transition among the different catalytic sites. In the '80s, Boyer proposed that the rotation of the γ subunit within the $\alpha_3\beta_3$ hexamer could determine the cyclic conversion of the sites; in order to accomplish this task the γ subunit should be located in the axial centre of the hexamer.

This revolutionary theory was strongly supported by the structural data obtained in the '90 by Walker and coworkers (Abrahamas et al., 1994). By X-ray crystallography they studied the structure of the $\alpha_3\beta_3\gamma$ complex and they first showed the asymmetric conformation of these subunits. Moreover their studies revealed a striking correspondence between the three conformations found for the β subunit (β_{TP} , β_{DP} and β_E) and the three conformations postulated by Boyer (T,L and O sites). They hypothesized that the asymmetry of the whole complex could be determined by the asymmetric disposition of γ with respect to the $\alpha_3\beta_3$ hexamer.

In the subsequent years a number of studies were carried out to verify these hypothesis; the supposed rotation of the γ subunit was supported by Duncan and coworkers in 1995 by crosslinking experiments and by Sabbert and coworker in 1996 by fluorescence correlation spectroscopy. In 1997 the research group of Yoshida and Kinoshita provided an incontrovertible evidence by fluorescence microscopy of a unidirectional rotation of the γ subunit induced by the ATP hydrolysis reaction (Noji et al., 1997). All the data supporting the hypothesis of Boyer and Walker led to a general acceptance of the model, and the two scientists won the Nobel prize for Chemistry in 1997. According to this model, the expression “rotational catalysis motor” started to be used to describe the catalytic activity of this enzyme. Biochemical studies on the *E. coli* ATP synthases



provided evidence that the rotor part of the enzyme is represented by the $c_{10-12} \gamma \epsilon$ subunits and the stator portion by the $\alpha_3 \beta_3 \delta a b_2$ (Rodgers & Capaldi, 1998), (Fig.1.3.2.).

Fig.1.3.2. Model of ATP synthase in which the rotor and the stator part are indicated. (from <http://www.answersingenesis.org/docs/3799.asp>).

1.3.2. The binding change mechanism in the presence of saturating concentration of ATP.

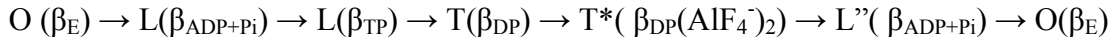
In 2001, Walker and coworker published a crystal-structure of the bovine heart mitochondrial F_1 -ATPase in which the enzyme was inhibited by aluminium fluoride (Menz et al., 2001). The crystallographic analysis of this inhibited form of the ATP synthase revealed a new structure characterized by nucleotides occupancy of all the three catalytic sites. In the intentions of the authors, the transition state was simulated by the ADP- AlF_4^- complex, mimicking the pentacoordinate transition state of P_i . In all the structures previously solved in J. Walker's laboratory (see §1.3.1.), one of the β subunit always was in the open conformation, without any bound nucleotide (β_E). Unexpectedly, the new crystal structure of the AlF_4^- -inhibited-form of the ATP synthase showed that the β subunit can bind ADP together with sulphate (which can be considered a structural analog of P_i); under these conditions the β subunit adopts a "half closed" conformation (β_{HC}). β_{HC} differs from β_E and β_C for several aspects:

- relative to the β_E conformation, the C-terminal domain is rotated 16° around the axis of the $\alpha_3 \beta_3$ barrel, a feature which determines the closing of the α_E/β_E interface;
- relative to the β_C conformation, the subunit undergoes a 23° rotation around an axis perpendicular to the previous one; this event favours an optimal facing of the two catalytic residues, βGlu188 and βArg189 , towards the P_i moiety of the nucleotide.

Based on this finding, the authors proposed a modified binding change mechanism in which all three catalytic sites are occupied by nucleotides. This model was based on the hypothesis that, in the presence of saturating ATP concentration, the half-life of the β open conformation had to be very short in order to ensure the highest turnover rate.

The binding of ATP to an open catalytic site (O), causing a conformational change, would determine the transition to an half-closed conformation, which in turn would induce the hydrolysis of ATP in the contiguous catalytic site (T^*). This sequence would explain the cyclic inter-conversion of the sites: T^* sites turns into an half closed site

(L''), L site turns into T and L' site turns into L (Fig.1.3.3.). Each β undergoes the following transitions:



The crystal structure of ADP- AlF_4^- F_1 -ATPase would represent, according to this model, a newly discovered intermediate in the catalytic pathway, which occurs after the hydrolytic step but before the release of products. The authors assume that this hydrolytic pathway also takes place, in the opposite direction, during the ATP synthesis reaction.

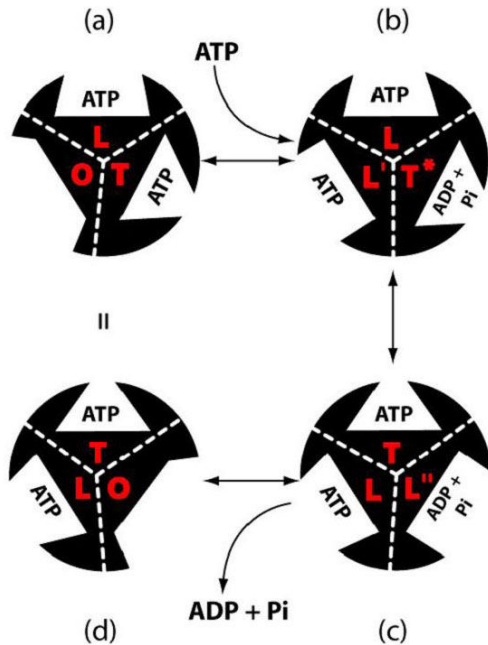


Fig.1.3.3. Model of the binding change mechanism in the presence of saturating concentration of ATP.
(Menz et al., 2001).

1.3.3. The rotation of the γ subunit.

In two works published in 2001 and 2003, Yoshida and coworker, using epifluorescence microscopy, investigated in more detail the rotation of the γ subunit (Yasuda et al., 2001; Shimabukuru et al., 2003). They showed that the rotation step of 120° can be split into two substeps of 80° and 40° , both of them lasting a fraction of millisecond. The binding of ATP to the catalytic sites would determine the 80° rotation and, subsequently, the products release would cause the 40° step. Between the two events, two mechanically silent reactions (lasting approximately 1ms) would occur:

1. the hydrolysis of bound ATP;
2. the release of the hydrolysis products (ADP or Pi).

Only after this second event, the 40° rotation would occur, coupled to the release of the second hydrolysis product. At this point F_1 would be ready to start a new catalytic cycle (Fig.1.3.4.).

In the direction of the ATP synthesis the proton flux through F_0 would determine the 40° rotation of the γ subunit ($A' \rightarrow C$ in Fig.1.3.4.) and the transition $\beta_E \rightarrow \beta_{DP}$ (in which ADP is loaded and bound). The release of ATP, synthesized during the previous catalytic cycle and bound to the β_{TP} site, would be associate to the next 80° rotation; indeed this rotation would determine a decrease of the affinity for the bound ATP. It has been hypothesized that the γ subunit has a high degree of internal flexibility and can

couple, in an elastic way, the c -ring rotation to the conformational change of the catalytic sites in the subunit β .

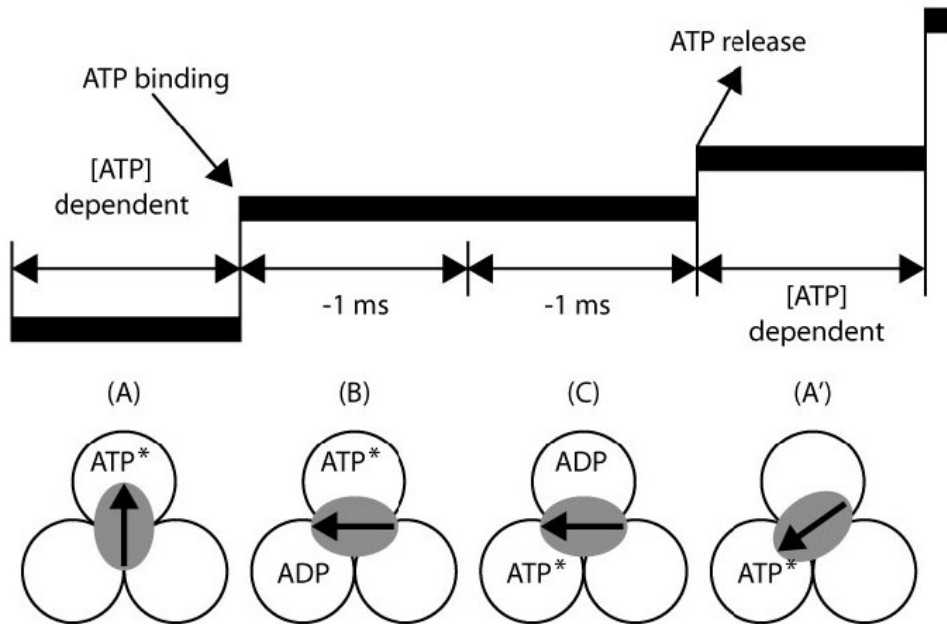


Fig.1.3.4. Schematic mechanism describing the catalytic substeps during the γ subunit rotation. ATP* indicate either ATP or ADP+Pi, (from Yasuda et al. 2001).

1.3.4. Hypothesis on the catalytic mechanism of the F_0 portion.

It is likely that the rotation of the γ subunit can be transmitted to the c -ring of F_0 ; indeed several data, supporting the rotation of F_0 in the presence of ATP, have been published (see e.g. Tsunoda et al., 2000). However, the structural information relative to the F_0 complex is still incomplete. Therefore, the models proposed to explain the rotational mechanism of F_0 remain highly speculative; some of them are based on models of the rotational motion of bacterial flagella.

The model proposed by Junge and coworker (Junge et al., 1997).

The model of Junge is based on three main assumptions:

1. the carboxylic group of Asp61 (present in each subunit of the c -ring) has to be protonated when it faces the membrane lipids while it is supposed to be deprotonated, i.e. negatively charged, when it faces the amino acids residues of subunit **a**(Fig.1.3.5.);
2. for the **a/c** subunits assembly to provide unidirectional rotation, the two proton entry points, located on the two membrane side of the subunit **a**, have to be non-colinear;
3. the c -ring rotates backwards and forwards relative to **a** by Brownian motion; these random rotations are an essential requirement for the ensuing unidirectional rotation.

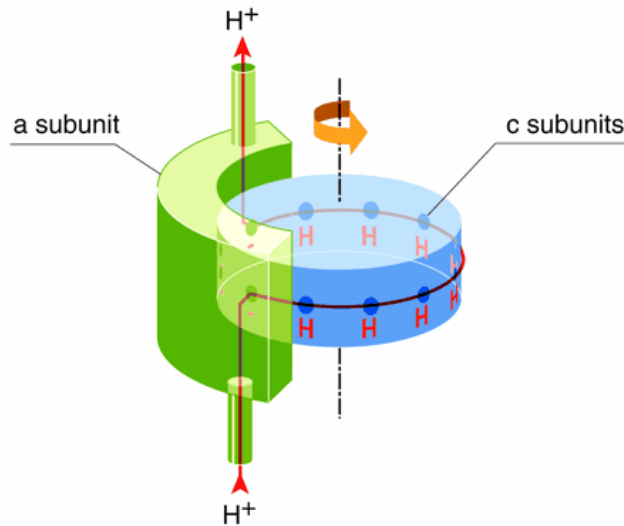


Fig.1.3.5. Model explaining the F₀ rotation.

The picture shows the c-ring and the a subunit with both the cytoplasmic and periplasmic H⁺ entry points. (from Junge et al., 1997).

Based on this model, each c subunit has a carboxylic group (from Asp61), located at half height of the thickness of the lipid bilayer, protruding into the proton channel.

The deprotonation of one of these aspartates negatively charges the c subunit, which, in order to escape from the hydrophobic environment of the membrane, moves and orients the COO⁻ of Asp61 at the interface with the a subunit. When Asp61 is protonated and electroneutral, the c subunit, and with it the whole c-ring, moves again. The rotation can be clockwise and anticlockwise depending on the probability for the proton to move into one of the two entry points on the two sides of the membrane. If the periplasmic space has a proton concentration higher than the cytoplasm, the c-ring will rotate anticlockwise, conversely it will rotate clockwise.

The model proposed by Rastogi and Girvin (Rastogi & Girvin, 1999)

Girvin and Rastogi have shown by NMR spectroscopy that the c subunit undergoes interesting structural transitions when the protonation state of Asp61 changes. Indeed, ranging from acidic to slightly alkaline pH, one of the two transmembrane α -helices of the c subunit undergoes a conformational change, through a 140° rotation of the C-terminal helix. Two different structures are observable at pH 8.0 and 5.0 respectively. Since Asp61 is not exposed on the membrane surface, hydrophilic pathways have to exist at both sides of the membrane in order to protonate Asp61. The authors suggest that the most probable pathway is the one which links Arg210 (a subunit) to the surface of the membrane. Indeed a cluster of polar residues (e.g. Gln252, Asn214, Asn148,

Asp119, His245, Glu219, Ser144 and Asn238) can be traced within a structural model of the a subunit. This cluster forms an hydrophilic pathway across the membrane connecting Arg210 with the surface of the membrane (Fig.1.3.6.).

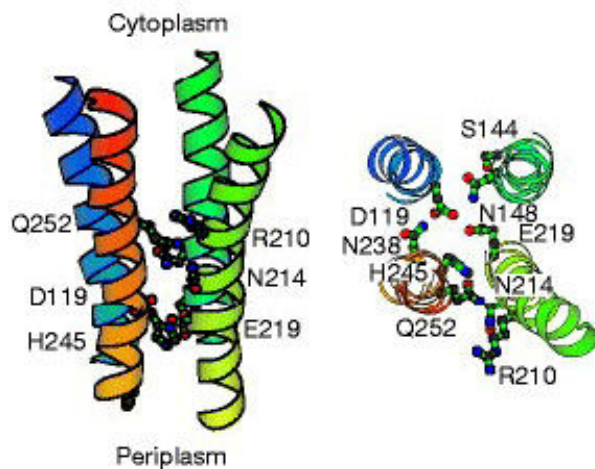
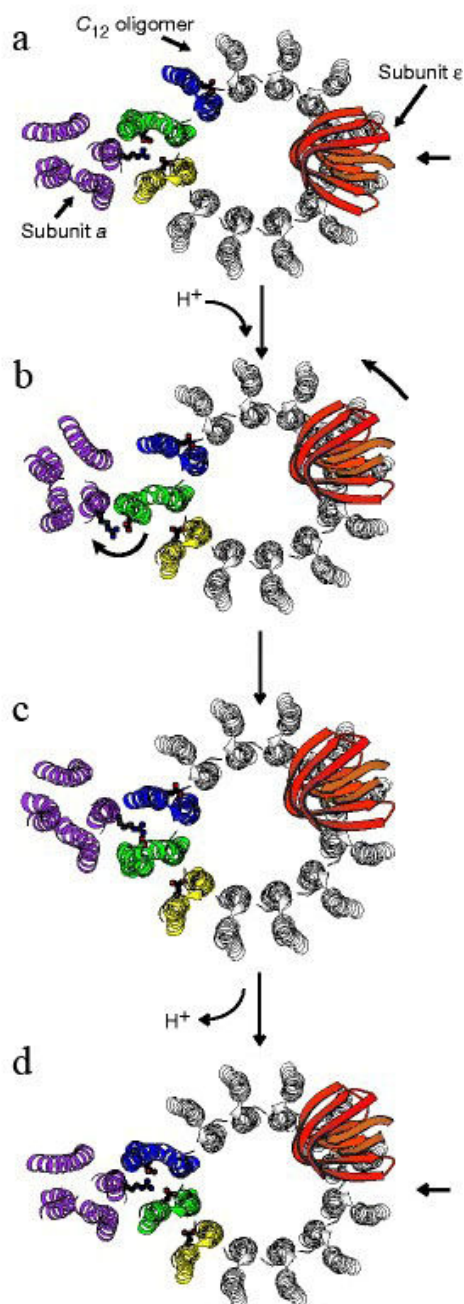


Fig. 1.3.6. Lateral view (on the left) and section (on the right) of the a-c interface in the structural model proposed by Rastogi and Girvin (1999), (adapted from Rastogi & Girvin, 1999).

During ATP synthesis, the proton electrochemical potential is higher in the periplasmic space than in the cytoplasm, favouring an inward proton flux. Based on the structural data obtained by NMR spectroscopy, the authors hypothesize that only one **c** subunit is deprotonated and that its subsequent protonation determines a clockwise rotation of the C-terminal α -helix of **c** (Fig.1.3.7.). During this rotation, the α -helix of the **a** subunit which carries Arg210 moves in concert with the helix of the **c** subunit (thanks to hydrogen bonds and steric interactions between the **a** and **c** subunits residues) and stops when the **a** subunit is positioned between the two next **c** subunits (panel *b* and *c* in Fig.1.3.7.). The **c** subunit would rotate in this way 1/12 revolution. After this rotation, in order to switch back to the starting point conformation, Asp61 in the next monomer has to deprotonate (blue monomer in panel *c* and *d* of Fig.1.3.7.). Again, analysis of the structural model revealed a potential hydrophilic pathway, running along the cytoplasmic membrane side. formed by: Ser206, Lys203 and Ser199



(**a** subunit), Arg50 (**c** subunit) and Thr51 (next **c** subunit). The subunit γ and ϵ interact with the **c**-ring through its protruding polar loops, and they should rotate together with it. If the stoichiometry of the **c**-ring is 12 subunits, the described four steps would occur during one 120° rotation of the $\gamma\epsilon$ complex within the internal core of F₁. This rotation would drive, in turn, the binding change mechanism required for catalysis at the nucleotide binding sites.

Fig. 1.3.7. The model by Girvin & Rostogi of the catalytic cycle explaining the translocation of protons across the F₀ complex (from Rastogi & Girvin 1999).

1.4. Regulation of the ATP synthase.

As far as we know, the regulation of the catalytic activity of the ATP synthase varies among different species, even though the catalytic mechanism is substantially conserved. In chloroplasts, the activity of the ATP synthase is modulated by the oxidation/reduction of a disulphide bond between two cysteines of the γ subunit (which are conserved in chloroplasts). The redox state of this bond is controlled by thioredoxins, which are reduced by the photosynthetic transport chain. It has been shown that the ATPase activity of the isolated CF₁ is enhanced when the disulfide bond between these conserved cysteines is cleaved by reduction (Mills et al., 1980; Nalin & McCarty, 1984). The structural basis for this redox regulation is assigned to the portion of the γ subunit, which consists of 37 amino acid residues (Pro194-Ile230 in the case of spinach CF₁) including two cysteine residues (Cys199 and Cys205 in spinach) (Miki et al., 1988), which resides only in the γ subunit of the redox-sensitive ATP synthase. Hisabori and coworker showed that this regulatory region of the γ subunit of chloroplast, inserted into the γ subunit gene of the thermophilic bacterial F₁-ATPase, can modulate the rotational activity of this redox insensitiveness enzyme (Bald et al., 2001). They showed in addition that this chimeric enzyme, under oxidizing conditions, had attenuated activity and was characterized by frequent and long pauses of rotation of γ (Ueoka-Nakanishi et al., 2004).

In mitochondria the enzyme is inhibited by a 9kDa basic protein, involving a pH-dependent interaction. All ATP synthases (from chloroplasts, mitochondria and bacteria) are inhibited by Mg-ADP; the binding of this complex in a catalytic site blocks the enzymatic activity (in both hydrolysis and synthesis direction). The presence of a $\Delta\tilde{\mu}_H^+$ induces the release of Mg-ADP and the activity of the enzyme is reestablished (Boyer, 2002; Feniouk et al.); moreover the binding of ATP in a non-catalytic site in the α subunit also appears to promote the release of Mg-ADP (Boyer, 2002).

The ϵ subunit has been shown to act as an endogenous inhibitor of the catalytic activity of bacterial ATP synthases; this subunit undergoes a drastic conformational change between a non-inhibitory form (down-form) and an inhibitory one (up-form) (see §1.5.).

1.4.1. Inhibition of *E. coli* ATP synthase activity by ADP and P_i.

Data obtained with *E. coli* ATP synthases which had been isolated and reconstituted into liposomes showed that the hydrolytic activity was inhibited by the binding of ADP and P_i to the enzyme and that this inhibition could be released by imposing a high transmembrane $\Delta\tilde{\mu}_H^+$ (Fischer, et al. 2000). It is intriguing to hypothesize that these phenomena might have a regulatory role in the bioenergetics of *E. coli*.

1.5. Structural changes of the ϵ subunit and their relevance to the catalytic and regulatory processes of the enzyme.

In the last decade much experimental evidence has accumulated indicating that the ϵ subunit can adopt at least two very different conformations within the ATP synthase complex. In the following paragraphs, a summary of such results is presented.

1.5.1. Up- and down-state of the ϵ subunit.

The high resolution structure of the isolated *E. coli* ϵ , solved by both X-ray crystallography (Uhlin et al., 1997) and NMR spectroscopy (Wilkins et al., 1995; Wilkins & Capaldi, 1998), shows a two domains protein with an N-terminal 10-stranded β -barrel (residues 1–87, indicated as the N-domain) and a C-terminal helix-turn-helix domain (residues 88–138, indicated as the C-domain), (see §1.2.1).

Cross-linking data and crystals analysis have shown that the β barrel domain of ϵ has contacts with the membrane and with the upper part of F_0 (subunit *c*); the structure of this domain remains substantially constant, even though its orientation varies. The helix-loop-helix motif forms an hairpin which comes in contact with the bottom of the $(\alpha\text{-}\beta)_3$ hexamer; this hairpin undergoes drastic structural and positional changes.

Based on this high flexibility of the C-terminus domain, two different conformations of the ϵ subunit have been predicted; both of them have been found in the holoenzyme (Hausrath et al., 2001). By considering the structural changes of the ϵ subunit, Yoshida et al. have proposed in 2003 that the ATP synthase could undergo two different conformational states: up-state and down-state (Tsunoda et al., 2001; Suzuki et al., 2003). According to these authors, in the down conformation the two α -helices of the C-domain fold on themselves and lie next to the N-domain on top of the c_{10} oligomer (panel B in Fig.1.5.1.). In this conformation the ATP hydrolysis would be active and coupled with the proton pumping, while the ATP synthesis would decrease its activity. In the up conformation the helices of the C-domain are extended and partially wrapped around the γ subunit to make contact with $\alpha_3\beta_3$ barrel (panel C in Fig.1.5.1.); in this conformation the ATP hydrolysis coupled with the proton translocation would be inhibited, whereas the ATP synthesis activity would remain unaffected.

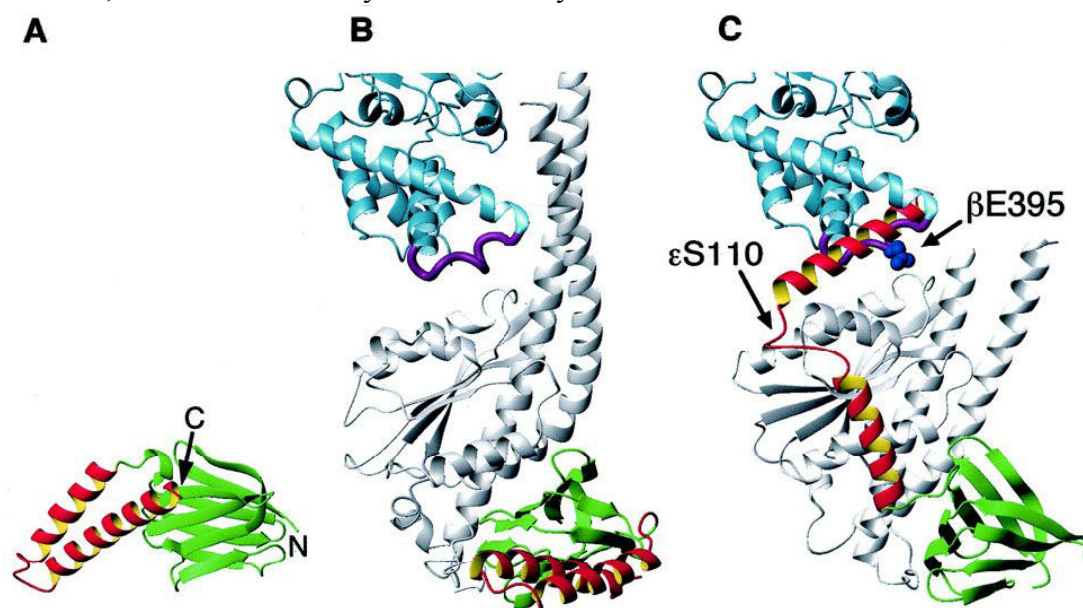


Fig.1.5.1. Conformational changes of the ϵ subunit.

The γ subunit is grey the C-terminus α -helices of the ϵ subunit are red (from Suzuki et al., 2003).

Panel A, structure of the ϵ subunit isolated from the *E. coli* ATP synthase (Uhlin et al., 1997);

Panel B, down conformation of the ϵ subunit from the bovine heart mitochondrial ATP synthase (Gibbon et al., 2000);

Panel C, down conformation of the ϵ subunit from the *E. coli* ATP synthase (Rodgers & Wilce, 2000).

Under normal conditions, it can be speculated that the up conformation is transient, but that it may occur at relatively high frequency under conditions of reduced rate of hydrolysis. It can be hypothesized that the ϵ subunit regulates the efficiency of the hydrolysis reaction but not of the synthesis reaction, since the up conformation strongly inhibits the ATP hydrolysis but it does not affect the ATP synthesis. According to Yoshida, the catalytic model of the ATP synthase, based on the rotational mechanism, could explain this phenomenon. It can be assumed that during the up-state the $\alpha_3\beta_3/\epsilon$ interactions prevent the conformational changes of the β which cause the rotation of the central stalk. These blocking interactions could be quickly removed when the enzyme rotates clockwise, so the ATP synthesis could normally occur. During the anticlockwise rotation, these interactions between the α -helix of the ϵ subunit and the α/β heterodimer would not be released (due to steric or electrostatic constraints) and the ATP hydrolysis

would be blocked. Therefore the ϵ subunit would work like a blocking pawl in a gear wheel (Fig.1.5.2.). This blockage function would enable the ϵ subunit to regulate, to various degrees, the hydrolysis and the synthesis activity.

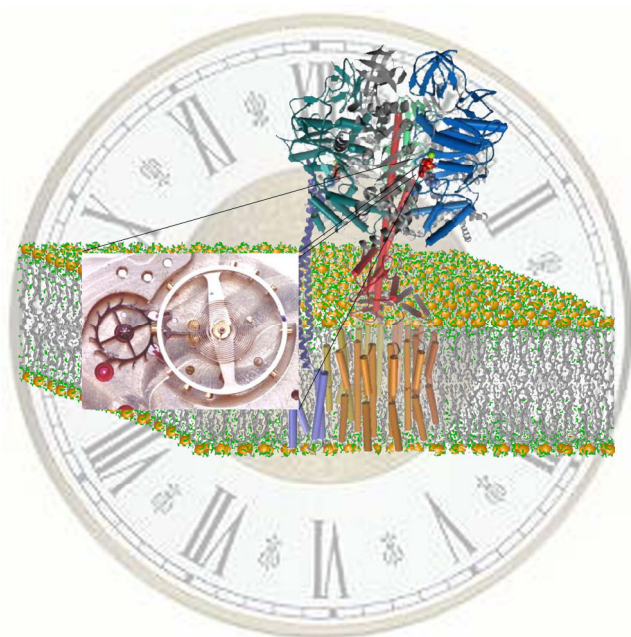


Fig. 1.5.2. A pictorial model suggesting how the ϵ subunit can work like a blocking pawl in a gear wheel (from <http://www.public.asu.edu/~frasch/catchloop.htm>; Greene & Frasch, 2003)

Tsunoda and coworker (2001) have suggested that this regulatory function of the ϵ subunit is ancestral and characteristic of bacterial ATP synthases. In eukaryotic enzymes a more complicated system of functional regulation would exist, and the structural and inhibitory roles of the ϵ subunit would be performed by two different polypeptides, δ and IF_1 . Tsunoda suggests that, in mitochondria, the δ subunit (homologous of the ϵ subunit in *E. coli*) is constantly blocked in a “down” conformation and a specific protein (instead of a conformational change) inhibits the ATP hydrolysis. It has been shown (Suzuki et al., 2003) that the presence of ATP, ADP and of the protonmotive force can influence the switch up/down-state of the enzyme: without any nucleotide, ϵ is in the up-state, ATP induces the transition to the down-state, and ADP counteracts the action of ATP; the proton motive force stabilizes the up-state (right panel in Fig.1.5.3.). In that work Yoshida and co-worker suggest that two factors would determine the conformational switches of ϵ : the ADP/ATP ratio and the protonmotive force. Therefore their model predicts that at high proton motive force and low ATP, ϵ is predominantly in the up-state, and F_0F_1 is geared to the ATP synthesis mode. At low proton motive force and high ATP, ϵ adopts the down-state and F_0F_1 hydrolyzes ATP to

pump out protons, generating a proton motive force with enough magnitude to drive uptake of nutrients and flagella motion.

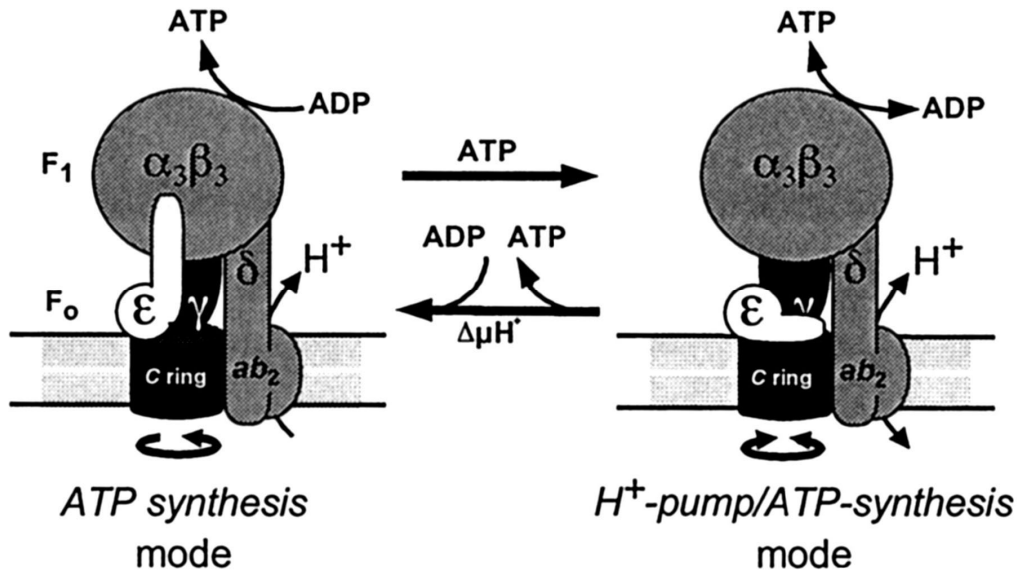


Fig. 1.5.3. Schematic model of the up-state and down-state of the ϵ subunit.

In the up conformation the enzyme synthesizes but does not hydrolyze ATP (right part of the picture); when the ϵ subunit is in down conformation the enzyme both hydrolyzes and synthesizes ATP; (from Suzuki et al., 2003).

1.5.2. Role of the C-terminal helices of the ϵ subunit.

In some bacteria, such as *Chlorobium limicola* (Xie et al., 1993) and *Thermotoga neapolitana* (Iida et al., 2002), the native ϵ subunit lacks the C-terminal helical domain; under these conditions the ϵ subunit is forced to adopt a conformation that is functionally similar to the down-state. These bacteria grow in anaerobic environments and they do not carry out ATP synthesis coupled to oxidative phosphorylation; therefore they use their F_0F_1 as an ATP hydrolysis-driven proton pump to establish a $\Delta\tilde{\mu}_{H^+}$, which energizes several cellular processes, like active transport and motion. Since the up-state of the ϵ subunits inhibits the ATP hydrolysis coupled to proton pumping, this conformation would be a disadvantage for these bacteria; therefore the selective pressure would have acted in the direction of the loss of the C-terminus domain of ϵ , responsible of the up-state (Suzuki et al., 2003). Nevertheless, when ϵ is in down-state, the enzyme can catalyze both ATP synthesis and ATP hydrolysis; indeed mutant *E. coli* strains, carrying ATP synthase lacking the C-terminal domain of ϵ (up-state forbidden), can grow in aerobic condition by oxidative phosphorylation (Kuki et al., 1988). Since the deletion of the C-terminal domain of ϵ is not lethal, it has been suggested (Suzuki et al., 2003) that the up-state in ATP synthases from *E. coli* cells could have an important role under nutrients-shortage or starving conditions of the cells. Indeed Suzuki and co-worker observed that by decreasing the ATP concentration in the growth media, the population of F_0F_1 in the up-state increased, i.e. in the absence of ATP, the hydrolysis reaction was largely inhibited. Indeed each organism needs to regulate the synthesis/hydrolysis balance, according to the physiological needs of the cells and in response of quick changes in the nutrient availability.

1.6. Intrinsic uncoupling.

The term "uncoupling" was first utilized to indicate the effects of the uncoupler dinitrophenol on the oxidative phosphorylation. In the inner membrane of mitochondria, this compound separates the flow of electrons and the pumping of H^+ ions from ATP synthesis, so that the energy from electron transfer cannot be used for ATP synthesis. According to the Mitchell's chemiosmotic theory, the mitochondria establish across their membranes a proton gradient, and the uncouplers dissipate this gradient. Dinitrophenol acts as an extramolecular protonophore, which inhibits ATP synthesis by collapsing the $\Delta\tilde{\mu}_H^+$. From this observation, a number of other uncouplers have been

reported, which act as ionophores and collapse the transmembrane $\Delta\tilde{\mu}_H^+$. Besides this kind of uncoupling, which we can call "extrinsic", a different kind of uncoupling has been characterized, consisting in a slip between the chemical turnover and the transport activity within the same protein complex, and which we can call "intrinsic".

An intrinsic uncoupling has been reported for other chemiosmotic enzymes such as cytochrome oxidase (reviewed in Kadenbach, 2003), V-ATPases (Moriyama & Nelson, 1988; Davies et al., 1994; Müller et al., 1999), and Ca-ATPases (reviewed in Berman, 2001), in which its possible regulatory role has been discussed. In general the uncoupling affects the enzymatic functional state and can determine physiological effects, which can influence the cellular metabolism and/or can be associated to pathological conditions (Berman et al., 2001).

1.6.1. Intrinsic uncoupling in the complexes of the mitochondrial oxidative phosphorylation.

The stoichiometric efficiency of the oxidative phosphorylation is represented by the ratio P/O, i.e. by the amount of P_i incorporated into ATP per reduced O_2 . An uncoupling of the oxidative phosphorylation involves any process characterized by a decrease of the P/O ratio due to a decrease of the protonmotiveforce. Such an event determines a waste of redox energy and a correlated increase of thermogenesis. Different agents can collapse the transmembrane proton gradient and decrease the P/O ratio: classical

uncouplers (fatty acid), uncoupler proteins (es UCP1), carriers which decrease the $\Delta\tilde{\mu}_H^+$ by actively transporting ions across the membrane. According to Kadenbach (2003), these agents collapse the proton gradient and act as "extrinsic uncouplers"; nevertheless also a reduction of the efficiency of one of the proton pumps present in the respiratory chain can determine a decrease of the P/O ratio (e.g. a decrease of the $H^+_{TRASP.}/e^-_{TRASP.}$ in the respiratory chain, or a reduction of the stoichiometry $H^+_{TRANSL.}/ATP_{HYDR}$ in the ATP synthase). This phenomenon can be defined as "intrinsic uncoupling" or "slip of the proton pump". Only complex IV and complex V could undergo intrinsic uncoupling (Kadenbach, 2003). In particular Kadenbach emphasizes that the slip of the cytochrome oxidase can influence the interplay of the rate of respiration and the efficiency of ATP synthesis, two points of possible regulatory control.

Indeed both the proton leak (unspecific proton permeability of membranes at high Δp) and the intrinsic uncoupling (decreased degree of coupling between electron transport and proton translocation) induce a degree of variability in the ATP synthesis efficiency, since they affect the degree of coupling between the protonmotive force and the rate of respiration. It is possible that the state of intrinsic uncoupling in complex IV could be due to a rearrangement of the proton exit pathway within the enzyme.

According to Kadenbach, several factors can determine an intrinsic uncoupling; noteworthy for their functional implications are the “slip by high proton motive force” and the “tissue-specific slip”.

- **Slip by high protonmotive force:**
by increasing the membrane potential ($\Delta\psi_m$), the cytochrome oxidase has been shown to undergo a progressive state of intrinsic uncoupling and a decrease of its H^+/e^- stoichiometry. The slip of the enzyme, in the presence of high $\Delta\psi_m$, could have the physiological role of preventing or slowing down the production of ROS (oxygen free radicals), enhanced by the high membrane potential. Such a safety mechanism would preserve the cellular integrity during conditions of stress, when the presence of a high $\Delta\psi_m$ can promote the production of ROS, harmful for the organism.
- **Tissue-specific slip:**
In heart and skeletal muscle, at increasing ATP/ADP ratios, it has been observed that the cytochrome oxidase undergo slippage, and that the ensuing decrease in the H^+/e^- ratio promotes thermogenesis. This phenomenon is particularly evident at rest (or during sleep) when no heat is produced by the work of the muscles, and the intramitochondrial ATP/ADP ratio is expected to rise. Moreover also in non-skeletal muscle, palmitate induces slip of the cytochrome oxidase and the decreased H^+/e^- ratio stimulates thermogenesis.

Finally, according to Kadenback (2003) it has not been demonstrated yet whether uncoupling of the ATP synthase does occur in vivo and if it is involved in regulatory phenomena.

1.6.2. Intrinsic uncoupling elicited by lowering the [ADP] and [Pi] concentrations in the ATP synthase from *Rb. capsulatus*.

Melandri and coworkers have recently shown that the efficiency of proton transport in the ATP synthase of the photosynthetic bacterium *Rhodobacter capsulatus* can be decreased during physiological ATP hydrolysis, under specific conditions (See Fig.1.7.2)(Turina et al., 2004). These studies showed that by increasing the concentration of P_i , the proton pumping is increased. Nevertheless, experiments of ATP hydrolysis, carried out under the same experimental conditions, showed that by increasing [Pi], the rate of hydrolysis was constant. These data, taken together, clearly indicated that in the presence of low P_i concentration the enzyme was uncoupled. Similar results were obtained in the presence of increasing concentrations of ADP. This work represented the first evidence of the existence of an intrinsic uncoupling in a bacterial ATP synthase.

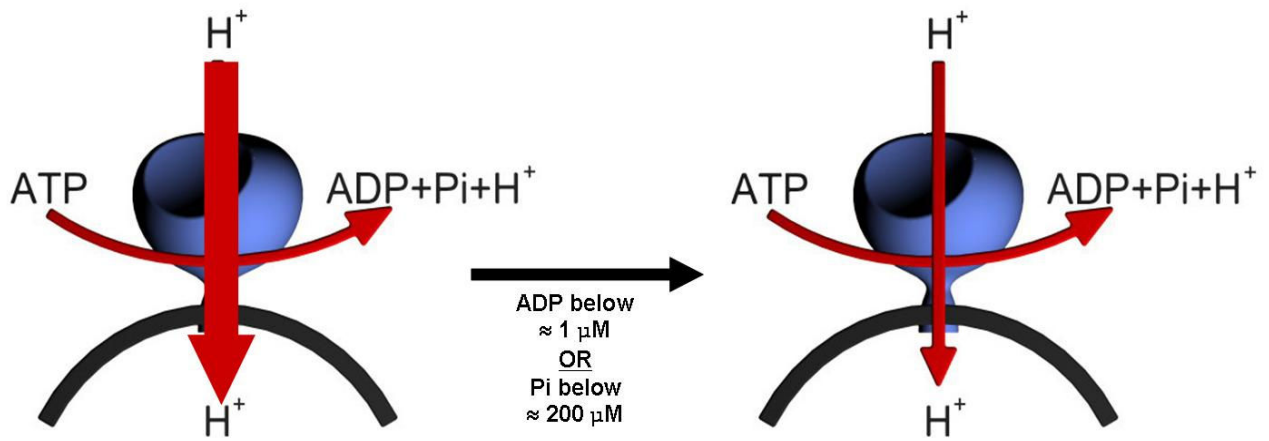


Fig.1.7.1. Schematic model to explain the phenomenon of intrinsic uncoupling in the ATP synthase

1.7. Aim of the present work

The aim of the present work has been to show the occurrence of an intrinsic uncoupling in the ATP synthases of *E. coli*, in order to reinforce the hypothesis that this phenomenon occurs in all Prokaryotes, and to clarify how this phenomenon can be regulated. This task was first tackled in native membranes, isolated from *E. coli*, and subsequently in isolated and reconstituted *E. coli* ATP synthase, in order to rule out artefactual interferences from other enzymes. Finally we decided to explore the role of a possible structural candidate involved in this phenomenon. As such possible candidate we have focused our attention on the α -helical C-terminal domain of the ϵ subunit, generating a truncated mutant lacking this domain.

Chapter 2.

MATERIALS AND METHODS

2.1. *E. coli* membrane preparation

During the membranes preparation the cells and the buffers were kept on ice. The membranes were prepared according two different methods.

2.1.1. *E. coli* membrane preparation according to Mosher et al., 1985

Cells from the XL1Blue *E. coli* strain carrying the kanamycin resistance on the plasmid pNK1 (Stratagene) were grown on LB* media supplemented with 25mg/l kanamycin, and harvested at a late exponential phase. Membranes were isolated from cells essentially as described in Mosher et al., 1985. Cells were resuspended in 5 ml/g wet weight of a BufferA* and disrupted at 138 Mpa (20,000 p.s.i.) with a French-Press, (during the breaking the polarity of the membranes gets inverted, with the cytoplasmic F₁ pointed toward the external medium). Unbroken cells were removed by centrifugation at 16,000 rpm and the remaining supernatant was recentrifuged in a Beckman type 50.2 Ti rotor at 40,000 rpm for 90 min. The pellet was resuspended in a small volume of the same buffer, rapidly frozen as 50 µl aliquots in liquid nitrogen, and stored at -80 °C. Total protein concentration was measured by the Bradford method (§2.10.1) and ranged between 40 and 55mg/ml.

*LB: 10g/l tryptone, 5g/l yeast extract, 10g/l NaCl

*BufferA: 10 mM Tricine/NaOH pH 7.5, 5 mM MgCl₂, 10% glycerol, 6 mM paminobenzamide

2.1.2. *E. coli* membranes preparation according to Elliot Hertzberg & Peter Hinkle (1974)

This procedure is essentially similar to the method of Elliot Hertzberg & Peter Hinkle (1974) except that these authors grew cells on a defined medium with glycerol as the carbon/energy source.

Cells from the DK8 *E. coli* strain carrying the ampicillin resistance on the plasmid pDC44 or pDC45 and the streptomycin resistance on the plasmid pEXT21 or its derivatives, were grown on LB* media supplemented with sodium phosphate (pH 7.0) to a final concentration of 10 mM and with 40mg/l ampicillin and 24mg/l streptomycin. Cells were harvested when A₆₀₀ was about 3.0 and resuspended in 25ml of BufferA*, centrifuged at 10,000 rpm for 10min and resuspended in a volume of BufferB* equal to 10 times the value in grams of the original packed wet weight of the pellet. PMSF to a final concentration of 1mM was added to the solution. Cells were disrupted in French-Press at 138 Mpa (20,000 p.s.i.). Unbroken cells were removed by centrifugation at 10,000 rpm and the remaining supernatant was recentrifuged in a Beckman type 45 Ti rotor at 38,000 rpm for 90 min. Pellet was washed twice in Buffer C*. After the second centrifugation step, the pellet was resuspended in a small volume of the same buffer, rapidly frozen as 50 µl aliquots in liquid nitrogen, and stored at -80 °C.

Total protein concentration was measured by the Lowry method (§2.10.2) and ranged between 50 and 60 mg/ml.

*LB: 10g/l tryptone, 5g/l yeast extract, 10g/l NaCl

*BufferA: 50mM Sodium Phosphate (pH 7.0), 5mM MgCl₂.

*BufferB: 50mM Sodium Phosphate (pH 7.0), 5mM MgCl₂, 10% Glycerol.

*BufferC: 10mM MOPS NaOH (pH 7.5), 250mM Sucrose, 5mM MgCl₂, 10% methanol, NaOH to pH 7.5.

2.2. ATP hydrolysis

The ATP hydrolysis methods described below were carried out under the same conditions both on the membranes and on the proteoliposomes samples.

2.2.1. Phenol Red Assay

All reactions were carried out in sample holders thermostated at 26 °C. In the absence of pyruvate kinase (PK), ATP hydrolysis was measured by detecting the scalar protons released upon ATP hydrolysis with the colorimetric pH indicator Phenol Red (Fig.2.2.1.). Membranes were suspended in BufferA*, and 1 μM valinomycin was added to minimize Δφ. Phenol Red was added to 100 μM.

Prior to each measurement, the sample pH was adjusted to 8.0 with NaOH. The pH changes of the suspension were followed as a function of time by the absorbance changes at 625–587 nm, and were calibrated after about 200 s of reaction by 3 sequential addition of 15 μM HCl. The overall pH

change of the suspension at the end of the measurements was never higher than 0.3 units. The calibration signals showed that the addition of 3mMPi in the poorly buffered assay medium caused an increase of the buffering power of 30%. This change was corrected for in all calculations. The changes of proton concentration were transformed to changes of ATP concentration as described in Nishimura et al., 1962. At pH 8.0 an H⁺/ATP ratio of 0.94 was used. When ATP hydrolysis was measured in parallel samples with the malachite green assay (Lanzetta et al., 1979), the same rates were obtained within experimental error, indicating absence of significant artefacts in either assay methods.

*BufferA: 1mM Tricine, 50 mM KCl, 2.0 mM MgCl₂, NaOH to pH 8.0.

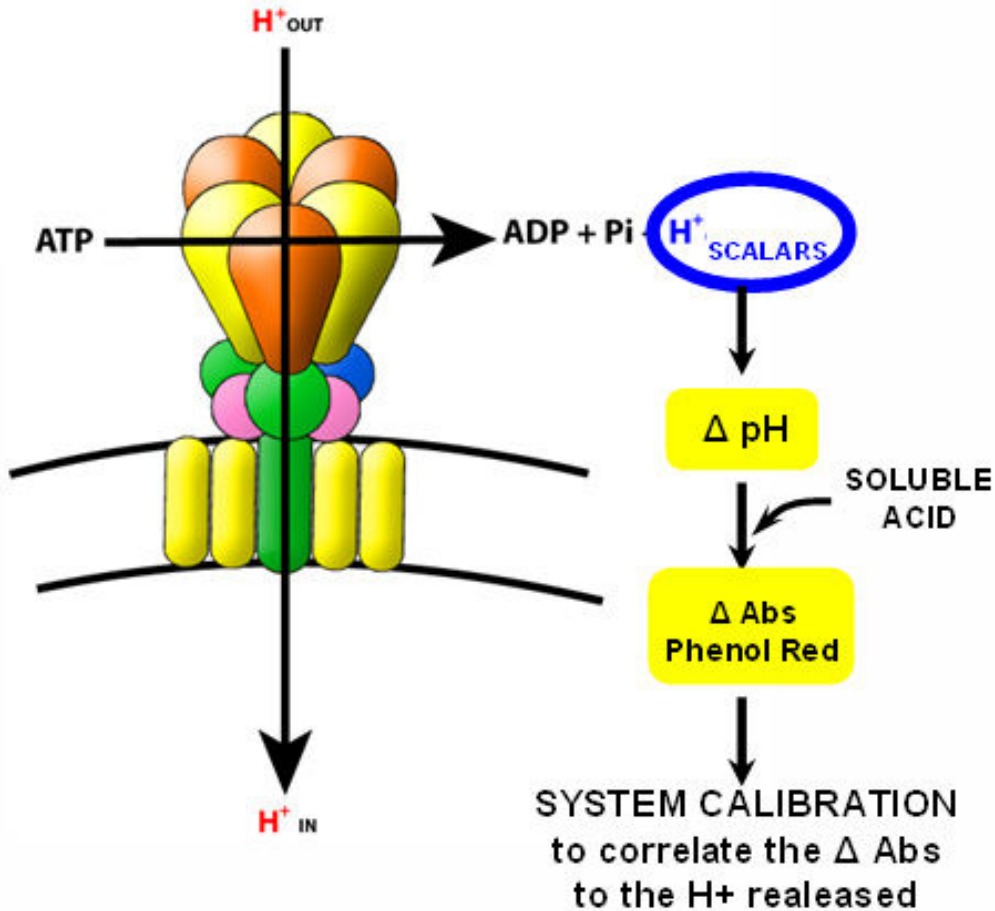


Fig.2.2.1. Simplified model explanation of the Phenol Red assay.

2.2.2. Piruvate Kinase-ADP trap Assay

In several experiments it was of interest to modulate the ADP concentration in the system. An ADP-trap coupled to the NADH oxidation, based on the enzymes pyruvate kinase (PK) and lactic dehydrogenase (LDH), was used to phosphorylate the endogenous ADP.

As shown in (Fig.2.2.2.), PK uses phospho(enol)pyruvic acid (PEP) to phosphorylate the ADP produced during the hydrolysis reaction, with formation of ATP and pyruvate. Then the LDH reduces pyruvate to lactate with oxidation of a molecule of NADH. Reduced NADH absorbs at 340nm, so the rate of disappearance of this substrate is proportional to the Absorbance decrease measured by a spectrophotometer.

This enzymatic assay serves two purposes at the same time:

- 1) it modulates the ADP concentration in the system;
- 2) it measures the ATP hydrolysis rate, since hydrolyzed ATP and oxidized NADH are in the stoichiometric ratio 1:1.

The assay was conducted in the presence of potassium cyanide (KCN), an inhibitor of the cytochrome oxidase, to exclude that NADH was oxidised by the enzymes of the respiratory chain.

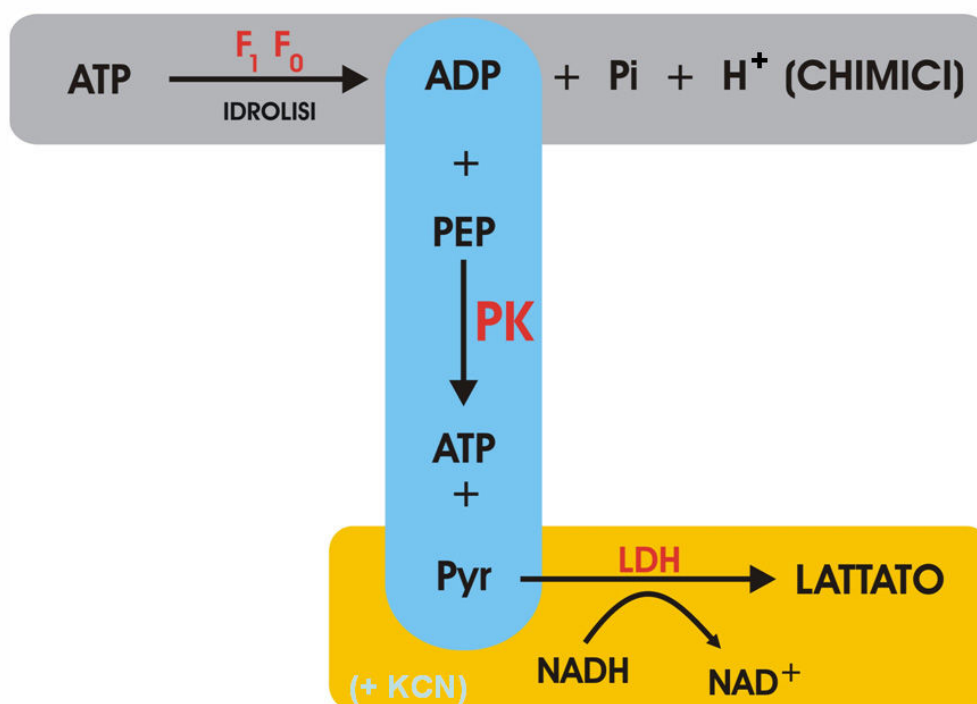


Fig.2.2.2. Reactions coupled to the activity of the enzyme Piruvate Kinase.

For measurements in the presence of PK (ADP trap), the reaction temperature and ATP hydrolysis mixtures were the same as the ones used in the Phenol Red assay, including the low buffer concentration. However for these measurements 2 mM PEP, PK to variable amounts, 25 U/ml of LDH, 0.15 mM NADH and 2 mM KCN were present and no Phenol Red was added (in the proteoliposomes samples the KCN was omitted). The PK was supplied from Sigma (P- 9136) as ion-free lyophilized powder. The ADP trap was thus coupled to NADH oxidation, and the absorbance changes at 340 nm were followed as a function of time. Again, control samples were set up in which ATP hydrolysis was measured with the malachite green assay in the presence of the ATP regenerating system, and the same rates were obtained within experimental error. In the absence of ATP, no significant NADH oxidation could be detected, and in control ACMA assays it was confirmed that 2 mM KCN were enough to completely inhibit the NADH-driven ACMA quenching, indicating a sufficient inhibition of the *E. coli* respiratory chain.

The hydrolysis rate in the presence of the ADP-trap is linear. The changes of absorbance were transformed to changes of ATP concentration on the basis of an extinction coefficient for NADH of $6.22 \text{ mM}^{-1} \cdot \text{cm}^{-1}$.

2.2.3. Malachite Green Assay

The malachite green assay is a colorimetric assay for the determination of nanomole amounts of inorganic phosphate. This procedure is a modification of the Hess & Derr methods (Hess & Derr, 1975); by introducing citrate into the mixture, the colour reaction is rendered more stable and insensitive to nascent phosphate (Lanzetta et al, 1979).

Solutions:

0.045% Malachite green (MG)

4.2% ammonium molybdate in 4N HCL (AM)

2% Tween (Tw)

34% Sodium citrate• 2H₂O (w/v)

10mM NaH₂PO₄; appropriate dilutions were made from this stock and used as standard.

The colour reagent was prepared from the above solutions as follows:

- 1) 3:1 mixture of MG and AM solutions; mixed for 30 min and then passed through Whatman N°5 filter paper (MG/AM)
- 2) 100µl of Tw added to 5 ml of MG/AM solution (MG/AM/Tw).

To 50µl of sample, 800µl of the MG/AM/Tw solution is added and mixed. After 1min, 100µl of the citrate solution is added and mixed. The full green colour development is completed after 30min and is stable for at least 4h. This solution can be read at 660nm in the spectrophotometer.

ATP hydrolysis measurements. The detection of inorganic phosphate, released upon ATP hydrolysis in our samples, is a measure of the ATP hydrolysis rate.

After the addition of ATP to the sample solution the hydrolysis reaction was stopped at different times by adding 5% Trichloroacetic acid. The released P_i, measured with the malachite green assay, was plotted as a function of the hydrolysis reaction time. Assays were always performed in duplicate.

The amount of released phosphate was subtracted from the amount of endogenous P_i. A calibration curve was obtained by carrying out the assay in the presence of standard amounts of P_i.

2.2.3.1. Measurement of the inorganic phosphate in PhosphoEnolPyruvate solution.

The P_i content in the PEP was measured with the malachite green assay (Lanzetta et al, 1979). It was found to be 10µM and was neglected in the calculations

2.3. Dicyclohexylcarbodiimide (DCCD) assay

DCCD inhibition was obtained by incubating the membranes for at least 30 min in the presence of 250 µM inhibitor; under such conditions the activity measured in the presence of 0.5% LDAO, lauryldimethylamine oxide (LDAO) was not significantly affected, indicating that the observed inhibition did not involve the F₁ sector.

2.4. Measurement of pyruvate kinase activity

The activity of PK under the experimental conditions of the present work was measured at 26 °C. The buffer in the absence of any membranes was supplemented with 2 mM PEP, 2 mM ADP, 0.15 mM NADH, 25 U/ml LDH. The reaction was started in the spectrophotometer by addition of PK (corresponding to the theoretical value of 0.03 U/ml) and the coupled NADH oxidation was recorded at 340 nm.

2.5. 9-Amino-6-chloro-2-methoxyacridine (ACMA) assay

ACMA (Fig.2.5.1.) was purchased from Molecular Probes, Inc. Eugene, Oregon, USA. The ACMA assays were carried out under experimental conditions as close as possible to those used for ATP hydrolysis measurements. The ACMA fluorescence emission was recorded as a function of time (RC=0.25 s) in a Jasco FP 500 spectrofluorometer (wavelength 412 and 482 nm for excitation and emission respectively) at 26 °C. For measurements in the absence of PK, the assay mixture was the same as used for Phenol Red assay, including the low buffer capacity, except that Phenol Red was omitted and 1.5 μ M ACMA was added. When an ADP trap was present, the assay mixture was the same as used for measurements of ATP hydrolysis in the presence of PK, except that LDH, NADH and KCN were omitted. In control measurements it was shown that pyruvate up to 100 μ M did not affect the quenching signals.

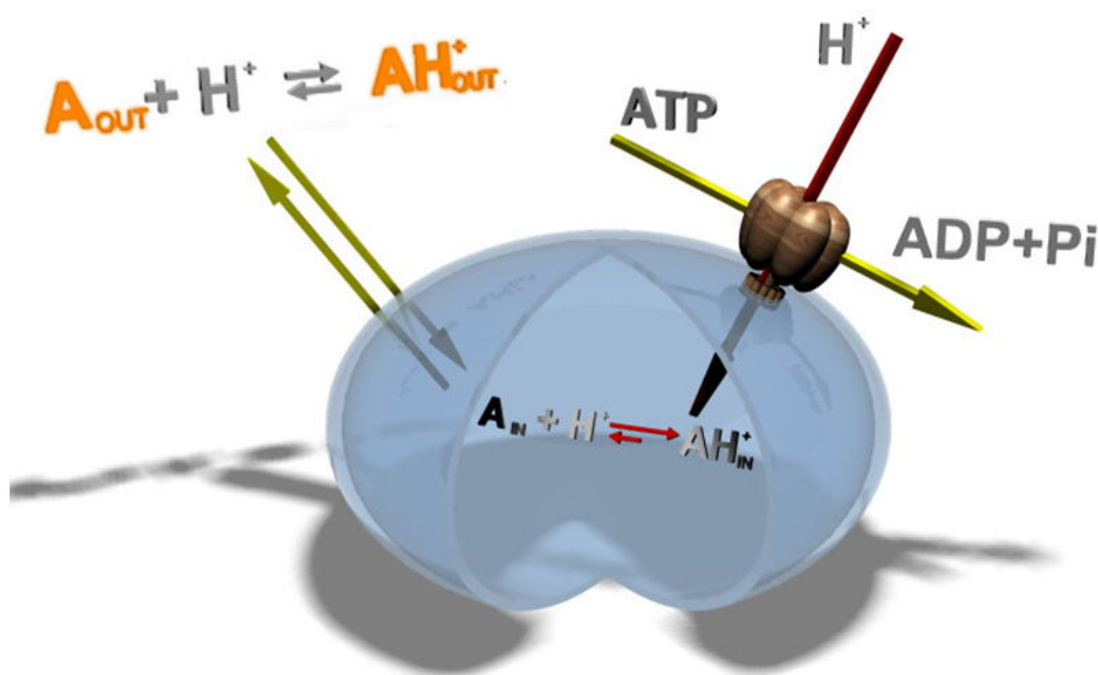


Fig.2.5.1. Simplified model explanation of the ACMA assay.

2.6. Plasmid construction and mutagenesis

Recombinant DNA procedure were carried out by standards methods, either as described by Sambrook et al. (1989) or as recommended by suppliers of enzymes used in the procedures.

2.6.1. Development of a low copy number expression vector carrying extra copy of mutated *uncC*

Plasmid pSD15 containing the 1182-bp PstI fragment of the *unc* operon cloned into the PstI site of pUC8 (Vieira & Messing, 1982) and plasmid pDC47 containing an AvrII site just after the stop codon of the ϵ gene (Cipriano & Dunn, 2006) were the starting point for the construction of the insert cloned into the low copy expression vector pEXT21.

The 335-bp HindIII/NcoI fragment of pDC47 was moved into pSD15 which was cut with the same enzymes to produce pMDA1, a plasmid with the AvrII site after the stop codon of the ϵ gene of pSD15. pMDA1 was cut with PstI to obtain a 1179-bp fragment carrying the *uncC* gene and the AvrII site; this fragment was cloned into the PstI site of pEXT21 to produce pMDA2.

The PstI site downstream *uncC* was removed to obtain pMDA5, a plasmid containing the WT ϵ gene flanked by two unique site PstI and AvrII. The small PstI/AvrII restriction fragment from pDC45 was cloned into pMDA5 to obtain pMDA7, a plasmid containing the $\epsilon_{88\text{-stop}}$ gene.

pExt21, pMDA5 and pMDA7 were transformed into DK8 *E. coli* strains already containing pDC44 (WT) and pDC45 ($\epsilon_{88\text{-stop}}$ truncation) to produce 4 new *E. coli* strains.

2.6.2. Transformation of *E. coli* cell with plasmids

The *unc*-less DK8 *E. coli* strains was transformed with different combinations of the following plasmids:

- pDC44, an ampicillin resistant plasmid that contains all genes encoding ATP synthase with wild-type ϵ (Cipriano & Dunn, 2006);
- pDC45, an ampicillin resistant plasmid that contains all genes encoding ATP synthase with the mutation $\epsilon_{88\text{-stop}}$ (Cipriano & Dunn, 2006);
- pEXT21, a low copy number streptomycin resistant expression vector, which contains an expression cassette comprised of the *lacI^q* gene, the *tac* promoter, a multiple cloning site and a downstream transcriptional terminator (Dykxhoorn et al., 1996);
- pMDA5, a derivative of pEXT21 in which the *uncC* gene with wild-type ϵ was cloned;
- pMDA7, a derivative of pEXT21 in which the mutated *uncC* gene with $\epsilon_{88\text{-stop}}$ was cloned

2.6.3. Transformation of *E. coli* competent cells.

The transformation of *E. coli* competent cells was carried out as described in the following protocol:

- a) The DNA mixture is added to competent cells.
- b) The sample are incubated on ice for 30 min.
- c) Cells are heat shocked in a 42°C water bath for 90s, then returned immediately on ice.
- d) Then the samples are incubated in 0.8ml of culture medium at 37°C for 1h.
- e) Sample cells, positive and negative controls are plated on selective media and incubated overnight at 37°C.

2.6.4. Transformation of strains with plasmids

The transformation of strain with plasmids was carried out as described in the following protocol:

- a) the recipient strain is grown in LB at 37°C to an A_{600} of 0.5.
- b) the culture is placed on ice for 10min and then centrifuged for 5min at 570 rpm in a JA-20 rotor.
- c) the pellet is resuspended in half of the original volume of ice-cold Buffer1* and the solution is dispensed in 0.2ml aliquots.
- d) DNA (up to 40ng) is added to the aliquots. The samples are stored on ice for 40min.

- e) The samples are transferred to a 42°C water bath for 2min, then returned immediately on ice.
- f) Then the samples are incubated in 1ml of LB at 37°C for 1h.
- g) Sample cells, positive and negative controls are plated on selective media and incubated overnight at 37°C.

*Buffer1: 50mM CaCl₂, 10mM Tris-HCl, pH 8.0.

2.6.5. Induction and analysis of protein from plasmid.

This procedure is good for detecting expression of several vectors that have either *tac* or *lac* promoters.

- a) 5ml of LB are inoculated with a colony and are grown at 37 °C.
- b) When the cultures become slightly turbid, 1 ml of them is transferred into a tube containing IPTG 1mM. The tubes are grown at 37 °C for 3-4 hours. before extracting the protein.
- c) Samples are spun down, the pellets are re-suspended in 1X SDS sample buffer and placed in a boiling water bath for 5 min.
- d) Samples are analyzed by running 10µl per well on SDS gel and staining with Coomassie blue.

2.7. Purification of *E. coli* ATP synthase and its reconstitution into liposomes

2.7.1. *E. coli* and growth conditions

Cells from the XL1Blue *E. coli* strain carrying the kanamycin resistance on the plasmid pNK1 (Stratagene) were grown on LB media, and harvested at a late exponential phase.

2.7.2. Preparation of membrane vesicles and isolation of ATP synthase

Washing of the cells. Fifteen grams of bacteria (wet weight) in 400ml of BufferA* and centrifuged at 10.000 rpm. Pellet was resuspended in 200ml BufferB*; 10 µg/ml of DNase, 100µM PMSF and 6mM p-ABA were added to the solution.

Cells were passed through a French press (pressure set at 1200psi). The mixture was centrifuged at 13.000 rpm for 10 min. The supernatant fraction was removed and centrifuged at 43.000 rpm for 90 min. The pellet was suspended in 15ml of BufferC*. The protein concentration was measured by the Bradford method (§2.10.1.) and was brought to 10mg/ml by adding an appropriate volume of BufferC*. The mixture was incubated at 0° for 10min in the presence of 2% Octyl glucoside.

The supernatant obtained by centrifugation at 34.000rpm for 60min was applied to a sucrose gradient (20-45%) containing BufferD* (total volume 12 ml, 6 tubes), and centrifuged at 35.000rpm with a Beckman type 50.2 Ti rotor for 14 h. The ATPase activity was recovered in the middle of the gradient, and fractions 5-9 (from the bottom) were combined and stored at -80 °C.

The total protein concentration of every fraction was measured by the Bradford (§2.10.1.) method. Molecular mass of 530 kDa for EF₀F₁ was used.

The measurement of ATPase activity of every fraction was carried out by an ATP regenerating system assay. To start the hydrolysis reaction, 20 μ l of fraction were added to 1ml of BufferE* containing the standard ATPase reaction mixture. NADH oxidation and its absorbance changes at 340 nm were followed as a function of time in a Jascow V-550 spectrophotometer. The rate of hydrolysis was expressed as nM ATP per sec.

2.7.3. Preparation of liposomes. Liposomes from phosphatidylcholine and phosphatidic acid were prepared by dialysis. 18 g/l phosphatidylcholine and phosphatidic acid in a mass ratio 19:1 were suspended in the sonication BufferF* . The lipid detergent solution was sonicated in an ice bath for 3*30 s (Branson sonifier at 20 kHz and 150 W) and dialyzed against the 4000-fold volume of dialysis BufferG* at 30°C overnight using a Diachema membrane type 10.14 MWC 5000. The lipid concentration of the liposomes after dialysis was approximately 16 g/l.

2.7.4. Reconstitution of EF_0F_1 into liposomes. EF_0F_1 was reconstituted into preformed liposomes according to the method described by Richard et al. (1990). 100 μ l liposomes (16 mg/ml lipid; no corrections were included for losses during the dialysis process) were mixed with 5 μ l 100mM $MgCl_2$ and 10 μ l 1M KCl. 27 μ g EF_0F_1 was diluted with reconstitution BufferD* to yield a final volume of 60 μ l to which 13 μ l Triton X-100 (10%) was added. Subsequently, the enzyme/detergent solution and liposome solution were mixed and incubated for 60 min. To remove the detergent, 64mg Bio- Beads SM-2 (extensively washed as described in Holloway, 1973) were added (Fig.2.7.1.). The solution was incubated at room temperature for 60 min under constant stirring. The resulting EF_0F_1 , proteoliposomes with a final lipid concentration of 8mg/ml and a final enzyme concentration of approximately 850nM (assuming a 100% purity of the EF_0F_1) were stored at room temperature for up to three days without any loss of ATP synthesis activity.

*BufferA: 50mM Tris-HCl, pH 8.0

*BufferB: 50mM Tris-HCl, pH 8.0, 140mM KCl, 1mM DTT, 10% Glycerin.

*BufferC: 40mM MOPS, 2mM $MgCl_2$, 5mM Thioglycerin.

*BufferD: 20mM MOPS, 0.5mM $MgCl_2$, 5mM Thioglycerin, 0.6% Octyl glucoside.

*BufferE: 20mM Tricine, 2mM $MgCl_2$, 10mM KCl, 1mM ATP, 2mM PEP, 0.15mM NADH, 5mM KCN, 25U/ml LDH, 25 U/ml PK, NaOH to pH 7.5.

*Sonication Buffer F containing 7.2 g/l cholic acid, 3.6 g/l sodium desoxycholate, 500 μ M dithiothreitol, 100 μ M ethylenediaminetetraacetic acid and 10 mM Tricine/NaOH (pH 8).

*Dialysis Buffer G (2.5 mM $MgCl_2$, 250 μ M DTT, 200 μ M EDTA and 10mM Tricine/ NaOH, pH8).

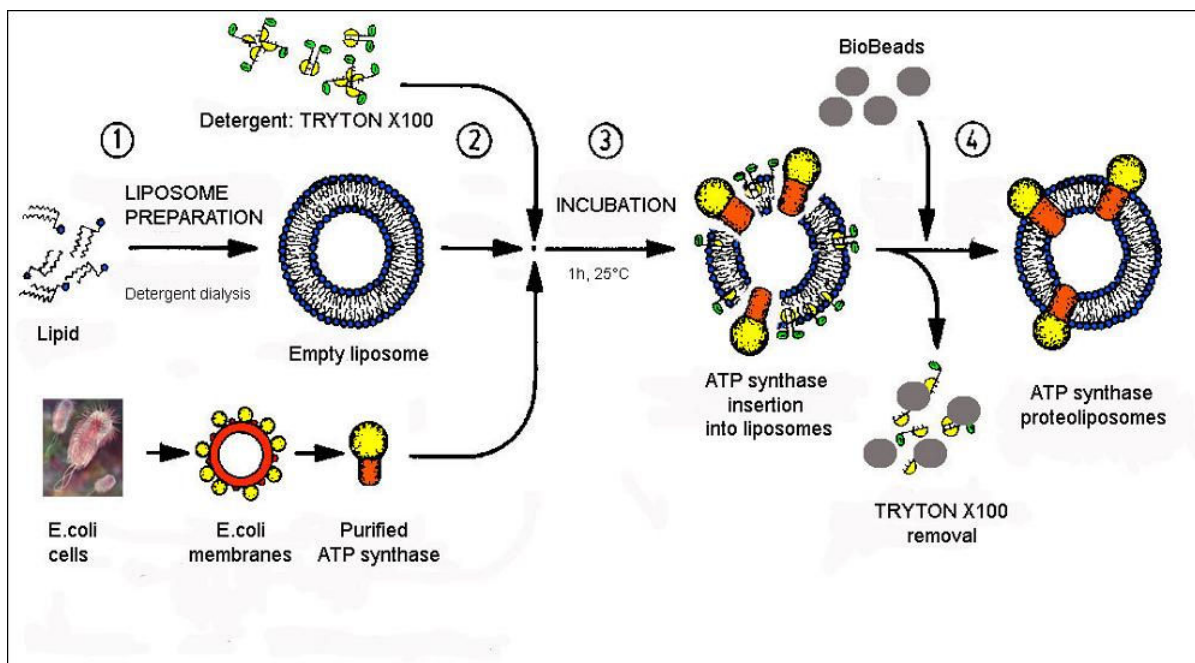


Fig.2.7.1. Isolated ATP synthase reconstitution into preformed liposomes.

Adapted from http://www.mpsd.de/MPSD_MPro.html (T. Nawroth).

2.7.5. SDS polyacrylamide gel electrophoresis In order to separate the ATP synthase subunits SDS-PAGE according to Schägger *et al.* (1987) has been used, at 15% or 20% of acrylamide concentration. In the following the composition of the separating and stacking tricine gels are summarized (Tab.2.7.1.). All the solution were prepared using bidistilled (BD) water. Ammonium Persulfate (APS) was freshly prepared.

Tab.2.7.1. Composition of the separating and stacking tricine gels.

15% Resolving gel, 10 ml	20% Resolving gel, 10 ml	4% Stacking gel, 5 mL
Gel Buffer* 3.33 mL 30% Acrylamide, 30:1 5 ml BD H ₂ O 1.6 ml 25% APS 30 µl Temed 10 µl	Gel Buffer* 3.33 ml 30% Acrylamide, 30:1 6.66 ml BD H ₂ O --- 25% APS 30 µl Temed 10 µl	Gel Buffer* 1.25 ml 30% Acrylamide 0.8 ml BD H ₂ O 2.95 ml 25% APS 30 µl Temed 10 µl

*Gel Buffer: 3M Tris-HCl, pH 8.45, 0.3% w/v SDS

*Loading Buffer: 8% w/v SDS, 24% v/v Glycerol, 100 mM Tris -HCl, 8% v/v β-mercaptoethanol, 0.02% w/v Serva Blue G R250

*Anode Buffer: 0.2 M Tris -HCl, pH 8.9

*Cathode Buffer: 0.1 M Tris-HCl, 0.1 M Tricine, pH 8.25, 0.1% w/v SDS.

Electrophoresis conditions: 15 min 30 V constant to concentrate the sample at the edge of the running gel, then 110 V constant at least for 2 h, at room temperature.

The best resolution of the bands is achieved by loading the sample at a concentration of 1.6 µM. The EF₀F₁ subunits bands were fixed and stained by Coomassie Brilliant Blue.

The Marker used for the assay was M4038 from Sigma. It covers the range of molecular weights common to most proteins or their subunits and it is formulated to yield a

distribution of well-defined bands of approximately equal intensity after electrophoresis and Coomassie blue staining. M4038 yields 13 protein bands with Coomassie Blue staining.

A densitometric analysis of the protein band on the gel was performed using a the densitometric function of the Fluor S-Max Biorad. By comparison of the bands from the EF₀F₁ samples and the ones of the marker it was possible to recognize on the gel all the subunits of the enzyme. Purity of subunits was estimated by using the software Quantity One to measure the volume of every band of a sample strip on the gel. The purity was expressed as the percentage of the ratio between the total volume of EF₀F₁ bands and the total volume of all the bands present on the strip.

2.8. Measurement of ATP synthesis

The rate of ATP synthesis catalyzed by EF₀F₁ was measured at 25°C as described in Schmidt and Graber, 1985. Proteoliposomes were energized by an acid/base transition and an additional K⁺/valinomycin diffusion potential (Fig.2.9.1.B.) The ATP concentration was monitored continuously with luciferin/luciferase (Merlin) in a luminometer (LKB 1250). In order to generate $\Delta\tilde{\mu}_H^+$, the Buffers LI and LII reported in Tab.2.8.1. were used in the acid-base transition. ATP synthesis and detection of ATP with the luciferin/luciferase assay were carried out simultaneously as follows: 890µl Buffer LII was mixed with 10µl luciferin/luciferase reagent, placed in the luminometer and the baseline was recorded. 30µl of the diluted proteoliposomes (113nM EF₀F₁) were mixed with 90µl Buffer LI and incubated at 25°C for 1-6 min. ATP synthesis was initiated by injection of 100µl of this solution (final pH 5.0) with a Hamilton syringe directly into the cuvette containing LII and luciferin/luciferase (final pH 8.5). The increase in ATP concentration was followed by the increase luminescence. At the end of the ATP synthesis reaction, the luminol signal was calibrated by addition of 10µl of an ATP solution of known concentration (10 µM).

Tab. 2.8.1. Composition of Buffers LI and LII

Acidic medium- BufferLI	Basic medium-BufferLII
20mM succinate, 0.5mM KOH, 2mM MgCl ₂ , 5mM NaH ₂ PO ₄ , 20µM valinomycin (freshly added); titrated to pH 4.5 with NaOH.	200mM tricine, 160mM KOH, 2mM MgCl ₂ , 5mM NaH ₂ PO ₄ , 0.1 mM ADP; titrated to pH 8.8 with NaOH.

2.9 ACMA calibration

ACMA was purchased from Molecular Probes. Inc. Eugene, Oregon, USA. It was dissolved in ethanol at a final concentration of 2mM.

Using the procedure described in Casadio & Melandri (1985), ΔpH's were artificially imposed on proteoliposomes with an acid-to-base transition (Fig.2.9.1.B.).

Proteoliposomes were equilibrated for 30 min at initially imposed acidic pH values ranging from 4.2 to 8.00. The quenching of ACMA fluorescence was recorded at 25 °C upon addition of a suitable volume of 1M NaOH directly in the spectrofluorimetric cuvette, so that the outside pH was brought rapidly (within about 0.5s) to a constant

value equal to 8.00. This procedure induced a transient transmembrane pH difference (varying from 3.8 to 0 pH units) that relaxed within 150 s due to the proton passive flow occurring in opposite directions. A decrease of fluorescence intensity, expressed as percentage quenching of fluorescence, was observable during the period of persistence of ΔpH . Under conditions in which a rapid re-equilibration of the transmembrane pH difference was induced, i.e. upon the addition of 1 μM Nigericine prior to NaOH, no quenching of fluorescence after the transition to pH = 8.00 was detected. The initial and final pH of the suspensions were determined using a Radiometer PH M 62 pHmeter, and the imposed ΔpH was calculated. The maximum quenching value upon the acid-to-base transition was taken as the ACMA fluorescence response to these calculated ΔpH values.

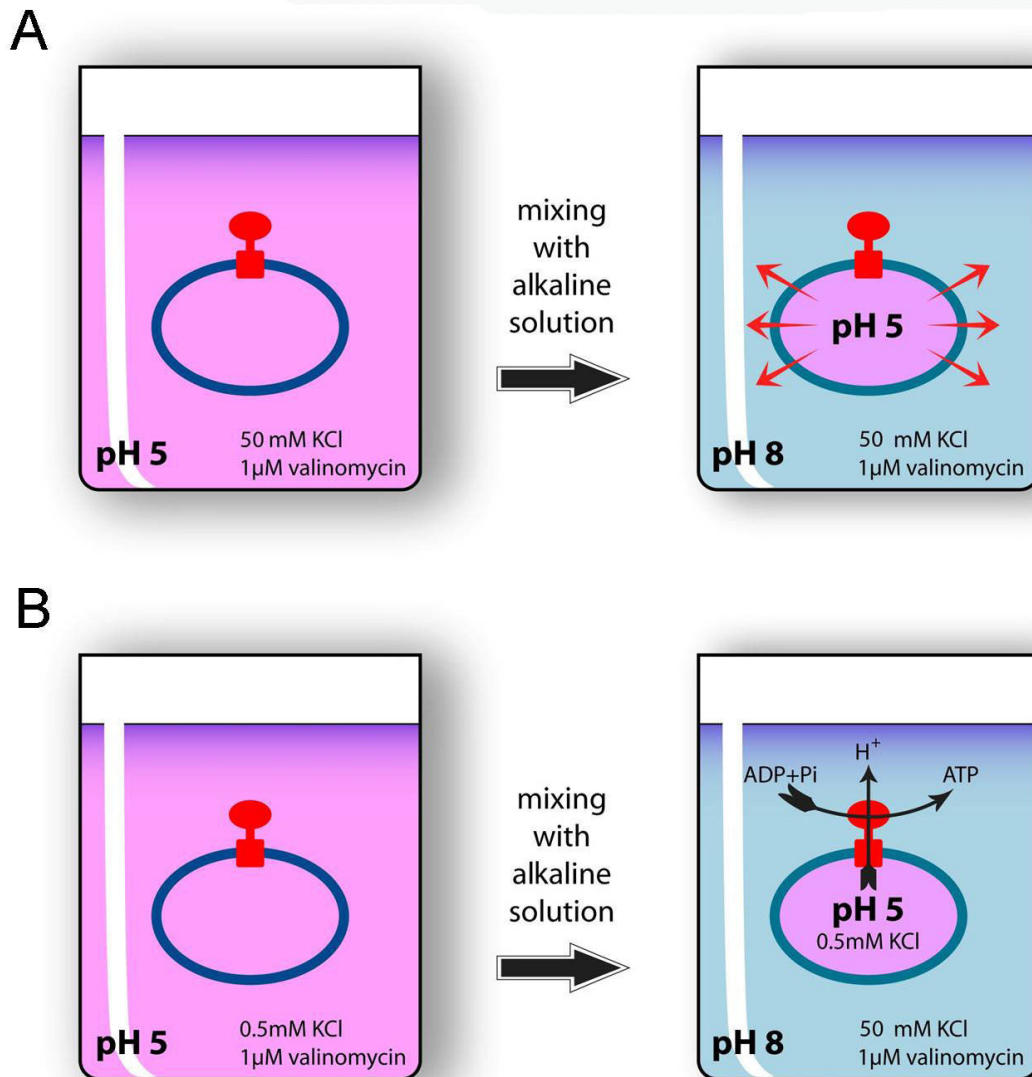


Fig.2.9.1. Acid-base transition: calibration of ACMA signal (A) and measurement of the activity of ATP synthesis (B).

2.10. Measurement of protein concentration.

2.10.1. Bradford method

The assay, first described by Bradford 1976, is based on the observation that the absorbance maximum for an acidic solution of Coomassie Brilliant Blue G-250 shifts from 465 nm to 595 nm when binding to protein occurs. Both hydrophobic and ionic interactions stabilize the anionic form of the dye, causing a visible color change.

Reagents:

1) Bradford reagent: Dissolve 100 mg Coomassie Brilliant Blue G-250 in 50 ml 95% ethanol, add 100 ml 85% (w/v) phosphoric acid. Dilute to 1 liter when the dye has completely dissolved, and filter through Whatman #1 paper just before use.

2) BSA: 0.1%

3) SDS: 0.1%

Assay:

1. The samples were diluted to obtain between 5 and 100 μg protein in at least one assay tube containing 100 μl sample. 25 μl SDS (0.1%) were added to each sample (the same volume of SDS 0.1% was added to standards as well). The standards, for the calibration, were prepared by adding a range of 5 to 100 micrograms BSA 0.1% in 100 μl volume
2. 2 ml of dye reagent were added to the mixture and incubated for 5 min, before measuring the absorbance at 595 nm.

2.10.2. Lowry method.

The protein concentration was determined by the method of Lowry et al., 1951.

The assay was carried out as described in the follow protocol:

- a) Blanks, background (buffer present in the sample), standard (BSA 0.5mg/ml) and samples (diluted if needs) were prepared, in duplicate, in a glass 10*75 tube , then water was added to a final volume of 0.5ml.
- b) 0.5ml of Buffer1* were added to the samples, and each tube was incubated for 10min.
- c) 33 μl of Folin Reagent were added, again staggering the times. The incubation time was 10 min.
- d) The absorbance was read at 750nm.

*Buffer1: 4% Sodium Tartrate, 2%CuSO₄*5H₂O, 0.2M NaOH/6%Na₂CO₃.

2.11. Measurement of the ADP content in the ATP solution.

The ADP content in the ATP was measured in a spectrophotometer by detecting the decrease in NADH in an enzymatic coupled assay (Rosing et al., 1975). It was found to be 1%.

2.12. Western Blot

Western blotting was carried out as described by Dunn, 1986 with modifications that allowed quantification of the truncated form of ϵ subunit; this polypeptide is usually lost from the blot during processing steps and is not detected (Cipriano et al, 2006). Samples of membrane proteins in SDS sample buffer (1 mg or 2 mg of protein) were separated by SDS-PAGE on 15 % polyacrylamide gels. Polypeptides were transferred to polyvinylidene difluoride membrane (Immobilon-FL) using carbonate blot buffer as described in Dunn, 1986. Following transfer, glutaraldehyde cross-linking were used to enhance detection of the truncated form. After the membrane was blocked using the Li-Cor Biosciences blocking reagent, it was incubated overnight with a mixture of monoclonal antibodies α -II (Aggeler et al, 1992) and ϵ -1 (Dunn et al, 1985), each labeled with Li-Cor IRDye 800CW. Unbound antibodies were removed by washing the blot three times, for 10 min each, then the bound fluorescent antibodies were visualized using a Li-Cor Biosciences Odyssey infrared imaging system. Band intensities were quantified and corrected for local background using software provided by the manufacturer.

Chapter 3.

RESULTS

3.1. Intrinsic uncoupling in the ATP synthase of *E. coli*.

The stoichiometry of protons transported per ATP hydrolyzed or synthesized has usually been considered a fixed parameter under physiological conditions (but see Schemidt et al., 1998; Olsson et al., 2003), although there have been several reports of conditions under which this stoichiometry was decreased, i.e. in mutated or chemically modified ATP synthases (see e.g. Zhang & Fillingame, 1995; Aggeler et al., 1995; Gardner & Cain, 1999; Peskova & Nakamoto, 2000; Cipriano et al., 2002; Cipriano & Dunn, 2006 and references therein), or when using non-physiological ligands such as Ca^{2+} in place of Mg^{2+} (Pick & Weiss, 1988; Casadio & Melandri, 1996) or sulfite in place of P_i during hydrolysis (Cappellini et al., 1997). Recently, we have found that the efficiency of proton transport in the ATP synthase of the photosynthetic bacterium *Rhodobacter capsulatus* can be decreased during physiological ATP hydrolysis, provided the concentrations of either P_i or ADP are kept sufficiently low (Turina et al., 2004).

One of the best known and most investigated ATP synthases, from a biochemical, functional and structural point of view, is that of *E. coli*. Therefore, it was of interest to check whether the same phenomenon could be found in this organism. It is already known that its ATP synthase, purified and reconstituted into liposomes, is inhibited in the hydrolysis direction by the binding of ADP and P_i , with apparent K_d 's of 10 and 470 μM , respectively, and that the inhibited ATP hydrolysis activity is recovered if a protonmotive force is applied (Fischer et al., 2000).

In this Chapter, our goal was to investigate whether the binding of ADP and P_i to the *E. coli* ATP synthase was not only inhibitory of hydrolysis but would also elicit the transition from a partially uncoupled to a fully coupled form of the enzyme. Our results show that regulatory phenomena of proton transport involving ADP and P_i binding are operative also in the ATP synthase of *E. coli*, although their features differ somewhat from those shown in *Rb.capsulatus*. They open the way to mutational studies, easily performed in this bacterium, aimed at investigating the coupling mechanism in the ATP synthases. These results have been presented in (Turina et al., 2006; D'Alessandro et al., 2008).

In order to evaluate the relative coupling degree of the *E. coli* enzyme as a function of P_i and ADP, we carried out both hydrolysis and proton pumping measurements in parallel in the isolated membrane vesicles, taking special care in keeping constant all experimental conditions in each double series of measurements.

3.2. Effect of P_i on ATP hydrolysis and proton pumping.

Inorganic phosphate has been reported to strongly inhibit the ATP hydrolysis of the isolated, reconstituted EF_0F_1 (Fischer et al., 2000) and of the isolated EF_1 (Muneyuki et al., 1991; Turina, 2000), with apparent K_d 's in the order of a few hundred micromolar. Therefore, we first measured ATP hydrolysis as a function of P_i , to check whether this behavior could be reproduced in the isolated internal membranes. Fig. 3.2.1.A shows

the amount of hydrolyzed ATP as a function of time after addition at $t=0$ s of 25 μM ATP, in the presence of increasing P_i concentrations; valinomycin and 50 mM K^+ were also present, in order to have the same assay composition as used in the ACMA assay (see below). The rates of ATP hydrolysis at $t=0$ s and $t=50$ s were evaluated by fitting the spectrophotometric data (collected at a rate of 1/s) with a monoexponential function and taking the first derivatives at $t=0$ s and $t=50$ s respectively. These rates decreased at increasing P_i concentrations, confirming that P_i inhibited the hydrolysis activity also in the non-isolated enzyme. The DCCD insensitive activity is also shown for comparison. At each P_i concentration, the hydrolysis rates decreased with time, an effect which can be attributed to decreasing ATP and/or accumulating ADP, since the same reactions carried out in the presence of an enzyme-coupled ATP regenerating system had a fully linear time-course (see below). By plotting the initial rates as a function of P_i (Fig. 3.2.1.B, full circles), an hyperbolic trend was obtained, with a best-fitting value of 140 μM for the apparent K_d . The rates at $t=50$ s are also plotted (full triangles), which can be similarly interpreted as having an hyperbolic trend.

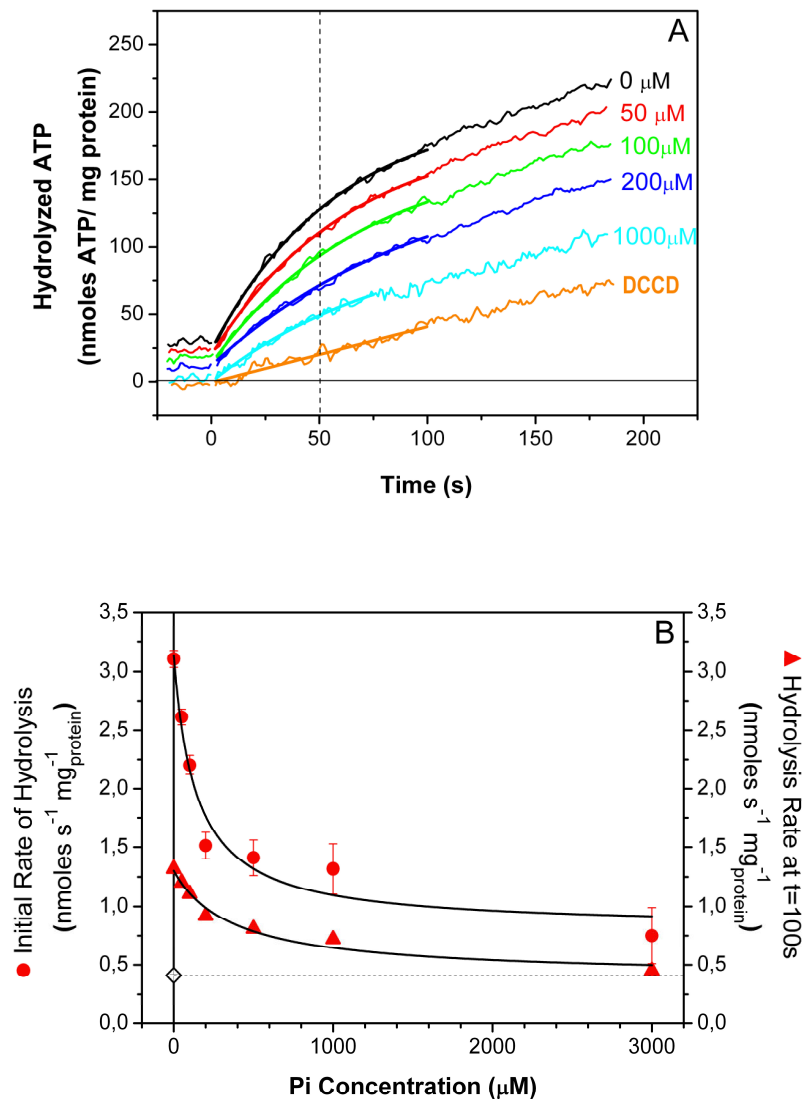


Fig. 3.2.1. ATP hydrolysis rate as a function of P_i concentration.

The ATP hydrolysis assay was carried out with Phenol Red as a pH indicator for the release of scalar protons as described in the §2.2.1.

Panel A. The ATP hydrolysis reaction was started at time $t=0$ s in the spectrophotometer by addition of 25 μM ATP and the absorbance (625–587 nm) was measured as a function of time. Absorbance values were converted to hydrolyzed ATP as described in the §2.2.1. Different P_i concentrations were added to each assay as indicated. For specifically inhibiting the ATP synthase activity, the reaction mixture was incubated in the presence of 250 μM DCCD for 30 min before starting the reaction. The experimental traces were best fitted by monoexponential functions (or linear in the case of DCCD) up to 100 s (75 s for $P_i=1$ mM).

Panel B. Rates of ATP hydrolysis at $t=0$ s (\bullet) and at $t=50$ s (\blacktriangle) and DCCD-insensitive rate (\diamond) are from Panel A and additional measurements, and have been calculated from the fitting functions; the errors of the rates at $t=0$ s have been calculated from the errors associated with the amplitude and time constant of the monoexponentials. The curves through the ATP hydrolysis data points are the best fit to the data of the hyperbolic function $P1-P2 \cdot x/(P3+x)$, with resulting best fit parameters $P3=140 \pm 50$ μM (\bullet) and $P3=400 \pm 200$ μM (\blacktriangle) respectively, corresponding to the apparent K_d values.

The proton translocating activity of the ATP synthase was estimated using the fluorescent ΔpH -sensitive acridine dye ACMA. The fluorescence measurements were carried out under the same experimental conditions of the ATP hydrolysis measurements, except for the absence of Phenol Red and the presence of ACMA. Valinomycin and 50mM K^+ were always present in order to minimize the electrical

component of the protonmotive force, so that the $\tilde{\Delta\mu}_H^+$ consisted of ΔpH only.

Fig. 3.2.2.A shows the ACMA fluorescence as a function of time in the presence of different added P_i concentrations. After starting the proton transport reaction by addition of 25 μM ATP at $t=0$ s, a rapid fluorescence quenching was observed in all cases, indicating a rapid acidification of the vesicles' interior, which settled to a steady state quenching level within 1–2 min, and could be reversed by the addition of nigericin. No significant fluorescence quenching was detected in samples pre-treated with DCCD (not shown). Notably, this steady state level was increased in the presence of P_i concentrations up to 100 μM (black, red and green traces in Fig. 3.2.2.A), while higher concentrations resulted in a progressive inhibition of proton pumping (blue, cyan, magenta and olive traces in Fig. 3.2.2.A). A similar biphasic response to P_i could also be observed in the initial rates of fluorescence quenching (Fig. 3.2.2.B). In Fig. 3.2.2.C and D both the steady state (at $t=50$ s) and the initial rate values of fluorescence quenching were plotted as a function of added P_i (open symbols). In the same figures the hydrolysis rates from Fig. 1B (at $t=0$ s and $t=50$ s) are also reported for comparison (full symbols). The plot highlights the different courses of both quenching curves, markedly biphasic (first activatory and then inhibitory), and of the two hydrolysis curves, monotonically inhibitory. Analogous experimental results had been preliminarily obtained using vesicles from the ATPase superproducer strain of *E. coli* AN1460, carrying a copy of the *unc* operon on the multicopy pAN45 plasmid (data not shown). The very fast fluorescence response of ACMA observed using these vesicles had prevented us, however, from performing an analysis in terms of initial rates.

In the case of a pumping enzyme which keeps the number of protons translocated per hydrolyzed ATP constant, a parallel behavior of hydrolysis and ACMA response is expected. In such a case, a higher initial rate of hydrolysis will be associated, at constant internal buffering capacity, with a higher rate of ACMA quenching. In fact, the ACMA quenching has been shown to be a monotonically increasing, though not linear, function of transmembrane ΔpH (see e.g. Schuldiner et al., 1972 for a theoretical model and

Casadio, 1991; Casadio et al., 1995; Casadio & Melandri, 1985 for an experimental calibration of the response of ACMA and other acridine dyes by means of acid-base transitions). Similarly, again in the case of a constant number of protons transported per hydrolyzed ATP, the steady state transmembrane ΔpH , and therefore the steady state fluorescence quenching, is expected to increase or decrease in parallel with the rate of ATP hydrolysis, provided the passive proton permeability coefficient of the membrane does not change. In fact, the higher the inward proton flux, the higher will be the ΔpH at which this active inward proton flux will be balanced by the passive outward proton flux (which at constant proton permeability coefficient is an increasing function of the ΔpH itself).

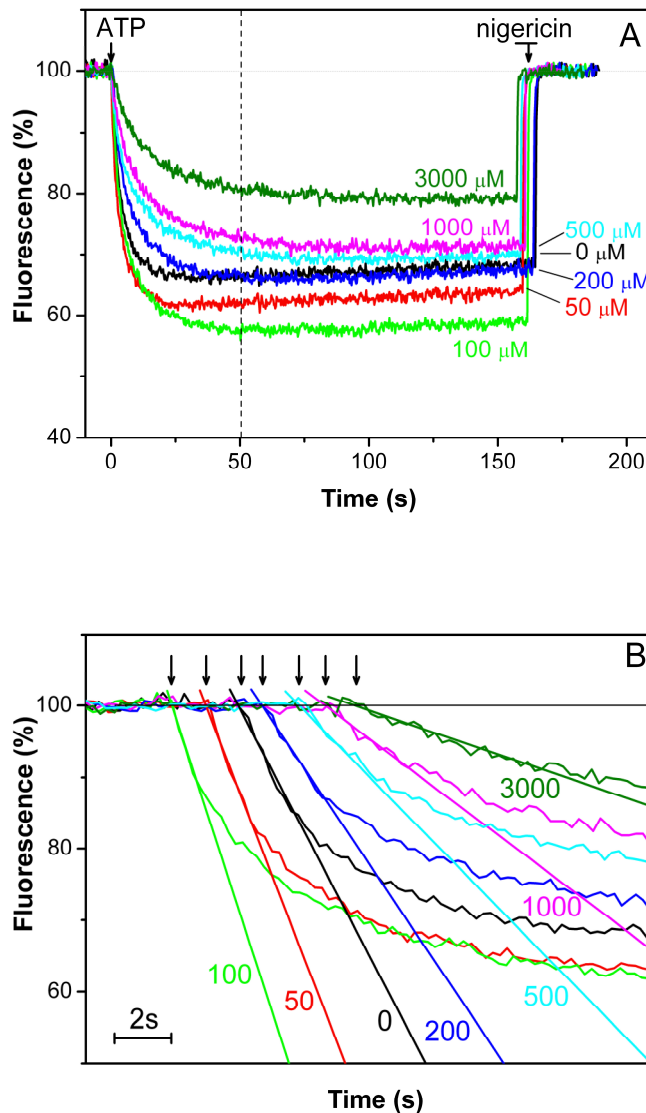


Fig. 3.2.2. A, B. see next page for the full caption.

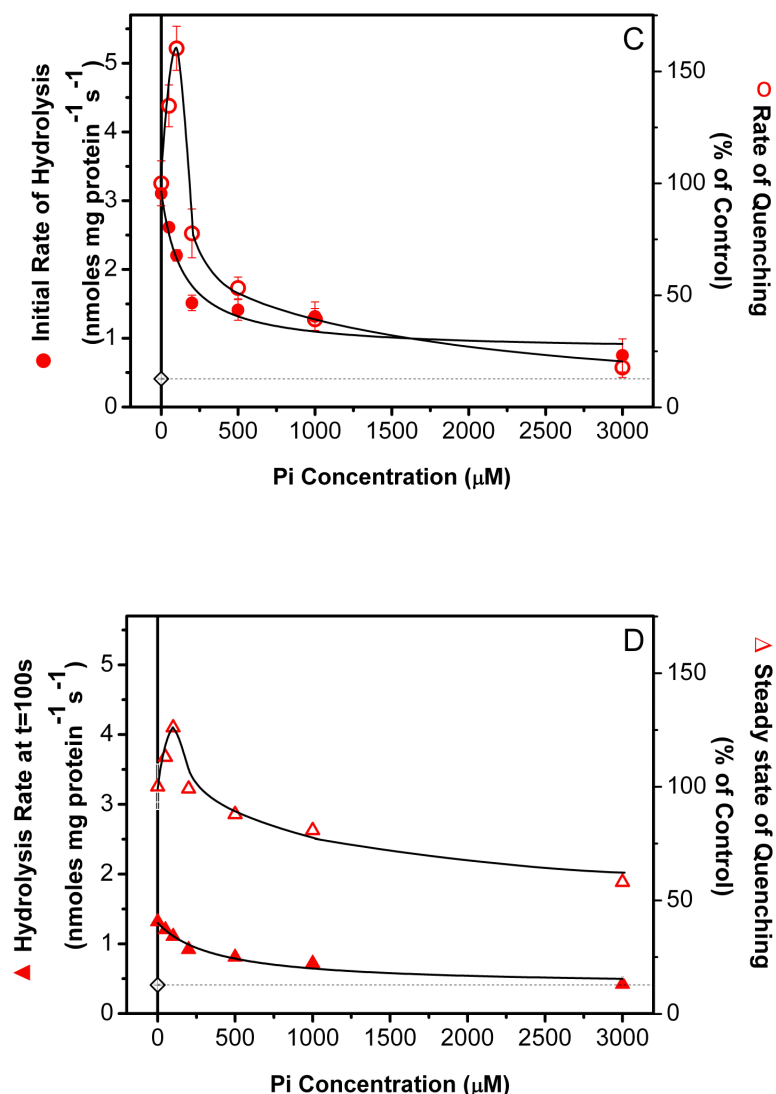


Fig. 3.2.2. ACMA fluorescence quenching as a function of P_i concentration.

The ACMA assay was carried out as described in the §2.5.

Panel A. The proton pumping reaction was started in the spectrofluorimeter cuvette by addition of 25 μM ATP at time $t=0$ s and the ACMA fluorescence was recorded as a function of time. Different P_i concentrations were added to each assay as indicated. For each trace, addition of 1 μM nigericine recovered the 100% fluorescence level.

Panel B. The traces in (A) are reported here on a shorter time scale and displaced along the time axis for showing the initial rates of quenching. The arrows indicate the time points of ATP addition, the numbers the P_i concentrations. The linear fits were calculated over 1 (0–500 μM P_i) or 2 (1–3 mM P_i) s of reaction (5 or 9 data points).

Panel C. The percentage values of the initial rates of fluorescence quenching (\circ) relative to controls (7.6% \cdot s⁻¹) were determined from (B). The errors of the initial rates of quenching are the errors associated with the first-order coefficients of the linear regressions. The values of the initial rates of ATP hydrolysis (\bullet) are reported for comparison from Fig. 3.2.1B. The curve through the quenching data points was drawn by hand.

Panel D. The percentage values of fluorescence quenching at $t=50$ s (Δ) relative to controls (33.8%) were determined from (A). The values of the rates of ATP hydrolysis at $t=50$ s (\blacktriangle) are reported for comparison from Fig. 3.2.1B. The curve through the quenching data points was drawn by hand.

3.3. Evaluation of the ACMA response in the *E. coli* membrane system.

The following measurements were carried out in order to confirm that also in our system the response of ACMA increased in parallel to increasing steady state ΔpH and initial rate.

The ACMA response was measured as a function of ATP concentration, and the results were indeed as expected, in that the steady state quenching increased in parallel with ATP (Fig. 3.3.1.A, traces (a) through (e)), and so did the initial rate of quenching (Fig. 3.3.1.B). These initial rates of quenching are plotted as a function of ATP concentration together with the initial rates of ATP hydrolysis (Fig. 3.3.1.C), which were measured in parallel in the Phenol Red assay under the same experimental conditions. The increase in the rate of hydrolysis was almost linear in the measured range, consistent with a K_M value in the hundreds of μM range ($K_M=140 \mu\text{M}$ ATP was obtained in the isolated and reconstituted enzyme in Löbau et al., 1998) and was closely paralleled by the initial rate of quenching, which had a less linear run, consistent with the non-linear response of ACMA to the trans-membrane ΔpH (Casadio, 1991; Casadio et al., 1995; Casadio & Melandri, 1985). During the recording of the trace at $5 \mu\text{M}$ ATP ((a) in Fig. 3.3.1.A), the further addition of $50 \mu\text{M}$ ATP restored a steady state quenching value similar to the one of the $50 \mu\text{M}$ ATP trace (d), indicating that the slow regain of fluorescence in trace (a) was mainly due to substrate depletion. Addition of $50 \mu\text{M}$ NADH (both trace (a) and trace (e)) showed that the activation in parallel of a second source of proton translocation (respiratory chain) further increased the steady state quenching, consistent with a parallel increase of inward proton flux and consequently with a higher steady state ΔpH . Finally, it can be noted that in Fig. 3.3.1.C the highest quenching rate values obtained as a function of ATP concentration are in the same range as the highest rates obtained as a function of P_i (Fig. 3.2.2.C and D), indicating that these latter were not significantly limited by lack of kinetic competence of ACMA. This kinetic competence is consistent with the data reported in (Casadio, 1991; Turina et al., 1990), indicating that acridines respond to ΔpH changes within hundreds of milliseconds.

As mentioned, the interpretation of the increasing rates of ACMA quenching (data in Fig. 3.2.2.) as corresponding to increasing rates of proton translocation mainly requires that the internal buffer capacity of the vesicles remains constant in the range of P_i concentration in which the phenomenon is observed. Assuming complete permeation of P_i through the membrane (which is an extreme assumption in view of its 1–2 charges at pH 8), it can be excluded that a few hundred μM P_i (with $\text{pK}=7.2$) could significantly alter the buffer capacity of the inner bulk phase, which should be buffered by 1 mM Tricine ($\text{pK}=8.2$), and even in this case, the buffering would determine a decrease of the initial rate, relative to the initial rate at $\text{P}_i=0$, and not an increase. As to the decreasing phase of the P_i dependency of the quenching rate, it cannot be excluded that a small part of the observed decrease was due to P_i permeation to the vesicle inside, but a very similar decrease was observed also when the buffer contained 20 mM Tricine (not shown). The interpretation that the increasing steady state of ACMA quenching, seen with increasing P_i (data in Fig. 3.2.2.), corresponds to increasing rates of proton translocation also requires, as mentioned, that the proton permeability of the membrane is not changed by the changing concentration of P_i (e.g. through P_i binding to, and activation of, membrane channels). We checked for this possibility by measuring, as a function of P_i , the steady state quenching signal induced by $50 \mu\text{M}$ NADH, or, in order to include nucleotides as well, by repeating the same measurements in the presence of $20 \mu\text{M}$ ATP and $5 \mu\text{M}$ ADP in a DCCD inhibited sample (not shown). No significant change in the steady state quenching could be detected in either case.

We conclude that the interpretation of increasing initial quenching rates and increasing steady state quenching in the low P_i concentration range as being due to increasing proton translocation rates by the ATP synthase is warranted in our system. According to this interpretation, the binding of P_i at low concentration to ATP synthase increases its rate of proton translocation while decreasing its rate of ATP consumption. The only plausible explanation for this phenomenon that we can see is that P_i binding at low concentration increases the ratio of protons translocated per hydrolyzed ATP, or, in other words, that it increases the efficiency of proton translocation from a relatively inefficient state to a much more efficient one.

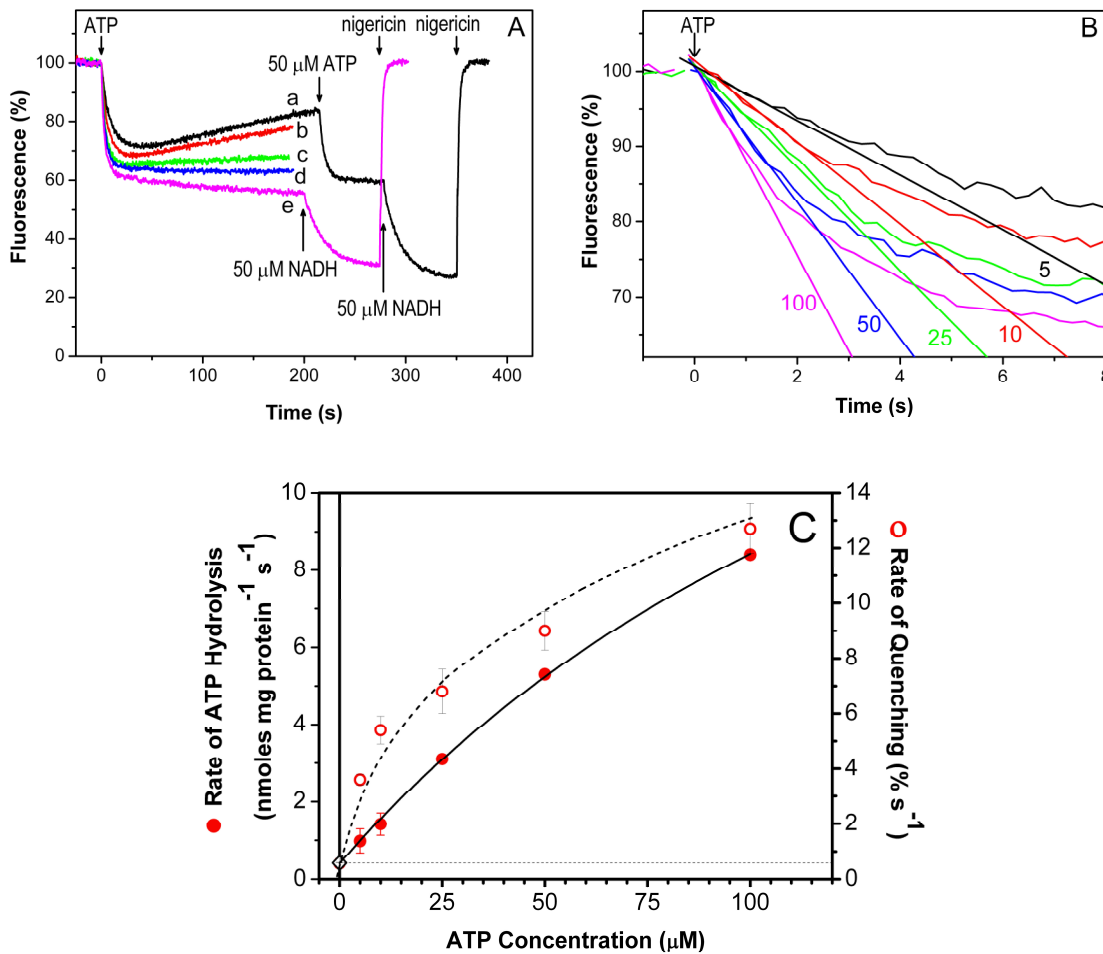


Fig. 3.3.1. ACMA fluorescence quenching as a function of ATP concentration.

The ACMA assay was carried out as described in the legend of Fig. 3.2.2. The ATP concentrations were (a) 5 μM , (b) 10 μM , (c) 25 μM , (d) 50 μM , (e) 100 μM . For the trace at 5 μM ATP, a second addition of 50 μM ATP after about 200 s is indicated by an arrow. The further additions of 50 μM NADH for the traces at (5+50) μM and 100 μM ATP are indicated by arrows.

Panel B. The traces from Panel A. are reported on a shorter time scale. The numbers indicate the ATP concentrations. The linear fits were calculated over 1 or 2 s of reaction (5 or 9 data points).

Panel C. The values of the initial rates of fluorescence quenching (\circ) (from Panel B) are reported as a function of ATP concentration. The errors of the initial rates of quenching are the errors associated with the first-order coefficients of the linear regressions. The values of the initial rates of ATP hydrolysis (\bullet) and their errors were determined, similarly as described for Fig. 3.2.1., from monoexponential fitting of Phenol Red traces of ATP hydrolysis measurements carried out as a function of ATP concentration. The curve through the quenching data points was drawn by hand, the curve through the hydrolysis data points is a best fitting hyperbole with apparent $K_M = 190 \pm 20$.

3.4. Effect of ADP depletion on the P_i inhibited ATP hydrolysis.

The inhibition by saturating P_i of the ATP hydrolysis by the isolated and reconstituted *E. coli* ATP synthase has been shown to be strongly enhanced by the presence of ADP and, vice versa, the inhibition by saturating ADP was strongly enhanced by P_i (Fisher et al., 2000).

We checked, therefore, whether the same phenomenon could be shown in the enzyme embedded in native membranes. Given the high P_i inhibition observed in the absence of added ADP, it was likely that ADP was already present in our system, either pre-bound to the synthase or present in sufficient amounts in the ATP solution. In order to deplete our system from ADP, we measured the rate of ATP hydrolysis with an enzyme-coupled ATP regenerating system (see §2.2.2.), in which PK and PEP operated as an ADP trap, and LDH and NADH (in the presence of KCN for inhibiting the NADH driven respiratory chain) coupled the ATPase reaction (through the PK and LDH reaction) to the absorbance changes at 340 nm. The steady state ADP concentration was modulated through the amount of added PK: different series of measurements as a function of P_i were carried out in the presence of increasing amounts of PK in the assay, i.e. at decreasing concentration of steady state ADP. At all P_i and PK concentrations, addition of 25 μ M ATP started a decrease in the absorbance, i.e. ATP hydrolysis, which was linear over the whole measuring time (200 s), except for an initial fast phase of 1–2 s, which could be attributed to rapid phosphorylation of the ADP present as a contaminant in the ATP solution, since it could be observed also in the absence of membranes. The hydrolysis rates are plotted in Fig. 3.4.1. as a function of P_i concentration for all tested PK activities, together with the hydrolysis rates from Fig. 3.2.1.B (black circles) obtained in the absence of PK. The curves through the data points are hyperbolic functions best-fitted to the data. An effect of PK on the inhibition by P_i is evident: at intermediate PK amounts (2, 10, and 55 U/ml) the apparent K_d 's for P_i shift to progressively higher values (290, 520, and 1100 μ M respectively) until, at the highest PK amount (110 U/ml), an inhibition by P_i is barely detectable. The asymptotic levels of inhibition were gradually decreased as well. Therefore the activating effect of the ADP trap is most evident at the highest P_i concentrations.

These results confirm and extend those first obtained in the isolated and reconstituted EF_0F_1 (Fisher et al., 2000), in showing that ADP bound to the enzyme is required for P_i to be able to inhibit ATP hydrolysis. Analogously, P_i is required for a stronger inhibition by ADP, although the inhibitory effect of ADP can be observed also in the absence of added P_i .

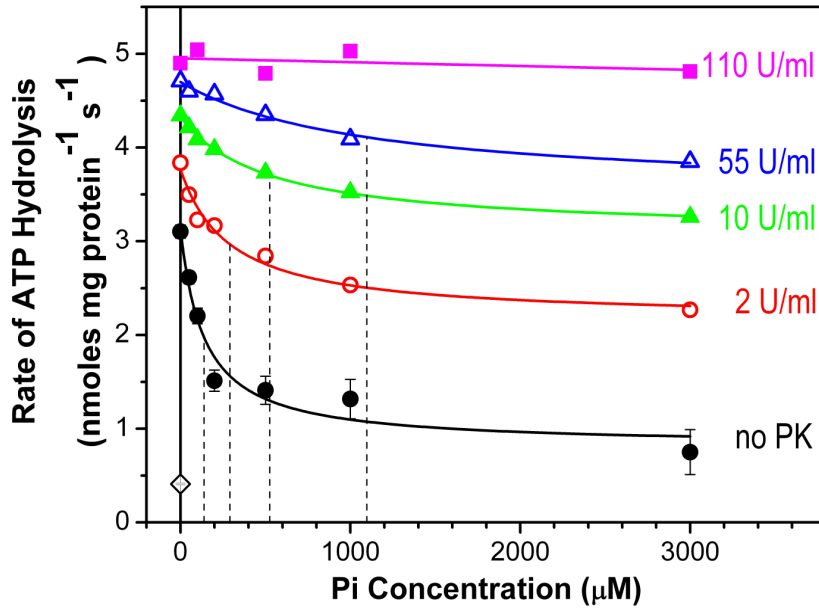


Fig. 3.4.1. ATP hydrolysis rate as a function of P_i concentration in the presence of increasing PK activity. ATP hydrolysis reactions as a function of P_i concentration were started in the presence of PK by adding 25 μ M ATP and were measured as the disappearance in time of NADH absorbance in the presence of an enzyme-coupled ATP regenerating system, as described in §2.2.2.. Data points obtained in the absence of PK (\bullet), or after inhibition by DCCD (\diamond) are reported from Fig. 3.2.1.B for comparison. The ATP regenerating system contained increasing activities of PK as indicated. The curves through the data points at 0 (\bullet), 2 (\circ), 10 (\blacktriangle) and 55 U/ml (\triangle) are the best fit to the data of the hyperbolic function $P_1 - P_2 \cdot x / (P_3 + x)$, with resulting best-fit parameters $P_3 = 140 \pm 50$, 290 ± 80 , 520 ± 60 and 1100 ± 400 μ M, respectively, as indicated by the dashed lines. The curve through the data points at 110 U/ml (\blacksquare) is a linear fit.

3.5. Effect of ADP depletion on proton pumping.

We then measured the ATP-driven ACMA fluorescence quenching under the same experimental conditions of Fig. 3.4.1. The assay compositions were identical to those of Fig. 3.4.1. except that LDH, NADH and KCN were omitted and ACMA was present. In the fluorescence traces shown in Fig. 3.5.1, P_i was kept constant at 200 μ M, and the amount of PK added to the assay was progressively increased from 0 to 110 U/ml. After addition of 25 μ M ATP at $t=0$ s, a fast rate of fluorescence quenching was observed in all cases, which declined with time. Such decline was most pronounced in the case of no added PK, showing that substrate depletion and ADP accumulation contributed to this decline. Noticeably, the overall quenching signal was significantly increased, relative to no addition, by the presence of 2 U/ml of PK, but such high quenching level was progressively decreased when increasing PK activities were added. A very similar trend could be observed in the initial rate of fluorescence quenching (Fig. 3.5.1.B). The increase in both overall quenching signal and initial quenching rate at 2 U/ml PK was in agreement with the increase of the hydrolysis rate observed at 200 μ M P_i at the corresponding level of PK (see Fig. 3.4.1.). By contrast, while the hydrolysis rate kept increasing with the PK activity (Fig. 3.4.1.), both the overall quenching signal and the initial quenching rate were markedly decreased (Fig. 3.5.1.A, B). To check for possible interferences of the PK/PEP components with the permeability system of the membrane, the NADH-induced quenching was monitored in the presence of PEP and of

increasing PK amounts, or the ATP-induced quenching was monitored in the presence of PEP alone or of PK alone or pyruvate. Again, no alteration of the quenching signal could be detected under these conditions, letting us conclude that the decrease in the quenching was due to a decrease of the proton translocation rate by the ATP synthase with increasing PK, in spite of the increasing rate of ATP hydrolysis.

The ADP concentrations present at the different PK activities can be calculated by imposing a steady state concentration for ADP, in which its rate of production by the ATP hydrolysis reaction (v_{hyd}) balances the rate of ADP depletion by the PK (v_{PK}). The attainment of a steady state [ADP] is consistent with the fact that, after an initial pre-steady state, the hydrolysis rate in the presence of the PK-LDH system is constant. Assuming a Michaelis–Menten kinetics of the PK reaction, one has:

$$v_{\text{[hyd]}} = v_{\text{[PK]}} = \frac{v_{\text{max}}^{\text{ADP}} \cdot [\text{ADP}]_{\text{SS}}}{[\text{ADP}]_{\text{SS}} + K_{\text{M}}^{\text{ADP}}}$$

where $[\text{ADP}]_{\text{ss}}$ is the ADP concentration in the steady state, and $v_{\text{max}}^{\text{ADP}}$ and $K_{\text{M}}^{\text{ADP}}$ refer to the PK reaction. $v_{\text{max}}^{\text{ADP}}$ was measured directly (see §2.4.), $K_{\text{M}}^{\text{ADP}} = 0.3 \text{ mM}$ was taken from the literature (Mcquate & Utter, 1959). v_{hyd} were those measured in the PiruvateKinase-ADP trap assays. While competition between ATP and ADP, and other possible kinetic alterations of the PK activity, have not been considered here, this calculation should provide a good first estimate of $[\text{ADP}]_{\text{ss}}$.

In Fig. 3.5.1.C, the hydrolysis rates from Fig. 3.4.1. (full circles) and the quenching data from Fig. 3.5.1.A, B (open circles: quenching rates, triangles: quenching value at $t=50 \text{ s}$) were plotted as a function of the calculated steady state ADP concentration. The lowest calculated ADP concentration corresponds to the highest PK activity (110 U/ml). In such a plot the diverging course between the ATP hydrolysis and the quenching data can be fully appreciated, as well as their dependency on the estimated ADP concentration. Noticeably, the very low ADP concentrations calculated in such a way (submicromolar range) indicate that a very high affinity binding site for ADP is involved.

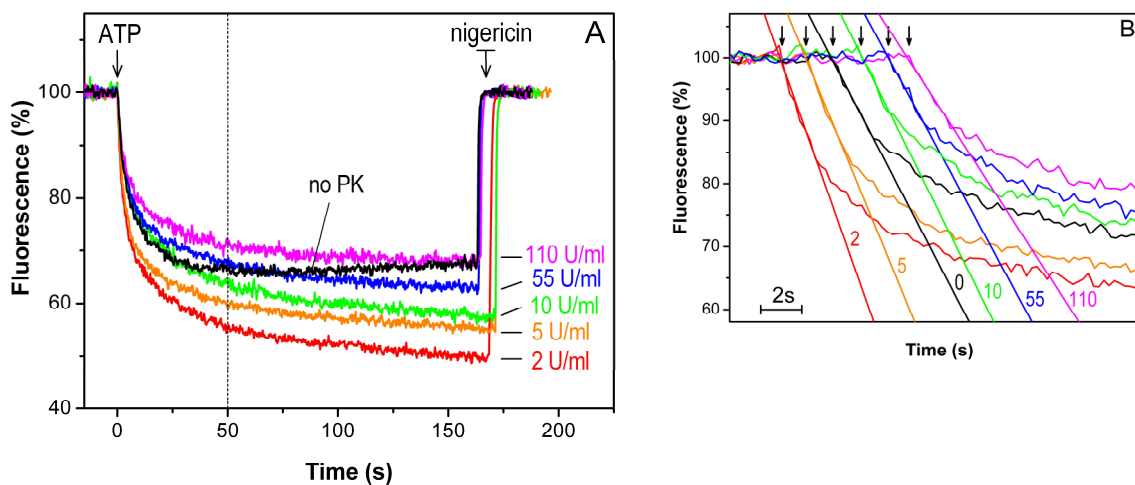


Fig. 3.5.1. A, B. see next page for the full caption.

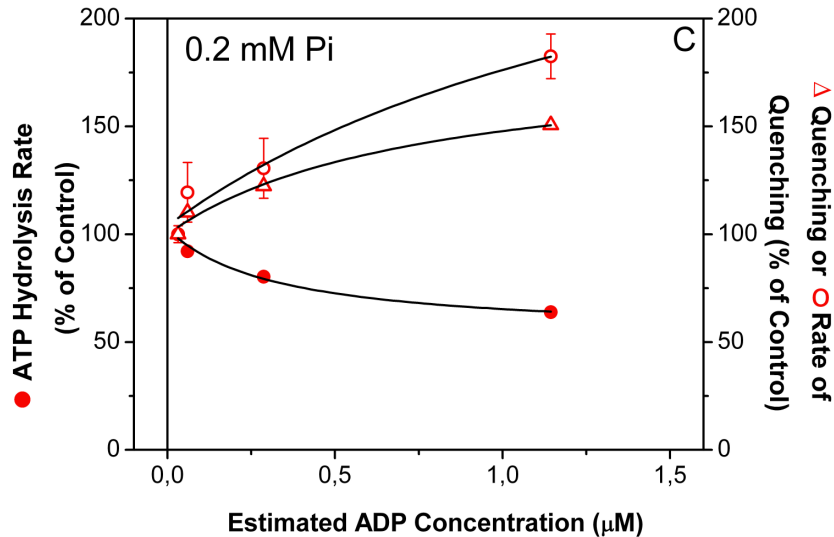


Fig. 3.5.1. ACMA fluorescence quenching at constant P_i concentration in the presence of increasing PK activity.

Panel A. The ACMA assay was carried out as described in the legend of Fig. 3.2.2., but the reaction mixture contained in addition 200 μM P_i , 2mMPEP and increasing activities of PK as indicated.

Panel B. The traces from Panel A are reported on a shorter time scale and displaced along the time axis for showing the initial rates of quenching. The arrows indicate the time points of ATP addition. The linear fits were calculated over 2 s of reaction (9 data points).

Panel C. The steady state ADP concentration for each PK concentration was estimated as described in the text. The percentage values of the initial rates of fluorescence quenching (○) and the percentage values of fluorescence quenching at $t=50$ s (Δ) relative to controls, i.e. to the values obtained at the lowest estimated ADP concentration estimated in the presence of 110 U/ml of PK (5.0% \cdot s $^{-1}$ and 29.5%, respectively), were determined from Panel B and A, and the values of the initial rates of ATP hydrolysis (●) relative to control (5.0 nmol ATP \cdot s $^{-1}$ \cdot mg protein $^{-1}$) were measured in an enzyme-coupled ATP regenerating system as described in the text. The errors of the initial rates of quenching are the errors associated with the first-order coefficient of the linear regression. The curves through the data points are the best fit to the data of a hyperbolic function.

3.6. Effect of ADP depletion on proton pumping as a function of P_i concentration.

Similar experiments were performed at different concentrations of P_i and the final results are summarized in Fig.3.6.1., where the quenching level at $t=50$ s (Fig.3.6.1.A) and the initial quenching rates (Fig. 3.6.1.B) at different PK activities are plotted as a function of P_i . At all intermediate PK activities, a maximum of both quenching level and initial quenching rate was observed close to 100–200 μM P_i , followed by a decrease at higher concentrations. This biphasic course, as well as the extent of P_i inhibition in the high concentration range, were progressively attenuated at the highest PK activities, until no biphasicity was detectable at PK=110 U/ml, and a very weak inhibition was left. The biphasic trend observed at the intermediate PK activities was similar to what was found in the absence of PK (reported for comparison in Fig.3.6.1.A, B, open symbols) and was again particularly striking, given that the ATP hydrolysis rates were, on the contrary, monotonically decreasing as a function of P_i (see Fig.3.4.1.) at all the intermediate PK activities tested.

In addition, for all tested P_i concentrations, a trend similar to the one recorded at $P_i=200$ μM (Fig. 3.5.1.) was evident: the lowest PK activity was the one at which both quenching level at $t=50$ s and initial quenching rate were the highest, and increasing PK

activities induced a decrease of both these parameters. Also for these series of data, it was possible to calculate the steady state ADP concentration present in each assay and to plot the hydrolysis and quenching data as a function of $[\text{ADP}]_{\text{ss}}$ for each P_i concentration. In Fig. 3.6.1.C one such plot is presented, in which the P_i concentration was 1 mM. In Fig. 3.6.1.D the analogous plot is presented for the data obtained in the absence of added P_i ; also in this latter case, the same divergent trend between hydrolysis and quenching is evident, as in the presence of P_i , indicating that ADP alone was also able to induce the phenomenon, although to a lower extent and with a lower binding affinity (the P_i present at the beginning of the reaction as a contaminant in the ATP solution was not higher than $0.5 \mu\text{M}$, as measured by the green malachite method (Turina et al., 2006), and the P_i released during 50 s of ATP hydrolysis can be calculated and was not higher than $6 \mu\text{M}$, i.e. negligibly small).

We conclude that the binding of ADP at very low concentration, and more markedly when P_i is present, induces in the ATP synthase a higher efficiency state, in which more protons per hydrolyzed ATP are translocated across the membrane.

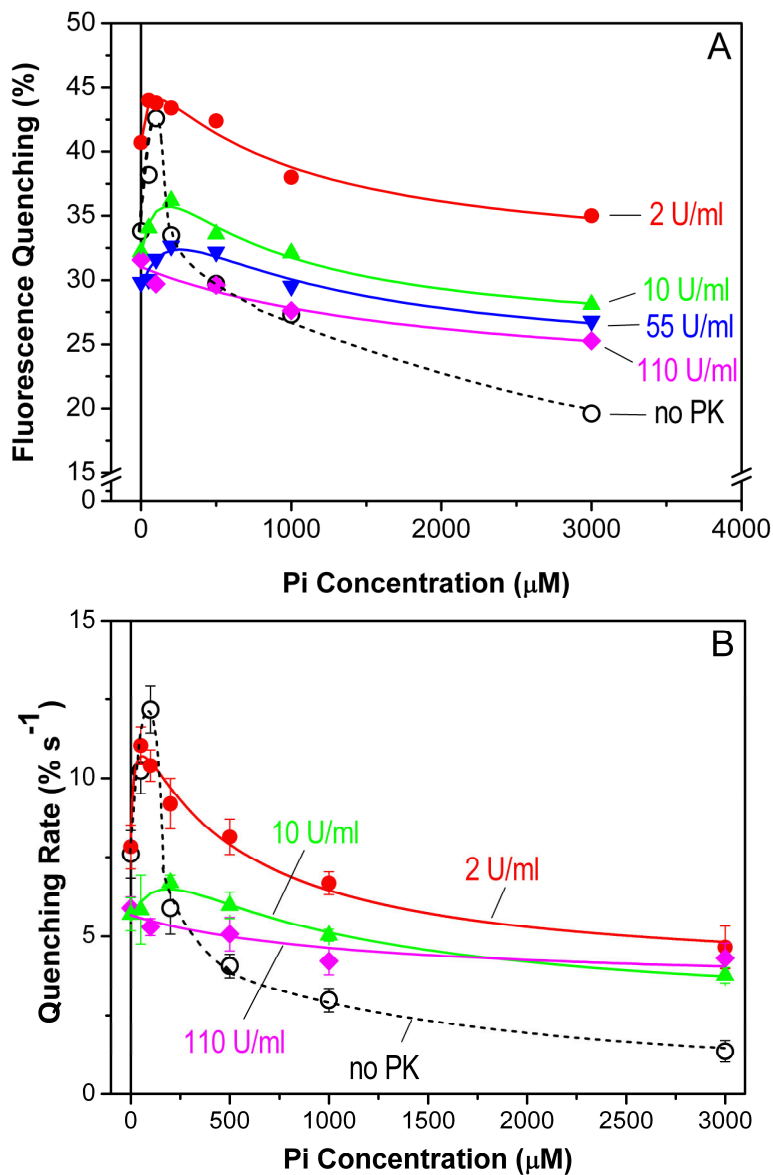


Fig. 3.6.1. A,B. see next page for the full caption.

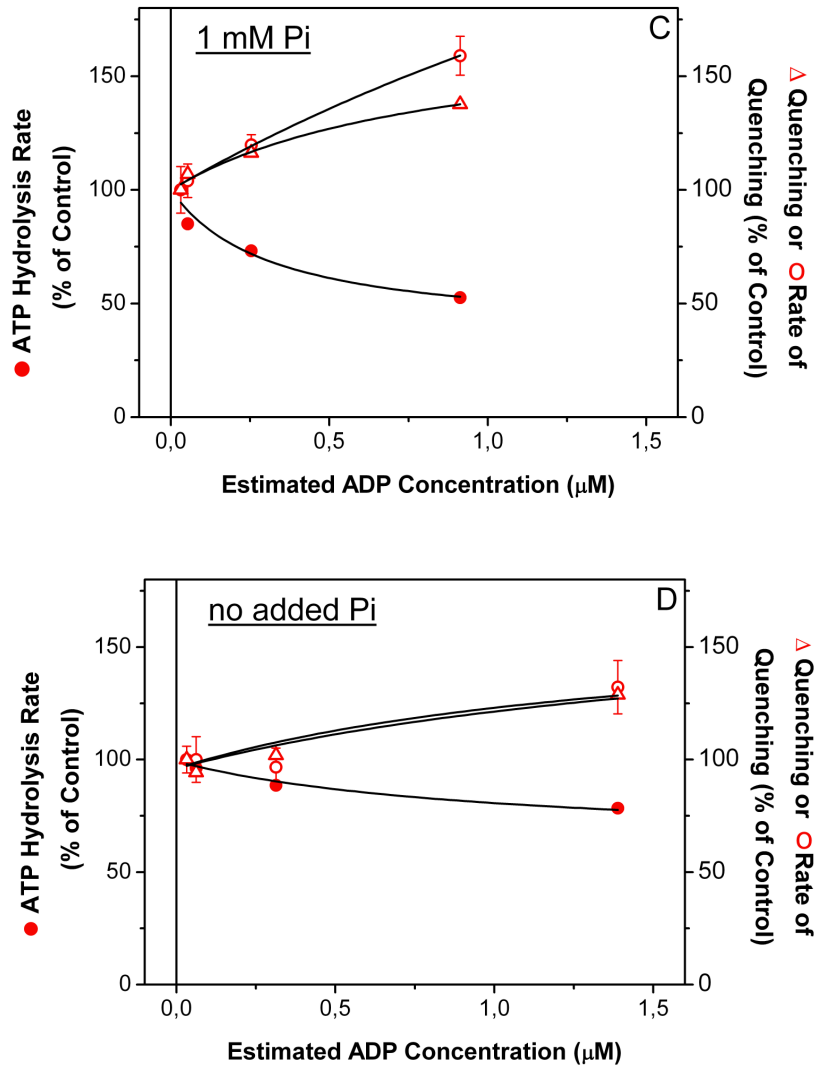


Fig. 3.6.1. ACMA fluorescence quenching as a function of P_i concentration in the presence of increasing PK activity.

The ACMA assay was carried out as described in the legend of Fig. 3.2.2., but contained in addition 2 mM PEP and variable concentrations of PK and P_i as indicated.

Panel A. The fluorescence quenching at $t=50$ s is plotted as a function of the added P_i concentration for each PK activity. The open symbols (no added PK) are reported from Fig. 3.2.2.D for comparison.

Panel B. The initial rates of fluorescence quenching were determined by the linear fits calculated over 1 s of reaction (5 data points) and are plotted as a function of the added P_i concentration for each indicated PK activity. The data at PK=55 U/ml were omitted for clarity. The errors of the initial rates of quenching are the errors associated with the first-order coefficient of the linear regression. The open symbols (no added PK) are reported from Fig. 3.2.2.C for comparison.

Panel C. The ADP concentration for each PK activity at 1 mM P_i was estimated as described in the text. The percentage values of the initial rates of fluorescence quenching (○) and the percentage values of fluorescence quenching at $t=50$ s (Δ) relative to controls, as specified in the legend of Fig. 3.5.1. ($4.2\% \cdot \text{s}^{-1}$ and 27.6% , respectively), are from Panel B and A (values at 1 mM P_i), and the rate values of ATP hydrolysis (●) relative to control ($4.8 \text{ nmol ATP} \cdot \text{s}^{-1} \cdot \text{mg protein}^{-1}$) are from Fig. 3.4.1. (values at 1 mM P_i). The curves through the data points are the best fit to the data of a hyperbolic function.

Panel D. The ADP concentration for each PK activity at no added P_i was estimated as described in the text. The percentage values of the initial rates of fluorescence quenching (○) and the percentage values of fluorescence quenching at $t=50$ s (Δ) relative to controls, as specified in the legend of Fig. 3.5.1. ($5.9\% \cdot \text{s}^{-1}$ and 31.6% , respectively), are from Panel B and A (values at 0 mM P_i), and the rate values of ATP hydrolysis (●) relative to control ($4.9 \text{ nmol ATP} \cdot \text{s}^{-1} \cdot \text{mg protein}^{-1}$) are from Fig. 3.4.1. (values at 0 mM P_i). The curves through the data points are the best fit to the data of a hyperbolic function.

3.7. Discussion

The major finding of the work reported in this chapter is that low concentrations of ADP and P_i inhibit the rate of ATP hydrolysis by the ATP synthase in *E. coli* internal membranes, while at the same time increasing the rate of inward proton translocation. This experimental observation can be rationalized if it is assumed that, in binding these two ligands, the ATP synthase changes its catalytic mode, shifting from a partially uncoupled to a fully coupled ATP hydrolysis. This general conclusion parallels the one previously reached for the ATP synthase of *Rb. capsulatus* (Turina et al., 2004). The occurrence of this phenomenon in these two Prokaryotes suggests that it might be a common feature in the prokaryotic ATP synthases, and possibly in the eukaryotic ones as well.

To our knowledge, a modulation of the coupling efficiency by physiological ligands has never been documented in any other ATP synthase so far, even though states of uncoupling have been reported in mutated, or chemically modified, ATP synthases (Zhang & Fillingame, 1995; Aggeler et al., 1995; Gardner & Cain, 1999; Peskova & Nakamoto, 2000; Cipriano et al., 2002; Cipriano & Dunn, 2006), and in the presence of non-physiological ligands, such as Ca_2^+ and sulfite (Pick & Weiss, 1988; Casadio & Melandri, 1996; Cappellini et al., 1997). The results obtained in the laboratories of Capaldi (Tsunoda et al. 2001), and Yoshida (Suzuki et al., 2003), according to which the trapping of the ϵ subunit in two different conformations generates either a “synthase” or a “hydrolase” form, can be considered consistent with the existence of two conformations having different coupling efficiencies, although alternative mechanisms could also explain those experimental findings. An intrinsic uncoupling has been reported for other chemiosmotic enzymes such as cytochrome oxidase (reviewed in Kadenbach, 2003), V-ATPases (Moriyama & Nelson, 1988; Davies et al., 1994; Müller et al., 1999), and Ca-ATPases (reviewed in Berman, 2001), in which its possible regulatory role has been discussed. Analogously, a regulatory role can also be hypothesized for the intrinsic uncoupling we observe in the ATP synthase, since it is possible that the intracellular P_i concentration varies in the hundreds of micromolar range. On the other hand, it seems likely that the protonmotive force also have a role in modulating the pump efficiency, and the binding competition with ATP as well, even though these possibilities have not been explored in the present work.

Similarly as seen in the ATP synthase of *Rb. capsulatus*, the ADP concentrations which could induce this phenomenon were in the submicromolar range, and could be attained during hydrolysis only by supplementing the assays with an ATP regenerating system acting as an ADP trap. This implies the involvement of a site for ADP binding, whose very high affinity, manifest even in the presence of a large excess of ATP, is a strong indication in favour of its catalytic nature. Very recently, ADP trapping with an ATP regenerating system has revealed also in the ATP synthase of *P. denitrificans* a high affinity ADP binding site, whose occupancy was required for maintaining the activated state of the enzyme (Zharova & Vinogradov, 2006).

The uncoupling/coupling transition observed in the present chapter was dependent on P_i as well, similarly again to what was shown in *Rb. capsulatus*. However, a striking difference was that P_i , which slightly activated the hydrolysis in the photosynthetic bacterium, was instead inhibitory for hydrolysis in the *E. coli* enzyme, which makes the stimulation of the proton translocation rate observed at P_i concentration up to 100 μ M even more striking. The bell shaped dependence of proton transport on P_i concentration

suggests that two P_i binding sites are involved, one with higher affinity, whose occupancy increases the pumping efficiency (leading to an overall higher rate of proton translocation in spite of the underlying inhibition) and a second one with lower affinity, causing inhibition of hydrolysis (reflected in the inhibition of proton translocation visible at higher P_i concentrations). The apparent K_d measured for P_i inhibition of ATP hydrolysis was 140 μM (Fig. 3.2.1.), while the steep rise of the ACMA quenching rate and steady state between 0 and 100 μM P_i (Fig. 3.2.2.) indicates that the K_d for the high affinity site could be in the order of tens of μM . The effect on the hydrolysis rate of the higher affinity binding site cannot be determined from our results, since the experimental data as a function of P_i could be fitted not only by a single hyperbolic function but equally well by the sum of two hyperbolic functions with two K_d 's, one higher and one lower than 140 μM . The occurrence of two P_i binding sites has been shown in the isolated EF_1 by direct binding studies, and the resulting K_d (at pH 7.5) were both in the range of 0.1 mM (Penefsky, 2005). In addition, P_i binding to EF_1 has been demonstrated indirectly through its effect on the trypsinization pattern of the ϵ subunit (apparent $K_d=50 \mu\text{M}$), (Mendel-Hartvig & Capaldi, 1991), and its binding to EF_1 and EF_0F_1 through the changes induced in the emission intensity of a fluorescent probe covalently bound to the γ subunit (apparent $K_d=280 \mu\text{M}$) (Turina, 2000). An inhibition of ATP hydrolysis by P_i has also been reported, under deenergized conditions, in the isolated and reconstituted EF_0F_1 (apparent $K_d=500 \mu\text{M}$) (Fischer et al., 2000), and in the isolated EF_1 (apparent $K_d=280 \mu\text{M}$) (Turina, 2000). In the light of the present data (Fig. 3.4.1.), it should be considered that the value of the apparent K_d can depend on the fraction of ATP synthase molecules which have ADP bound. Moreover, according to data obtained in chloroplasts (Shoshan & Strotmann, 1980) and in *P. denitrificans* (Zharova & Vinogradov, 2006), the ATP synthase affinity for P_i may depend on the extent of the protonmotive force.

Both the P_i -inhibition of hydrolysis and the P_i -induced enhancement of coupling efficiency were lost in our system when the ADP concentration was drastically lowered by the presence of high amounts of the ADP-trapping PK (Figs. 3.4.1. and 3.6.1.), indicating that these P_i effects were strictly dependent on the occupancy of a very high affinity binding site for ADP. The ADP requirement for the P_i -inhibition of hydrolysis is in agreement with the results obtained in the isolated and reconstituted EF_0F_1 (Fischer et al., 2000).

Chapter 4.

RESULTS

4.1. Purity and concentration of the ATP synthase.

The ATP synthase of *Escherichia coli* has been purified by using the methods described in §2.7.2. we decided to measure the purity of the sucrose gradient fraction enriched with ATP synthase Fig. 4.1. shows an SDS PAGE analysis of two different dilution of purified F_0F_1 (fraction n°7). By comparison of the bands from the F_0F_1 samples and the ones of the marker it was possible to recognize on the gel all the subunits of the enzyme, as indicated in Fig.4.1. The purity of the protein preparation was estimated, as described in §2.7.5., from the ratio of the sum of the ATP synthase bands and the total band intensity. This densitometric analysis suggested that the F_0F_1 constituted about 40% of the total proteins (Fig.4.1.2.). By considering this purity the concentration of purified F_0F_1 was 0.6mg/ml.

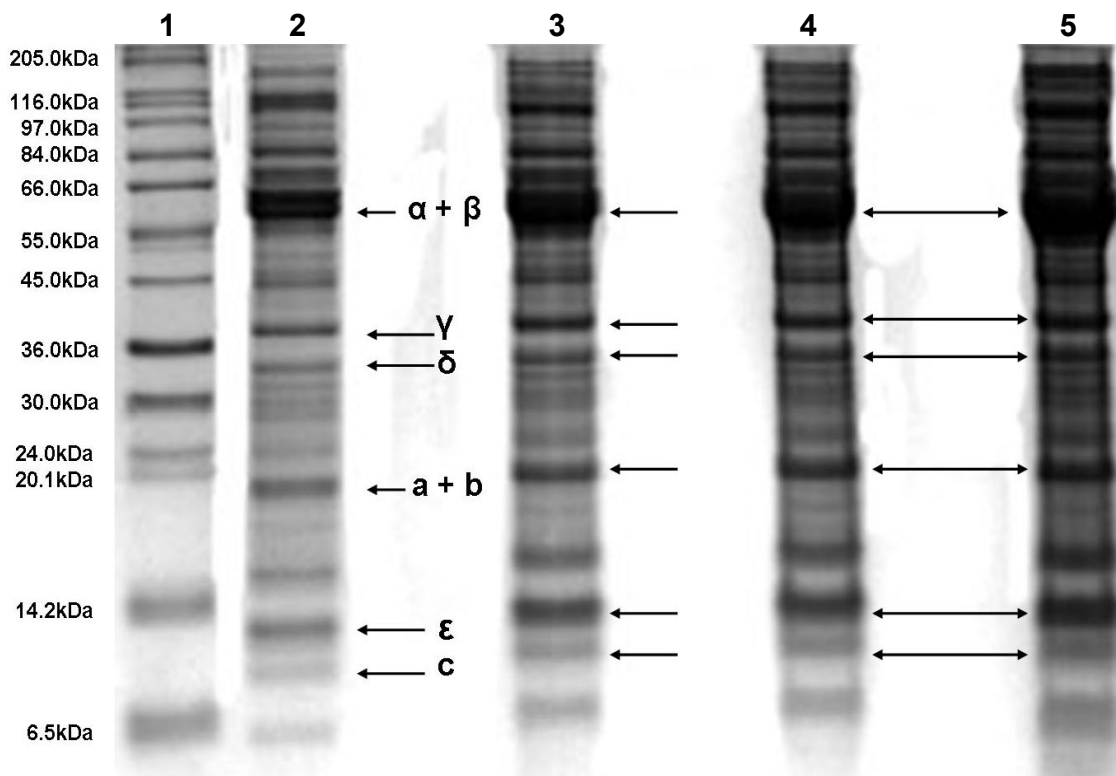


Fig.4.1.1. SDS/PAGE analysis of four different fractions of purified F_0F_1 from *E. coli*.

Proteins were separated on a 15%-polyacrylamide gel and stained with Coomassie Blue R-250.

Lane 1, molecular-mass markers (kDa) ; lane 2, purified F_0F_1 from fraction6 of Sucrose gradient; lane3, purified F_0F_1 from fraction7 of Sucrose gradient; lane 4, purified F_0F_1 from fraction8 of Sucrose gradient; lane 5, purified F_0F_1 from fraction9 of Sucrose gradient . The different subunits of the ATP synthase are indicated by arrows.

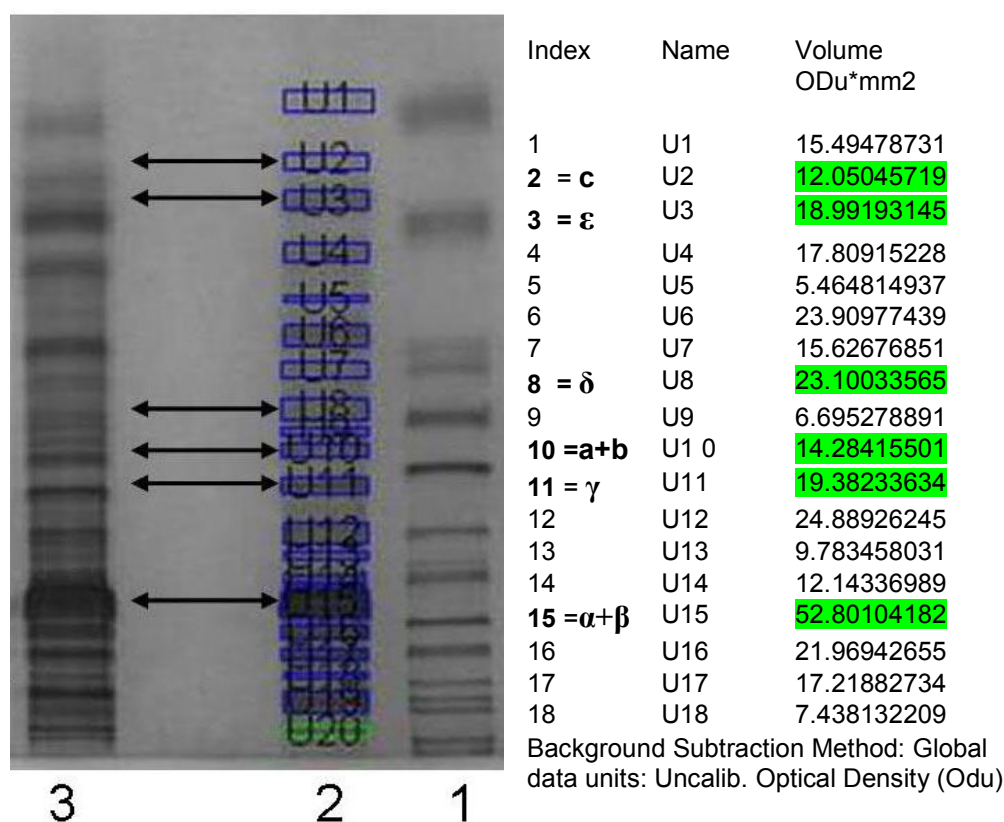


Fig.4.1.2. Densitometric analysis of the protein bands on the gel.

Lane 1,2,3 are from Fig.4.1.1. The purity of the protein preparation was estimated by the ratio of the sum of the ATP synthase bands and the total band intensity, from lane2:

Volume of the sum of the ATP synthase bands = 141.419 ODu*mm2; Volume of the total band = 358.969 ODu*mm2; EF₀F₁ Purity = 141.419/358.969*100 = 40%

4.2. Proton Pumping, ATP hydrolysis rate and ATP synthesis rate in the presence of different protein-to-lipid ratios during the reconstitution.

We measured in parallel both the ATP hydrolysis rate and the ATP synthesis rate and the proton pumping by liposomes containing different protein-to-lipid ratio, in order to check the proper working of our proteoliposomes. Different reconstitutions were set up, containing different protein-to-lipid ratios; the volume of added liposomes was kept constant, while the volume of F₀F₁ was varied, ranging from 2 up to 60 μl (or, in terms of F₀F₁ concentration, ranging from 0.1 up to 305 nM F₀F₁). Each assay contained the same amount of vesicles (expressed as phospholipid concentration, 2.31 μmoles of phospholipid).

4.2.1. Proton pumping.

The proton translocating activity of the ATP synthase was estimated using the ACMA assay. The fluorescence measurements were carried out under the same experimental conditions described in §2.5.

The 0 % signal was recorded in absence of ACMA, and was due to the scattering of the measuring beam; the 100% fluorescent was recorded at the end of the assay after addition of 1 μM nigericin. The fluorescence data were expressed as percentage of the 100-0% fluorescence difference.

Fig. 4.2.1. shows the ACMA fluorescence as a function of time in the presence of different F_0F_1 concentrations. The concentration of F_0F_1 in every sample was calculated by considering: **a)** the concentration of purified F_0F_1 estimated by Bradford (1.4mg/ml; §2.10.1.), **b)** the purity (40%), **c)** the volume of F_0F_1 added in every reconstitution of 200 μl (ranging from 0 up to 60 μl), **d)** the volume of proteoliposomes added in every sample of 2ml (20 μl). After starting the proton transport reaction by addition of 50 μM ATP at $t=0$ s, a fluorescence quenching was observed in all cases, indicating an acidification of the vesicles' interior, which settled to a steady state quenching level within 1–2 min, and could be reversed by the addition of nigericin. Notably, both the initial rate and the steady state quenching were increased in the presence of increasing F_0F_1 concentrations. No significant fluorescence quenching was detected in the absence of F_0F_1 (black plot in fig 4.2.1.), in samples where the reconstitution was carried out with F_0F_1 concentration below 50nM and in samples pre-treated with DCCD (not shown).

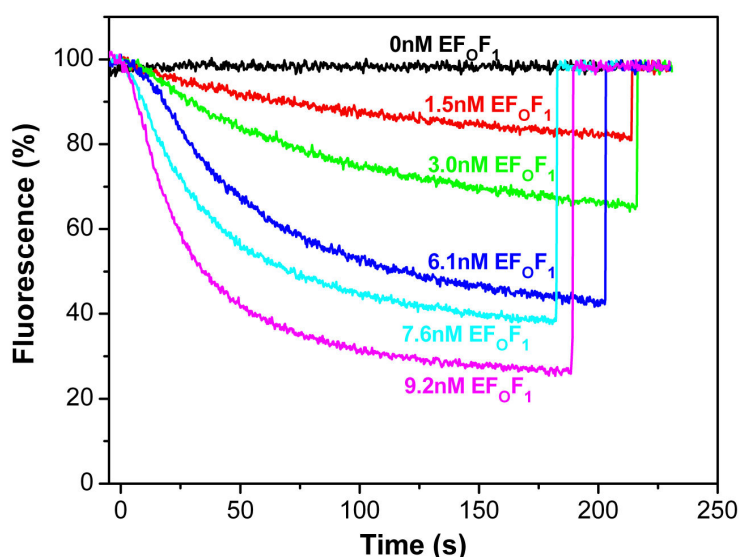


Fig. 4.2.1. ACMA fluorescence quenching as a function of time.

The ACMA assay was carried out as described in the §2.5.

The proton pumping reaction was started in the spectrofluorimeter cuvette by addition of 50 μM ATP at time $t=0$ s and the ACMA fluorescence was recorded as a function of time. Different EF_0F_1 concentration were added to each assay as indicated. For each trace, addition of 1 μM nigericin recovered the 100% fluorescence level.

In Fig. 4.2.2. A,B both the initial rate and the steady state (at $t=100$ s) values of fluorescence quenching were plotted as a function of the F_0F_1 concentration. The plots show that, in our reconstitution system, both the rate and the steady state of proton pumping increase by increasing the protein-to-lipid ratio. The increase of the initial rate is not linear. This result can be predicted since at low protein-to-vesicle ratios, the fraction of vesicles devoid of ATP synthase is not negligible (see below Fig.4.4.1.), and that fraction will not contribute to establish a ΔpH and therefore a fluorescence quenching.

The linearity of the steady state of quenching as a function of the concentration of F_0F_1 (Fig.4.2.2.B) can be considered as resulting from a combination of the non linear trend shown by the initial rate of quenching (Fig.4.2.2.A) and a compensating non-linear trend shown in the regions of the function which links Q and ΔpH (see Fig.4.5.3.).

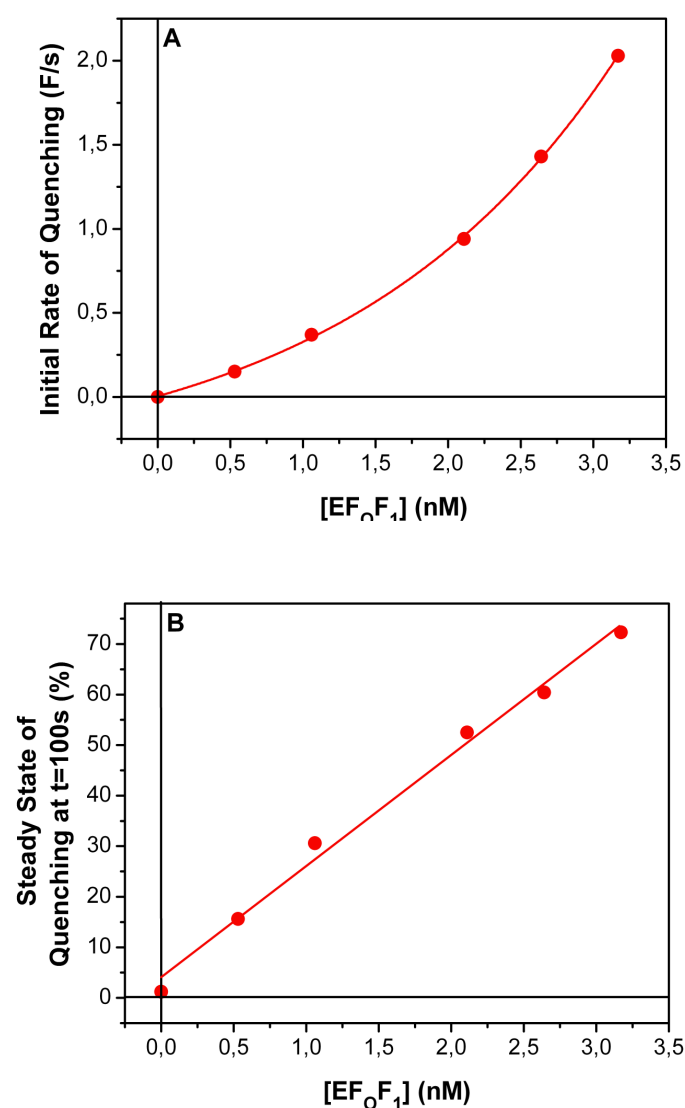


Fig.4.2.2. Initial rate (A,) and steady state at $t=100$ s (B,) of quenching as a function of EF_0F_1 concentration.

Panel A. The values of the initial rates of fluorescence quenching are from Fig.4.2.1. The curve through the quenching data points is a best fitting arbitrary function to guide the eye.

Panel B. The values of fluorescence quenching at $t=100$ are from Fig.4.2.1. The curve through the quenching data points was best fitted by linear function.

4.2.2. ATP hydrolysis rate

The rate of ATP hydrolysis was estimated using the Phenol Red assay. The hydrolysis measurements were carried out under the same experimental conditions described in §2.2.1.

Fig. 4.2.3.A shows the amount of hydrolyzed ATP as a function of time in the presence of different F_0F_1 concentrations. The concentration of F_0F_1 in every sample was calculated by considering the same assumptions reported in §4.2.1. The addition of 50 μM ATP started an increase in the absorbance, i.e. ATP hydrolysis, which was linear over the whole measuring time (100 s). The slope of the curves increased at increasing F_0F_1 concentrations. The DCCD insensitive activity was not significant (data not shown). The rates of ATP hydrolysis were evaluated by fitting the spectrophotometric data (collected at a rate of 1/s) with linear functions and were plotted as a function of the concentration of F_0F_1 (Fig.4.2.3.B). The plot clearly shows that the rate of hydrolysis increases linearly by increasing the protein-to-lipid ratio in the reconstitution, as expected, since the hydrolysis rate does not depend on the fraction of vesicles devoid of ATP synthases.

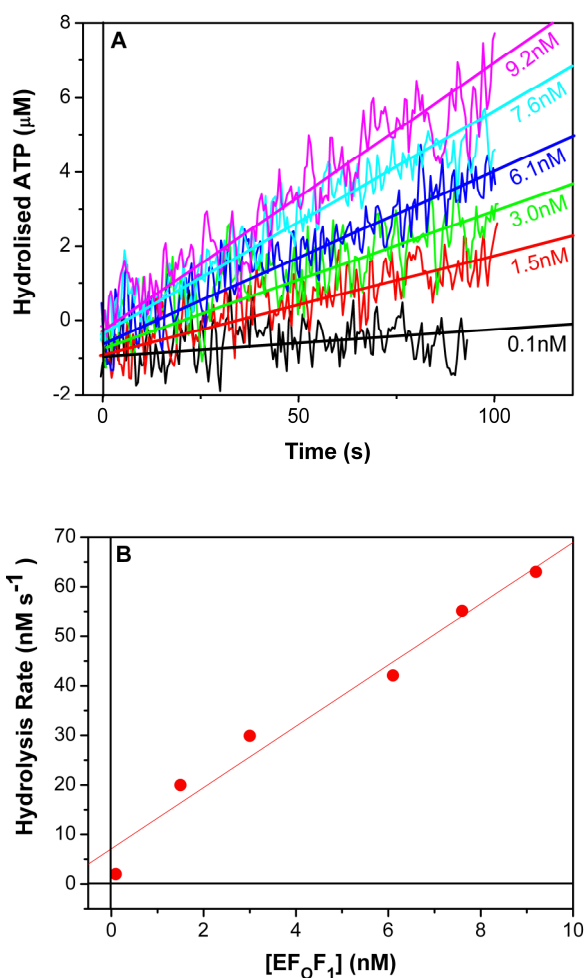


Fig.4.2.3. ATP hydrolysis rate as a function of EF_0F_1 concentration.

The ATP hydrolysis assay was carried out with Phenol Red as a pH indicator for the release of scalar protons as described in the §2.2.1.

Panel A. The ATP hydrolysis reaction was started at time $t=0$ s in the spectrophotometer by addition of 50 μM ATP and the absorbance (625–587 nm) was measured as a function of time. Absorbance values were converted to hydrolyzed ATP as described in the §2.2.1. Different EF_0F_1 concentrations were added to each assay as indicated.

Panel B. Rates of ATP hydrolysis are from Panel A and have been calculated from the fitting functions. The curve through the hydrolysis data points was best fitted by a linear function.

4.2.3. ATP synthesis

The ATP synthesis measurements were carried out under the following conditions. After reconstitution of the enzyme into phosphatidylcholine/phosphatidic acid (19 : 1) liposomes, the proteoliposomes were energized by a transmembrane pH difference (acid/base transition: $\text{pH}_{\text{out}} = 8.5$, $\text{pH}_{\text{in}} = 5.0$) and a K^+ /valinomycin diffusion potential ($[\text{K}^+]_{\text{out}} = 150$ mM, $[\text{K}^+]_{\text{in}} = 0.5$ mM) and ATP synthesis was measured with the luciferin/luciferase system as described in §2.8. In Fig.4.2.4. an example of an experimental curve, collected by using this measurement method, is depicted. After addition of F_0F_1 proteoliposomes preincubated in buffer LI to buffer LII, the luminescence intensity, i.e. the ATP concentration, increased linearly for nearly 1s and kept increasing for approximately 15s. The rate of ATP synthesis was calculated from the slope at $t = 0$. The slope was calculated after fitting the curve by an exponential function. In Fig.4.2.4. the initial rate of ATP synthesis was 110 nM ATP s^{-1} resulting in a turnover number of 17.5s^{-1} , since the final enzyme concentration was 6.3 nM. The calculation of the turnover number is based on the following assumptions: **a)** the molar mass is 530 kg \cdot mol $^{-1}$; **b)** the enzyme preparation is 40% pure; **c)** all added F_0F_1 is reconstituted; **d)** all reconstituted F_0F_1 molecules are orientated so that the ADP and P_i binding sites are directed to the medium (outside). After a few seconds, the rate declined due to the decrease of the driving force, reaching a final ATP concentration of 320 nM after about 40 s. This corresponds to an average value of 51 turnovers for each F_0F_1 molecule present in the proteoliposomes. No ATP synthesis was observed in the absence of any pH difference obtained by titration of buffer LI to pH 8.8 (data not shown), indicating that ATP is generated by a proton-transport-coupled synthesis reaction catalyzed by F_0F_1 reconstituted into liposomes.

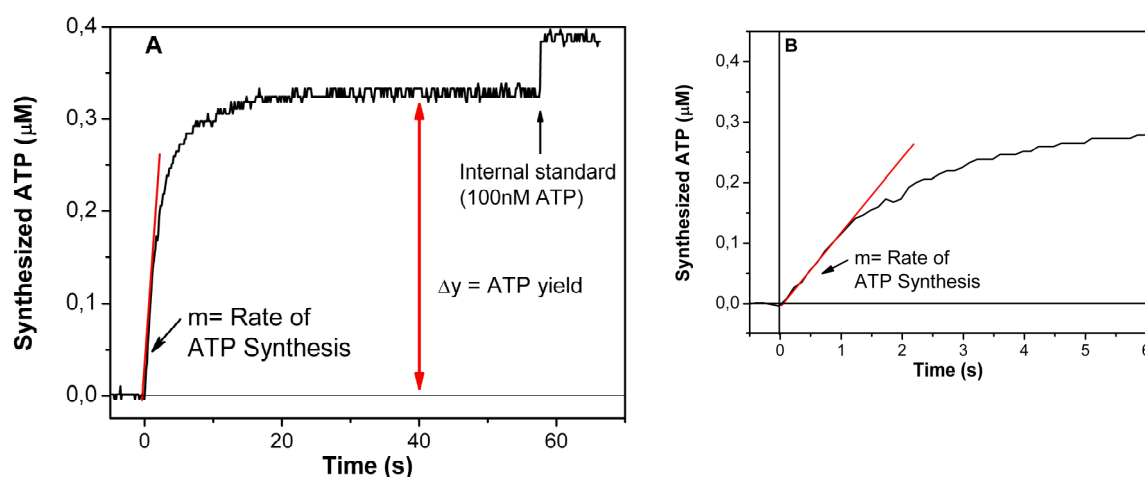


Fig.4.2.4. $\Delta\tilde{\mu}_{\text{H}^+}$ driven ATP synthesis catalyzed by EF_0F_1 proteoliposomes of *E. coli*.

The preparation of the EF_0F_1 liposomes and the ATP synthesis reaction were performed as described in §2.7. and §2.8. Panel A. the rate of ATP synthesis was monitored continuously with the luciferin/luciferase system in a luminometer. The basic medium LII contained luciferin/luciferase, 0.1 mM ADP and 5 mM P_i . At time zero the proteoliposomes in LI were injected; after a reaction time of 60 s the signal was calibrated by addition of an ADP standard solution. Luminescence intensity values were converted to hydrolyzed ATP as described in the §2.8. Panel B. the graph was rescaled to show the initial rate of ATP synthesis.

The rate of ATP synthesis was then measured, as described, as a function of the ATPase concentration. Fig. 4.2.5.A shows the amount of synthesized ATP as a function of time in the presence of different F_0F_1 concentrations. The concentration of F_0F_1 in every sample was calculated by considering: **a)** the concentration of purified F_0F_1 estimated by Bradford method (1.4mg/ml) (§2.10.1.), **b)** the purity (40%), **c)** the volume of F_0F_1 added in every reconstitution of 200 μl (ranging from 2 up to 60 μl), **d)** the volume of proteoliposomes added in every sample of 1ml (30 μl).

Again, the rates of synthesis were calculated from the initial slopes and then were plotted as a function of the concentration of F_0F_1 (full circles in Fig.4.2.5.B). The plot shows that by increasing the protein-to-lipid ratio in the reconstitution, the rate of ATP synthesis increases linearly, indicating that the reconstitution efficiency, in the concentration range tested, did not depend on the lipid-to-protein ratio. Also the total yield of synthesized ATP increased linearly with the F_0F_1 concentration, as expected given the similar time interval in which synthesis occurs.

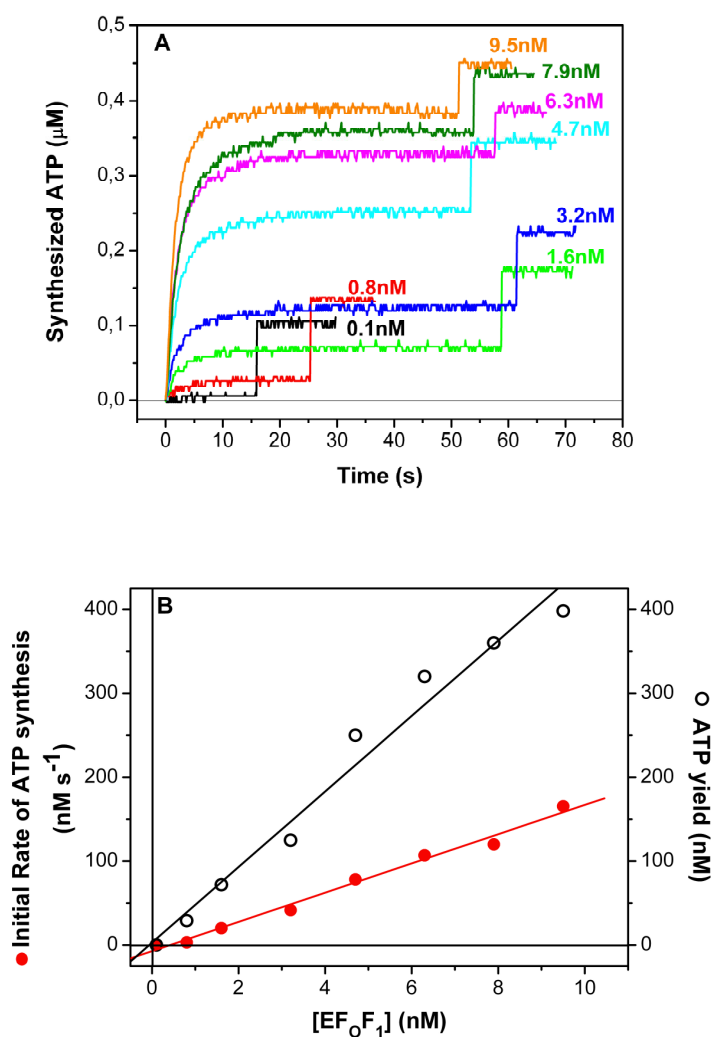


Fig.4.2.5. ATP synthesis as a function of EF_0F_1 concentration.

ATP synthesis was performed as described in §2.8. and in the legend of Fig. 4.2.4..

Panel A. Luminescence intensity values were converted to hydrolyzed ATP as described in §2.8. Different EF_0F_1 concentrations were added to each assay as indicated.

Panel B. The rate of ATP synthesis (●) were calculated from the initial slope of the curves from Panel A.. The maximum ATP yield (○) was the value of y at approximately $t = 40\text{s}$. The curves through the hydrolysis data points were best fitted by linear functions.

4.3. ATP hydrolysis and synthesis as a function of the average number of ATP synthases per liposome.

Under the assumptions which are reported in §4.2.3. we calculated the turnover number of the hydrolysis and synthesis data from Fig.4.2.3.B and 4.2.5.B respectively, by dividing each rate value by the corresponding concentration of F_0F_1 .

We then estimated the number of ATPase per liposomes for each reconstitution at different F_0F_1 concentration using the following calculations. We assumed for our liposomes an external diameter of 200 nm, (Zimmermann et al., 2005).

A vesicle with a diameter of 200 nm has a surface of $2.5 \times 10^5 \text{ nm}^2$ (inner plus outer surface). Assuming an area of $0.6 \text{ nm}^2/\text{lipid molecule}$ (Nagle & Wiener, 1988), each vesicle contains about

4.2×10^5 lipid molecules (Eq. (1) and (2)).

$$\text{Liposome surface}_{\text{ext+int}} = 2 \cdot (4 \cdot r^2 \cdot \pi) \quad \text{Eq. (1)}$$

where $r=100\text{nm}$ is the liposomes radius.

$$\frac{\text{Lipid molecules}}{\text{Liposome}} = \frac{\text{Liposome surface}}{\text{Lipid area}} \quad \text{Eq. (2)}$$

where lipid area= 0.6 nm^2 was taken from the literature (Zimmermann et al., 2005).

Using an average molecular mass of 780 Da for a lipid molecule, $100\mu\text{l}$ of liposomes with a lipid concentration of 18 g/l are equal to 2.31 μmoles of liposomes, and this corresponds to 3.31×10^{12} liposomes (Eq. (3) and (4)).

$$\text{Liposome}_{\text{moles}} = \frac{\text{lipids}_{\text{weight}}}{\text{lipids}_{\text{molecular mass}}} \quad \text{Eq. (3)}$$

where the $\text{lipids}_{\text{weight}}$ was calculated from the volume of liposomes added in the reconstitution (0.1ml) and the lipid concentration of the liposome preparation (18mg/ml).

$$\text{Liposome}_{\text{number}} = \frac{\text{Liposome}_{\text{moles}} \cdot N_A}{\text{Lipid}_{\text{molecules}} \cdot \text{Liposome}} \quad \text{Eq. (4)}$$

where N_A is the number of Avogadro (6.022×10^{23}).

The different concentrations of F_0F_1 in the reconstitution mixture can be estimated on the basis of the concentration of purified F_0F_1 as estimated by the Bradford method (1.4mg/ml) (§1.10.1.), and of the purity, calculated as described in §4.1, which was 40%.

The resulting moles of ATP synthase were divided by the number of liposomes present in the reconstitution. This ratio gives the number of ATPase per liposome, when the enzyme concentration is varied at constant lipid concentration.

4.4. Poisson distribution of ATP synthases/vesicle.

Reconstituted proteoliposomes offer the opportunity for a quantitative analysis of the proton pumping, since the ACMA response can be calibrated as a function of a pH difference induced by an acid-base transition. The utilization of such calibration curves requires the absence of vesicles devoid of ATP synthase, since they will respond to the imposed ΔpH but will not contribute to an ACMA fluorescence change due to ATP hydrolysis coupled proton pumping.

Assuming a Poisson distribution of ATP synthases, the probability of the presence of a given number (x) of ATP synthase molecules per vesicle can be predicted for different values of the average number of the ATPase per vesicle (n), according to the equation:

$$P(x,n) = \frac{n^x e^{-n}}{x!} \quad \text{Eq. (5)}$$

The distribution shown in Fig. 4.4.1. demonstrates that the probability of containing liposomes completely deprived of ATP synthase, within the population of reconstituted vesicles containing an average of 1,2 and 3 ATP synthase / vesicle, is respectively 37.0%, 13.7% and 5.2%.

Therefore, in order to reduce this probability to values lower than 5% , the average number of ATP synthase /vesicle must exceed 3.

On this basis, vesicles containing 3.5 ATP synthases (corresponding to 317nM in terms of F_0F_1 concentration in the reconstitution mixture) were systematically utilized in the subsequent experiments.

It is interesting to note that the results shown in Fig. 4.2.2.A are consistent with this theoretical calculation, since a lack of linearity of the initial rate of quenching as a function of the ATP synthase concentration is evident up to approximately 1 ATP synthase per vesicle (corresponding to a concentration of 3nM in the quenching assay).

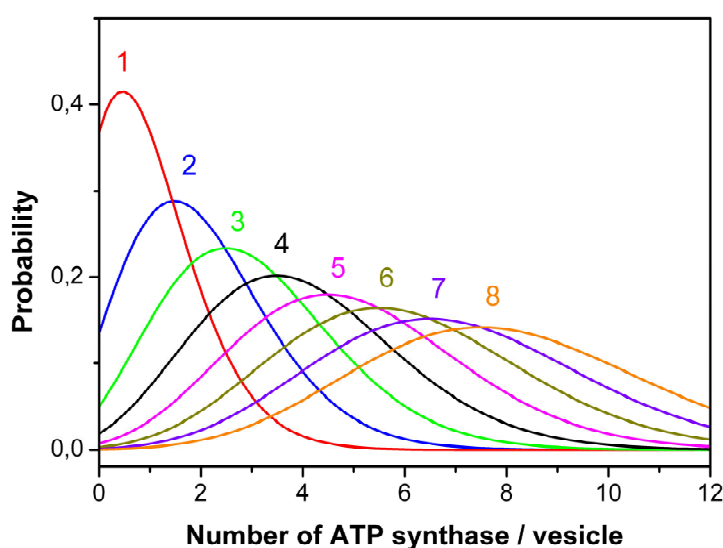


Fig.4.4.1. Poisson distribution ATP synthase/vesicle at different average number of ATP-synthase/vesicle.
The probability $P(x,n)$ of having x ATPase per vesicle, was calculated by using the equation (5).

4.5. Calibration of the ACMA response in proteoliposomes.

Fluorescent amine have been largely used to detect a transmembrane proton concentration difference (ΔpH_{i-o}) in natural and artificial membrane systems in which direct measurements are generally precluded by the small dimensions of the inner osmotic volume. The model for an interpretation of energy-dependent fluorescence changes was originally proposed by Schuldiner et al.(1972). This model assumes that amines behave ideally, are freely permeable through the membrane phase in their neutral form and re-distribute between the inner and outer aqueous compartments following the protonation-deprotonation equilibria which occur upon the generation of a trans-membrane ΔpH (acidic inside). In the case of fluorescent amines, this equilibrium re-distribution is associated with a quenching of their fluorescence (Q) which, according to the model, would be promoted by accumulation of the probe in the inner aqueous compartment. This notion is based on the observation that the fluorescence is restored to its original level when the transmembrane ΔpH is dissipated by effectors such as uncoupling agents, ionophores and specific inhibitors of proton pumping.

On the basis of these assumption, for monoamine of high pK_a ($pK_a \gg pH_i, pH_o$), ΔpH is therefore determined as:

$$\Delta pH_{i-o} = \text{Log}\left(\frac{C_i}{C_o}\right) = \text{Log}\left(\frac{Q}{100-Q}\right) + \text{Log}\left(\frac{V_o}{V_i}\right) \quad \text{Eq.(6)}$$

Where C_i and C_o are the concentrations of the amine in the inner V_i and outer V_o aqueous compartments respectively, and Q is the percentage quenching of fluorescence.

This model has been tested over an extended period of time, the conclusion of these experiments was that the probe behaves non-ideally, especially when it concentrates within the inner compartment of a vesicle system. In particular the empirical V_o/V_i value extrapolated from the experimental data was unreasonably high.

The model by Schuldiner et al. (1972) has been modified by Casadio (1991), who considered also the partition of ACMA, a particularly lipophilic probe, into the lipid phase and the differential partition equilibria on the inner and outer liposome faces, exposed to different pH values of the inner and outer aqueous phases. In this modified model the amine distribution in the two aqueous phases follows the protonation equilibria, as in Schuldiner et al.(1972):

$$pH_i = -\text{Log}\left(\frac{C_i}{C_o} \cdot (10^{-pH_o} + 10^{-pK_a}) - 10^{-pK_a}\right) \quad \text{Eq.(7)}$$

while at both the inner and outer membrane interfaces the partition equilibrium obeys the isotherm:

$$C_{o,i} = K_A \cdot \left(\frac{\sigma S_{o,i}}{\sigma_{\max} S_{o,i} - \sigma S_{o,i}}\right) \cdot e^{\left(\frac{\sigma S_{o,i}}{\sigma_{\max} S_{o,i} - \sigma S_{o,i}} + D \cdot \sigma S_{o,i}\right)} \quad \text{Eq.(8)}$$

where

$C_{o,i}$ is the concentration of the amine free in the aqueous volumes V_o and V_i ;

σ is the surface density of the amine;

$S_{o,i}$ are the adsorbing surfaces of the outer and inner membrane;

K_a , σ_{max} and D are three parameters of the adsorption isotherm of the amine.

If the adsorption isotherm is assumed to be identical on both faces of the membrane and the residual fluorescence is assumed to be a measure of the amine present in the outer aqueous phase (being the amine adsorbed in the lipid totally quenched and the amine present in the inner aqueous phase contributing very little to the total fluorescence due to the very small internal volume), a complex equation can be written that can be solved only numerically.

However the response of ACMA can be obtained empirically by imposing a known ΔpH and measuring the quenching response the data thus obtained can be fitted with the following equation, which reflects the protonation and partition equilibria:

$$\Delta pH = pH_i - pH_o = A \cdot \frac{Q}{B-Q} e^{\left(\frac{Q}{B-Q} + C \cdot Q\right)} \quad \text{Eq. (9)}$$

where the three empirical fitting parameters A, B and C are related to the three parameters defining the adsorption isotherm.

4.5.1. Calibration of the quenching of ACMA fluorescence in terms of ΔpH 's of known extents.

When acid/base transitions are imposed on the assay medium containing known concentrations of ACMA and proteoliposomes, a transitory quenching of the fluorescence of the probe is detected (Fig. 4.5.1.). The fluorescence intensity keeps increasing until, after about 150s, the quenching is completely relaxed. Addition of nigericine 1 μ M at this point in time had no effect on ACMA fluorescence. Addition of Nigericine prior to the pH transition prevented the transient quenching of fluorescence (orange trace in Fig. 4.5.1.). Under these conditions, however, a fluorescence change was still observable; this change was due to the different quantum yield of ACMA at different pH values. Therefore the fluorescent intensity after nigericine addition was considered as the 100% fluorescence intensity recorded at the pH of the outside buffer and in the absence of ΔpH .

A collection of traces obtained at different values of ΔpH (i.e. at variable inside pH's and constant outside pH= 8.0) and normalized to 100% fluorescence is shown in Fig. 4.5.2..

The maximum extent of quenching, measured when the imposed ΔpH had not been dissipated by passive proton fluxes, increases for increasing ΔpH values indicating that the response of ACMA fluorescence is an increasing function of ΔpH .

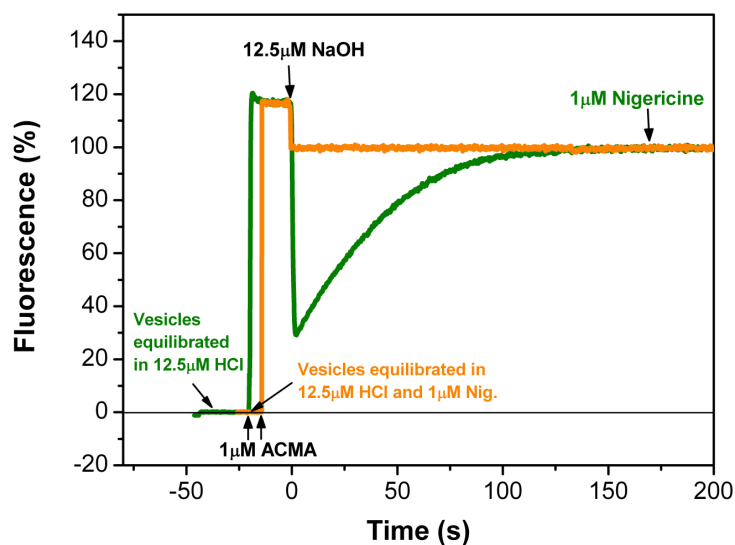


Fig.4.5.1. Reversible decrease of the ACMA fluorescence upon energization by acid-base transition.

The acid-base transition was performed as described in § 2.9..

After addition of NaOH, the alkalization of the external medium relative to the internal aqueous compartment of the proteoliposomes, determines a rapid transient ΔpH and consequently a quenching of the ACMA fluorescence that is fully decayed within 150s.

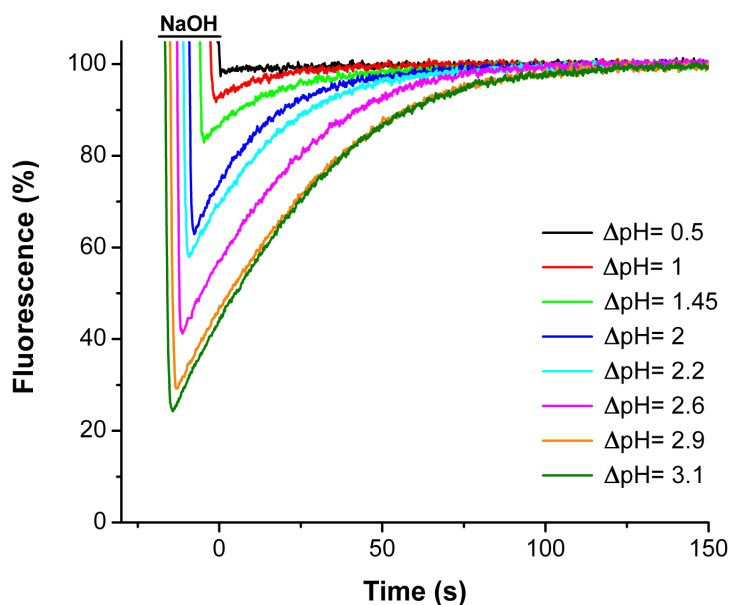


Fig.4.5.2. Time course of the transient quenching signal of the ACMA fluorescence in suspensions of proteoliposomes exposed to artificially induced ΔpH 's of different extent.

The acid base transitions were performed as described in § 2.9..

The traces are displaced along the time axis for clarity..

The values of the fluorescence quenching measured at different imposed ΔpH are shown in Fig.4.5.3. as a function of the imposed ΔpH value. These data constitute a calibration of the ACMA response to ΔpH and were utilized for the empirical determination of parameter A, B and C in Equation (9). In Fig. 4.5.3. the data points were fitted utilizing the Equation (9), thereby following the model of Casadio described above. The experimental data points could be fitted very well by the sigmoidal trend described by Equation (9), indicating that they are consistent with the model of Casadio.

This calibration curve and the fitting equation were utilized for converting the quenching data into the corresponding values of pH_{in} , resulting from ATP hydrolysis-coupled proton pumping in liposomes containing ATP synthase.

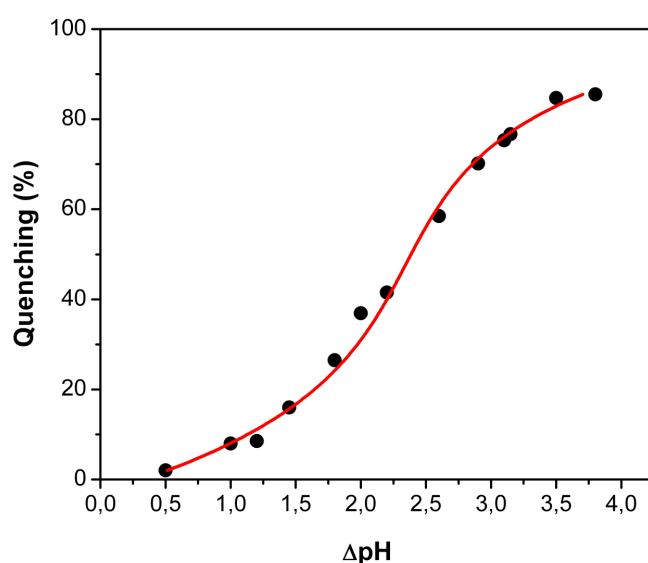


Fig.4.5.3. Dependence of the quenching of ACMA fluorescence on ΔpH .

The ACMA quenching values are from Fig.4.5.2. and additional not shown measurements.

Each value of ACMA quenching measured after the imposed pH transition was plotted as function of the corresponding calculated ΔpH . The red curve corresponds to the fitting equation (9):

$$\Delta\text{pH} = \text{pH}_i - \text{pH}_o = A \cdot \frac{Q}{B-Q} e^{\left(\frac{Q}{B-Q} + C \cdot Q\right)}$$

The values of the fitting parameter are $A=19.24623 \pm 0$, $B=149.12463 \pm 6.11294$, $C=-0.03831 \pm 0.0023$.

4.6. Discussion

The data of the present work show that our reconstitution method gave well energized proteoliposomes as demonstrated by their high rates of ATP synthesis, and by their high ACMA fluorescence quenching (Figs.4.2.1. and 4.2.5.).

Moreover the presence of a negligible amount of vesicles devoid of ATP synthase, as evaluated by Poisson distribution, enabled the use of the calibration of ACMA response in proteoliposomes, obtained by acid-to-base transitions, for a quantitative evaluation of the proton pumping data in chapter 5.

Chapter 5.

RESULTS

5.1. Functional studies in the isolated and reconstituted EF₀F₁

In Chapter 3 we have showed that low concentrations of ADP and P_i inhibit the rate of ATP hydrolysis by the ATP synthase in *E. coli* internal membranes, while at the same time increasing the rate of inward proton translocation. We decided to check if the same phenomena were still present in our reconstituted system, in which the possibility of interference by other *E. coli* enzymes is highly unlikely. Moreover, since in these proteoliposomes it has been possible to calibrate empirically the ACMA response to ΔpH (Chapter 4.), we were in a position to analyze the proton pumping data, obtained by ACMA fluorescence assay, in a more quantitative way.

5.2. Effect of P_i on ATP hydrolysis and proton pumping.

Inorganic phosphate monotonically inhibited the ATP hydrolysis of ATP synthase in *E. coli* membranes with an apparent K_d of 150 μM (D'Alessandro et al., 2008). Therefore, we first measured ATP hydrolysis as a function of P_i, to check whether this trend could be reproduced in the isolated, reconstituted EF₀F₁. Fig. 5.2.1.A shows the amount of hydrolyzed ATP as a function of time after addition at t=0 s of 50 μMATP, in the presence of increasing P_i concentrations; valinomycin and 50 mM K⁺ were also present, in order to carry out the experiment under the same conditions used in the ACMA assay (see below). The hydrolysis rates were largely linear over the measured range. They decreased by increasing P_i concentrations. By plotting the rate from Fig. 5.2.1.A as a function of P_i, an hyperbolic trend is obtained (Fig. 5.2.1.B), with a half-maximal effect at [P_i]=440μM. The residual activity after DCCD inhibition was not detectable (data not shown).

The proton translocating activity was estimated using the ΔpH probe ACMA under the same experimental conditions. The ionophore valinomycin and 50 mM K⁺ were present in order to minimize the electrical component of the protonmotive force.

Fig. 5.2.2. shows the ACMA fluorescence as a function of time and in the presence of increasing P_i. In contrast to the inhibitory trend observed for hydrolysis, increasing amounts of added P_i, up to 200μM, induced an increase both of the initial rate (Fig. 5.2.2.B) and of the average steady state value of ACMA fluorescence quenching (Fig. 5.2.2.A), indicating that P_i induced an increase in the rate of the inward proton flux, in spite of the fact that it decreased the rate of ATP hydrolysis.

When higher P_i concentrations were added (up to 3 mM), both the initial rate and the average steady-state level of quenching were decreased. Under these conditions the strong reduction of the hydrolysis rate overcame the stimulating effect of P_i on the proton pumping.

The experimental results of Fig. 5.2.1 and Fig. 5.2.2 are summarized and compared in Fig. 5.2.3., which clearly shows that the ATP hydrolysis rates decrease monotonically as a function of P_i (red circles), whereas the initial rates and the steady state values of

fluorescence quenching are biphasic, first increasing at $[P_i] < 200 \mu\text{M}$ and then decreasing (respectively open and full black circles).

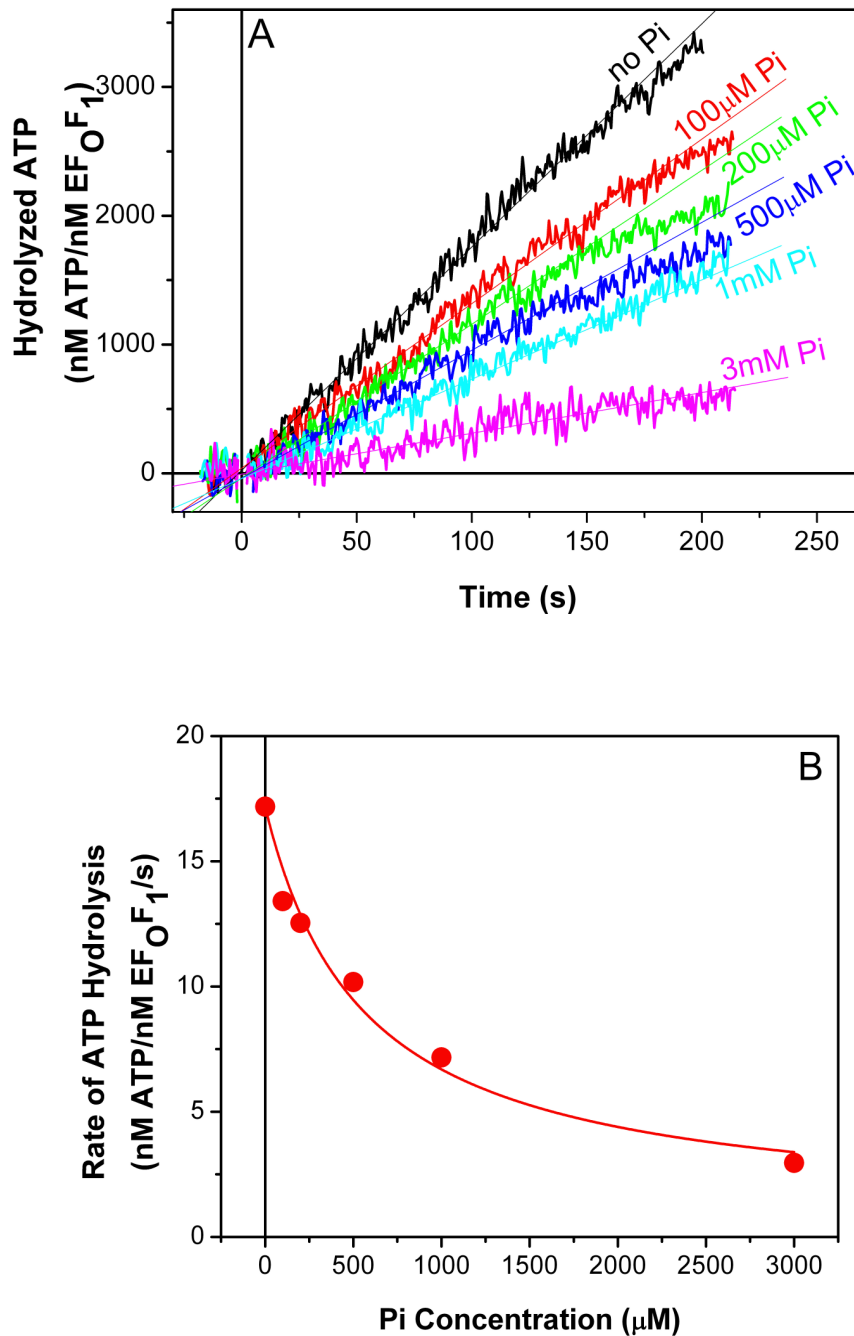


Fig. 5.2.1. ATP hydrolysis rate as a function of P_i concentration.

The ATP hydrolysis assay was carried out with Phenol Red as a pH indicator for the release of scalar protons as described in §2.2.1.

Panel A. The ATP hydrolysis reaction was started at time $t=0$ s in the spectrophotometer by addition of $50 \mu\text{M}$ ATP and the absorbance ($625\text{--}587$ nm) was measured as a function of time. Absorbance values were converted to hydrolyzed ATP as described in the §2.2.1. Different P_i concentrations were added to each assay as indicated. The experimental traces were best fitted by linear functions up to 100 s.

Panel B. Rates of ATP hydrolysis (●) are from Panel A; the curve through the ATP hydrolysis data points was the best fit to the data of the hyperbolic function $P1 - P2 \cdot x / (P3 + x)$, with resulting best fit parameter $P3 = 440 \pm 120 \mu\text{M}$ (●), corresponding to the apparent K_d value.

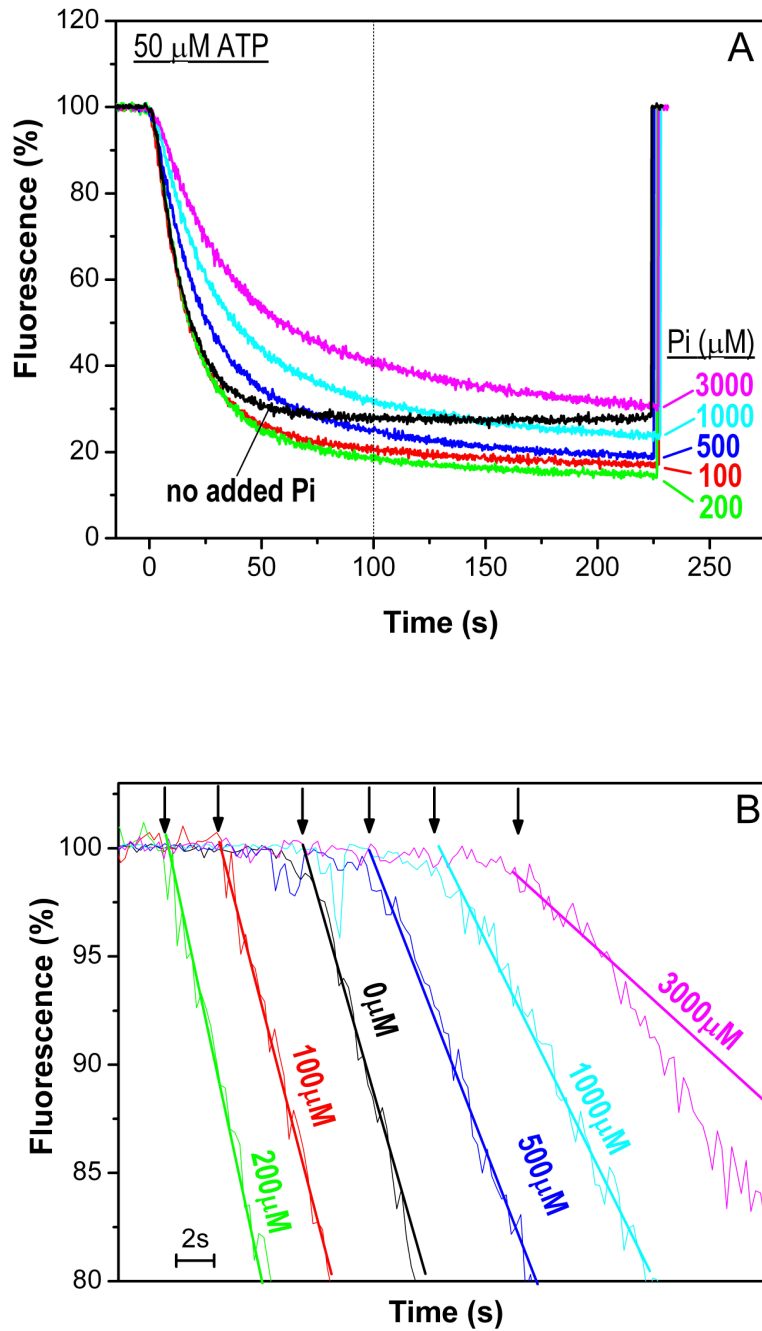


Fig. 5.2.2. ACMA fluorescence quenching as a function of P_i concentration.

The ACMA assay was carried out as described in §2.5..

Panel A., The proton pumping reaction was started in the spectrofluorimeter cuvette by addition of 50 μ M ATP at time $t=0$ s and the ACMA fluorescence was recorded as a function of time. Different P_i concentrations were added to each assay as indicated. For each trace, addition of 1 μ M nigericine recovered the 100% fluorescence level.

Panel B. The traces in (A) are reported here on a shorter time scale and displaced along the time axis for showing the initial rates of quenching. The arrows indicate the time points of ATP addition, the numbers the P_i concentrations. The linear fits were calculated over 1 (0–200 μ M P_i) or 2 (0.5–3 mM P_i) s of reaction (5 or 9 data points).

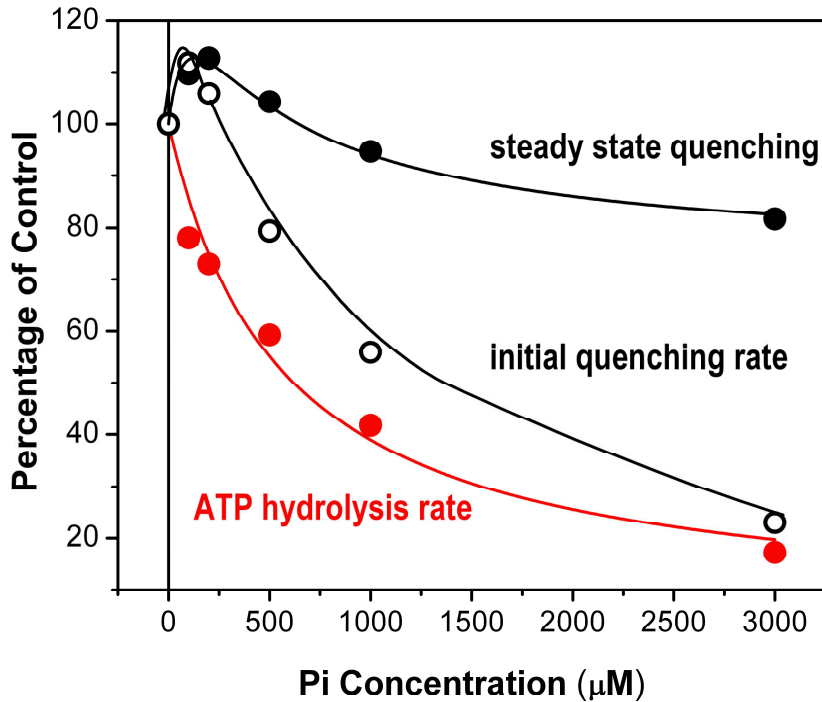


Fig. 5.2.3. ACMA fluorescence quenching and ATP hydrolysis as a function of [Pi].

The percentage values of the initial rates of fluorescence quenching (\circ) relative to controls ($3.4\% \cdot s^{-1}$) were determined from (Fig.5.2.2.B). The percentage values of fluorescence quenching at $t=100$ s (\bullet) relative to controls (72.2%) were determined from (Fig.5.2.2.A). The curves through the quenching data points were drawn by hand. The percentage values of the rate of ATP hydrolysis (\bullet) relative to controls ($17.2 \cdot nM \text{ ATP} \cdot nM \text{ EF}_0\text{F}_1 \cdot s^{-1}$) were determined from (Fig.5.2.1.) and were reported for comparison. The curve through the ATP hydrolysis data points was the best fit to the data of the hyperbolic function described in Fig. 5.2.1B.

5.2.1. Conversion of the quenching values into $\Delta p\text{H}$ and $[\text{H}^+]_{\text{in}}$ values.

Based on the calibration of the ACMA response to $\Delta p\text{H}$ (§ 4.5.), we converted the fluorescence values from Fig. 5.2.2 into quenching values, $\Delta p\text{H}$ values and $[\text{H}^+]_{\text{in}}$ values (respectively Fig. 5.2.4.A, B and C).

Fig. 5.2.4.B and C show that the $\Delta p\text{H}$ and the $[\text{H}^+]_{\text{in}}$ at first increase and then decrease at higher P_i concentration.

We measured the steady state $\Delta p\text{H}$ after 100s the addition of ATP and the initial rate of internal acidification ($\Delta p\text{H}$ formation); both these values were plotted as a function of added P_i (respectively full and open black circles in Fig.5.2.5.). In the same figure the hydrolysis rates from Fig. 5.2.1.B are also reported for comparison (red circles). This plot, similarly to the plot of Fig. 5.2.3., again highlights a strong contradiction since the rate of hydrolysis and the rate of internal proton concentration should run in parallel, but they diverge.

In our opinion, this result can be explained only by assuming that the P_i -induced increase of the ATP-driven inward proton flux rate, observed in spite of the P_i -induced decrease of the ATP hydrolysis rate, is due to an increase in the number of protons transported per hydrolyzed ATP. As for the ATP synthase in the internal membranes (Chapter 3.), we can conclude that by increasing the P_i concentration also the isolated and reconstituted enzyme reaches a state of higher coupling efficiency.

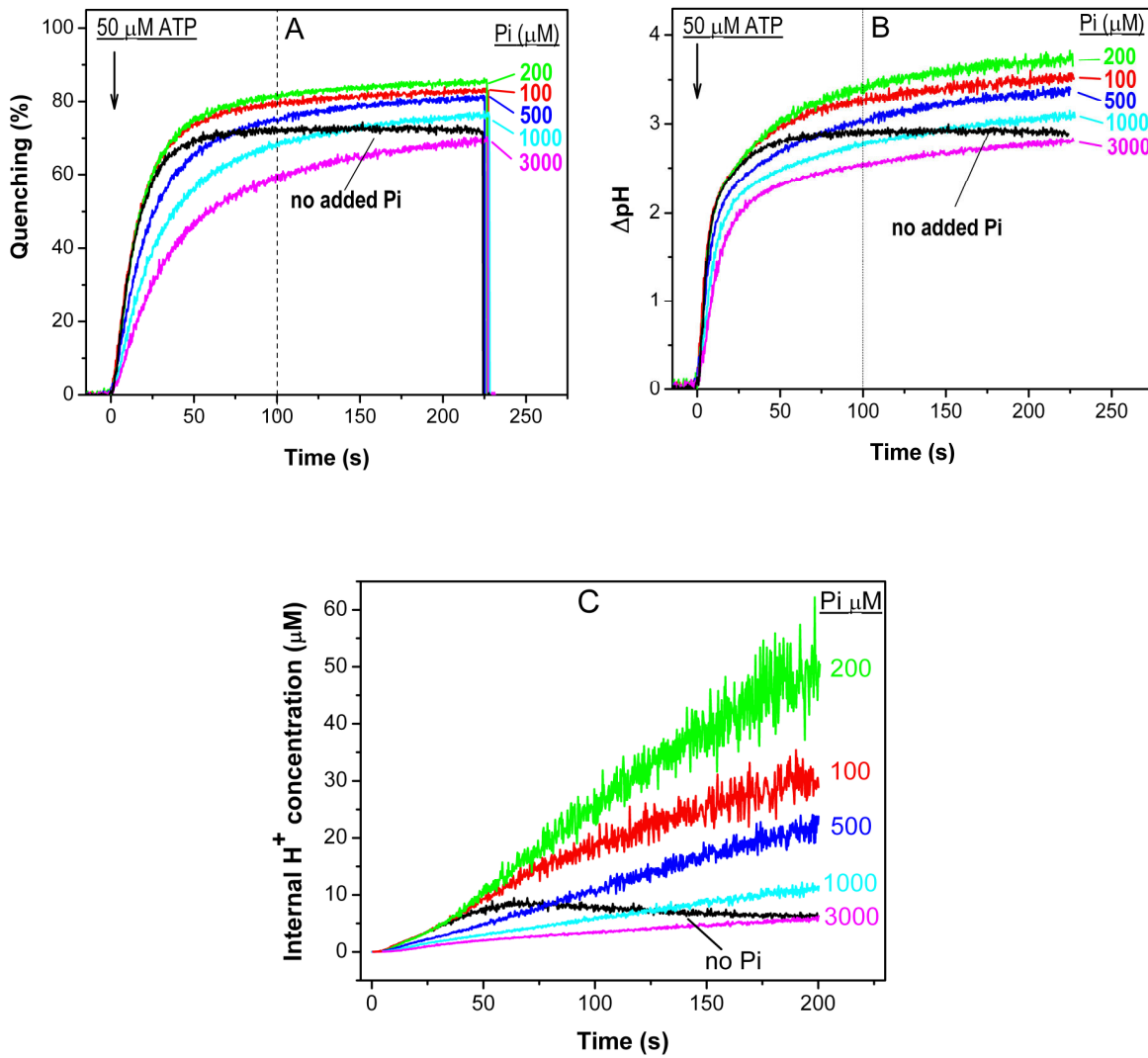


Fig. 5.2.4. Quenching (A), ΔpH (B) and internal proton concentration (C) as a function of time in the presence of different P_i concentration.

Panel A., the ACMA fluorescence traces from Fig.5.2.2.A. were transformed into the corresponding quenching traces through the following equation: $Q\% = 100\% - F\%$.

Panel B., the quenching traces from Panel A. were transformed into the corresponding ΔpH traces through the correspondent fitting equation obtained from the ACMA calibration curve (Eq. (9) in §4.5.1.):

$$\Delta pH = pH_i - pH_o = A \cdot \frac{Q}{B - Q} e^{\left(\frac{Q}{B - Q} + C \cdot Q\right)}$$

with $A=19.24623$, $B=149.12463$, $C=-0.03831$.

Panel C, ΔpH traces from Panel B. were transformed into the corresponding internal proton concentration traces through the following steps:

1. $pH_{int} = 8 - \Delta pH$
2. $[H^+]_{int} = 10^{-pH_{int}}$

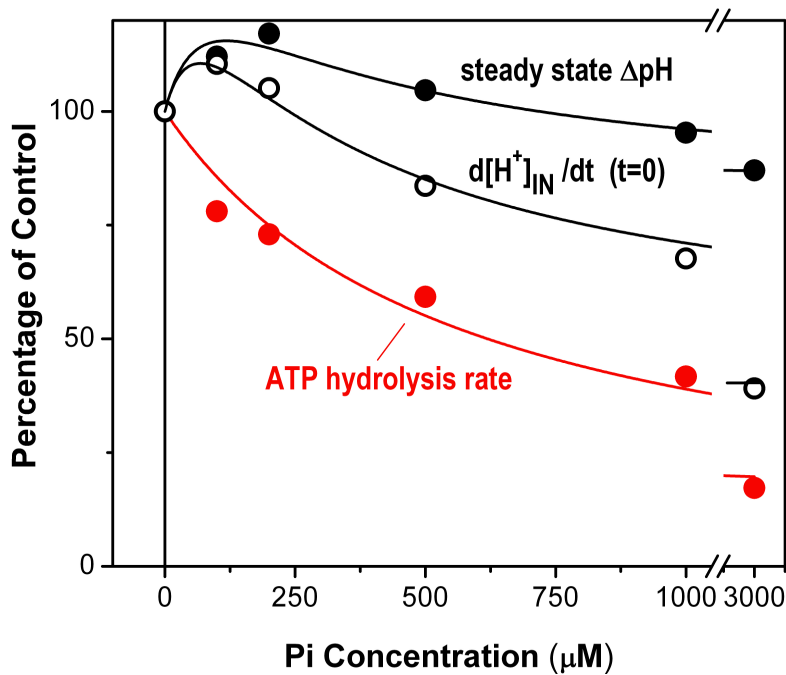


Fig. 5.2.5. ΔpH and ATP hydrolysis as a function of [Pi].

The percentage values of the initial rates of internal acidification (○) relative to controls (0.4 units of $\text{pH} \cdot \text{s}^{-1}$ or $4.0 \text{ nM}[\text{H}^+]_{\text{in}} \cdot \text{s}^{-1}$) and the percentage values of steady state ΔpH at $t=100 \text{ s}$ (●) relative to controls (2.9 units of pH) were determined from (Fig.5.2.4.B). The curves through the quenching data points were drawn by hand. The percentage values of the rate of ATP hydrolysis (●) relative to controls ($17.2 \cdot \text{nM ATP} \cdot \text{nM EF}_0\text{F}_1 \cdot \text{s}^{-1}$) were determined from (Fig.5.2.1.) and were reported for comparison. The curve through the ATP hydrolysis data points was the best fit to the data of the hyperbolic function described in Fig. 5.2.1B.

5.2.2. Quantitative evaluation of the uncoupling degree induced by P_i depletion

In order to evaluate quantitatively the degree of uncoupling induced by P_i depletion, we converted the rates of internal pH changes into rates of $[\text{H}^+]_{\text{in}}$. In order to obtain the real value of translocated protons per hydrolysed ATP, one would need to know the internal buffer capacity and the total internal volume of the vesicles. However, in the absence of a determination of these two parameters, one can determine relative values, which will be proportional to the real ones and will constitute an estimation of the degree by which the H^+/ATP stoichiometry is decreased, relative to the H^+/ATP stoichiometry of the fully coupled enzyme. The real value of such stoichiometry is still controversial, since in *E. coli* a stoichiometry of 10 c subunits has been reported (Jiang et al., 2001), which would imply an H^+/ATP stoichiometry of 3.3, but also a value of 4 has been obtained from thermodynamic measurements (Steigmiller et al., 2008).

Tab.5.2.1. collects, for each P_i concentration, the ratios of the initial rates of $[\text{H}^+]_{\text{in}}$ translocation over the initial rate of ATP hydrolysis, and the relative values of these ratios for H^+/ATP equal to 3.3 and 4 respectively. In this calculations the state of the enzyme at 3mM P_i has been considered to be a state of full coupling.

Tab.5.2.1. Quantitative evaluation of the uncoupling degree induced by P_i depletion

The initial rate of H⁺ translocation (V[H⁺]_{in}) were obtained by converting the initial rate of ΔpH formation in the following way:

$$\frac{d[H^+]_{in}}{dt} = -[H^+]_{in} \cdot \frac{dpH_{in}}{dt} = -[H^+]_{in} \cdot \frac{\Delta pH_{in}}{dt}$$

where ΔpH/dt values are from Fig.5.2.5..

The initial rates of hydrolysis (V_{Hyd}) are from Fig.5.2.1. In the fifth column the ratios of V[H⁺]_{in}/V_{Hyd} have been referred to the V[H⁺]_{in}/V_{Hyd} value at 3mM P_i, at which value the enzyme has been considered fully coupled. In columns sixth and seventh the H⁺/ATP ratios for each P_i concentration have been calculated by assuming a fully coupled H⁺/ATP ratio of 3.3 or 4.0 respectively.

[P _i]	V[H ⁺] _{in} (d[H ⁺] _{in} /dt, at t=0)	V _{Hyd}	V[H ⁺] _{in} /V _{Hyd}	0.01 / V[H ⁺] _{in} /V _{Hyd}	3.3 / 0.01 / V[H ⁺] _{in} /V _{Hyd}	4 / 0.01 / V[H ⁺] _{in} /V _{Hyd}
μM	nM H ⁺ /s	nMATP/s	nMH ⁺ /nMATP			
0	0.25	54.46	0.0046	2.27	1.45	1.76
100	0.28	42.51	0.0066	1.60	2.06	2.49
200	0.27	39.75	0.0067	1.57	2.09	2.54
500	0.21	32.27	0.0066	1.61	2.05	2.49
1000	0.17	22.73	0.0075	1.40	2.36	2.86
3000	0.10	9.38	0.0105	1.00	3.30	4.00

As evident from Tab.5.2.1., the calculated H⁺/ATP ratio is maximal at 3mM P_i and decreases monotonically as a function of decreasing P_i, up to a factor of nearly 2.3 at P_i=0, reaching values of 1.5 or 1.8, assuming fully coupled H⁺/ATP ratios of 3.3 or 4.0 respectively.

5.3. Evaluation of the ACMA response in proteoliposomes during ATP hydrolysis.

In order to show that the ACMA fluorescence rates measured at low P_i or ADP (see below) concentrations were not kinetically limited, we measured both ATP hydrolysis and proton pumping at increasing ATP concentrations (from 10 to 500μM ATP). Fig.5.3.1.A shows that the initial rates of ATP hydrolysis increased as a function of ATP concentration (black circles), with a K_M at 58 μM ATP. Fig. 5.3.1.B shows that also the initial rate of proton pumping increased with increasing amounts of ATP (black circles). The values from Fig. 5.2.1. and 5.2.2. are also reported (orange circles). The comparison shows that the ACMA quenching data obtained as a function of P_i were not limited by kinetic incompetence of the probe. The initial rate of quenching values were transformed in the initial rate of ΔpH formation and are reported as a function of ATP in Fig. 5.3.1.C together with the rate of ATP hydrolysis (respectively blue and black circles). This comparison shows that both the rate of ΔpH formation and the hydrolysis rate have a comparable K_M in the range of the experimental error, as it should be if the proton pumping efficiency does not vary as a function of ATP.

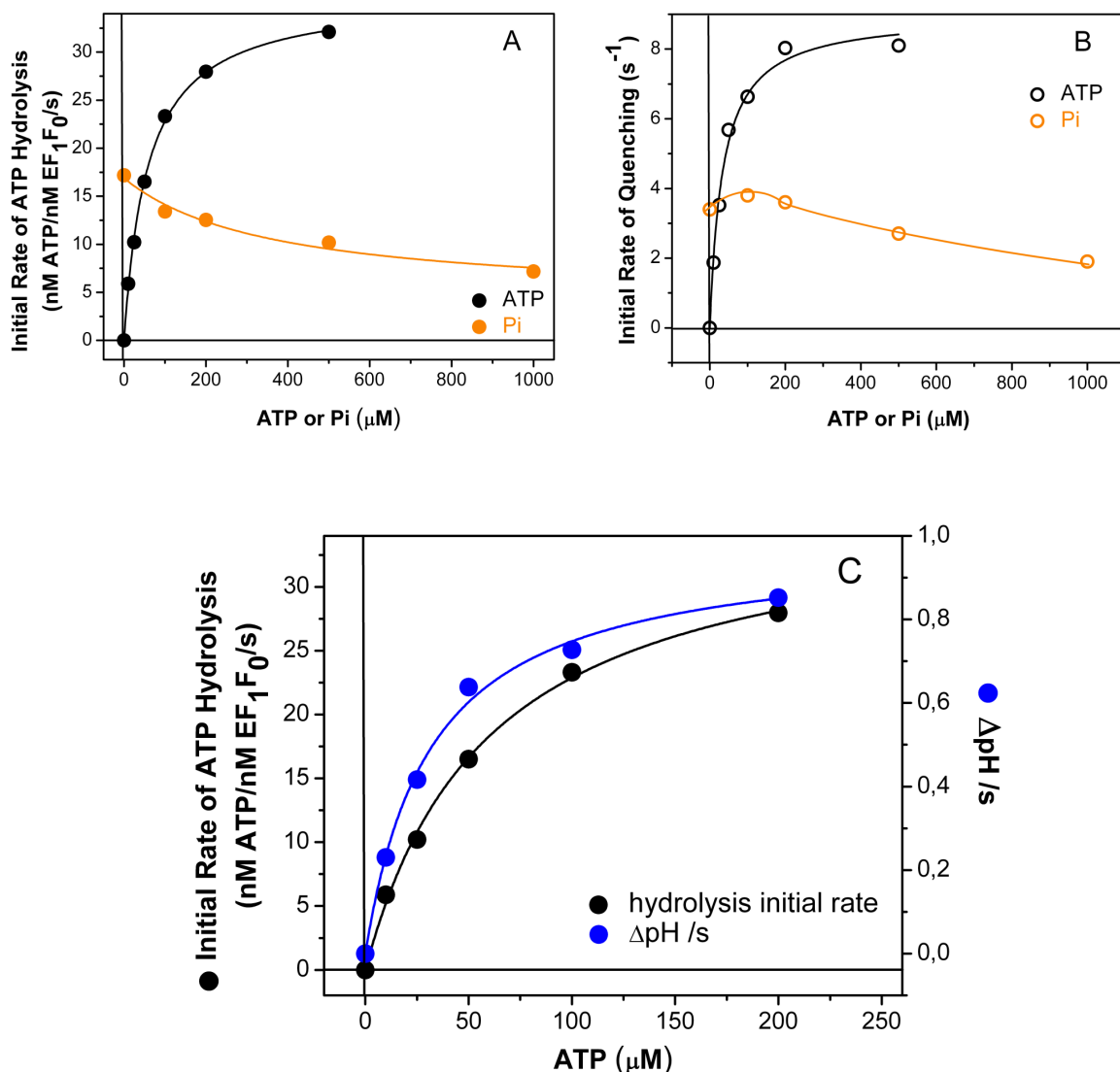


Fig. 5.3.1. Initial rates of ATP hydrolysis (A) and of ACMA quenching (B) as a function of ATP or P_i (P_i data are from Fig. 5.2.1. and Fig. 5.2.2.) and initial rates of ATP hydrolysis and ΔpH formation as a function of ATP (C).

Panel A., the curves through the hydrolysis data points were hyperbolic functions best fitted to the data. The K_M values for the hydrolysis reaction was $58 \pm 8 \mu\text{M ATP}$ (●) and the apparent K_d for [P_i] was $440 \pm 120 \mu\text{M}$ (○).

Panel B., for ATP data (○) the curves through the quenching data points was best fitted by an hyperbolic function with best-fitting K_M of $33 \pm 5 \mu\text{M ATP}$. For P_i data (○) the curve through the quenching data points was drawn by hand.

Panel C., ΔpH data have been calculated using the ACMA calibration function Eq.(9) from §4.5.1.:

$$\Delta pH = pH_i - pH_o = A \cdot \frac{Q}{B - Q} e^{\left(\frac{Q}{B - Q} + C \cdot Q\right)}$$

with $A=19.24623$, $B=149.12463$, $C=-0.03831$.

The curves through the hydrolysis data points were best fitted by hyperbolic functions. The K_M values were $58 \pm 8 \mu\text{M ATP}$ for the hydrolysis data (●) and $32 \pm 4 \mu\text{M}$ for the ΔpH data (●).

5.4. Effect of ADP depletion on ATP hydrolysis and proton pumping.

In Chapter 3, we have shown that the binding of ADP at very low concentrations induces in the ATP synthase a higher efficiency state, in which more protons per hydrolysed ATP are translocated across the membrane. Nevertheless, due to the very low ADP concentrations required, in *E. coli* membranes this phenomenon could be revealed only by pre-incubating the membranes with an ATP regenerating system acting as an ADP trap. Therefore, we checked whether the same phenomenon could be shown in the isolated, reconstituted EF_0F_1 .

At first we measured the rate of ATP hydrolysis as a function of different PK activities (i.e. of different steady-state [ADP]); we utilized the same conditions described in §3.4, except for the absence of KCN. The hydrolysis assay was carried out in the presence of LDH and NADH that coupled the ATPase reaction, through the PK reaction, to the absorbance changes at 340 nm. Fig. 5.4.1.A shows that at all the PK concentrations, addition of 50 μ M ATP started a decrease in the NADH absorbance, i.e. an increase in the hydrolysed ATP, which was linear over the whole measuring time (200 s). The hydrolysis rates were plotted in Fig. 5.4.1.B. as a function of all tested PK activities. The plot shows that increasing amounts of PK in the assay (i.e. decreasing amount of steady state [ADP]) increased the rate of ATP hydrolysis.

The ATP-driven ACMA fluorescence quenching were then measured under the same experimental conditions of 5.4.2.A.. The assay compositions were identical to those of Fig. 5.4.1.A except that LDH and NADH were omitted and ACMA was present. In the fluorescence traces shown in Fig. 5.4.2.A, the amount of PK added to the assay was progressively increased from 0 to 25 U/ml. After addition of 50 μ M ATP at $t=0$ s, a fast rate of fluorescence quenching was observed in all cases, which declined with time. Such decline was most pronounced in the case of no added PK, showing that substrate depletion and ADP accumulation contributed to this decline.

Both the initial rate of ACMA fluorescence quenching (Fig.5.4.2.B) and the extent of quenching, measured at $t=100$ s, (Fig.5.4.2.A) increased by the addition of small amounts of PK (2.5 U/ml), but decreased for larger amounts of added PK. In suitable controls it was shown that neither PEP alone nor PK alone, even at highest concentrations, affected the quenching, so that a direct effect of these reagents on the proteoliposomes permeability can be excluded (data not shown).

In Fig.5.4.3. we have summarized and compared the experimental results of Fig. 5.4.1 and Fig. 5.4.2.; both the initial rate of quenching and its steady-state value decreased when ADP was removed from the system (respectively open and full black circles), in contrast to the trend observed for the hydrolysis rates, which under the same conditions were stimulated (red circles).

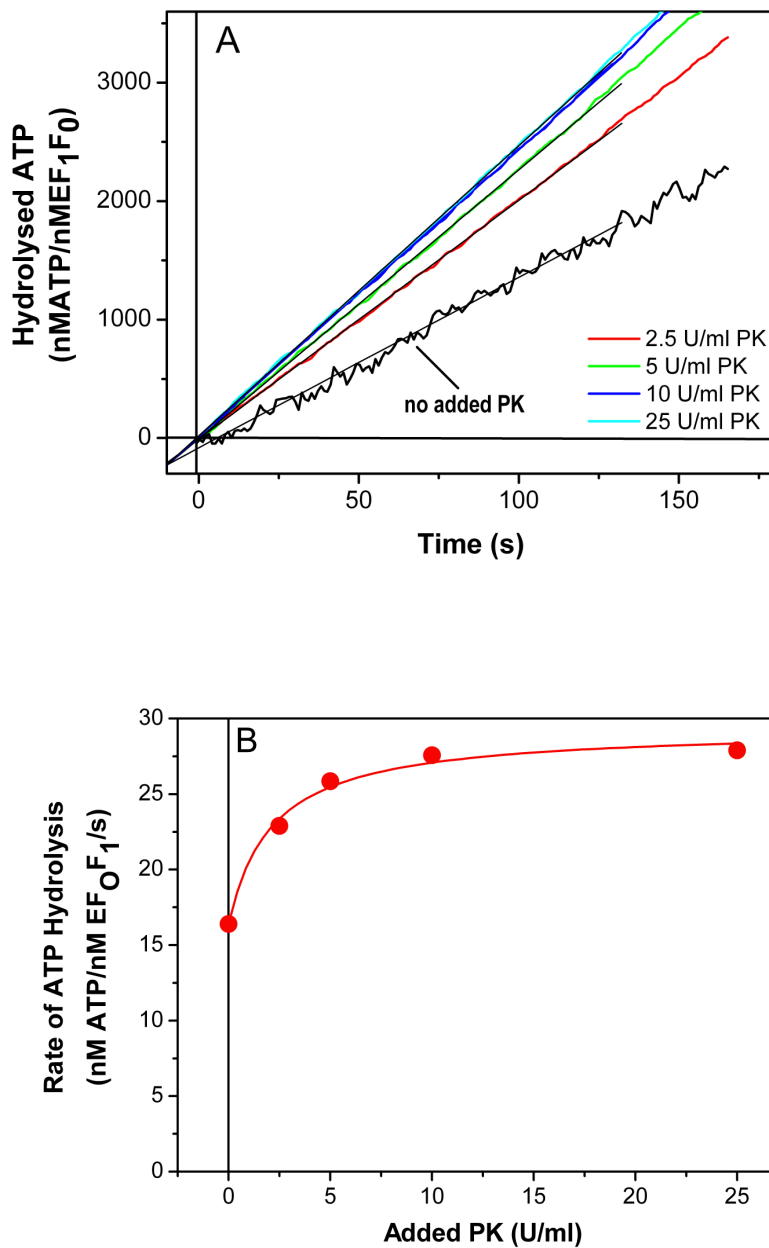


Fig. 5.4.1. ATP hydrolysis rate as a function of PK concentration.

The ATP hydrolysis assay was carried out with a PK ADP-trap coupled to the NADH oxidation as described in §2.2.2.

Panel A. The ATP hydrolysis reaction was started at time $t=0$ s in the spectrophotometer by addition of $50 \mu\text{M}$ ATP and the absorbance (340 nm) was measured as a function of time. Absorbance values were converted to hydrolyzed ATP as described in §2.2.2. Different PK activities were added to each assay as indicated. The experimental traces were best fitted by linear functions up to 100 s. The trace without added PK was measured with the Phenol Red assay.

Panel B. Rates of ATP hydrolysis are from Panel A, and have been calculated from the fitting functions. The curve through the hydrolysis data points is a best fitting arbitrary function drawn to guide the eye.

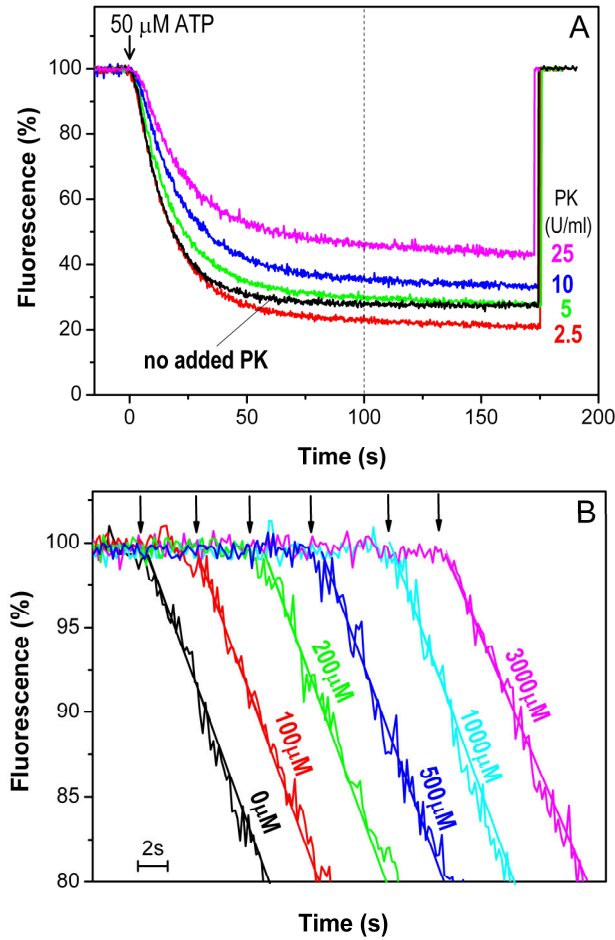


Fig. 5.4.2. ACMA fluorescence quenching in the presence of increasing PK activities.

Panel A. The ACMA assay was carried out as described in the legend of Fig. 5.2.2., but the reaction mixture contained in addition 2mMPEP and increasing activities of PK as indicated. Panel B. The traces from Panel A are reported on a shorter time scale and displaced along the time axis for showing the initial rates of quenching. The arrows indicate the time points of ATP addition. The linear fits were calculated over 2 s of reaction (9 data points).

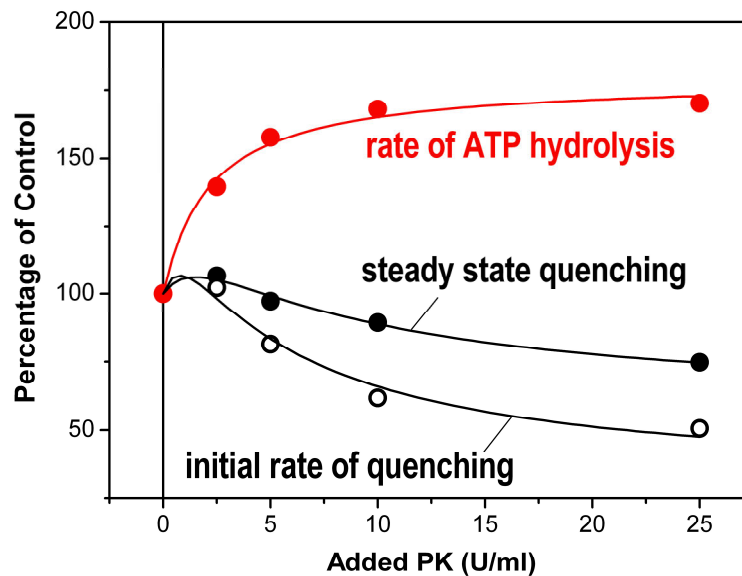


Fig. 5.4.3. ACMA fluorescence quenching and ATP hydrolysis as a function of PK activities.

The percentage values of the initial rates of fluorescence quenching (\circ) relative to controls ($3.6\% \cdot s^{-1}$) were determined from (Fig.5.4.2.B). The percentage values of fluorescence quenching at $t=100$ s (\bullet) relative to controls (72.2%) were determined from (Fig.5.4.2.A). The curves through the quenching data points were drawn by hand. The percentage values of the rate of ATP hydrolysis (\bullet) relative to controls ($16.4 \cdot nM \text{ ATP} \cdot nM \text{ EF}_0\text{F}_1 \cdot s^{-1}$) were determined from (Fig.5.4.1.) and were reported for comparison. The curve through the ATP hydrolysis data points is reported from Fig. 5.4.1B.

In Fig. 5.4.4.A and C the fluorescence values from Fig. 5.4.2. have been converted into ΔpH values and $[\text{H}^+]_{\text{in}}$ values respectively (see §4.5.); the biphasic trend observed, as a function of PK activity, in the fluorescence quenching data was maintained after conversion to ΔpH and to $[\text{H}^+]_{\text{in}}$. In Fig. 5.4.4.B the initial rate of internal acidification and the steady state ΔpH at $t=100\text{s}$ were plotted as a function of added PK (respectively open and full black circles). In the same figure the hydrolysis rates from Fig. 5.4.1.B are also reported for comparison (red circles). As already observed for the set of experiments obtained in the presence of different $[\text{Pi}]$, the rate of hydrolysis and the rate of internal proton concentration should run in parallel, but they totally diverge. In our view, this contradictory behaviour could be explained only by assuming that the removal of ADP induces in the enzyme a condition of intrinsic uncoupling.

5.4.1. Calculation of the ADP concentrations present at the different PK activities

As already described in §3.5., the ADP concentrations present at the different PK activities can be calculated by imposing a steady state concentration for ADP, in which its rate of production by the ATP hydrolysis reaction ($v_{(\text{hyd})}$) exactly balances the rate of ADP depletion by the PK ($v_{(\text{PK})}$).

In Fig.5.4.4.D, the initial rate of internal acidification, the steady state ΔpH at $t=100\text{s}$, and the hydrolysis rates values from Fig. 5.4.4.B are reported as a function of the corresponding ADP concentrations. This plot further confirms that at increasing ADP concentrations the enzyme reaches a state of higher coupling efficiency.

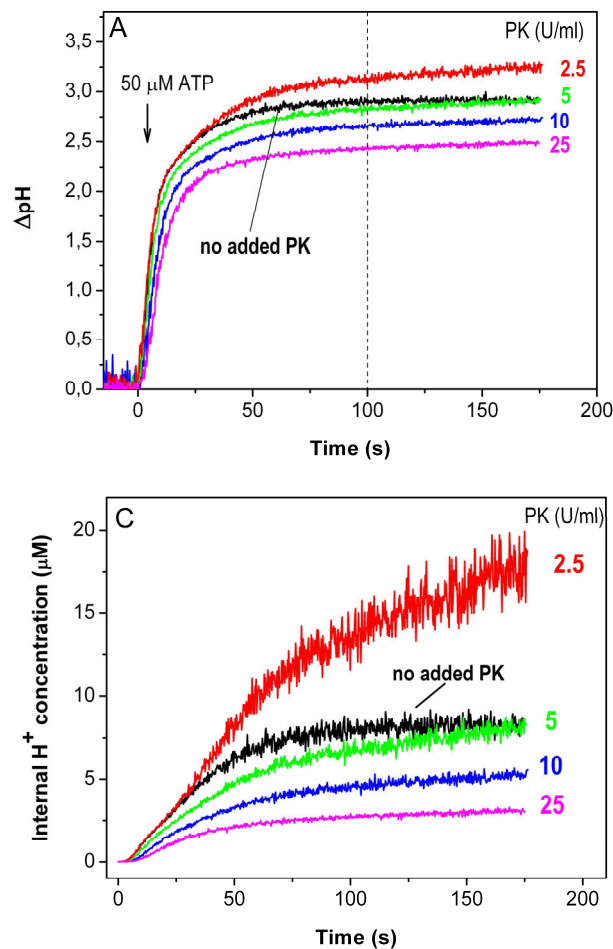


Fig. 5.4.4. A, C see next page for the full caption

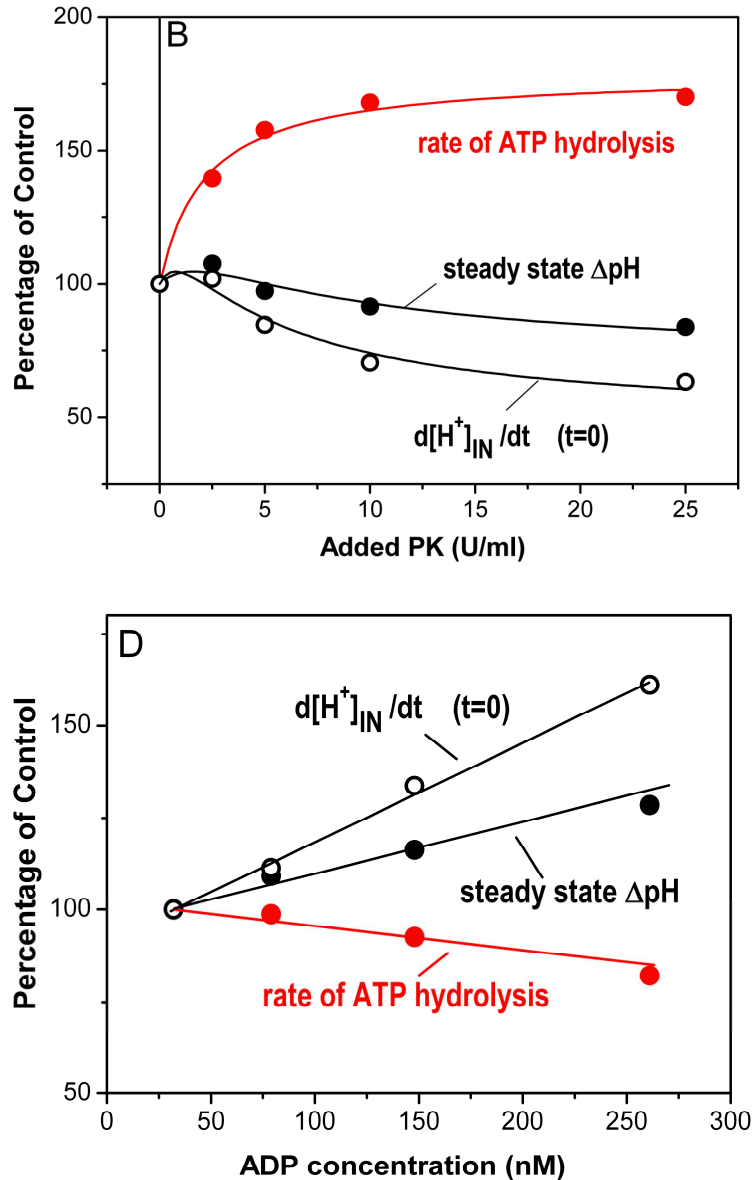


Fig. 5.4.4. ATP hydrolysis and proton pumping as a function of PK activity and of estimated steady-state ADP concentration .

Panel A., the ACMA fluorescence traces from Fig.5.4.2.A. were transformed into the corresponding ΔpH traces as described in the legend of Fig. 5.2.4.

Panel B., the percentage values of the initial rates of internal acidification (\circ) relative to controls (0.03 units of $\text{pH} \cdot \text{s}^{-1}$ or $0.3 \text{ nM}[\text{H}^+]_{\text{in}} \cdot \text{s}^{-1}$) and the percentage values of steady state ΔpH at $t=100 \text{ s}$ (\bullet) relative to controls (2.9 units of pH) were determined from Panel A. The curves through the quenching data points were drawn by hand. The percentage values of the rate of ATP hydrolysis (\bullet) relative to controls ($16.4 \cdot \text{nM ATP} \cdot \text{nM EF}_0\text{F}_1 \cdot \text{s}^{-1}$) were determined from (Fig.5.4.1.) and were reported for comparison. The curve through the ATP hydrolysis data points is reported from Fig. 5.4.1B.

Panel C, ΔpH traces from Panel A. were transformed into the corresponding internal proton concentration traces as described in the legend of Fig. 5.2.4.C.

Panel D, the steady state ADP concentration for each PK concentration was estimated as described in the text (see below, §5.4.1.). The percentage values of the initial rates of internal acidification (\circ) and the percentage values of steady state ΔpH at $t=100 \text{ s}$ (\bullet) relative to controls, i.e. to the values obtained at the lowest estimated ADP concentration (i.e. in the presence of 25 U/ml of PK) ($0.017 \text{ units of } \text{pH} \cdot \text{s}^{-1}$ or $0.17 \text{ nM}[\text{H}^+]_{\text{in}} \cdot \text{s}^{-1}$ and 2.43 units of pH , respectively), were determined from Panel A, and the values of the initial rates of ATP hydrolysis (\bullet) relative to control ($24.5 \text{ nM ATP} \cdot \text{nM EF}_0\text{F}_1 \cdot \text{s}^{-1}$) were determined from (Fig.5.4.1.). The curves through the data points were the best fit to the data of a hyperbolic function.

5.4.1.1. Measurement of the apparent K_M^{ADP}

In Chapter 3, the value of $K_M^{ADP} = 300\mu\text{M}$, taken from the literature, was utilized for calculation of $[\text{ADP}]_{\text{SS}}$ (§3.5). For the work presented in this chapter we decided to measure the K_M^{ADP} value directly, under the experimental conditions of our experiments. We have measured the K_M^{ADP} by coupling the ATP production from ADP to the NADH oxidation. The rate of disappearance of the reduced NADH is proportional to the Absorbance decrease at 340nm, measured by a spectrophotometer (see §2.5.). All experimental conditions, in terms of pH, temperature, PEP concentration, and buffer, were equal to those of our standard experiments. Every samples contained all the reagents used for the PK-ADP-trap assay (LDH 25U/ml, PEP 2mM, NADH 0.15mM) and ADP at different concentrations (from 0 up to 2mM).

The reaction was started by adding 0.03U/ml PK; the absorbance change at 340nm was followed in a spectrophotometer and was proportional to the production of ATP.

In Fig.5.4.5., $v_{(\text{PK})}$ is plotted as a function of ADP concentration. The resulting apparent K_M^{ADP} was $150\mu\text{M}$. The extrapolated V_{max}^{ADP} was $6.98\mu\text{M/s}$.

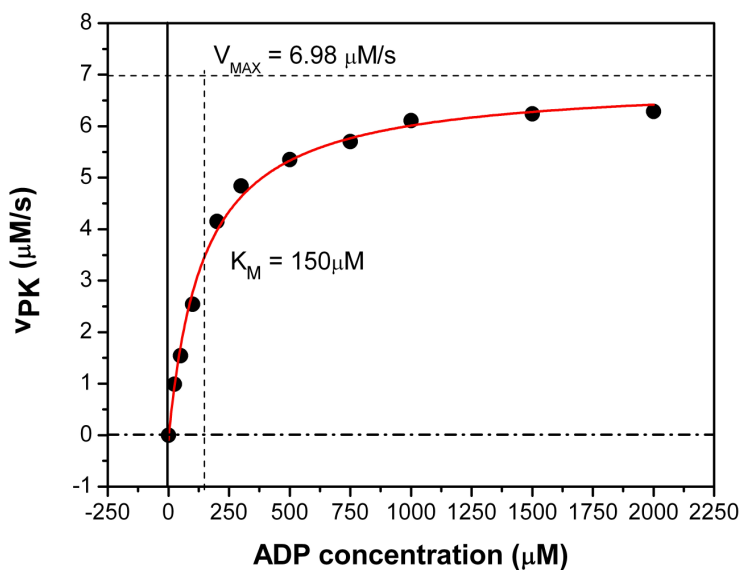


Fig.5.4.5. $v_{(\text{PK})}$ as a function of ADP concentration.

The curve through the data points was a best fitting hyperbole with apparent $K_d = 150 \pm 10\mu\text{M}$.

5.4.1.2. Measurement of competitive inhibition by ATP

To evaluate the inhibition constant for the competitive inhibition by ATP, K_i^{ATP} we have used the Dixon plot for competitive inhibition: $1/v_{(\text{PK})}$ versus $[\text{ATP}]$, (Segel, 1975).

The measurement of K_i^{ATP} was carried out under the same experimental conditions described in §2.4., except for the presence of ATP at different concentrations (from 0 up to 2mM). Moreover the concentration of added ADP was 100 μM in every sample.

The reaction was started by adding 0.03U/ml PK; the absorbance change at 340nm was followed in a spectrophotometer and was proportional to the production of ATP.

The $v_{(\text{PK})}$ for every sample were calculated and their reciprocal values were plotted as a function of ATP concentration. The curve through the data points yielded a straight line with positive slope (Fig.5.4.6.). We used the $V_{\text{max}}^{\text{ADP}}$ obtained as described in §3.5 to draw an horizontal line at $1/V_{\text{max}}^{\text{ADP}}$. The $-[I]$ value at the intersection of the two lines gives K_i as described in (Segel, 1975). The resulting K_i was 2mM. In our experiments the concentration of added ATP was not higher than 0.15mM, therefore we conclude that under our experimental conditions the competitive inhibition by ATP was negligible.

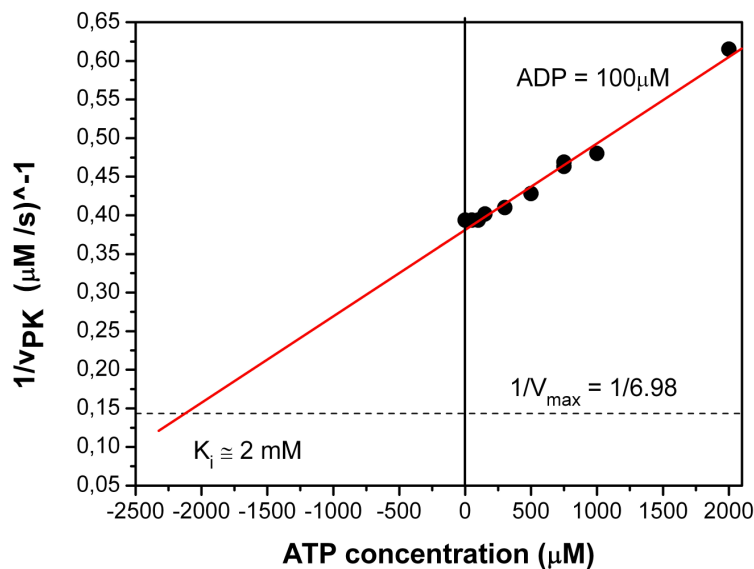


Fig. 5.4.6. $1/v_{(\text{PK})}$ as a function of ATP concentration.

The data points were best fitted by a linear function.

5.4.2. Quantitative evaluation of the uncoupling degree induced by ADP depletion

In order to evaluate quantitatively the degree of uncoupling induced by ADP depletion, we converted the rates of internal pH changes into rates of $[H^+]_{in}$ as described in §.5.2.2..

Tab.5.4.1. collects, for each PK activities, i.e. for each $[ADP]_{ss}$, the ratios of the initial rates of $[H^+]_{in}$ translocation over the initial rate of ATP hydrolysis, and the relative values of these ratios for H^+/ATP equal to 3.3 and 4 respectively. In this calculations the state of the enzyme in the absence of added PK has been considered to be a state of full coupling.

Tab.5.4.1. Quantitative evaluation of the uncoupling degree induced by ADP depletion

The initial rate of H^+ translocation ($V[H^+]_{in}$) were obtained by converting the initial rate of ΔpH formation in the following way:

$$\frac{d[H^+]_{in}}{dt} = -[H^+]_{in} \cdot \frac{dpH_{in}}{dt} = -[H^+]_{in} \cdot \frac{\Delta pH_{in}}{dt}$$

where $\Delta pH/dt$ values are from Fig.5.4.4.B.

The initial rates of hydrolysis (V_{Hyd}) are from Fig.5.4.1.B In the fifth column the ratios of $V[H^+]_{in}/V_{Hyd}$ have been referred to the $V[H^+]_{in}/V_{Hyd}$ value obtained in the absence of added PK, at which value the enzyme has been considered fully coupled. In columns sixth and seventh the H^+/ATP ratios for each PK (i.e.ADP) concentration have been calculated by assuming a fully coupled H^+/ATP ratio of 3.3 or 4.0 respectively.

PK	[ADP]	$V[H^+]_{in}$ ($d[H^+]_{in}/dt$ at $t=0$)	V_{Hyd}	$V[H^+]_{in}/V_{Hyd}$	0.05 / $V[H^+]_{in}/V_{Hyd}$	3.3 / 0.05 / $V[H^+]_{in}/V_{Hyd}$	4 / 0.05 / $V[H^+]_{in}/V_{Hyd}$
U/ml	nM	nM H^+ /s	nMATP/s	nM H^+ / nM ATP			
25	32	0.17	88.45	0.0019	2.69	1.23	1.49
10	79	0.18	87.37	0.0021	2.38	1.38	1.68
5	148	0.22	81.95	0.0027	1.86	1.77	2.15
2.5	261	0.27	72.57	0.0037	1.37	2.41	2.92
0	>500	0.26	51.99	0.0051	1.00	3.30	4.0

As evident from Tab.5.4.1., the calculated H^+/ATP ratio is maximal in the absence of added PK and decreases monotonically as a function of increasing PK (i.e. decreasing ADP), up to a factor of nearly 2.7 at $PK=25U/ml$ (or $ADP= 32nM$), reaching values of 1.2 or 1.5, assuming fully coupled H^+/ATP ratios of 3.3 or 4.0 respectively.

5.5. Effect of added ADP on ATP hydrolysis and proton pumping

Measurements similar to those described in § 5.2. and 5.4. were carried out in the presence of increasing concentrations of ADP. The results of both hydrolysis and proton pumping experiments are summarized in Fig.5.5.1.A.. The ATP hydrolysis rates (red circles) and the initial rate of ACMA fluorescence quenching (black open circles) decreased at increasing ADP concentrations. However, the extent of quenching, measured at $t=100s$ (black full circles), did not vary significantly up to $4\mu M$ ADP. Therefore, the steady-state ΔpH appears in this range of ADP concentrations, to be in contrast to the trend observed for the initial hydrolysis and proton pumping rates, which

under the same conditions were monotonically inhibited. Similar data were obtained in the presence of $200\mu\text{M P}_i$ (Fig.5.5.1.B.).

These results might suggest that, when considering the steady-state ΔpH values, there is an increase in pumping efficiency, and this increase can be due to the build-up of a proton motive force taking place during the 100s of hydrolysis reaction.

The results of the present section, taken together with the results in §5.4., support the conclusion that ADP, similar to P_i , increases the number of protons transported per hydrolyzed ATP.

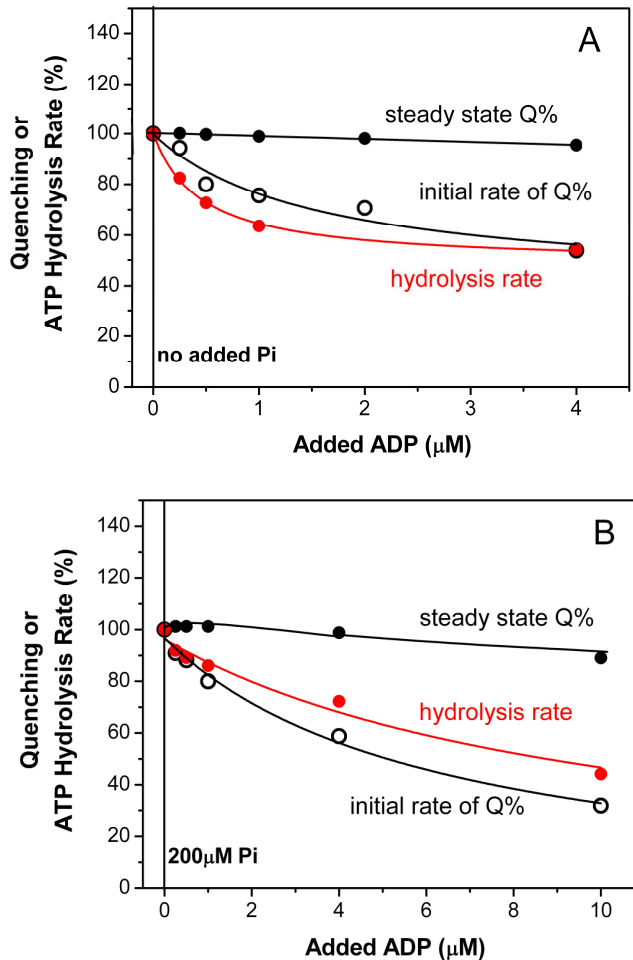


Fig. 5.5.1. ACMA fluorescence quenching and ATP hydrolysis as a function of [ADP] in the absence of added P_i (A) and in the presence of $200\mu\text{M P}_i$ (B).

Panel A., the absolute value of the initial rate of fluorescence quenching (○) at $t=0$ was $3.0\% \cdot \text{s}^{-1}$. The curve through the quenching data points is a best fitting hyperbole with apparent $K_d=1.6\pm 0.9 \mu\text{M}$. The absolute value of the fluorescence quenching (●) at $t=100\text{s}$ was 64.2% . The curve through the quenching data points was best fitted by a linear function.

The absolute value of the rate of ATP hydrolysis (●) at $t=0$ was $16.5 \cdot \text{nM ATP} \cdot \text{nM EF}_0\text{F}_1 \cdot \text{s}^{-1}$. The curve through the hydrolysis data points was a best fitting hyperbole with apparent $K_d=0.44\pm 0.04 \mu\text{M}$.

Panel B., experiments similar to those reported in Panel A. were carried out in the presence of $200 \mu\text{M P}_i$. The absolute value of the initial rates of fluorescence quenching (○) at $t=0$ was $3.7\% \cdot \text{s}^{-1}$. The curve through the quenching data points was a best fitting hyperbole with apparent $K_d=6.2\pm 2.2 \mu\text{M}$.

The absolute value of fluorescence quenching (●) at $t=100\text{s}$ was 77.7% . The curve through the quenching data points was drawn by hand.

The absolute value of the rate of ATP hydrolysis (●) at $t=0$ was $12.4 \cdot \text{nM ATP} \cdot \text{nM EF}_0\text{F}_1 \cdot \text{s}^{-1}$. The curve through the hydrolysis data points was a best fitting hyperbole with apparent $K_d=9.1\pm 0.9 \mu\text{M}$.

5.6. Effect of P_i on ATP hydrolysis and proton pumping in the presence of $1\mu\text{M}$ ADP and of 25U/ml PK.

A set of hydrolysis and quenching experiments similar to those described in §5.2. were carried out, either in the presence of $1\mu\text{M}$ ADP or in the presence of 25U/ml PK. The high PK activity was chosen in order to reduce as much as possible the steady state concentration of ADP in the system.

The results are summarized in Fig.5.6.1.A and B and compared with those obtained in the absence of added ADP (Fig.5.6.1.C).

In the presence of $1\mu\text{M}$ ADP the hydrolysis rate (red circles of Fig.5.6.1.A) decreased monotonically as a function of P_i . In the contrast the trend of the initial rate of quenching (open black circles of Fig.5.6.1.A) and the steady state values of fluorescence quenching (full black circles of Fig.5.6.1.A) were biphasic, first increasing at $[P_i] < 200\mu\text{M}$ and then decreasing, indicating once again a coupling effect of P_i .

In the presence of 25U/ml of PK, both the inhibitory effect of P_i on the ATP hydrolysis rate and the biphasic effect of P_i on the proton pumping disappeared (Fig.5.6.1.B). These results confirm those obtained in Chapter 3, in showing that ADP bound to the enzyme is required for P_i to be able to inhibit ATP hydrolysis and increase the efficiency of proton pumping.

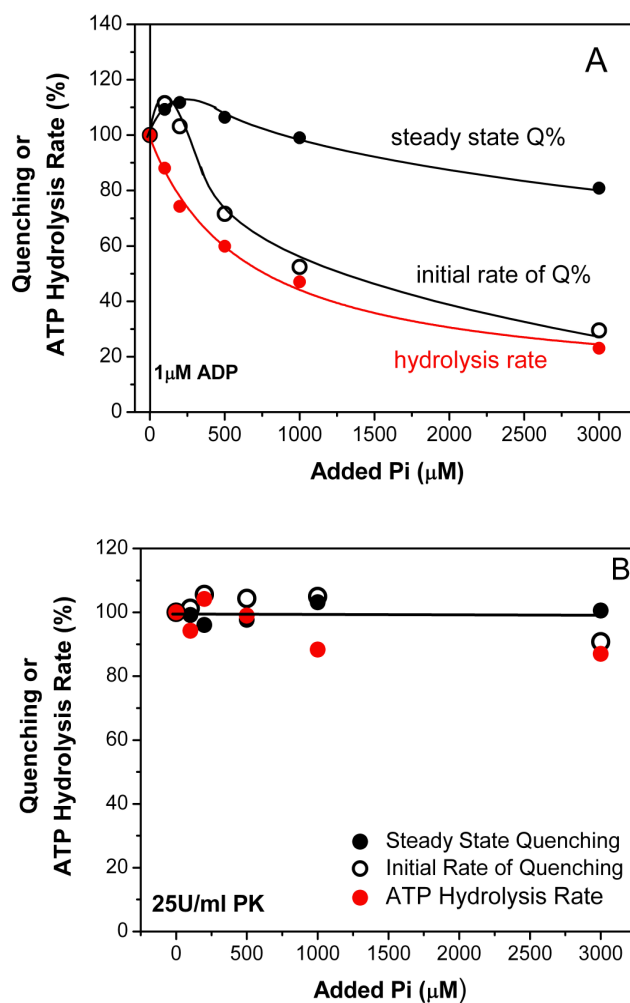


Fig. 5.6.1. A, B. see next page for the full caption.

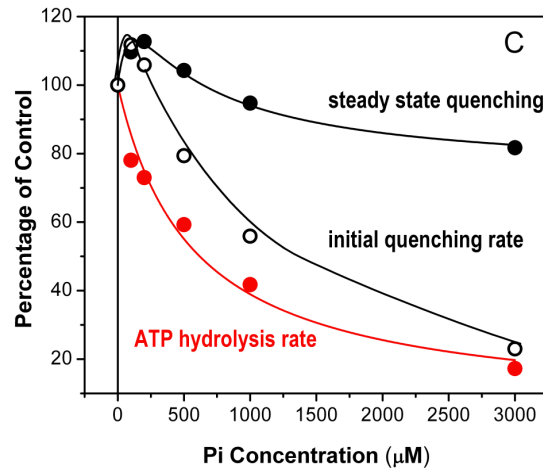


Fig. 5.6.1. ACMA fluorescence quenching and ATP hydrolysis as a function of [Pi] in the presence of 25U/ml PK (A), in the presence of 1µM ADP (B) and in the absence of added Pi (C).

Panel A., all measurements were carried out in the presence of 25U/mlPK. The absolute value of the initial rates of fluorescence quenching (\circ) at $t=0$ was $2.1\% \cdot s^{-1}$. The curve through the quenching data points was drawn by hand. The absolute value of fluorescence quenching (\bullet) at $t=100$ s was of 63%. The curve through the quenching data points was drawn by hand. The absolute value of the rate of ATP hydrolysis (\bullet) at $t=0$ was $10.1 \cdot nM \text{ ATP} \cdot nM \text{ EF}_0\text{F}_1 \cdot s^{-1}$. The curve through the hydrolysis data points was a best fitting hyperbole with apparent $K_d=650 \pm 130 \mu M$.

Panel B., experiments similar to those reported in Panel A. were carried out in the presence of 1 µM ADP. The absolute value of the initial rates of fluorescence quenching (\circ) at $t=0$ was $1.62\% \cdot s^{-1}$. The curve through the quenching data points was best fitted by a linear function. The percentage values of fluorescence quenching (\bullet) at $t=100$ s was 50.6%. The curve through the quenching data points was best fitted by a linear function. The percentage values of the rate of ATP hydrolysis (\bullet) at $t=0$ was $26 \cdot nM \text{ ATP} \cdot nM \text{ EF}_0\text{F}_1 \cdot s^{-1}$. The curve through the hydrolysis data points was best fitted by a linear function.

Panel C. data are from (Fig.5.2.3.) and are reported for comparison.

5.7. Discussion.

The results shown in the present chapter confirm that the binding of ADP and P_i inhibits the rate of ATP hydrolysis in the isolated and reconstituted F_0F_1 of *E. coli*. Moreover, the same ligands concomitantly increases its rate of proton pumping, so that, similarly as concluded for the internal membranes in Chapter 3, it is possible to conclude that its efficiency of proton pumping is increased. This higher efficiency of proton pumping, promoted by the binding of ADP and P_i , means that, in binding these two ligands, the ATP synthase changes its catalytic mode, shifting from a partially uncoupled to a fully coupled ATP hydrolysis.

Similarly as seen in the ATP synthase from *E. coli* membranes (Chapter 3), the ADP concentrations able to induce this phenomenon were in the submicromolar range, and could be attained during hydrolysis only by supplementing the assays with an ATP regenerating system acting as an ADP trap. The very high affinity for ADP supports the idea that the ADP binding site involved in this phenomenon is catalytic.

Similarly as concluded in Chapter 3, the biphasic dependence of proton transport on P_i concentration suggests that two P_i binding sites are involved, one with higher affinity, whose occupancy increases the pumping efficiency and a second one with lower affinity, causing inhibition of hydrolysis (Fig.5.2.5.).

The apparent K_d measured for inhibition by P_i of ATP hydrolysis was 440 μM (Fig. 5.2.1.), a value higher than the one measured in F_0F_1 from internal membrane (140 μM , see Chapter 3, Fig.3.2.1.). This difference could indicate that, in the isolated and reconstituted enzyme, the ADP binding site involved in this inhibitory role is partially empty. Indeed, in internal membranes a K_d value comparable to the one observed in the reconstituted system was obtained when the assay was supplemented with PK-ADP-trap between 2-10 U/ml PK.

Liposome membranes, which have a very low permeability for protons, have allowed us to calibrate the ACMA fluorescence quenching signal by means of ΔpH jumps of known extent. By transforming the ACMA fluorescence quenching values into ΔpH values and into their corresponding internal proton concentration values, we were able to give a quantitative estimation of the uncoupling elicited by either ADP or P_i , determining that the progressive removal of these ligands induces a nearly two-fold decrease of the number of proton translocated per hydrolyzed ATP (Tab.5.2.1. and Tab.5.4.1.).

As already observed for the ATP synthase of *E. coli* membrane (Chapter 3.), both the P_i -inhibition of hydrolysis and the P_i -induced enhancement of coupling efficiency were lost when the ADP concentration was drastically lowered in the presence of high amounts of the ADP-trapping PK (Fig. 5.6.1.B), indicating that these P_i effects were strictly dependent on the occupancy of a very high affinity binding site for ADP. The ADP requirement for the P_i -inhibition of hydrolysis is in agreement with the results obtained in the isolated and reconstituted EF_0F_1 by Fischer et al.(2000).

Interestingly, the presence of P_i has also been shown to be required for relief of ADP inhibition by means of the protonmotive force in TF_0F_1 , both in the wild-type and in a mutant lacking the C-terminal domain of the ϵ subunit (Feniouk et al., 2007). Similarly, data obtained in the bovine mitochondrial F_1 (Kozlov & Vulfson, 1985) showed that the preliminary incubation of ADP at concentrations equimolar with F_1 (μM range) was necessary for F_1 to bind P_i (present at 500 μM); this high affinity ADP binding site was also shown by the same group to be exchangeable and catalytic (Drobinskaya et al.,

1985). Such data and the present ones appears to indicate a synergy of binding of ADP and P_i . The most straightforward picture is that an ADP binds to a catalytic site, thereby closing the β subunit and forming a binding site for P_i .

In summary, the data presented in this section are in full agreement with the results showed in Chapter 3., and confirm that P_i can modulate the coupling efficiency of EF_0F_1 , by binding to a high affinity site filled with ADP.

One possible interpretation is that this modulation is brought about by the interconversion of two different conformational states of the enzyme, one of which has a lower coupling efficiency than the other. According to this hypothesis, the possibility of modulating the coupling efficiency might require the existence of a structural device acting somehow as a clutch. The ϵ subunit appears to us as a possible candidate for this role, since it has frequently been indicated as a key regulatory and structural feature in the coupling mechanism (see e.g. Zhang & Fillingame, 1995; Aggeler et al., 1995; Gardner & Cain, 1999; Peskova & Nakamoto, 2000; Cipriano et al., 2002; Cipriano & Dunn, 2006; Duvezin-Caubet et al., 2003; and for reviews Dunn, 1995; Capaldi & Schulenberg, 2000; Evron et al., 2000; Feniouk et al., 2006). In particular, the drastic changes in the ϵ trypsinization pattern induced by P_i (Mendel-Hartvig & Capaldi, 1991) are consistent with P_i triggering the interconversion between two conformations, and the occurrence of drastically different conformations in this subunit has been confirmed by structural (Gibbons et al., 2000; Rodgers & Wilce, 2000) and mutational studies (Tsunoda et al., 2001; Suzuki et al., 2003). One of these different conformations of the ϵ subunit could induce a more frequent slippage for instance within the rotor at the joint between the γ subunit and the c-subunit ring, or between stator and rotor at the interface $\alpha_3\beta_3$ -barrel/ γ -shaft. This last possibility would be consistent with the finding that mechanically driven ATP synthesis in TF_1 was more efficient if the ϵ subunit was added (Rondelez et al., 2005). Interestingly, the ϵ subunit appears to control the conformations of the γ subunit (reviewed in Capaldi & Schulenberg, 2000) and to modulate the rate of P_i release under unisite conditions (Dunn et al., 1987). It should be noted that, within this framework, if indeed the switching from a low to a high efficiency state of the enzyme is brought about by ADP and P_i binding to a high affinity catalytic site, this binding has to be transient, otherwise there would be no chance of observing a more coupled hydrolysis. In other words, the ligands have to dissociate from the enzyme in steps subsequent to the binding and to the conformational switch. The two ligands could be released as such, or even as ATP, if a sufficiently high protonmotive force is available. As already noted (Turina et al., 2004), it is interesting in this respect that low levels of ATP synthesis, from medium ADP and P_i , are always found during ATP hydrolysis in the presence of a protonmotive force (so called "ATP- P_i exchange") even at very high ATP/ADP ratios (Baccarini-Melandri & Melandri, 1971; Davenport & McCarty, 1981). Moreover, single molecule experiments have shown that the MgADP-inhibited TF_0F_1 could be reactivated by a forced rotation of the γ subunit not only in the hydrolysis but also in the synthesis direction (Hirono-Hara et al., 2005), which suggests that F_0F_1 can release tightly bound ADP either as such or, possibly, as ATP.

An alternative possibility is that the observed uncoupling phenomena could be related to a premature release of the hydrolysis products from a catalytic site perturbing the ordered release sequence necessary for a productive cooperative interaction within the $\alpha_3\beta_3$ hexamer. The analysis of such an interpretation would require a careful correlation between a kinetic reaction model, the rotational mechanism and the energetics of the

different catalytic sites (for this type of analysis see in particular Kinoshita et al., 2004; Gao et al., 2005).

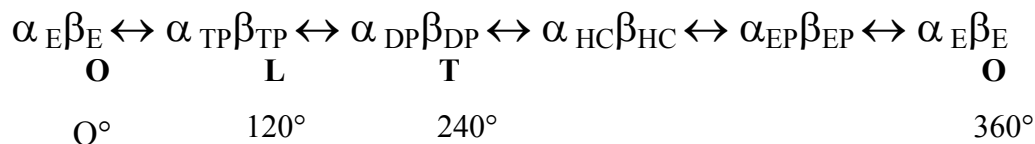
In the following we discuss a possible molecular mechanisms for the catalysis of hydrolysis of ATP in the absence of proton pumping. The model assumes that the central part of the enzyme rotates as a single body, and therefore excludes any mechanisms of slipping within the rotor structure. The model is based on some of the several molecular structures available for the bovine and yeast F_1 obtained in the presence of different ligands. These structure have been considered significant also for the *E. coli* F_1 , due to the extremely marked homology between these proteins.

The structures considered as significant for the present model are the following:

- bovine F_1 inhibited ADP and azide (Braig et al., 2000). In this structure one catalytic site is occupied by ANP, one by ADP and azide and the third is empty.
- bovine F_1 inhibited by ADP and BeF_3 (Kagawa et al., 2004). In this structure one catalytic site is occupied by ADP and BeF_3 , one by ADP and BeF_3 as well and the third is empty.
- bovine F_1 inhibited by ADP and AlF_4^- (Menz et al., 2001). In this structure one catalytic site is occupied by ADP and AlF_4^- , one by ADP and AlF_4^- as well and the third is occupied by ADP and P_i . This third site assumes a half closed conformation apt to the release of the hydrolysis products.
- yeast F_1 in two different structures (Kabaleesbaran et al., 2006). In the first structure (yF_1I) one catalytic site is occupied by AMP-PNP, one by AMP-PNP as well and the third is empty. In the second structure (yF_1II) the occupancy of the first two sites is the same but the third site contains bound P_i .

In all structures the rotor is differently rotated with respect to the stator. The position of the rotor is considered as a position in equilibrium with the structures of the catalytic subunits (the $\alpha\beta$ heterodimers) induced by the different ligands.

The present model considers the possibility that the catalytic mechanism of ATP hydrolysis could occur in the absence of a net anticlockwise rotation, but only assisted by limited clockwise and anticlockwise oscillations, eventually compensating each other, and due to thermal fluctuations. It is possible that the torsion exerted by a protonmotive force on the clockwise rotation of the rotor is involved in this effect. This mechanisms is alternative to the normal coupled hydrolytic cycle that occurs according to the scheme:



This sequence of conformations will promote the anticlockwise rotation of the rotor and the consequent pumping of proton.

On the contrary, an uncoupled hydrolysis mechanism will occur when a catalytic site containing ADP and P_i releases its ligands prematurely so that the enzyme contains two empty catalytic sites. This can occur when the ambient conditions favour ligand dissociation, i.e. at very low concentrations of ADP and P_i in the external medium.

These are exactly the conditions when no P_i is added to the reaction mixture and when ADP is consumed by a ATP regenerating system.

When two catalytic sites are empty there is a definite probability that ATP is bound to the wrong site, i.e. a site not consistent with the normal sequence of product release-substrate binding. This requires abnormal positions of the rotor and forwards and backwards oscillations in the synthesis and hydrolysis direction.

The two conformations containing ADP and P_i in the different structures listed above are the $\alpha_{HC}\beta_{HC}$ structure of Menz et al. (2001) (the structure with the enzyme in the reaction transition state) and the $\alpha_{DP}\beta_{DP}$ of Kagawa et al. (2004) (in which the position of BeF_3 mimics that of P_i). The conformation more suited for binding either ATP or ADP and P_i is that with the enzyme in the transition state (Menz et al., 2001), in which both the $\alpha_{DP}\beta_{DP}$ and the $\alpha_{TP}\beta_{TP}$ catalytic sites are occupied by ADP plus AlF_4^- .

The stability of the transition state conformation requires that the $\alpha_{HC}\beta_{HC}$ site is occupied by ADP and P_i . But under low P_i and ADP concentrations in the external medium this site is rapidly emptied. A limited rotation of about 28° in the synthesis direction will alter the conformation of the $\alpha_{DP}\beta_{DP}$ site, from a tight conformation (similar to the $\alpha_{DP}\beta_{DP}$ site in the Kagawa structure; (Kagawa et al., 2004)) to that of the transition state. This rotation is certainly favoured by the torsional action promoted by the protonmotive force, and the resulting conformation can facilitate the further, and premature, release of ADP and P_i . This series of events will produce an enzyme with two empty catalytic sites, thereby increasing the probability of binding ATP to the wrong site. The contribution of the protonmotive force for the rotation in the synthesis direction seems to be decisive, since the estimated energy appears too large for a spontaneous thermal fluctuation. This consideration is consistent with the observed proton pumping burst observed upon ATP addition, before a partially uncoupled ATP hydrolysis takes place (see e.g. Figs. 5.2.2.-5.2.4.)

A possible scheme for an uncoupled catalytic cycle of ATP hydrolysis is presented in Fig. 5.7.1.

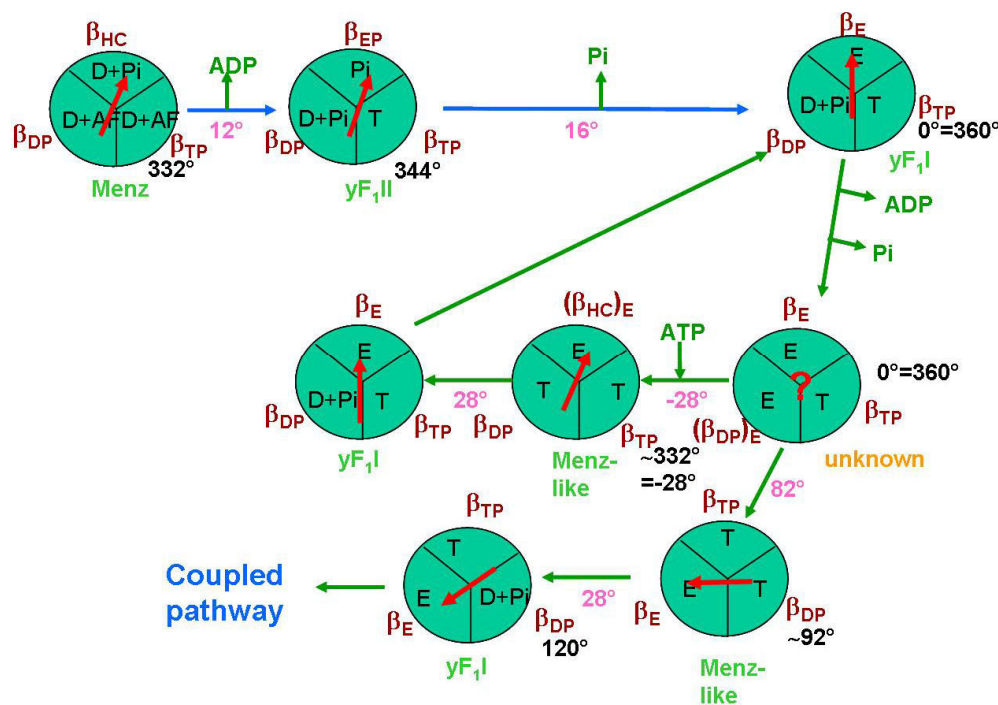


Fig.5.7.1. Model scheme of the hydrolysis taking place in the presence of high PK activity and in the absence of P_i ; futile cycle with limited clockwise and anticlockwise oscillations.

This model appears to offer a structural support to a mechanism of hydrolysis occurring in the absence of a net rotation of the rotor and therefore uncoupled from proton transport. The conclusions of this model are consistent with previous observations and conclusions by other authors. In particular Cipriano & Dunn (2006) documented the existence of an uncoupled ATP hydrolysis reaction in F_1 in which the rotation of the rotor was hampered by the fusion of bulky proteins to the ϵ -subunit. They proposed that this hydrolysis could occur in the absence of net rotation of the rotor. The model is also consistent with old observations by Kayalar et al., (1997) indicating that many exchange reactions ($ATP \leftrightarrow P_i$, $P_i \leftrightarrow H_2O$, $ATP \leftrightarrow H_2O$, $ATP \leftrightarrow ADP$) are inhibited by an ATP regenerating system, and by uncouplers as well, while the hydrolysis reaction is stimulated. These observations can be explained by considering exchange mechanisms depending on partial rotation both in the hydrolysis and in the synthesis direction (hence the effect of uncouplers), and in addition by the availability of ADP in the external medium at a concentration sufficiently high for the cooperativity phenomena at the basis of the alternate binding mechanism to take place. On the contrary an hydrolytic mechanism can occur in the absence of these conditions.

Chapter 6.

RESULTS

6.1. Functional studies on ϵ truncation mutants.

The last part of my research work was focused on looking for a possible structural candidate involved in the phenomenon of intrinsic uncoupling. This work was developed in collaboration with the laboratory of Prof. S.D. Dunn, at the Dept. of Biochemistry of the University of Western Ontario, Canada.

The ϵ subunit is an endogenous inhibitor of the hydrolytic activity of bacterial ATP synthases.

This subunit, which lies at the interface of F_1 and F_0 , has been suggested to function within the enzyme as an inhibitor, a regulator, or a coupling factor (Kato-Yamada et al., 1999; Xiao et al., 2000; Duvezin-Caubet et al., 2003; Tsunoda et al., 2001; Suzuki et al., 2003). The high-resolution structure of the isolated *E. coli* ϵ , solved by both X-ray crystallography (Uhlin et al., 1997) and NMR spectroscopy (Wilkins et al., 1995; Wilkins & Capaldi, 1998), shows a two domain protein with an N-terminal 10-stranded β -barrel (residues 1–87, termed the N-domain) and a C-terminal helix-turn-helix domain (residues 88–138, termed the C-domain). The latter is not absolutely required for oxidative phosphorylation, or photophosphorylation in the case of the chloroplast enzyme, but is necessary for the inhibition of ATPase activity (Kato-Yamada et al., 1999; Nowak & McCarty, 2004; KuKi et al., 1988; Xiong et al., 1998). The structure of ϵ in the ATP synthase complex has been controversial as two different conformations of ϵ , the “up conformation” (Rodgers & Wilce, 2000; Hausrath et al., 2001; Hausrath et al., 1999) and the “down conformation” (Gibbons et al., 2000; Stock et al., 1999), have been seen in crystal structures. A crystal of the up conformation has been published by Rogers et al., 2000. The crystal structures of the down conformation of ϵ are from bovine heart mitochondria and yeast EF_0F_1 (Gibbons et al., 2000; Stock et al., 1999). However in these organisms an additional subunit of the ATP synthase might be seen to prevent the ϵ up conformation. The N-domain is located in essentially the same position in both conformations, but in the up conformation the helices of the C-domain are extended and partially wrap around γ to make contact with $\alpha_3\beta_3$, whereas in the down conformation the two α -helices fold on themselves and lie next to the N-domain on top of the c_{10} oligomer. It has been recently suggested (Tsunoda et al., 2001; Suzuki et al., 2003) that when the cellular concentration of ATP is low, ϵ adopts the up conformation and inhibits ATP hydrolysis by allowing for rotation only in the direction of synthesis. The ϵ subunit was suggested to adopt the down conformation when ATP is high, allowing ATP synthase to catalyze either hydrolysis or synthesis of ATP. It has also been seen that the switch up/down of ϵ has regulatory effects on the enzymatic activity; this change of conformation is influenced by the binding of ADP and ATP to the enzyme and by the presence of a protonmotive force (Feniouk et al., 2006; Feniouk et al., 2007). Moreover it has been already shown that the C-terminal domain of ϵ is required for efficient energy coupling see (Cipriano & Dunn, 2006); in this paper Cipriano & Dunn used a double ϵ mutants carrying both the 20KDa flavodoxin fused to the N-terminal domain and the truncation of the entire C-terminal domain ($\epsilon_{88\text{-stop}}$). The flavodoxin was fused, by using a 13-residue flexible linker, at the end of the N-terminal

domain. The presence of this 20KDa extra-domain blocked the rotation of the rotor. With this rotation-blocking strategy, it was possible to demonstrate that the removal of the C-domain of ϵ determines an increased level of uncoupled ATPase activity.

We hypothesized that the highly mobile C-domain of ϵ could have a coupling function in the ATP synthase, and that the ϵ -down conformation could be associated to the intrinsic uncoupled state of the enzyme. To test this hypothesis we have planned to use a mutant form of EF_0F_1 carrying an ϵ subunits with a deletion in the α -helices hairpin. Our idea was that this mutation should be able to shed light on the possible role of the C-terminal domain in this regulatory effects. For the aim of our research we choose to work with a C-terminal truncated ϵ ATP synthase carrying the mutation $\epsilon_{88-stop}$ (Fig.6.1.1.). Since such a truncation could also reduce assembly or stability (see below), we have constructed a strain with a multicopy plasmid, expressing additional ϵ subunits of the same type as those on the *unc* operon.



Fig.6.1.1. Schematic representation of the ϵ mutant used for this study.

General structure of ϵ WT. The two domains of ϵ are shown in blue (N-domain) and orange (C-domain).

6.2. Plasmid construction and *E. coli* DK8 cells double transformation.

During the preparation of membranes carrying an ATP synthase with the ϵ truncation, some unpredictable phenomena might occur, like reduced/ incompletely assembly of the EF_0F_1 complex, degradation of the ϵ subunit and/ or of the holoenzyme.

To test this possibility we decided to construct a low copy number plasmid carrying the ϵ gene inserted between unique restriction sites. We used this vector to obtain *E. coli* strains able to express an extra amount of the ϵ subunit. We doubled transformed *unc*-less *E. coli* DK8 strains with plasmids carrying the entire *unc* operon (pDC44 and pDC45 derivatives of pACWU1.2, (Cipriano & Dunn, 2006; Cipriano et al., 2002)) and with plasmids carrying only the *uncC* gene (pMDA5 and pMDA7 derivatives of pEXT21, (Dykxhoorn et al., 1996)). The two type of plasmid, used to carry the *unc* operon and the *uncC* gene, were compatible, having different origins of replication and different antibiotic resistances, so that both could be maintained within the cells.

6.2.1. Development of a low copy number expression vector carrying extra copy of WT or mutated *uncC*.

Plasmid pSD15 containing the 1182-bp PstI fragment of the *unc* operon cloned into the PstI site of pUC8 (Vieira & Messing, 1982) and plasmid pDC47 containing an AvrII site just after the stop codon of the ϵ gene (Cipriano & Dunn, 2006), were the starting point for the construction of the insert which was cloned into the low copy expression vector pEXT21 (Dykxhoorn et al., 1996). pEXT21 is a low copy number expression vector streptomycin resistant which contains an expression cassette comprised of the *lacI^r* gene, the *tac* promoter, a multiple cloning site and a downstream transcriptional terminator (Fig. 6.2.1.).

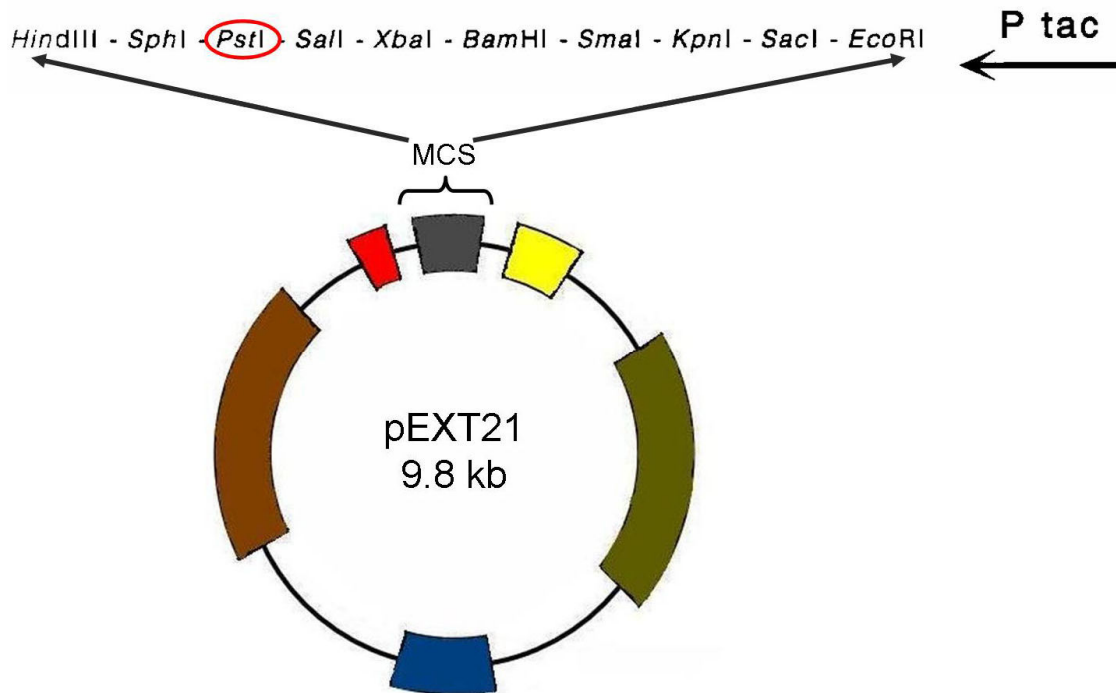


Fig. 6.2.1. Structure of the *tac* promoter expression vector pEXT21.

The expression cassette carried on this plasmid is composed of (1) the replication origin (*ori*, IncW), shown in blue; (2) the *lacI* gene, shown in olive; (3) the *tac* promoter (Ptac), shown in yellow; (4) a 51-bp EcoRI-*HindIII* fragment carrying the MCS, shown in grey (the orientation of the MCS is indicated by the position of the *HindIII* site and the restriction sites present in the MCS are indicated at the top); (5) the terminator (T2), shown in red; and (6) the streptomycin/spectinomycin resistance (Sm^R/Sp^R) gene, shown in brown (adapted from Dykxhoorn et al., 1996).

The 335-bp *HindIII*/*NcoI* fragment of pDC47 was moved into pSD15 which was cut with the same enzymes to produce pMDA1, in order to introduce the *AvrII* site after the stop codon of the ϵ gene of pSD15. The correctly cloned samples were identified by restriction mapping (with *HindIII*, *NcoI*, *AvrII*, *EcoRI*). pMDA1 was cut with *PstI* to obtain a 1179-bp fragment carrying the *uncC* gene and the *AvrII* site; this fragment was cloned into the *PstI* site of pEXT21 to produce pMDA2.

IPTG induction tests and different screening by restriction mapping were carried out to check if the insert was cloned into pEXT21 in single copy and in the right orientation and if the MCS was intact (data not shown). The *uncC* gene cloned into pEXT21 to produce pMDA2 has an *AvrII* unique site downstream of *uncC*; in order to facilitate future cloning steps, another unique site upstream of *uncC* was created by removing the *PstI* site downstream from *uncC*.

The *PstI* site in pMDA2 was removed by partial digestion with *PstI*, isolation of singly cut linear plasmid by gel purification, treatment with T4 DNA polymerase to remove the 3' overhangs, and ligation of the blunted ends. Transformants in which one of the two *PstI* sites within pMDA2 vector sequence had been removed were screened by restriction mapping. The positive samples were further on screened by restriction mapping in order to check which one of the two *PstI* sites was removed. Unfortunately, the *PstI* site upstream of *uncC* was removed in all samples. One of these samples was saved as pMDA3. The same result was invariably obtained for more than 30 tested transformants; it is likely that the two *PstI* sites in pMDA2 do not have the same

probability to be cut. pMDA3 was used as a starting point for a new strategy to remove the target PstI site.

The remaining PstI site in pMDA3 was removed by digestion with PstI, isolation of linear plasmid by gel purification, treatment with T4 DNA polymerase to remove the 3' overhangs, and ligation of the blunted ends. Transformants were screened by restriction mapping to identify pMDA4, a vector without PstI sites. Assignment of one transformant as pMDA4 is shown in Fig.6.2.2.. Upon double-digestion with PstI/EcoRI, pMDA4 shows only a 11.2 Kbp band whereas the control sample (pMDA2) shows two bands (respectively lanes 2 and 3 in Fig.6.2.2.); this test confirmed that the remaining PstI site was removed in pMDA4. After double-digesting with AvrII/EcoRI, both samples show the presence of two bands (lanes 4 and 5 in Fig.6.2.2.); these additional controls demonstrate that the treatment did not damage the AvrII site in pMDA4.

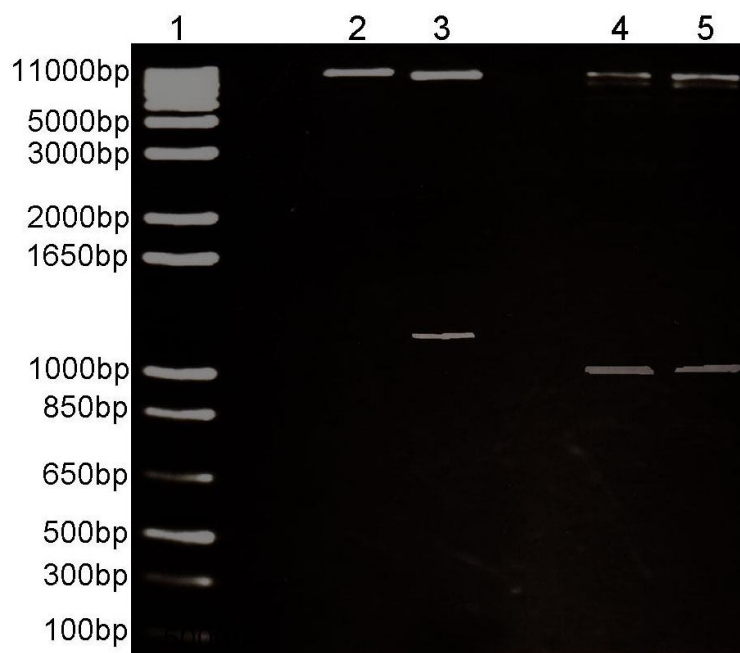


Fig. 6.2.2. Removal of PstI site from pMDA3 to produce pMDA4.

DNA isolated by mini-prep from 2 different cultures was digested with PstI/EcoRI and with AvrII/EcoRI.

Lane 1 1kb DNA marker.

Lanes 2 PstI/EcoRI-digestion of pMDA4 .

Lane 3 PstI/EcoRI -digestion of pMDA2 (control).

Lane 4 AvrII/EcoRI-digestion of pMDA4. Lane 5 AvrII/ EcoRI-digestion of pMDA2 (control).

Then pMDA2 was cut with EcoRI and AvrII and the small 1009-bp fragment (containing only the PstI site upstream of *uncC*) was isolated and ligated into the 9200-bp EcoRI/AvrII fragment of pMDA4 to produce pMDA5. This plasmid contains the ϵ WT gene flanked by unique PstI and AvrII sites. Three transformants were screened by restriction mapping (Fig.6.2.3.). When digested with PstI, both the three potential pMDA5 clones and the control sample (pMDA3) showed only a 11.2 Kbp band (lanes 2-5 in Fig.6.2.3.). After double-digesting with PstI/AvrII all potential clones from the pMDA5 construction showed the expected fragment of about 1000-bp (lanes 6-8 in Fig.6.2.3.), whereas this fragment was not present in the control sample (lane 9 in Fig.6.2.3.). Finally we checked if the cloning procedure could have disturbed the structure of pMDA5, by digesting pMDA5 and control samples with EagI. The pattern of bands observed in all pMDA5 samples (lanes 10-12 in Fig.6.2.3.) was identical to the one obtained in the control sample (lane 13 in Fig.6.2.3.).

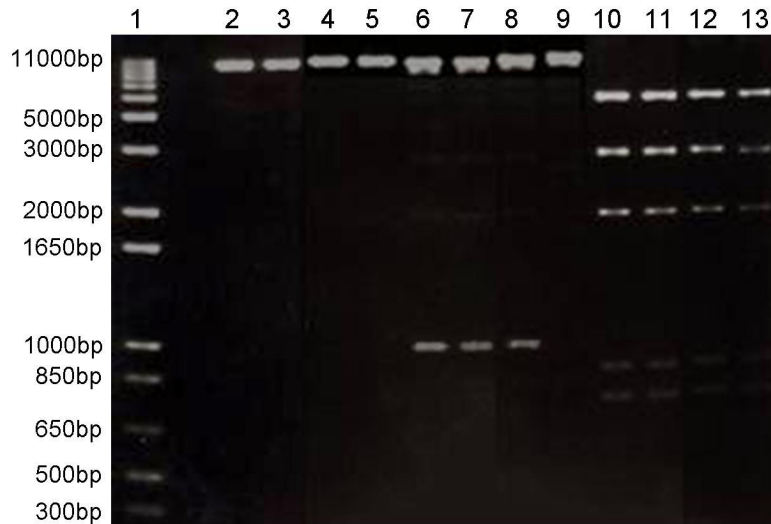


Fig.6.2.3. Restriction sites analysis of potential pMDA5 clones.

Plasmid preparation from three potential clones from the pMDA5 construction were digested by restriction enzymes and the fragments were compared to the one obtained from pMDA3. Samples were analyzed by electrophoresis in a 1% gel.

Lane 1, 1kb DNA marker.

Lanes 2-4, clones A, B and C were digested with PstI.

Lanes 5, pMDA3 was digested with PstI (control).

Lanes 6-8, clones A, B and C were digested with PstI/AvrII.

Lanes 9, pMDA3 was digested with PstI/AvrII (control).

Lanes 10-12, clones A, B and C were digested with EagI.

Lanes 13, EagI-digestion of pMDA3 (control).

Plasmid pDC45, containing the *unc* operon with the *uncC* gene encoding the $\epsilon_{88\text{-stop}}$ mutation, was the starting point for construction of the C-terminal ϵ deletion mutant plasmid. This plasmid has a PstI site before the ϵ initiation codon and an AvrII site immediately following the ϵ stop codon. These two restriction sites were cut and the small 832-bp fragment was inserted into pMDA5 cut with the same enzymes to make pMDA7. This plasmid contains the $\epsilon_{88\text{-stop}}$ gene flanked by unique PstI and AvrII sites. Positive transformants were screened by restriction mapping (Fig.6.2.4.). Upon double-digestion with PstI/AvrII, all potential clones from the pMDA7 construction showed an 800-bp fragment (lanes 2-4 in Fig. 6.2.4.), whereas the control sample showed a 1000-bp fragment, as expected (lane 5 in Fig.6.2.4.).

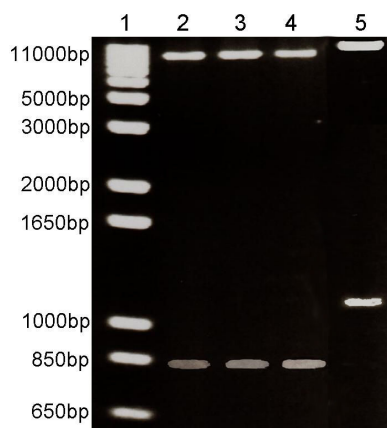


Fig.6.2.4. Restriction sites analysis of potential pMDA7 clones.

Plasmid preparation from three potential clones from the pMDA7 construction were digested by restriction enzymes and the fragments were compared to the ones obtained from pMDA3. Samples were analyzed by electrophoresis in a 1% gel.

Lane 1 1kb DNA marker.

Lanes 2-4, clones A, B and C were digested with PstI/AvrII.

Lanes 5, pMDA3 was digested with PstI/AvrII (control).

6.2.2. Transformation of DK8 *E. coli* strains with plasmids

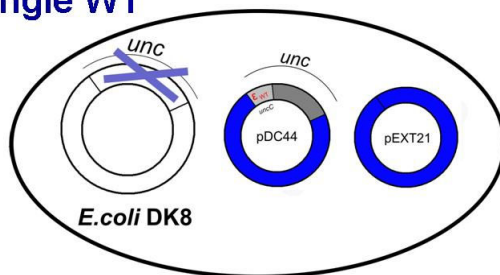
The *unc*-less DK8 *E. coli* strains the starting point for the setting up of four new *E. coli* strains, obtained after double transformation of different combinations of the plasmids, as summarized in Tab. 6.2.1. Firstly the *unc*-less DK8 *E. coli* strains were transformed with pDC44 and with pDC45. The cells were grown in a medium containing ampicillin (40mg/l). Transformant cells were further transformed with pEXT21, with pMDA5 and with pMDA7. The cells were grown in the presence of streptomycin (24mg/l). We obtained double transformant strains carrying the double ampicillin/streptomycin resistance. In fig.6.2.5. we summarized the different combinations used to transform pEXT21, pMDA5 and pMDA7 into DK8 *E. coli* strains already containing pDC44 (WT) and pDC45 (ϵ 88-stop truncation). We produced 4 new *E. coli* strains, which we called sWT (single WT), dWT (double WT), sMut (single Mutant) and dMut (double Mutant), respectively.

Tab. 6.2.1. Plasmids carried by single and double transformants.

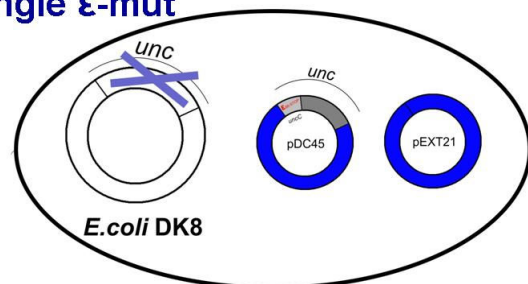
In the table the plasmid used for transformation are reported together with the antibiotic resistance, the origin of replication and the *UncC* gene they carried.

NAME	RESISTANCE	ORIGIN	<i>Unc</i> GENE CARRIED
pDC44	Ampicillin	P15A	<i>Unc I, B, E, F, H, A, G, D</i> and C (WT)
pDC45	Ampicillin	P15A	<i>Unc I, B, E, F, H, A, G, D</i> and C (88-stop)
pEXT21	Streptomycin	IncW	
pMDA5	Streptomycin	IncW	<i>Unc C (WT)</i>
pMDA7	Streptomycin	IncW	<i>Unc C (88-stop)</i>

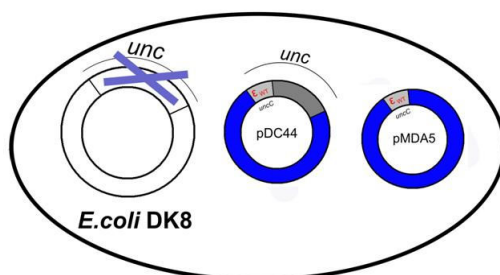
Single WT



Single ϵ -mut



Double WT



Double ϵ -mut

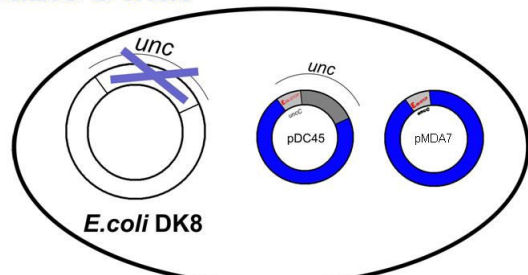


Fig.6.2.5. Schematic representation of the four *E. coli* strains obtained after double transformation of different combinations of the following plasmid:pDC44, pDC45, pEXT21, pMDA5 and pMDA7.

6.2.3. Western Blot analysis of expressed ϵ mutants and WT

Quantitative Western blot analysis were carried out, as described in §2.12., to estimate the amount of ϵ subunit in each strain.

Membranes from the four strains (double/single WT and double/single mutant), WT ATP synthase from SD381 strain membranes and isolated F_1 as control were loaded on the same gel (Fig.6.2.6.). Each sample was analyzed at two concentrations, 1 or 2 μg for membranes, 0.01 or 0.02 μg for F_1 . In these preliminary blots, the quantitative analysis of the spots (Tab.6.2.2.) showed that

- in membranes there are more ϵ per α than in pure F_1 (at least in membranes prepared as described in §2.1.2.);
- the doubles seem to have a bit more α in the membranes than the singles, implying that assembly or retention during membrane preparation is enhanced by the extra ϵ ;
- the mutants seem to have only a little less ϵ than the WT, relative to α . However it can not be excluded that some fraction of the truncated form has been lost (§2.12.), or that it is less reactive on the blot (e.g. because sites necessary for recognition are blocked by modifications). Clearly, though, it does assemble into the complex to an extent similar to that in the WT.

Work is in progress to optimize the blot method and enable a more definitive quantification.

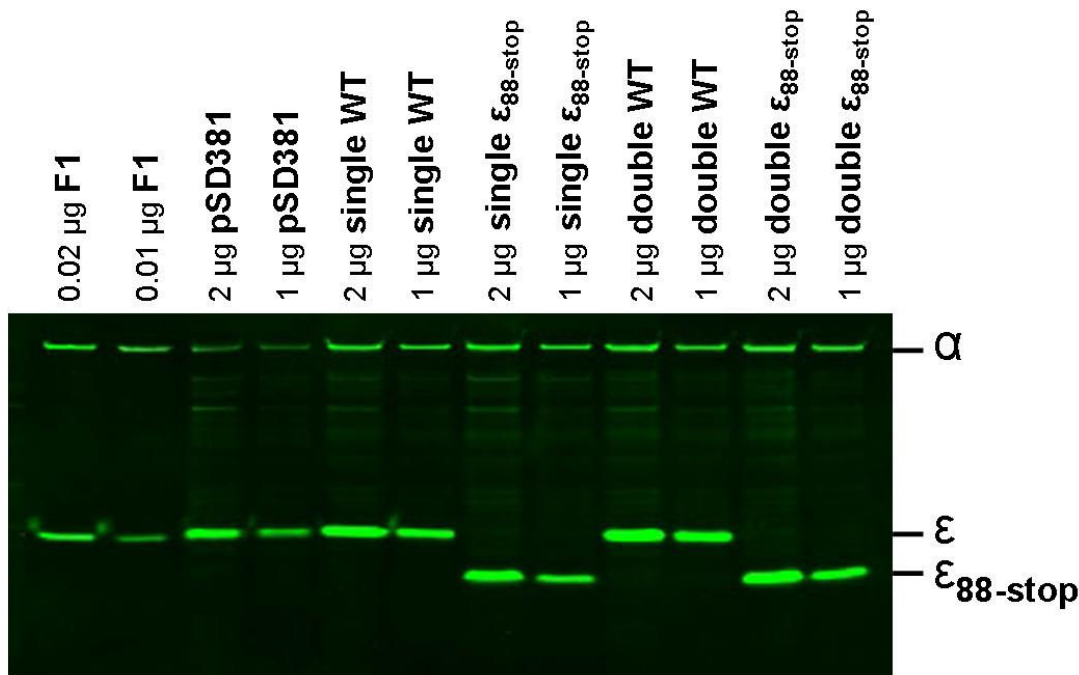


Fig.6.2.6. Western Blot analysis of expressed ϵ mutants and WT.

Samples of membrane protein (1 and 2 μg) and of isolated F_1 (0.01 and 0.02 μg) were subjected to SDS-PAGE analysis followed by Western blotting to PVDF membranes as described in §2.12.. Blots were probed with fluorescent (Li-Cor IRDye 800CW) antibodies raised against α and ϵ .

Tab.6.2.2. Quantitative analysis of the spots from Fig.6.2.5.

The first column of the table indicates the subunit analysed; the second column of the table indicates the amount of membrane or F₁ loaded in the blot; the third and the fourth columns indicate the intensity of each band and the change in signal obtained upon doubling the amount loaded for that sample, respectively; the fifth, sixth and seventh columns indicate the intensity ratio of double/single strain, mutant/WT strain and ϵ/α subunit, respectively.

subunit	amount	net intensity	load linearity	Double /single	$\epsilon_{88\text{-stop}}/\text{WT}$	ϵ/α
Alpha (α)	0.02 μg F ₁	724,3	1,59333891			
Alpha (α)	0.01 μg F ₁	454,58				
Alpha (α)	2 μg pSD381	239,04	1,38189386			
Alpha (α)	1 μg pSD381	172,98				
Alpha (α)	2 μg sWT	860,49	1,82857325			
Alpha (α)	1 μg sWT	470,58				
Alpha (α)	2 μg sMutant	949,4	1,7838823		1,10332485	
Alpha (α)	1 μg sMutant	532,21			1,13096604	
Alpha (α)	2 μg dWT	1058,89	1,57868921	1,23056631		
Alpha (α)	1 μg dWT	670,74		1,42534744		
Alpha (α)	2 μg dMutant	1052,04	1,45036947	1,10811039	0,99353096	
Alpha (α)	1 μg dMutant	725,36		1,36292065	1,08143245	
Epsilon (ϵ)	0.02 μg F ₁	972,45	2,79672716			1,34260665
Epsilon (ϵ)	0.01 μg F ₁	347,71				0,76490387
Epsilon (ϵ)	2 μg pSD381	1560,47	1,82949763			6,52807062
Epsilon (ϵ)	1 μg pSD381	852,95				4,93091687
Epsilon (ϵ)	2 μg sWT	4062,93	2,24101071			4,72164697
Epsilon (ϵ)	1 μg sWT	1812,99				3,85267117
Epsilon (ϵ)	2 μg sMutant	2791,19	2,54856647		0,68698944	2,93995155
Epsilon (ϵ)	1 μg sMutant	1095,2			0,60408496	2,05783431
Epsilon (ϵ)	2 μg dWT	5722,02	2,15271346	1,40834816		5,40379076
Epsilon (ϵ)	1 μg dWT	2658,05		1,46611399		3,96286191
Epsilon (ϵ)	2 μg dMutant	4377,63	2,33339197	1,56837406	0,76504976	4,16108703
Epsilon (ϵ)	1 μg dMutant	1876,08		1,71300219	0,70581065	2,58641226

6.3. Comparison of ATPase activity and ATP dependent proton pumping in membrane vesicles from the four *E. coli* strains at different P_i concentrations.

The internal membranes obtained from the four strains were first analyzed by measuring their ATP hydrolysis and proton pumping activities in the presence of different P_i concentrations.

We have measured both the ATP hydrolysis (Fig. 6.3.1.A-B) and the ACMA fluorescence quenching (Fig. 6.3.2.A-B) as a function of time, in the absence of added P_i and in the presence of two different P_i concentrations (1 and 3mM).

Both sWT and dWT confirmed the results obtained in Chapter 3: on one side the ATP hydrolysis rate was inhibited in the presence of increasing amount of added P_i (Fig. 6.3.1.A), on the other side certain concentrations of P_i promoted coupling (Fig. 6.3.2.A). However, the inhibitory effect of P_i on ATP hydrolysis and the P_i coupling effect are more evident in the dWT membranes.

As to the mutant strains, both in sMut and in dMut the coupling effect of P_i could still be observed (Fig. 6.3.2.B). On the contrary, the hydrolysis data show that membranes from mutant strains were almost completely insensitive to the inhibitory effect of P_i (Fig. 6.3.1.A). Comparing the behaviour of dMut and sMut, the effect of P_i on the enzyme appears to be much clearer in the former, similarly to what was already observed in the wild type strains. In particular, sMut still presents a slight P_i inhibition of hydrolysis, which is on the contrary totally lost in dMut.

Taken together, these data indicate that the expression of additional ϵ WT resulted in higher P_i inhibition of the ATP hydrolysis, while expression of additional ϵ truncation resulted in lower P_i inhibition. Similar effect could be observed in the proton pumping; the expression of additional ϵ resulted in a greater difference between WT and mutant.

These preliminary data, showing that the P_i effects on the ATP synthase are much more evident in the Double relative to the Single strains, support the hypothesis that strains expressing an extra amount of ϵ subunit could have a higher efficiency in retaining the full complement of the ϵ subunit.

This hypothesis is also consistent with the preliminary results from the Western blot analysis (§6.2.3.). For this reason, in the following experiments only double WT and double Mutant membranes have been used.

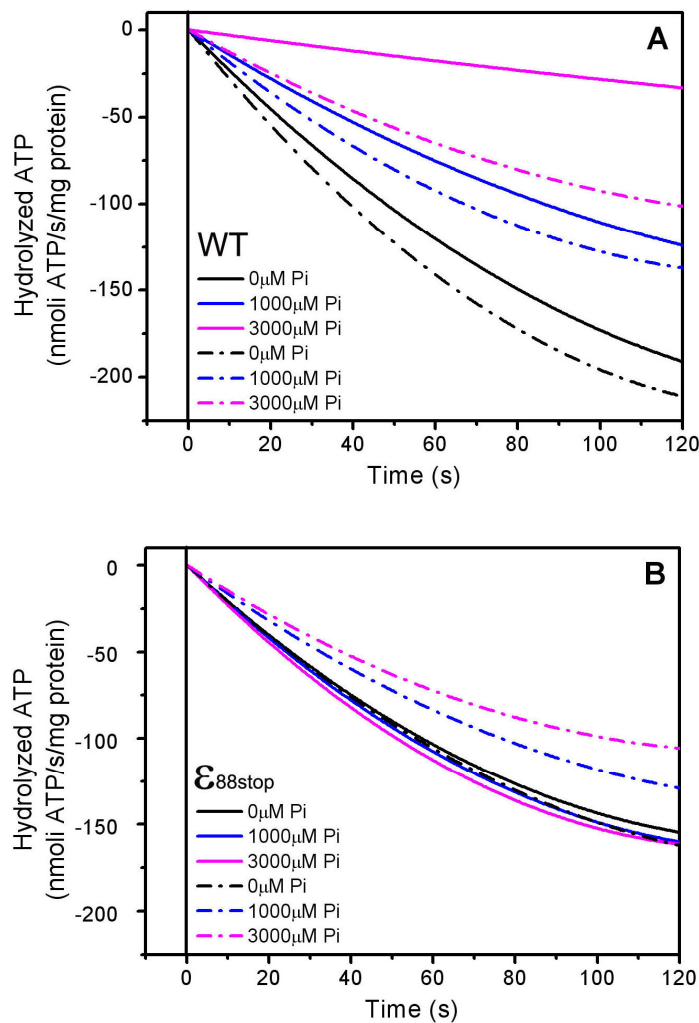


Fig.6.3.1. ATP hydrolysis as a function of time in the presence of 0, 1000, 3000 μM P_i , in ϵ WT *E. coli* membranes (A) and in $\epsilon_{88\text{-stop}}$ *E. coli* membranes (B).

The ATP hydrolysis reaction was started by adding 150 μM ATP at $t = 0\text{s}$ and the experimental traces have been best fitted by monoexponential functions (not shown). Each trace is the average of two determinations. Panel A. Broken lines = sWT, full lines = dWT; Panel B. Broken lines = sMut, full lines = dMut.

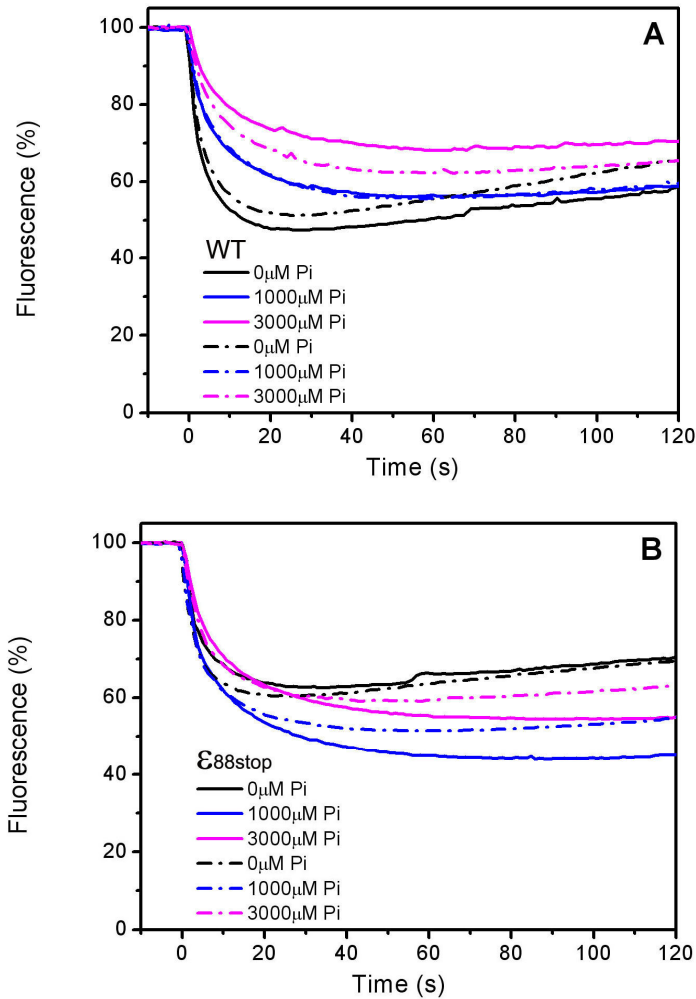


Fig.6.3.2. ACMA fluorescence quenching as a function of time in the presence of 0, 1000, 3000 μM P_i , in ϵ WT *E. coli* membranes (A) and in $\epsilon_{88\text{-stop}}$ *E. coli* membranes (B).

The fluorescence measurements were carried out under the same experimental conditions of the ATP hydrolysis measurements. For each trace, addition of 1 μM nigericine recovered the 100% fluorescence level. Each trace is the average of two determinations. Panel A. Broken lines = sWT, full lines = dWT; Panel B. Broken lines = sMut, full lines = dMut.

6.4. Effect of P_i on ATP hydrolysis and proton pumping.

In Chapter 3. and 4. low concentrations of P_i have been shown to inhibit the rate of ATP hydrolysis by the ATP synthase in *E. coli* internal membranes, while at the same time increasing the rate of inward proton translocation. The purpose of the following experiments was to check to what extent these effects were present in the membranes prepared from the double transformants, with and without ϵ truncation.

6.4.1. ATP hydrolysis in WT and in $\epsilon_{88\text{-stop}}$ mutant as a function of P_i concentration.

We first measured the ATP hydrolysis as a function of P_i in the dWT membranes. Fig. 6.4.1.A shows the amount of hydrolyzed ATP as a function of time after addition of 150 μM ATP at t=0s, in the presence of increasing P_i concentrations; valinomycin and 50mM K^+ were also present, in order to have the same assay composition as used in the ACMA assay (see below). The rates of ATP hydrolysis at t=0s and t=100s were evaluated by fitting the spectrophotometric data (collected at a rate of 1/s) with a mono-exponential function and taking the first derivatives at t=0s and t=100s respectively. In WT membranes, these rates decreased at increasing P_i concentrations, as expected.

By plotting the initial rates as a function of P_i (Fig. 6.4.2., open blue triangles), a hyperbolic trend was obtained, with a best-fitting value of $680\mu\text{M}$ for the apparent K_d . The rates at $t = 100\text{s}$ are also plotted (full blue circles), which can be similarly interpreted as having an hyperbolic trend. The DCCD insensitive activity was $1.5 \text{ nmolesATP}\cdot\text{s}^{-1}\cdot\text{mg}^{-1}$ (data not shown). The K_d value of $680\mu\text{M}$ is higher than the K_d value obtained with the membrane preparation of Chapter 3; this difference can be due to the different preparation methods, since this membranes have been extensively washed, possibly leading to a higher ADP depletion.

The same hydrolysis measurements were then carried out in the presence of $\epsilon_{88\text{-stop}}$ mutant membranes. Fig. 6.4.1.B shows the amount of hydrolyzed ATP as a function of time after addition at $t=0\text{s}$ of $150\mu\text{M}$ ATP; increasing P_i concentrations hardly inhibited ATP hydrolysis by the mutant enzyme. By plotting both the initial rates as a function of P_i and the rates at $t=100\text{s}$ (Fig. 6.4.2., open magenta triangles and full magenta circles respectively), it is evident that the P_i inhibitory effect totally disappeared. The DCCD insensitive activity was $1.0 \text{ nmolesATP}\cdot\text{s}^{-1}\cdot\text{mg}^{-1}$ (data not shown).

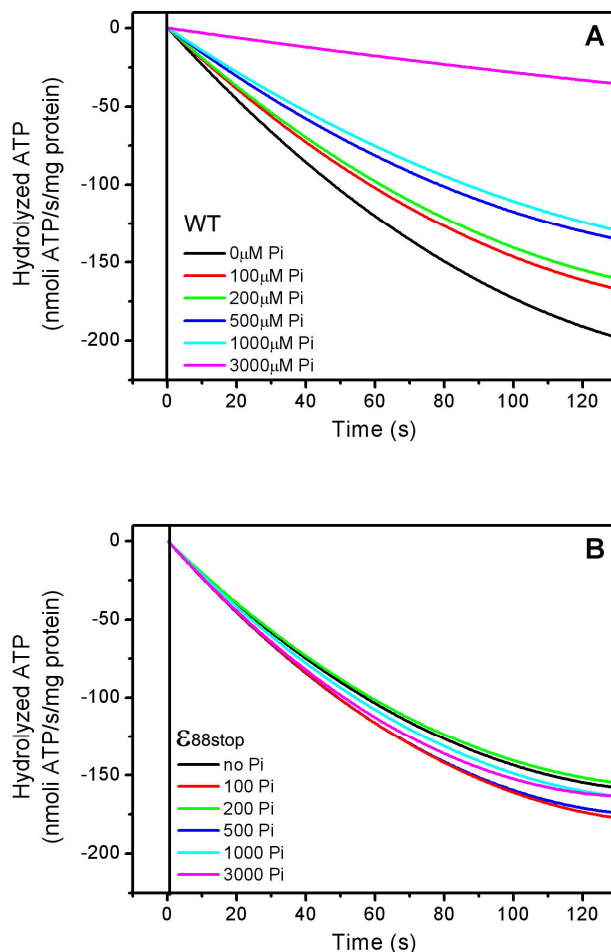


Fig. 6.4.1. ATP hydrolysis as a function of time in the presence of different $[P_i]$, in ϵ WT (A) and in $\epsilon_{88\text{-stop}}$ membranes (B).

The ATP hydrolysis reaction was started by adding $150\mu\text{M}$ ATP at $t = 0\text{s}$ and the experimental traces have been best fitted by monoexponential functions (not shown).

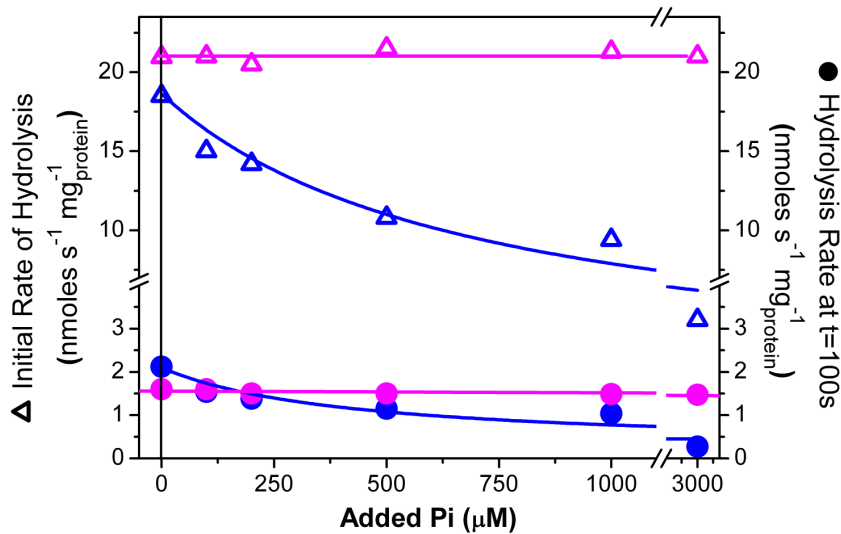


Fig. 6.4.2. ATP hydrolysis as a function of [Pi], in WT (blue) and in $\epsilon_{88\text{-stop}}$ *E. coli* membranes (magenta).

Initial rates of ATP hydrolysis (Δ) and rates at $t=100\text{s}$ (\bullet) are from Fig.6.4.1.A In WT membranes the curves through the hydrolysis data points were a best fitting hyperbole with apparent $K_d = 680 \pm 200 \mu\text{M}$ (Δ) and $K_d = 420 \pm 200 \mu\text{M}$ (\bullet). In $\epsilon_{88\text{-stop}}$ membranes the hydrolysis data points were best fitted by linear functions.

6.4.2. Proton pumping in WT and in $\epsilon_{88\text{-stop}}$ mutant as a function of P_i concentration.

The ACMA fluorescence as a function of time in the presence of different added P_i concentrations in WT membranes is shown in Fig. 6.4.3.A and B. As expected, both the initial rate of quenching and the steady state quenching have a biphasic trend. A similar biphasic response to P_i could also be observed in the data obtained in the presence of mutant membranes, but the inhibitory trend at high P_i concentrations was markedly reduced in the mutant. (Fig. 6.4.3.C and D).

In Fig. 6.4.4. both the steady state (at $t=100\text{s}$) and the initial rate values of fluorescence quenching were plotted as a function of added P_i (full circles and open triangle respectively). The data related to the WT membranes are in blue and the ones related to the mutant membranes are in magenta.

The plot shows that the ability of low concentrations of P_i to enhance the ACMA fluorescence quenching is retained in the ϵ truncation mutant. Consistently with the hydrolysis data above, quenching by the mutant membranes is less inhibited by high P_i concentration. As in the WT, low P_i concentrations (tens of μM) induced also in the mutant an increase of the coupling efficiency. The extent of this increase was similar in the two strains. We conclude that the phenomenon of intrinsic uncoupling found in ATP synthase from *E. coli* WT membranes (D'Alessandro et al., 2008) was still present in the truncated mutant. However the hydrolysis of the ATP synthase lacking the C-terminus of the ϵ subunit was much less sensitive than WT to inhibition by P_i .

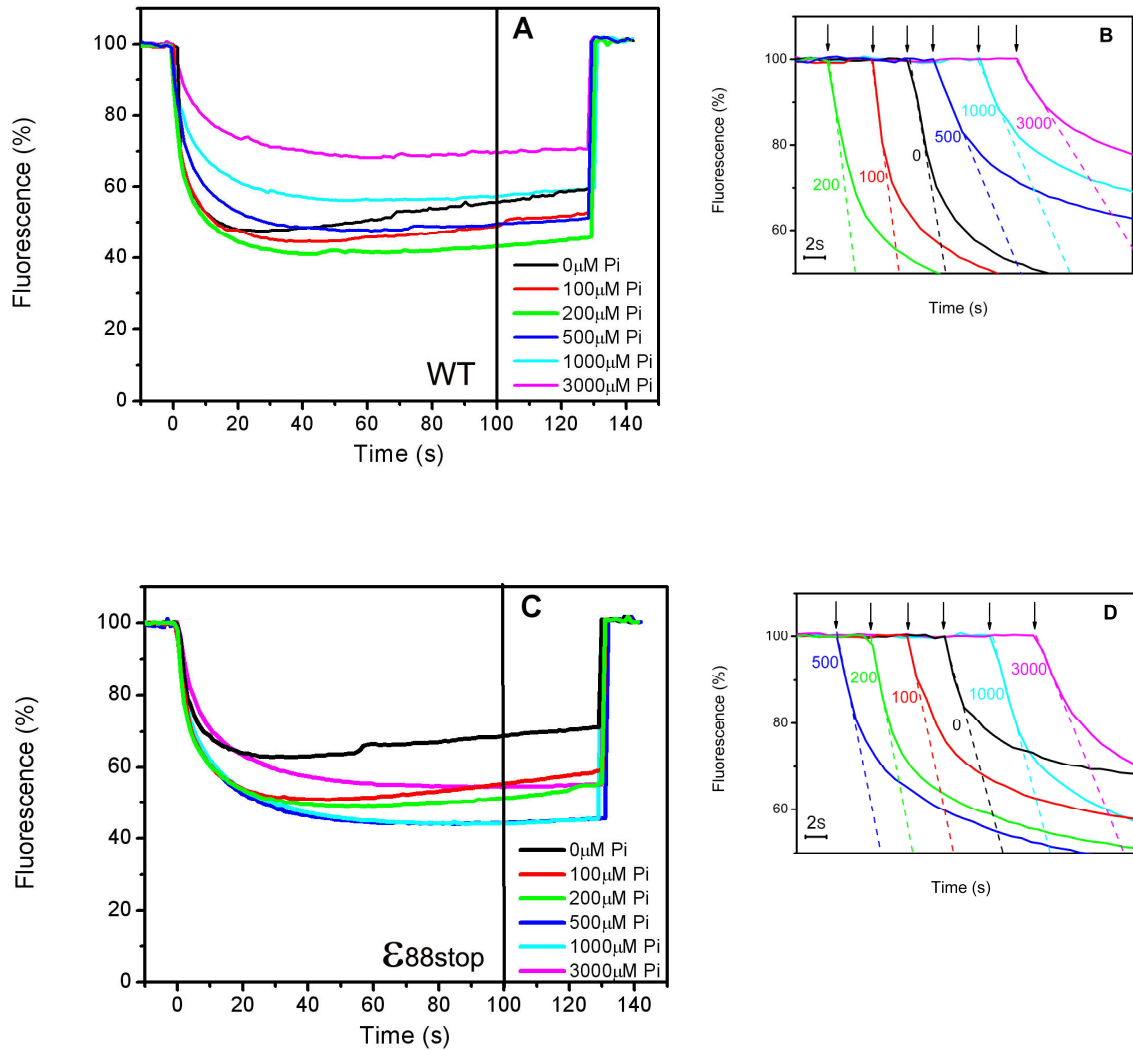


Fig.6.4.3. ACMA fluorescence quenching as a function of time in the presence of different [Pi], in ϵ WT *E. coli* membranes (A-B) and in $\epsilon_{88\text{-stop}}$ *E. coli* membranes (C-D).

The fluorescence measurements were carried out under the same experimental conditions as the ATP hydrolysis measurements. For each trace, addition of 1 μM nigericin recovered the 100% fluorescence level.

Panels A, C. The proton pumping reaction was started by addition of 150 μM ATP at $t=0$ and the ACMA fluorescence was recorded as a function of time. Different [Pi] were present in each assay.

Panels B, D. The graphs were rescaled to show the initial rate of quenching.

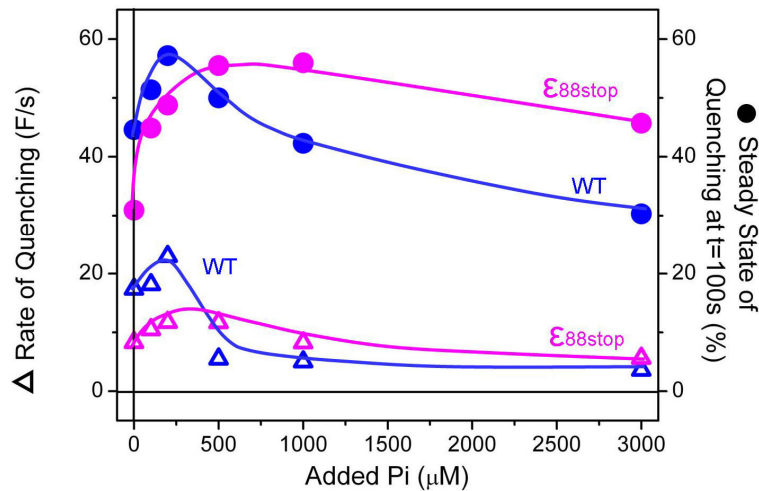


Fig.6.4.4. ACMA fluorescence quenching as a function of $[P_i]$, in ϵ WT (blue) and in $\epsilon_{88\text{-stop}}$ *E. coli* membranes (magenta).

Initial rates of quenching (Δ) and steady state values at $t=100$ s (\bullet) are from Fig.6.4.3. The curves through the quenching data points were drawn by hand.

6.4.3. Effect of P_i on ATP hydrolysis and proton pumping in WT and in $\epsilon_{88\text{-stop}}$ mutant in the presence of $1\mu\text{M}$ ADP, pre-incubated for an undefined time interval.

The P_i regulatory role can be observed only if ADP is bound to the enzyme (see §3.4. and §3.6.). Therefore, we re-examined the P_i effect both on the hydrolysis and on the proton pumping in the presence of $1\mu\text{M}$ ADP, to check whether the lack of hydrolysis inhibition by P_i in the $\epsilon_{88\text{-stop}}$ mutant could be due to lack of ADP bound to the enzyme. In this set of measurements no care was taken on the length of the pre-incubation time with ADP, since we were not aware yet that long incubation times could make a difference (see §6.6.).

The hydrolysis measurements were carried out under the same experimental conditions as described in §6.4.1. In Fig. 6.4.5. the observed initial rates of hydrolysis and the rates at $t=100$ s were plotted as a function of P_i (open triangles and full circles, respectively). Both in the WT membranes (blue symbols in Fig. 6.4.5.), and in the mutant membranes (magenta symbols in Fig. 6.4.5.), the presence of $1\mu\text{M}$ ADP affected the rate of hydrolysis. Compared with the data obtained in the absence of ADP (Fig.6.4.2.), the hydrolysis rate was reduced at $P_i=0$ to 66.5% for the WT and to 25% for the mutant for all P_i concentration. The inhibition as a function of P_i in the WT membranes was noticeable even though slight, whereas in the mutant no inhibitory trend was obtained by increasing P_i concentration. As to the ACMA fluorescence quenching, both the steady state (at $t=100$ s) and the initial rate values of fluorescence quenching were plotted in Fig. 6.4.6. as a function of added P_i (open triangles and full circles, respectively). In both strains, P_i induced a significant increase of proton pumping, which, compared to hydrolysis, indicates again a coupling effect of P_i regardless of the presence of the C-terminus.

We conclude that the presence of $1\mu\text{M}$ ADP did not alter substantially the P_i effects in the WT or in the mutant. In particular, the P_i modulation we were expecting to see in the mutant was not observed. It is likely that the chosen ADP concentration was already too strongly inhibitory, eventually masking the hypothesized P_i modulation.

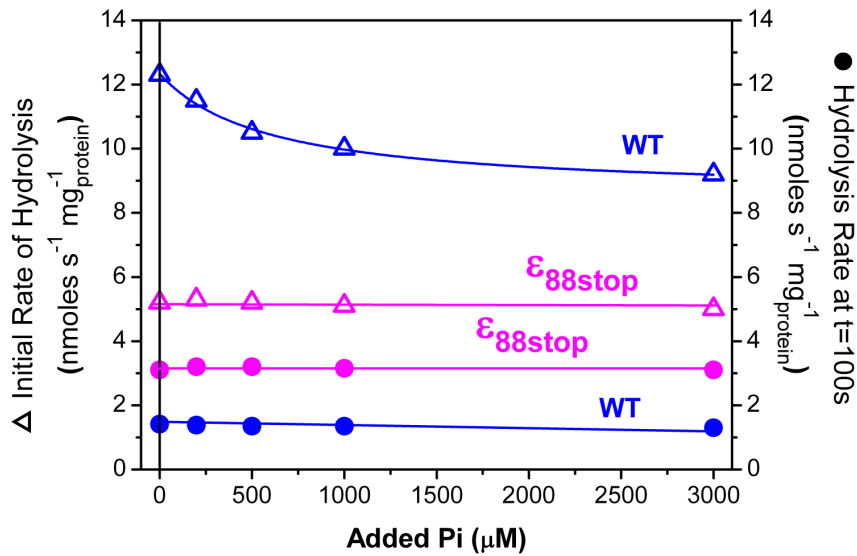


Fig. 6.4.5. ATP hydrolysis as a function of [Pi] in the presence of 1μM ADP, pre-incubated for an undefined time interval, in WT (blue) and in $\epsilon_{88\text{-stop}}$ *E. coli* membranes (magenta). Initial rates of ATP hydrolysis (Δ) and rates at $t=100\text{s}$ (\bullet). In WT membranes the hydrolysis data points were best fitted by a hyperbolic function with apparent $K_d = 590 \pm 110 \mu\text{M}$ (Δ) and by a linear function (\bullet). In $\epsilon_{88\text{-stop}}$ membranes the ATP hydrolysis data points were best fitted by linear functions.

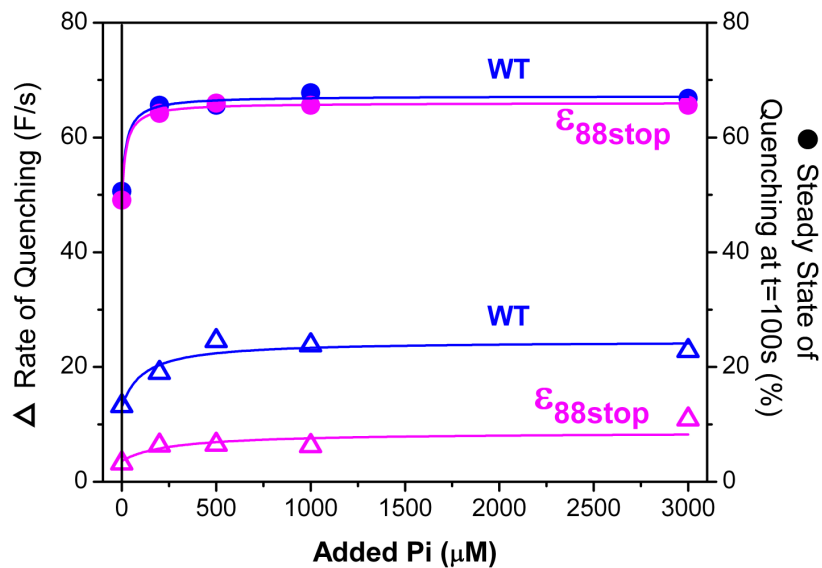


Fig. 6.4.6. ACMA fluorescence quenching as a function of [Pi] in the presence of 1μM ADP, pre-incubated for an undefined time interval, in WT (blue) and in $\epsilon_{88\text{-stop}}$ *E. coli* membranes (magenta). Initial rates of quenching (Δ) and steady state values at $t=100\text{s}$ (\bullet). In WT membranes the curves through the quenching data points were best fitting hyperboles with apparent $K_d = 112 \pm 100 \mu\text{M}$ (Δ) and $K_d = 23 \pm 20 \mu\text{M}$ (\bullet). In $\epsilon_{88\text{-stop}}$ membranes the curves through the quenching data points were best fitting hyperboles with apparent $K_d = 260 \pm 200 \mu\text{M}$ (Δ) and $K_d = 20 \pm 10 \mu\text{M}$ (\bullet).

6.5. ADP concentration dependence of the proton pumping in WT and in $\epsilon_{88\text{-stop}}$ mutant.

A set of preliminary fluorescence quenching measurement was carried out in the presence of four different concentrations of ADP (0, 0.25, 0.5 and 1 μM). The aim of this experiment was to find a range of ADP concentration that was not so strongly inhibitory of the ATP synthase and to use it to repeat the measurements reported in §6.4.3. Fig. 6.5.1. **A** and **B** show the ACMA fluorescence as a function of time in WT and mutant membranes, respectively. Membranes were diluted in the measuring buffer containing ADP at different concentration, subsequently ATP was added and the time course of fluorescence quenching was recorded.

The striking effect revealed by these measurements is the significant inhibition observed in a range of very low ADP concentrations (0 to 1 μM). We reasoned that this phenomenon must have had something to do with pre-incubation, since the 150 μM ATP added at the beginning of the reaction contained already 1.5 μM ADP (see § 2.11.). Moreover in the mutant the plots obtained in the presence of 0.5 and 1 μM ADP appear to be similar, pointing to a high scattering of the data: such scattering might have had something to do with the pre-incubation, in particular with the lack of control of the pre-incubation time. Therefore, we decided to study this effect in more detail.

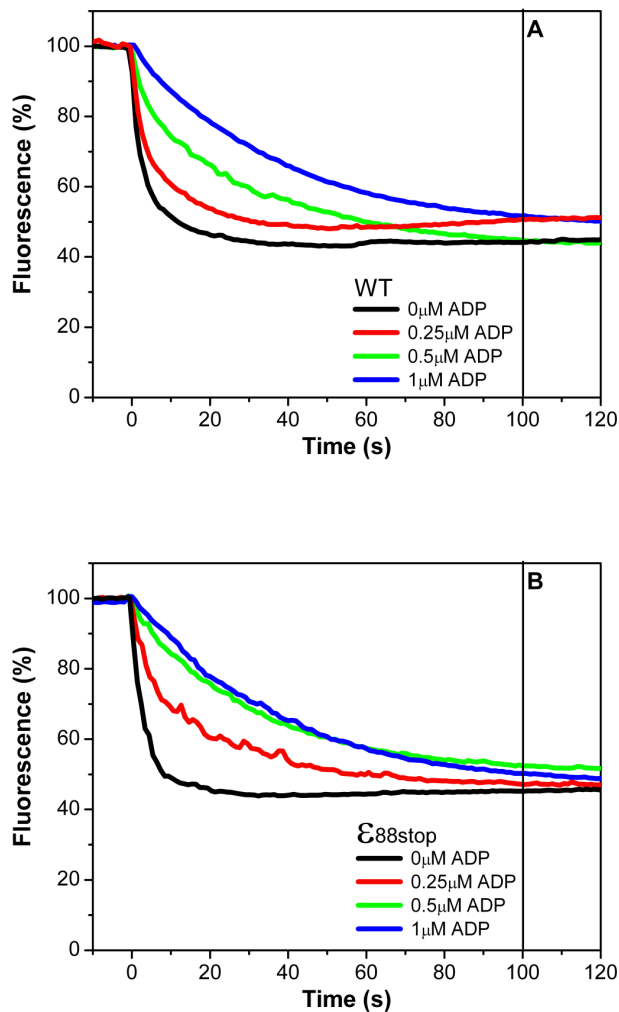


Fig.6.5.1. ACMA fluorescence quenching as a function of time in the presence of different [ADP], pre-incubated for an undefined time interval in WT (A) and in $\epsilon_{88\text{-stop}}$ *E. coli* membranes (B). The fluorescence measurements were carried out under the same experimental conditions of §6.4.2.

Panels A,B. The proton pumping reaction was started by addition of 150 μM ATP at $t=0$ and the ACMA fluorescence was recorded as a function of time. Different [ADP] were added to each assay.

6.6. Dependence of ATP hydrolysis and proton pumping on the pre-incubation time in the presence of ADP, in WT and in $\epsilon_{88\text{-stop}}$ mutant.

As mentioned, in the experiments reported in §§ 6.4.3. and 6.5. the pre-incubation time in the presence of ADP was not controlled (the length of the pre-incubation varied in a range usually from 5 up to 10 min, and occasionally even longer), but the results obtained gave some hints that the pre-incubation time could be a critical parameter. We decided to check if the pre-incubation time of the membranes with ADP could modulate the inhibitory effect of this substrate on the ATP synthase. Both WT and Mutant membranes were incubated in the presence of $1\mu\text{M}$ ADP for different lapses of time (ranging from 0 to 120 min). In parallel, the ATP hydrolysis rate and the ACMA fluorescence quenching were measured for every sample. The hydrolysis measurements were carried out under the same conditions of §6.4.3., except for the pre-incubation time, which was controlled.

In WT membranes the initial rate of hydrolysis was decreased by 40% and 50% after 30 min and 120 min, respectively, of pre-incubation in the presence of $1\mu\text{M}$ ADP (blue triangles of Fig 6.6.1.A). In mutant membranes (magenta triangles of Fig 6.6.1.A), after 30 and 120 min of pre-incubation, the hydrolysis rate was 75% lower than the control, in which ADP and ATP were added simultaneously. Interestingly, the hydrolysis values of controls were very similar to the ones obtained in the absence of ADP.

Both in WT and in mutant membranes, the extent of ADP inhibition increased by increasing the length of the incubation time. This effect was fully saturated in the WT after approximately 60 min of incubation, while in the mutant the saturation was prompter and the extent of inhibition larger.

The length of the pre-incubation time did not affect the rates of ATP hydrolysis at $t=100$ s, either in WT and in mutant membranes (Fig 6.6.1.B); it is likely that after 100s the amount of ADP generated by hydrolysis covers this time-dependant phenomenon.

As to the quenching measured under the same conditions, in WT membranes the initial rate of quenching was decreased by 30% and 70% after, respectively, 30 min and 120 min pre-incubation in the presence of $1\mu\text{M}$ ADP (blue triangles of Fig 6.6.2.A). Nevertheless, as seen also for the hydrolysis data, the decrease of the steady state (at $t=100$ s) quenching values as a function of pre-incubation time was negligible (blue circles of Fig 6.6.2.B).

In mutant membranes, after 30 min pre-incubation, the initial rate of quenching was already decreased by 95%, and the inhibition did not vary up to 120 min (magenta triangles of Fig 6.6.2.A); the decrease of the steady state (at $t=100$ s) of fluorescence quenching was somewhat stronger than in the WT (a 30% inhibition after 30 min and up to 120 min of pre-incubation; magenta circles of Fig 6.6.2.B), but was much less compared to the inhibition of the initial rate of quenching.

Given the high speed with which the quenching and the hydrolysis rate decreased in the mutant, it was worth to investigate what happened at lower concentration of ADP.

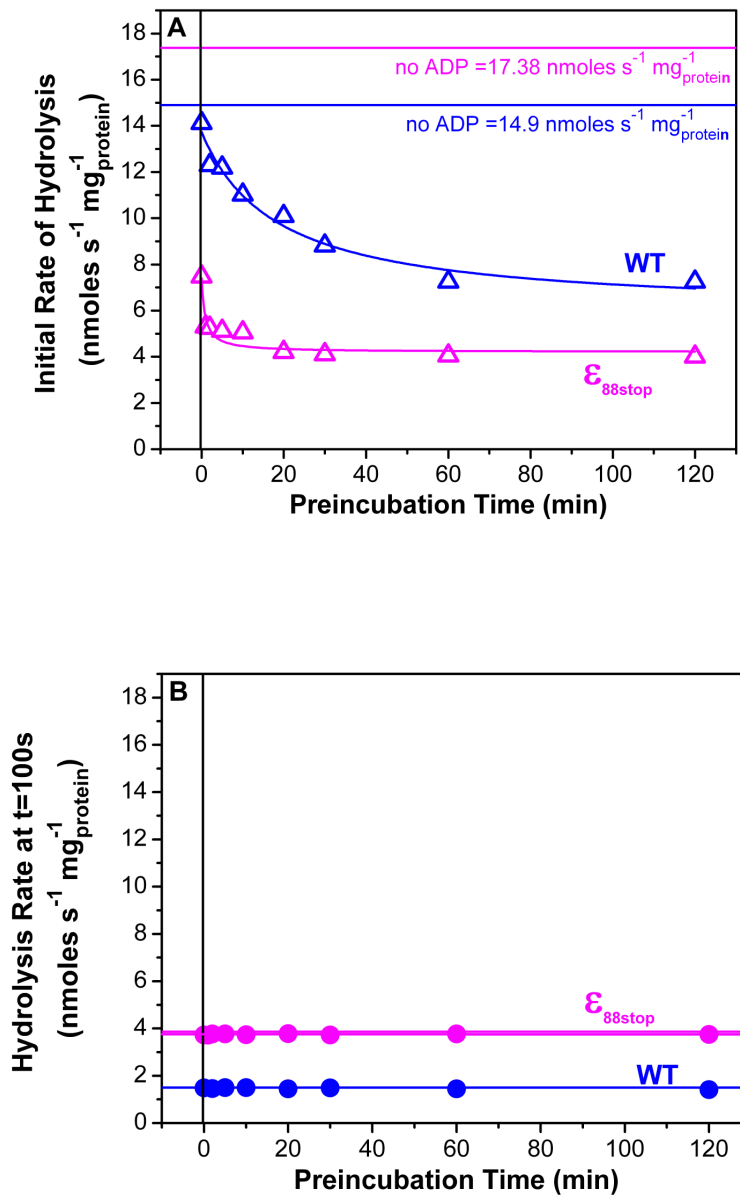


Fig.6.6.1. Initial rate (A) and rate at t=100s (B) of ATP hydrolysis as a function of the preincubation time in the presence of 1 μM ADP in WT and in $\epsilon_{88\text{-stop}}$ *E. coli* membranes (B).

Panel A. The curves through the hydrolysis data points were best fitting hyperboles with half maximal effects at 18 ± 6 min in WT (Δ), and at 0.9 ± 0.4 min in $\epsilon_{88\text{-stop}}$ membranes (Δ);

Panel B. Both in WT (\bullet), and in $\epsilon_{88\text{-stop}}$ membranes (\bullet) the ATP hydrolysis data points were best fitted by linear functions. In the absence of ADP the hydrolysis rates were 1.52 and 3.81 nmol s⁻¹ mg⁻¹ in WT and in $\epsilon_{88\text{-stop}}$ membranes, respectively.

The first time point in all data sets correspond to a pre-incubation time of 10sec.

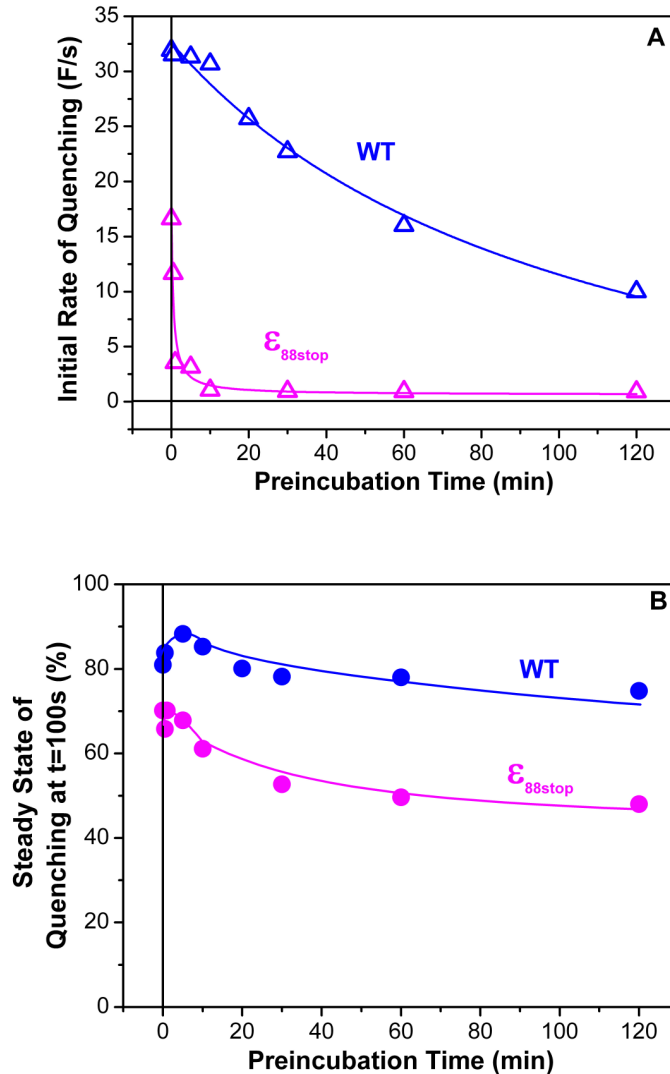


Fig.6.6.2. Initial rate (A) and steady-state at t=100s (B) of quenching as a function of the pre-incubation time in the presence of 1 μ M ADP in WT and in $\epsilon_{88\text{-stop}}$ *E. coli* membranes.

Panel A. The curves through the quenching data points were best fitting hyperboles with half-maximal effects at 106 ± 35 min in WT (Δ), and at 0.5 ± 0.2 min in $\epsilon_{88\text{-stop}}$ membranes (Δ);

Panel B. Both in WT (\bullet) and in $\epsilon_{88\text{-stop}}$ membranes (\bullet) the curves through the quenching data points were drawn by hand.

The first time point in all data sets correspond to a pre-incubation time of 10sec.

The same set of hydrolysis and quenching experiments were repeated in the presence of a lower concentration of ADP (0.1 μ M). The results are summarized in Fig.6.6.3. and 6.6.4..

In the presence of such low ADP concentration, the decrease of the hydrolysis initial rate as a function of pre-incubation time was negligible in WT membranes (blue triangles of Fig 6.6.3.A), but, surprisingly, it was still quite strong in mutant membranes (50% after 30 and 120 min of incubation; magenta triangles of Fig 6.6.3.A.).

The rates of ATP hydrolysis at t=100 s (Fig. 6.6.3.B), both in WT and in mutant membranes, had trends similar to the data observed in the presence of 1 μ M ADP (Fig.6.6.1.B). The decrease of the initial rate of quenching as a function of the incubation time in the presence of 0.1 μ M ADP was almost negligible in WT

membranes (5% after 30 and 120 min; blue triangles of Fig 6.6.4.A), but still significant in mutant membranes (90% after 30 and 100 min of incubation; magenta triangles in Fig. 6.6.4.A).

In WT membranes there was no decrease of the steady state (at $t=100$ s) quenching values as a function of pre-incubation time (blue circles of Fig. 6.6.4.B); in mutant membranes, a decrease of 25% after 30 and 100 min of incubation was observed (magenta circles of Fig. 6.6.4.B).

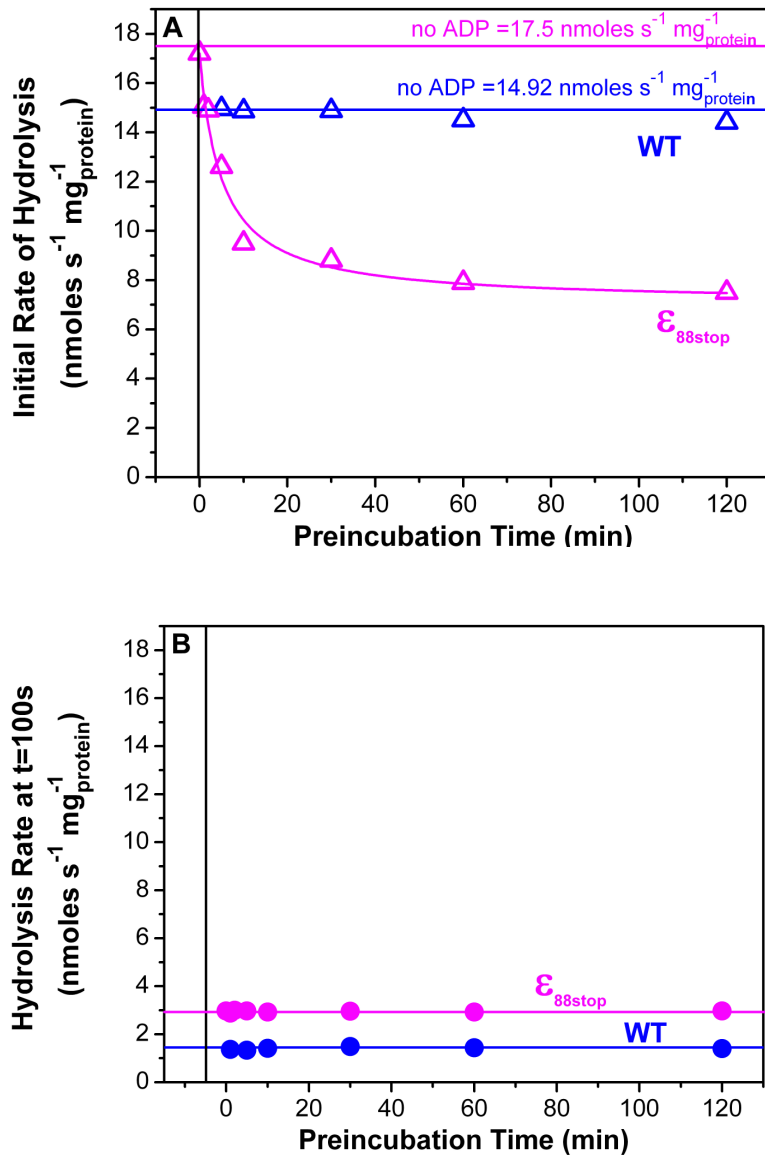


Fig. 6.6.3. Initial rate (A) and rate at $t=100$ s (B) of ATP hydrolysis as a function of the pre-incubation time in the presence of $0.1\mu\text{M}$ ADP in WT and ϵ_{88stop} *E. coli* membranes.

Panel A. In WT membranes (Δ) the hydrolysis data points were best fitted by a linear function; in ϵ_{88stop} membranes (∇) the curve through the ATP hydrolysis data points was a best fitting hyperbole with a half-maximal effect at 5 ± 1 min.

Panel B. Both in WT (\bullet), and in ϵ_{88stop} membranes (\bullet) the ATP hydrolysis data points were best fitted by linear functions. In the absence of ADP the hydrolysis rates were 1.45 and 3.32 nmoles s⁻¹ mg⁻¹ in WT and in ϵ_{88stop} membranes, respectively.

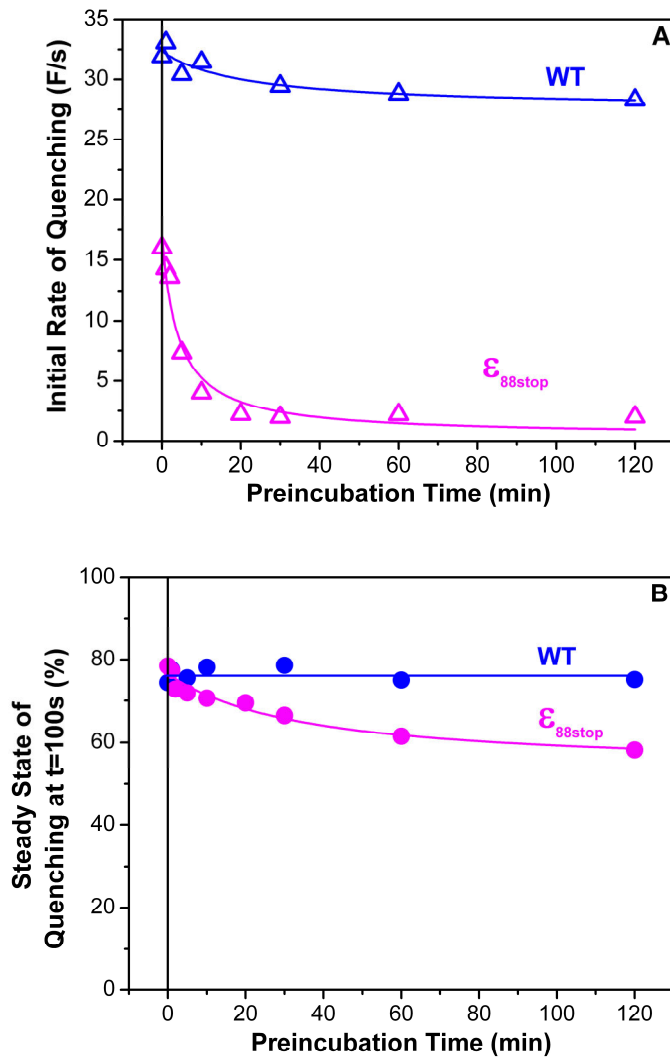


Fig. 6.6.4. Initial rate (A) and steady-state at $t=100\text{s}$ quenching (B) as a function of the preincubation time in the presence of $0.1\mu\text{M}$ ADP in WT and $\epsilon_{88\text{-stop}}$ *E. coli* membranes.

Panel A. The curves through the quenching data points were best fitting hyperboles with half-maximal effects at $20\pm 19\text{min}$ in WT (Δ), and at $4\pm 1\text{min}$ in $\epsilon_{88\text{-stop}}$ membranes (Δ);

Panel B. In WT (\bullet) the quenching data points were best fitted by a linear function; in $\epsilon_{88\text{-stop}}$ (\bullet) the curves through the quenching data points was a best fitting hyperbole with a half-maximal effects at $34.5\pm 15\text{min}$.

6.7. Dependence of ATP hydrolysis and proton pumping in WT and in $\epsilon_{88\text{-stop}}$ mutant on the ADP concentration during preincubation.

The dependence on ADP concentration, covering a range between 0.5nM and $2\mu\text{M}$, was studied. The pre-incubation was 30min for all samples.

Fig.6.7.1.A shows the initial rate of hydrolysis as a function of ADP. In the WT membranes (blue triangles) ADP monotonically inhibited the rate of hydrolysis with a half-maximal effect at approximately $1\mu\text{M}$.

The initial rate of hydrolysis in mutant membranes (magenta triangles of Fig.6.7.1.A,C) showed a similar inhibitory trend, but, surprisingly, two apparent K_d values were found, one in at 1nM and one in the hundreds of nM range.

In the rates of ATP hydrolysis at $t=100\text{ s}$ of WT membranes, the ADP inhibitory effect was barely detectable (blue circles of Fig.6.7.1.B). In mutant membranes, ADP was inhibitory also for the hydrolysis rate at $t=100$, with apparent K_d 's in the range of those measured for the initial rates (magenta circles of Fig.6.7.1.B, D).

In WT membranes, ADP monotonically inhibited the initial rate of proton pumping, starting from a concentration of 500nM (blue triangles of Fig.6.7.2.A). A similar inhibitory trend could also be observed in the steady state (at $t= 100\text{s}$) of fluorescence quenching (blue circles of Fig.6.7.2.B).

In mutant membranes, conversely, the initial rate of quenching was increased in the presence of ADP concentrations up to 0.75nM, while higher concentrations resulted in a progressive inhibition of proton pumping (magenta triangles of Fig.6.7.2.A,C). A similar biphasic trend could also be observed in the steady state (at $t = 100s$) of the fluorescence quenching values (magenta circles of Fig.6.7.2.B, D).

Data from Fig.6.7.1.A, C can be fitted in mutant membranes with two different apparent K_d values for ADP. These data indicate the existence of two ADP binding sites on the enzyme. In WT membranes, the fact that ADP starts to be inhibitory only at concentration higher than $0.1\mu M$ ADP, could indicate that in the WT enzyme the high affinity site is already filled with ADP.

In mutant membranes, the coupling effect of ADP appears to be linked to ADP binding to the high affinity site, i.e. it is evident in the range of few nM ADP.

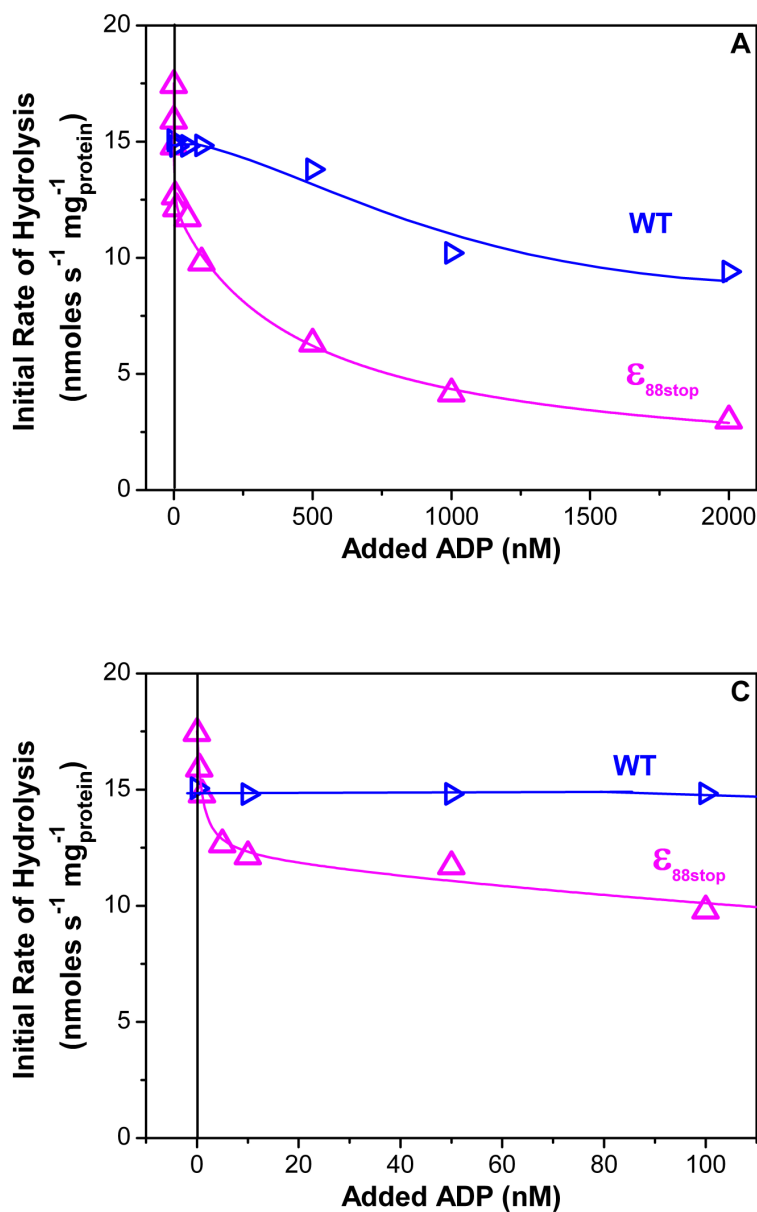


Fig. 6.7.1. A, C. see next page for the full caption.

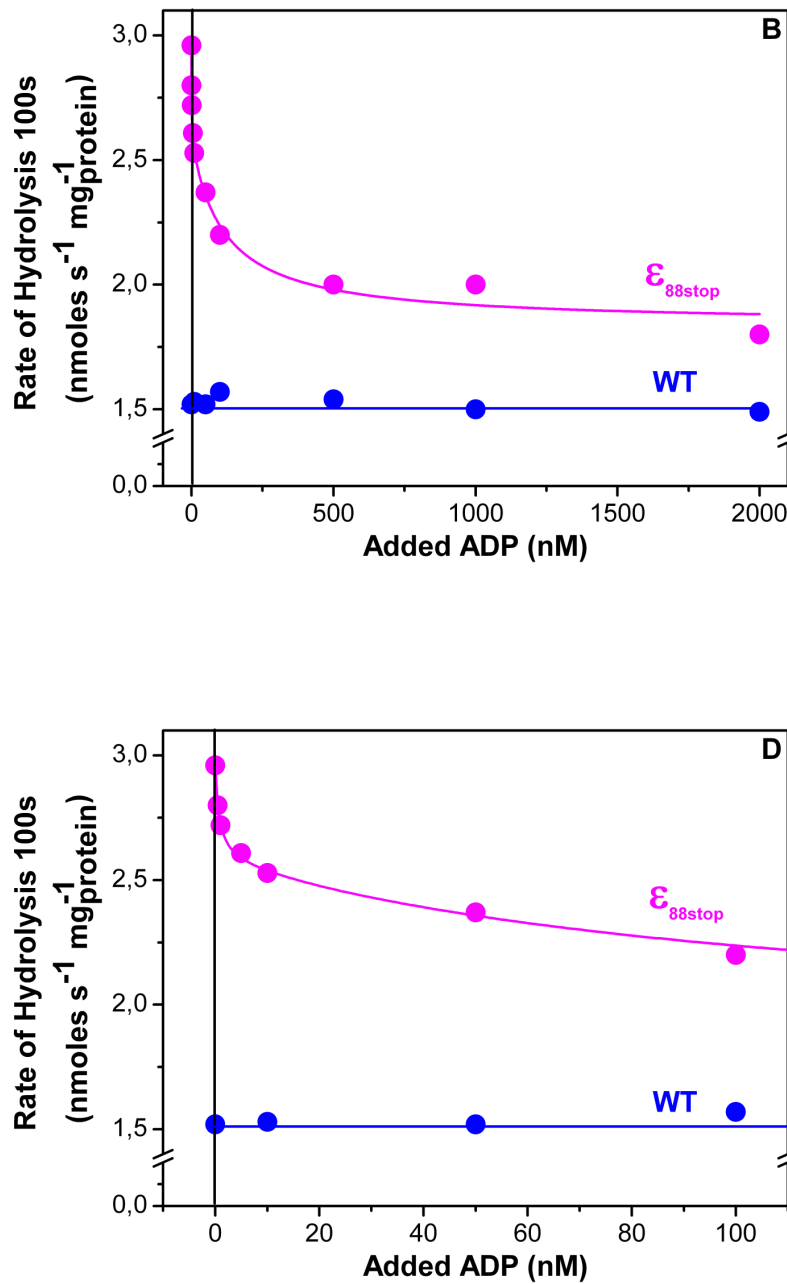


Fig. 6.7.1. Initial rate (A,C) and rate at t=100s (B,D) of ATP hydrolysis as a function of [ADP], in WT (blue) and in $\epsilon_{88\text{-stop}}$ *E. coli* membranes (magenta).

The preincubation time in the presence of different ADP concentrations was 30min for all samples. Panel A. The curve through the hydrolysis data points was drawn by hand in WT membranes (Δ) and was a best fitting double hyperbole with apparent $K_d = 1.0 \pm 0.3 \text{ nM}$ and $K_d = 117 \pm 0.5 \text{ nM}$ in $\epsilon_{88\text{-stop}}$ membranes (Δ);

Panel B. In WT membranes (\bullet) the hydrolysis data points were best fitted by a linear function.; in $\epsilon_{88\text{-stop}}$ membranes (\bullet) the curve through the ATP hydrolysis data point was a best fitting double hyperbole with apparent $K_d = 0.7 \pm 0.5 \text{ nM}$ and $K_d = 117 \pm 50 \text{ nM}$.

Panel C,D. The graphs A, B were rescaled to show the hydrolysis values in the hundreds of nM range.

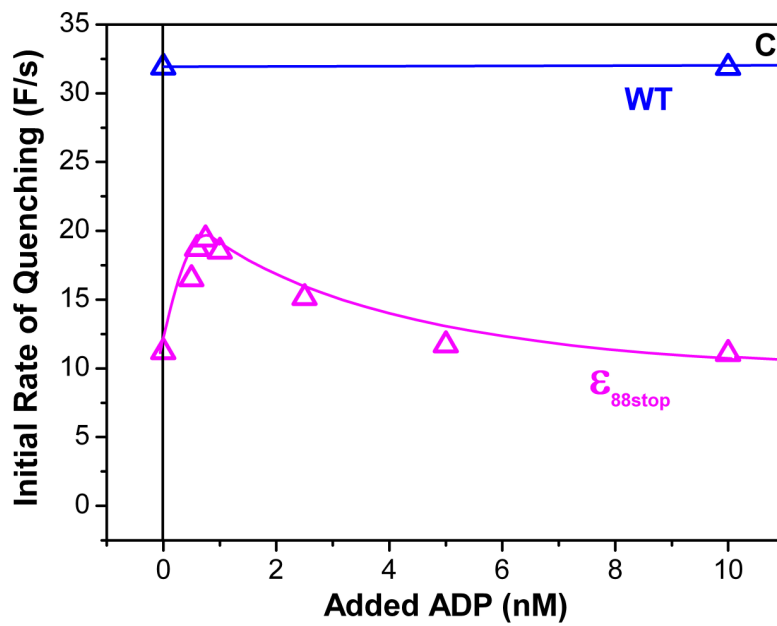
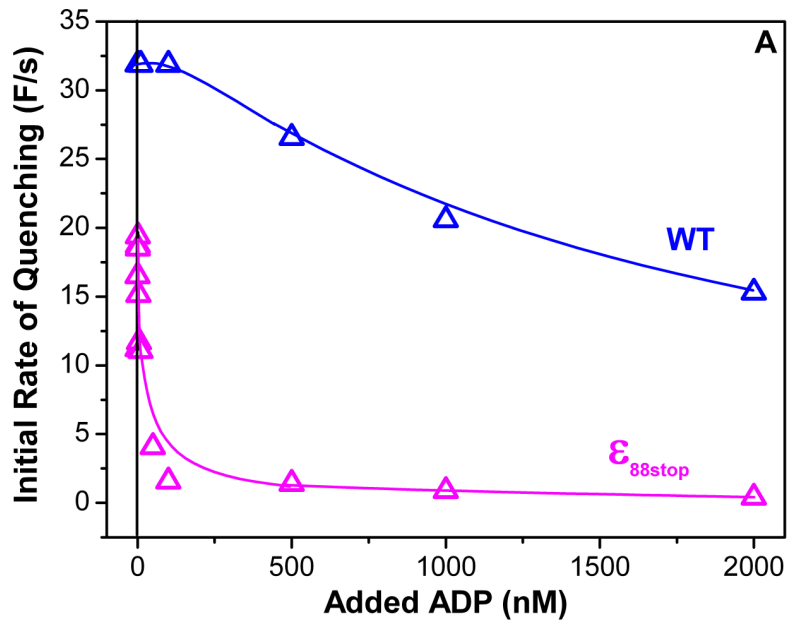


Fig. 6.7.2. A, C. See next page for the full caption.

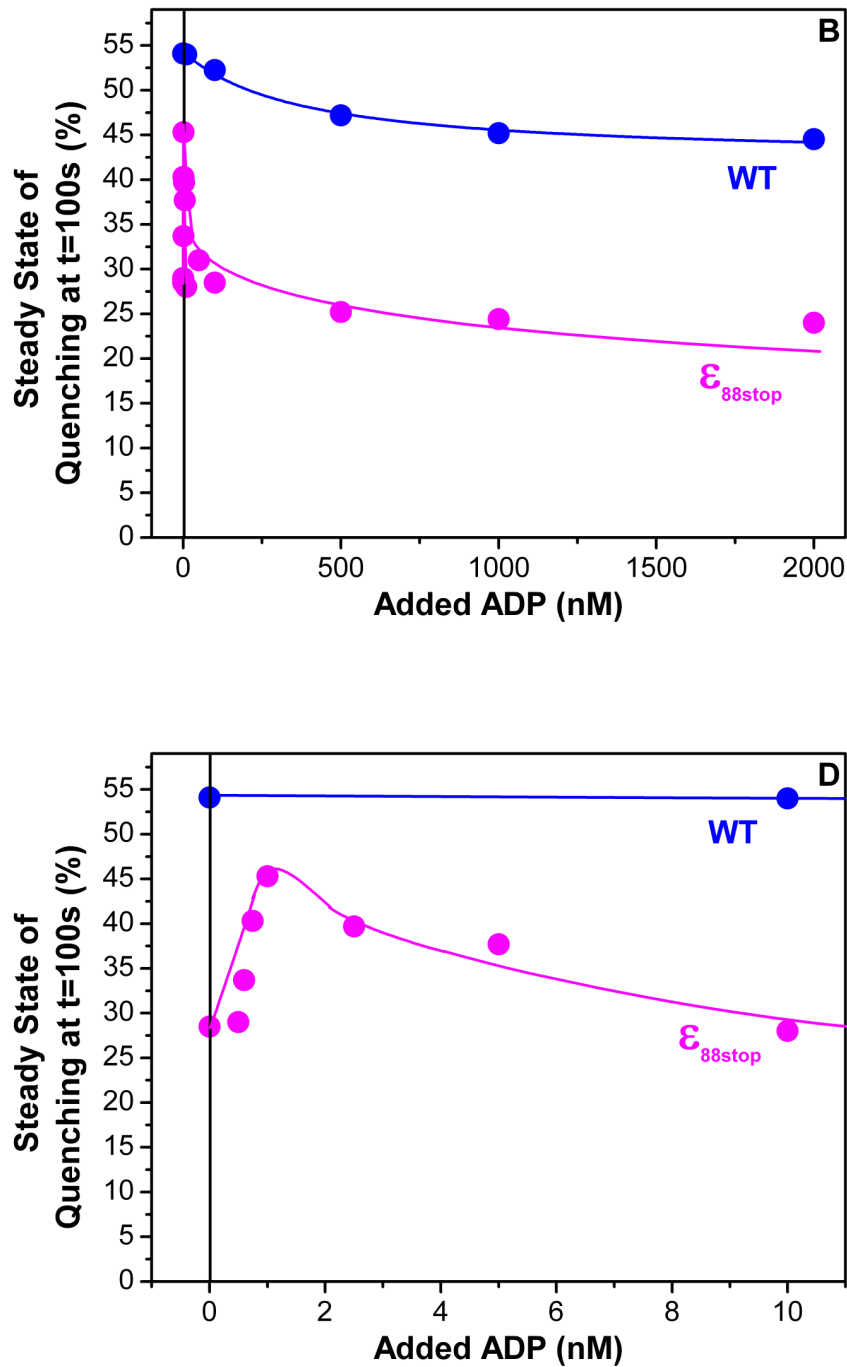


Fig.6.7.2. Initial rate (A,C) and steady-state values at t=100s (B,D) of quenching as a function of [ADP], in WT (blue) and in $\epsilon_{88\text{-stop}}$ *E. coli* membranes (magenta).

The preincubation time in the presence of different ADP concentrations was 30min for all samples.

Panel A. In WT membranes (Δ) and in $\epsilon_{88\text{-stop}}$ membranes (\triangle) the curves through the quenching data points were drawn by hand;

Panel B. In WT membranes (\bullet) and in $\epsilon_{88\text{-stop}}$ membranes (\bullet) the curves through the quenching data points were drawn by hand;

Panel C,D. The graphs A, B were rescaled to show the quenching values in the tens of nM range.

6.8. Effect of P_i on ATP hydrolysis and proton pumping in WT and in $\epsilon_{88\text{-stop}}$ mutant, after preincubation in the presence of ADP.

Considering the results obtained in §6.6. and §6.7., we decided to repeat the experiments shown in §6.4.3., but after pre-incubation in the presence of three different concentrations of ADP. The purpose was to check if the pre-incubation in the presence of ADP could reestablish, or affect to some degree, the inhibition by P_i of the hydrolysis rate in the mutant membranes. We incubated the membranes for 30 min with 1000, 100 and 1nM ADP and then we measured, in parallel, the corresponding ATP hydrolysis rates and the ACMA fluorescence quenching.

6.8.1. ATP hydrolysis and proton pumping as a function of P_i , after 30min of preincubation in the presence of 1 and 0.1 μM ADP.

Fig. 6.8.1.A-B show the initial rate of ATP hydrolysis as a function of P_i concentration in the presence and absence of 1 and 0.1 μM ADP, in WT (A) and in $\epsilon_{88\text{-stop}}$ membranes (B). In WT membranes the pre-incubation with both 0.1 and 1 μM ADP (respectively open triangles and squares of Fig. 6.8.1.A) increased the inhibition of ATP hydrolysis by P_i . The apparent $K_d = 1500 \mu\text{M}$, found in the absence of ADP, shifted to a value of about $700 \mu\text{M}$ in the presence of ADP. The pre-incubation in the presence of ADP strongly inhibited the hydrolysis rate at $t=100$; the P_i dependent inhibitory trend was similar to the one observed for the initial rate of hydrolysis data (Fig. 6.8.2.A).

In mutant membranes the ADP pre-incubation restored to some degree the inhibition by P_i . In the presence of 0.1 and 1 μM ADP we were able to measure an apparent K_d of 600 and $3000 \mu\text{M}$, respectively (open triangles and squares of Fig. 6.8.1.B). A similar response to P_i could also be observed in the hydrolysis rate at $t=100$ (Fig. 6.8.2.B).

The pre-incubation of membranes with 0.1 and 1 μM ADP prevented the enhancement of the initial rate of ACMA fluorescence quenching by low P_i concentrations for both WT and mutant membranes (6.8.3.A, B).

A biphasic response to P_i of the steady state fluorescence quenching (at $t=100$) in mutant membranes could be observed both in the absence and in the presence of ADP. The extent of the quenching increase, observed at low P_i concentration, was progressively smaller when the concentration of ADP was increased from 0 up to 1 μM (Fig.6.8.4.B). A slight biphasic trend was observed in WT membranes, in the presence of ADP (Fig.6.8.4.A).

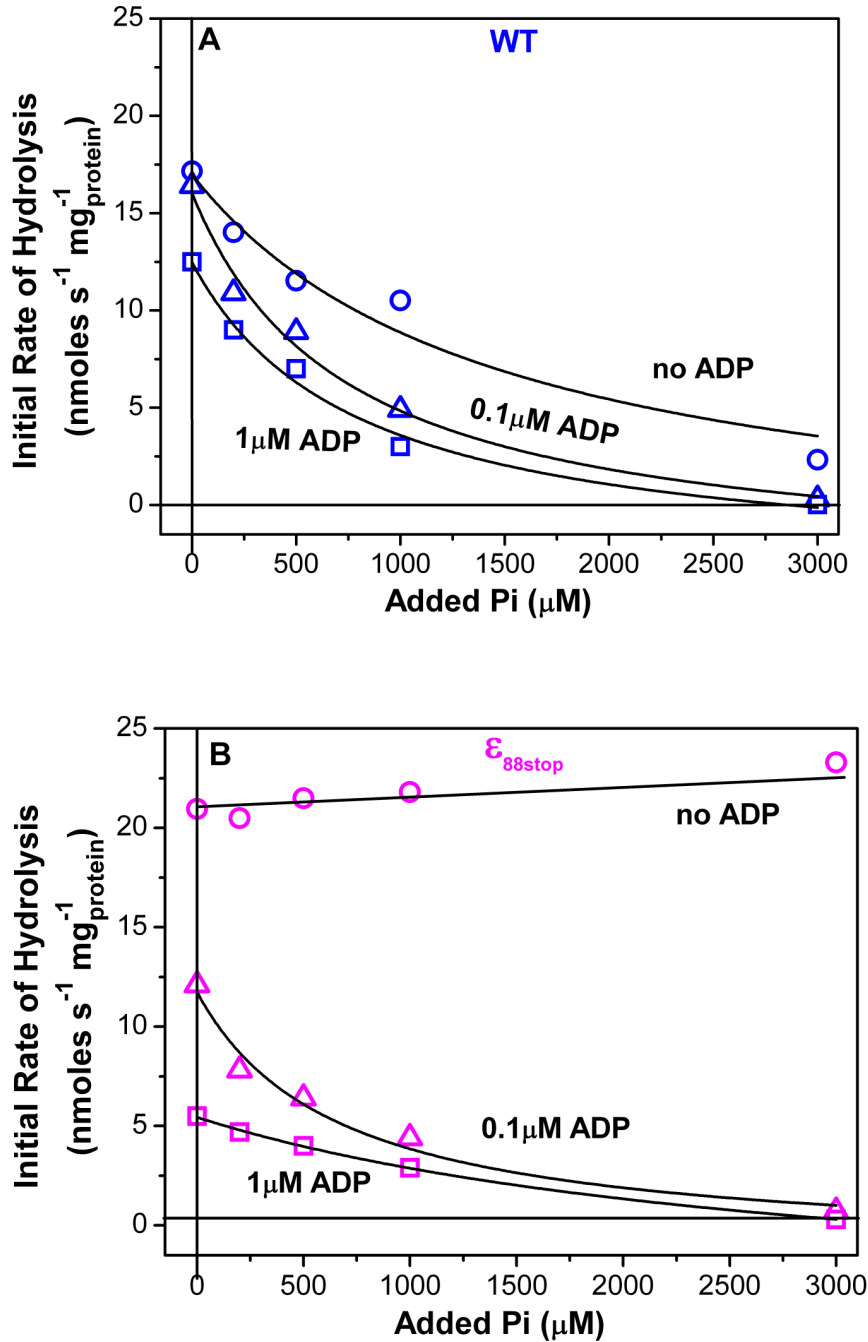


Fig. 6.8.1. Initial rate of ATP hydrolysis as a function of [Pi], after pre-incubation in the presence and absence of 0.1 and 1 μM ADP in WT (A) and in ε_{88-stop} *E. coli* membranes (B).

Panel A. The curves through the hydrolysis data points were best fitting hyperboles with apparent $K_d = 1500 \pm 200 \mu\text{M}$ in the absence of ADP (○), $K_d = 730 \pm 200 \mu\text{M}$ in the presence of 0.1 μM ADP (△) and $K_d = 790 \pm 200 \mu\text{M}$ in the presence of 1 μM ADP (□); Panel B. In the absence of ADP (○) the ATP hydrolysis data points were best fitted by a linear function; in the presence ADP the curves through the hydrolysis data points were best fitting hyperboles with apparent $K_d = 660 \pm 250 \mu\text{M}$ with 0.1 μM ADP (△) and $K_d = 3000 \pm 450 \mu\text{M}$ with 1 μM ADP (□).

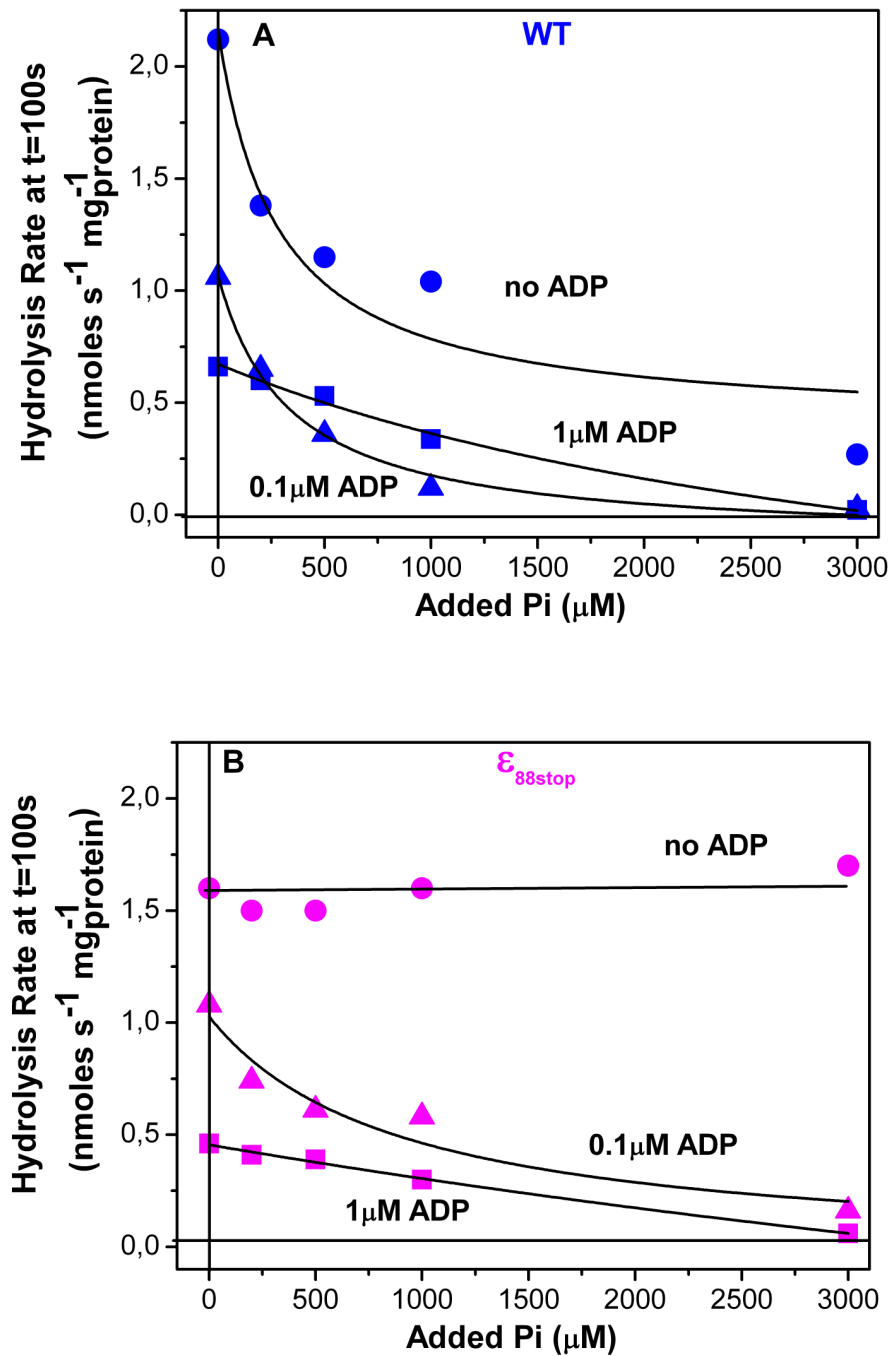


Fig. 6.8.2. Rate of ATP hydrolysis at $t=100s$ as a function of $[Pi]$, after pre-incubation in the presence and absence of 0.1 and $1\mu M$ ADP in ϵ WT (A) and in $\epsilon_{88-stop}$ *E. coli* membranes (B). Panel A. The curves through the hydrolysis data points were best fitting hyperboles with apparent $K_d = 470 \pm 100 \mu M$ in the absence of ADP (\bullet), $K_d = 330 \pm 70 \mu M$ in the presence of $0.1 \mu M$ ADP (\blacktriangle) and $K_d = 3800 \pm 1700 \mu M$ in the presence of $1 \mu M$ ADP (\blacksquare); Panel B. In the absence of ADP (\bullet) the ATP hydrolysis data points were best fitted by a linear function; in the presence of ADP the curves through the hydrolysis data points were best fitting hyperboles with apparent $K_d = 900 \pm 700 \mu M$ with $0.1 \mu M$ ADP (\blacktriangle) and $K_d = 13000 \pm 11000 \mu M$ with $1 \mu M$ ADP (\blacksquare).

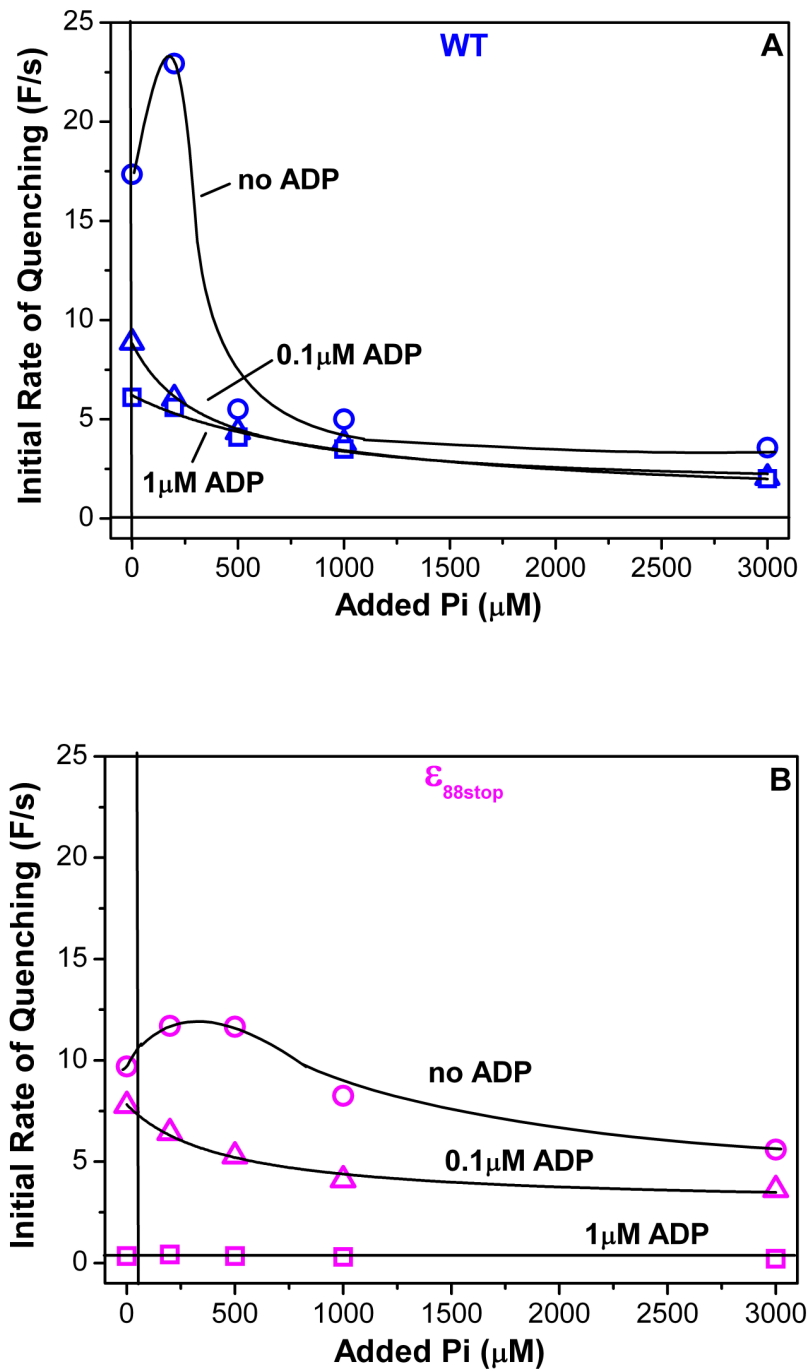


Fig. 6.8.3. Initial rate of quenching as a function of [Pi], after pre-incubation in the presence or absence of 0.1 and 1 μM ADP in WT (A) and in $\epsilon_{88\text{-stop}}$ *E. coli* membranes (B).

Panel A. The curve through the quenching data points obtained in the absence of ADP (○) was drawn by hand; the curves through the quenching data points, obtained in the presence of ADP, were best fitting hyperboles with apparent $K_d = 350 \pm 90 \mu\text{M}$ with 0.1 μM ADP (Δ) and $K_d = 1050 \pm 400 \mu\text{M}$ with 1 μM ADP (□);

Panel B. The curve through the quenching data points obtained in the absence of ADP (○) was drawn by hand; the curve through the quenching data points obtained in the presence of 0.1 μM ADP (Δ) was a best fitting hyperbole with apparent $K_d = 450 \pm 130 \mu\text{M}$; the quenching data points, obtained in the presence of 1 μM ADP (□), were best fitted by a linear function.

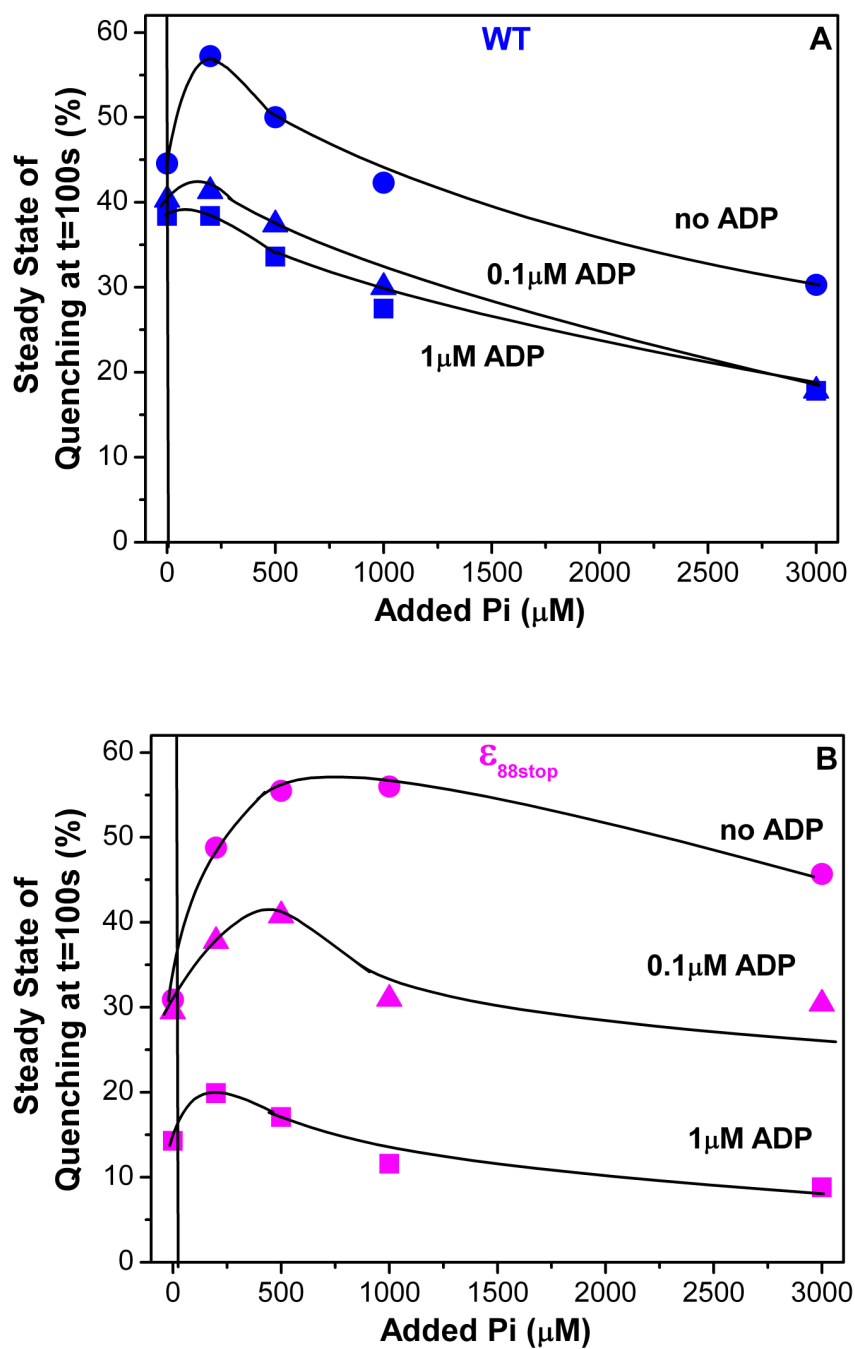


Fig. 6.8.4. Steady state of quenching at $t=100$ s as a function of $[\text{Pi}]$, after pre-incubation in the presence or absence of 0.1 and 1 μM ADP in WT (A) and in $\epsilon_{88\text{-stop}}$ *E. coli* membranes (B). Panel A. The curves through the quenching data points were drawn by hand; Panel B. The curves through the quenching data points were drawn by hand.

6.8.2. ATP hydrolysis and proton pumping as a function of P_i , after 30min of pre-incubation in the presence of 1 nM ADP.

The data presented in §6.8.1. show that a strong inhibition of the hydrolysis and a significant enhancement of proton pumping were still detectable by pre-incubating the mutant membranes in the presence of 0.1 μ M ADP. We decided to repeat the experiments in the presence of 1nM ADP.

Such a low ADP concentration did not affect the behaviour of WT membranes. As already observed for the data obtained in the absence of ADP (§6.4.), the hydrolysis rate was monotonically inhibited by P_i (Fig. 6.4.2.). In the proton pumping experiments, we reproduced the biphasic response to P_i already observed in the absence of ADP (Fig. 6.4.4.). Both the degree of the inhibition of the hydrolysis and the extent of the enhancement of the ACMA fluorescence quenching were in the same range as those observed in the absence of ADP (data not shown).

In mutant membranes, the pre-incubation in the presence of 1nM ADP was still able to restore the inhibition by P_i in the hydrolysis measurements (Fig.6.8.5.A). Based on the K_d values of the initial rate of hydrolysis data from the four data sets (P_i dependence in the presence of 0, 1, 100, 1000nM ADP), the highest efficiency for the inhibition by P_i was obtained in the presence of 1nM ADP (Fig.6.8.6.A).

In proton pumping experiments, we observed a biphasic trend both in the initial rate and in the steady-state of quenching data (open and full circles in Fig.6.8.5.B). The extent of the enhancement of ACMA fluorescence quenching by low P_i concentrations was stronger than the one observed in the absence of ADP (Fig.6.8.6.B).

In our view, the pre-incubation experiments shown in this section confirm the hypothesis that, in the WT membrane system, the high affinity site of the enzyme is already almost completely filled with ADP. Moreover the data obtained with mutant membranes indicate a strong effect of extremely low ADP concentrations (in the subnanomolar range) in both hydrolysis and proton pumping experiments.

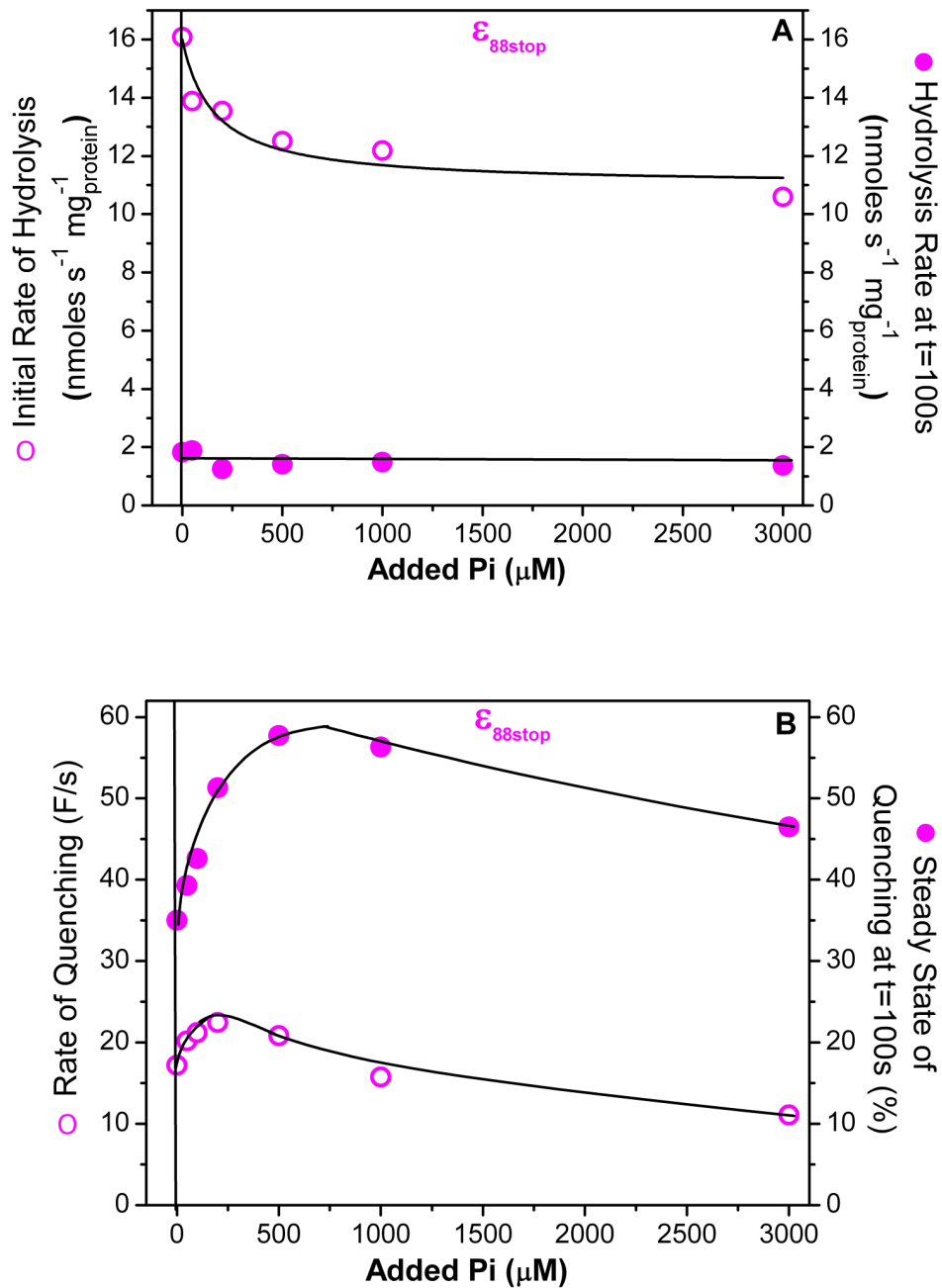


Fig. 6.8.5. ATP hydrolysis (A) and of ACMA fluorescence quenching (B) as a function of [Pi], after pre-incubation in the presence of 1nM ADP in ϵ_{88stop} *E. coli* membranes.

Panel A. Initial rates of ATP hydrolysis (○) and rates at $t=100\text{s}$ (●). The hydrolysis data points were best fitted by a hyperbolic function with apparent $K_d = 160 \pm 50 \mu\text{M}$ (○) and by a linear function (●).

Panel B. Initial rates of quenching (○) and steady state values at $t=100\text{s}$ (●). The curves through the quenching data points were drawn by hand.

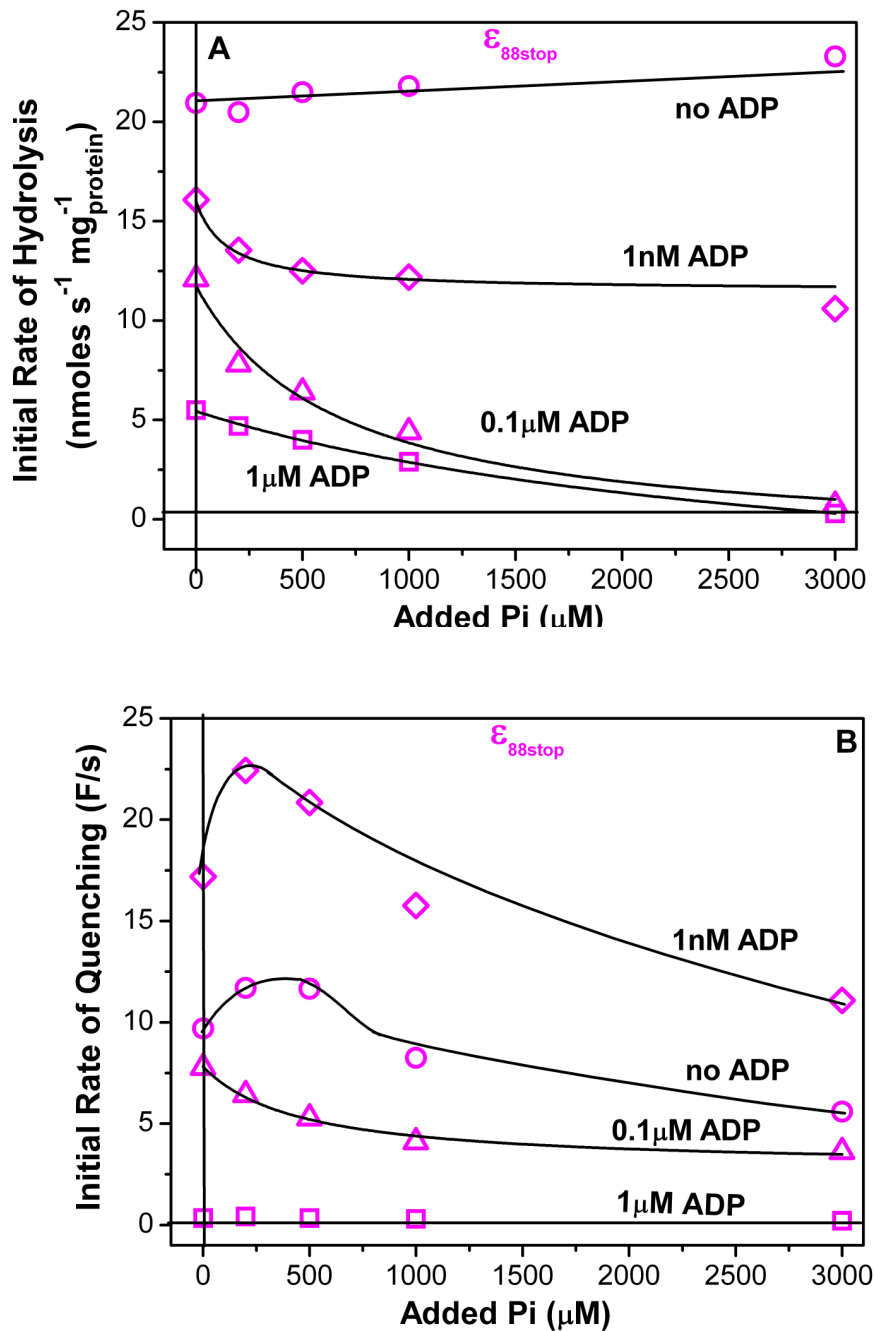


Fig. 6.8.6. Initial rate of ATP hydrolysis (A) and of ACMA fluorescence quenching (B) as a function of [Pi], after pre-incubation in the presence or absence of 1, 100 and 1000 nM ADP in $\epsilon_{88\text{-stop}}$ *E. coli* membranes.

Panel A. The ATP hydrolysis data points obtained in the absence of ADP (○) were best fitted by a linear function; the curves through the hydrolysis data points obtained in the presence of ADP were best fitting hyperboles with apparent $K_d = 160 \pm 50 \mu\text{M}$ (1 nM ADP(◇)), $K_d = 660 \pm 250 \mu\text{M}$ (0.1 μM ADP (△)) and $K_d = 3000 \pm 450 \mu\text{M}$ (1 μM ADP (□)).

Panel B. In the absence of ADP (○) and in the presence of 1 nM ADP(◇) the curves through the quenching data points were drawn by hand; in the presence of 0.1 μM ADP(△) the curve through the quenching data points was a best fitting hyperbole with apparent $K_d = 450 \pm 130 \mu\text{M}$; in the presence of 1 μM ADP (□) the quenching data points were best fitted by a linear function.

6.9. Effect of PK on ATP hydrolysis and proton pumping in WT and in $\epsilon_{88\text{-stop}}$ mutant.

The experiments described in §6.8. seem to indicate that the ATP synthases from mutant membranes have no pre-bound ADP. To check for this hypothesis we decided to carry out experiments of hydrolysis and quenching in the presence of PK.

In Chapter 3 we showed that 10 U/ml PK were able to significantly enhance the rate of hydrolysis in WT membranes. We measured the hydrolysis rate both in WT and in mutant membranes. As expected, in the WT membranes the rate of hydrolysis, which was constant over the entire time range, increased by a factor of almost 2 in the presence of 10 U/ml PK (Tab.6.9.1). In mutant membranes, the rate of hydrolysis measured in the presence of the ADP trap, similarly constant over the entire time range, was comparable to the one obtained in the absence of PK (Tab.6.9.1).

Tab 6.9.1. ATP hydrolysis rate in the presence or absence of 10 U/ml PK in WT and in $\epsilon_{88\text{-stop}}$ *E. coli* membranes.

	Hydrolysis Rate (nmoles·s ⁻¹ ·mg ⁻¹)	Hydrolysis Rate (nmoles·s ⁻¹ ·mg ⁻¹)
	No PK	10 U/ml PK
WT membranes	15.05	27.70
$\epsilon_{88\text{-stop}}$	17.44	17.31

Subsequently, we measured the proton pumping as a function of PK both in WT and in mutant membranes.

In WT membranes (blu circles, Fig. 6.9.1.), by increasing the amounts of added PK, the initial rate of quenching decreased (open circles) while the steady state of quenching, in parallel with the rate of hydrolysis, increased (full circles). In mutant membranes, the increase in the added PK determined a slight decrease in the initial rate of quenching (open magenta circles Fig. 6.9.1.). It can be thought that in the mutant, which largely lacks pre-bound ADP in the high affinity site, the ADP trap completely removes the residual ADP left in binding site. The biphasic trend observed in the steady state of proton pumping (full circles) can be promoted by the release of P_i and /or by the protonmotive force which has been built up during the 100s of hydrolysis activity.

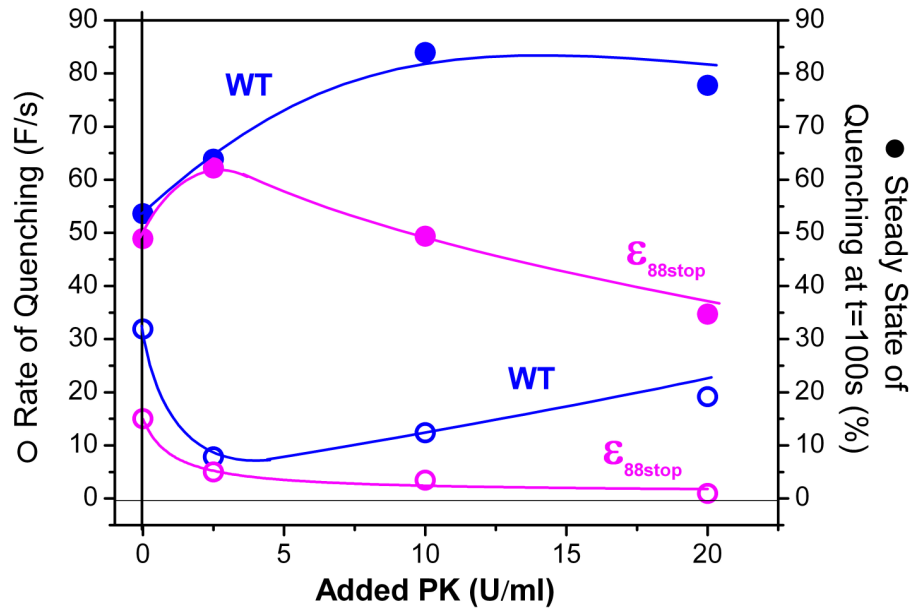


Fig.6.9.1. ACMA fluorescence quenching as a function of PK, in WT (blue) and in $\epsilon_{88\text{-stop}}$ *E. coli* membranes (magenta). Initial rates of quenching (○) and steady state values at $t=100\text{s}$ (●). The curve through the initial rate of quenching data points was drawn by hand in WT membranes (○) and was a best fitting hyperbole with apparent $K_d = 1 \pm 0.7 \mu\text{M}$ in $\epsilon_{88\text{-stop}}$ membranes (○). The curves through the steady state of quenching at $t=100\text{s}$ data points (●) were drawn by hand.

6.10. Discussion

The data presented in this Chapter show that the rate of ATP hydrolysis in the ATP synthase from WT membranes is inhibited by P_i , whereas proton pumping is first stimulated (up to about 250 μM P_i) and then inhibited (Fig.6.4.2. and Fig.6.4.4.). These data reproduce the behavior seen in Chapter 3. and 4., and, likewise, suggest the involvement of 2 P_i binding sites. In addition, the titration of ATP hydrolysis inhibition and proton pumping as a function of preincubated ADP directly indicated in the mutant the presence of two ADP binding sites, a high affinity site (HA-site) stimulating coupling, with $K_d=1$ nM, and a low affinity one (LA-site) inhibiting catalysis, with K_d in the hundreds of nanomolar range (see Fig. 6.7.1.).

Although the wild type titration data were not suited to quantitative analysis, they were qualitatively consistent with the occurrence of two ADP binding sites of different affinities and different functional effects (see Fig. 6.7.1. and Fig.6.7.2.). The wild type sites appeared to be filled considerably more slowly than those of the mutant (see e.g. Fig.6.6.1. and Fig.6.6.2.). Therefore, it is likely that for some data set, particularly at concentrations lower than 1 μM , the preincubation time was not long enough to reach the binding equilibrium. In addition, the ADP binding affinity of both the HA- and the LA-site is probably significantly lower than in the mutant (see below), leading to a permanent state of total or partial occupancy of these sites, which prevents a clear interpretation of the titration data.

The main pieces of evidence indicating a total or partial filling of the HA- and LA-sites with ADP in the wild type enzyme even in the absence of added nucleotides are: (1) the fact that a preincubation with PK stimulates the ATP hydrolysis rate by a factor of almost two, indicating enzyme activation due to removal by PK of inhibitory bound ADP; viceversa, the hydrolysis of the mutant was not stimulated under the same conditions, supporting the hypothesis that, in the absence of added nucleotides, the HA-site of the mutant is empty (Tab 6.9.1.); (2) the fact that the P_i inhibition of ATP hydrolysis, observable at first only in the wild type, could be restored in the mutant by a preincubation in the presence of ADP.

It is interesting to note that in the mutant, while the hydrolysis inhibition by P_i did require preincubation with ADP to be restored (Fig 6.8.1.), the strong increase in efficiency of the proton pumping seen after 100s reaction did not (Figg 6.4.2.-4.). This effect might indicate that the build-up of a protonmotive force is able to induce a faster binding of ADP and P_i to the HA-site.

A few features in the set of data reported in the present Chapter are, in our opinion, particularly novel and striking. One such feature is the extremely low K_d (1nM) for ADP found for the HA-site in the mutant. Remarkably, the affinity of the HA-site in the wild type is likely to be even lower. Moreover, this high affinity becomes evident only if the nucleotide is preincubated, since the ADP concentration present as contaminant in

the 150 μ M ATP, added to start the hydrolysis reaction, was 1500 nM (§1.11.), and nevertheless the effects of the 1nM ADP preincubation were very clear. This apparent paradox might be due to a competition of ATP with ADP for binding to the HA-site, which would also imply that ATP binding does not lead to enzyme coupling, but keeps the enzyme in the partially uncoupled state, or is even itself responsible for such uncoupled state. One more striking aspect is the clear functional separation between the HA- and LA-sites which emerges from the parallel ADP titration of the hydrolysis and the proton pumping activity of the mutant (Fig. 6.7.1. and Fig.6.7.2.). The HA-site has a clear efficiency-promoting effect for proton pumping, and in addition a partial inhibitory effect on the ATP hydrolysis, while the LA-site only shows inhibitory effects on both hydrolysis and proton pumping, consistent with its leaving unaffected the pump efficiency.

The occurrence of two ADP binding site, of which only the highest affinity one was involved in modulating the proton pumping efficiency, was already indicated by the data obtained in wild type membrane assayed in the presence of high concentrations of PK, acting as an ADP trap to deplete the HA-site (see Turina et al., 2004). However, the data of Figg 6.7.1.-2. represent a more direct evidence of such functional separation between the two sites.

According to the data of the present work, in view of the significantly higher affinity for ADP of the wild type HA- and LA-sites relative to the mutant sites, it is possible to speculate that one effect of the C-terminal α -helical domain of epsilon is to strongly stabilize the closed conformation of the β subunits. The existing structural data (see e.g. the crystal structure of the γ - ϵ -cocrystal of Rodgers & Wilce (2000), or the crosslinking data reviewed in (Capaldi & Schulenberg, 2000) and in (Vik, 2000), support this hypothesis, since in the up-state of the ϵ subunit, its C-terminal α -helical domain makes contacts with the DEELSED region of the β subunit, and could well acts as a wedge to keep in place the C-terminal domain of the β subunit, favoring the closed conformation.

Chapter 7.

CONCLUSIONS

The most salient conclusions of the present work can be summarized as follows.

1. The binding of ADP and P_i inhibits the rate of ATP hydrolysis in EF_0F_1 , both in internal membrane and in the isolated enzyme reconstituted into liposomes.
2. Unexpectedly, the inhibition of hydrolysis by ADP and P_i corresponds to an absolute stimulation of proton pumping, so that it can be concluded that these ligands appear to be necessary for an efficient coupling of proton pumping to ATP hydrolysis. The occurrence of this phenomenon in *E. coli*, here shown for the first time, parallels what had been found for the ATP synthase of the photosynthetic bacterium *Rb. capsulatus*.
3. This higher efficiency of proton pumping, promoted by the binding of ADP and P_i , means that, in binding these two ligands, the ATP synthase changes its catalytic mode, shifting from a partially uncoupled to a fully coupled ATP hydrolysis.
4. The calibration of the ACMA fluorescence quenching, carried out in proteoliposomes, enabled us to estimate quantitatively the degree of uncoupling elicited by either ADP or P_i , determining that the complete removal of either ligand induces a nearly two-fold decrease in the number of proton translocated per hydrolyzed ATP.
5. ADP binding is required for inhibition by P_i . Reciprocally, P_i is required for a stronger inhibition by ADP, although ADP inhibits ATP hydrolysis also in its absence. The same conclusions can be drawn for P_i /ADP stimulation of proton pumping.
6. The ADP concentrations able to induce these phenomena were in the submicromolar range, and such high affinity for ADP supports the idea that the involved binding sites are catalytic.
7. The biphasic dependence of proton transport on ADP and P_i concentrations and the data at low ADP concentration obtained in the truncated mutant suggest that two binding sites for either these ligands are involved: one with higher affinity, whose occupancy increases the pumping efficiency, and a second one with lower affinity, causing only inhibition of hydrolysis.
8. The complete removal of the α -helical hairpin at the C-terminal domain of the ϵ subunit ($\epsilon_{88\text{-stop}}$ truncated form) resulted in a loss of the P_i inhibitory effect on ATP hydrolysis. However, pre-incubation of the ϵ truncated enzyme in the presence of ADP at nanomolar concentrations restored this inhibition, indicating that the high affinity ADP binding site is characterized by a lower affinity for ADP (and possibly for P_i) relative to wild type.

9. Therefore, the C-terminal domain of the ϵ subunit appears to affect the coupling efficiency, at least in vitro, by modifying the affinity of one or more sites for nucleotides, particularly ADP.
10. We can hypothesize that both the mechanism of the uncoupling, documented by removal of ADP and the uncoupling observed by removal of C-domain of epsilon have as mechanistic basis that ADP (+P_i) is not bound at a site where it promotes coupling. When ϵ is intact it is a very high affinity site and hard to pull off; when epsilon is truncated ADP is lost more readily from this site. Thus the truncated mutant turned out to be an ideal system for investigating the role of the two ADP- and Pi-binding sites involved in the modulation of the proton pumping efficiency and in the inhibition of hydrolysis.

References

- Abrahams J.P., Leslie A.G., Lutter R., Walker J.E. (1994) *Nature* 370:621–628.
- Aggeler R, Capaldi RA, Dunn S, Gogol EP. (1992) *Arch Biochem Biophys.* 296:685-90.
- Aggeler R., Ogilvie I., Capaldi R.A. (1997) *J.Biol.Chem.* 272:19621-19624.
- Aggeler R., Weinreich F., Capaldi R.A. (1995) *Biochim. Biophys. Acta* 1230:62–68.
- Andrew J.W., Rodgers, Matthew C.J. Wilce (2000) *Nature Structural Biology* 7:1051-1054.
- Anraku, Y., Gennis, R.B. (1987). The aerobic respiratory chain of *Escherichia coli*. *TIBS* 12, 262-266.
- Baccarini-Melandri A., Melandri B.A. (1971) *Methods Enzymol.* 23:556–561.
- Bald, D., Noji, H., Yoshida, M., Hirono-Hara, Y., and Hisabori, T. (2001) *J. Biol. Chem.* 276, 39505–39507.
- Berman M.C. (2001) *Biochim. Biophys. Acta* 1513:95–121.
- Birkenhager R., Hoppert M., Deckers-Hebestreit G., Mayer F., Altendorf K. (1995) *Eur J Biochem.* 230:58-67.
- Boyer P.D. (1993) *Biochim. Biophys. Acta* 1140:215–250.
- Boyer P.D. (1997) *Annu. Rev. Biochem.* 66:717–749.
- Boyer PD. (2002) *J Biol Chem* 277:39045-61.
- Boyer P.D., Kohlbrenner W.E., in: B.R. Selman, S. Selman-Reimer (Eds.), *Energy Coupling in Photosynthesis*, Elsevier North Holland, New York, 1981, pp. 231–240.
- Bradford M.M., *Anal. Biochem.* 72 (1976) 248–254.
- Braig K, Menz RI, Montgomery MG, Leslie AG, Walker JE.(2000) *Structure.* 8:567-73.
- Brock D., Madigan M.D., Martinko J.M., Parker J. (2003) *Microbiologia*, Città Studi Edizioni.
- Calhoun M.W., Oden K.L., Gennis RB, de Mattos M.J., O.M. Neijssel (1993) *J.Bacteriol* 175:3020-3025.
- Capaldi R.A., Aggeler R. (2002) *Trends Biochem. Sci.* 27:154–160.

- Capaldi R.A., Schulenberg B. (2000) *Biochim. Biophys. Acta* 1458:263–269.
- Cappellini P., Turina P., Fregni V., Melandri B.A. (1997) *Eur. J. Biochem.* 248:496–506.
- Carmeli C., Lifschitz Y (1969) *FEBS Lett.* 5:227-230.
- Casadio R. (1991) *Eur. Biophys. J.* 19:189–201.
- Casadio R., Di Bernardo S., Fariselli P., Melandri B.A. (1995) *Biochim. Biophys. Acta* 1237:23–30.
- Casadio R., Melandri B.A. (1985) *Arch. Biochem. Biophys.* 238:219–228.
- Casadio R., Melandri B.A. (1996) *J. Bioinorg. Chem.* 1:284–291.
- Cipriano D.J., Bi Y., Dunn S.D. (2002) *J. Biol. Chem.* 277:16782–16790.
- Cipriano D.J., Dunn S.D. (2006) *J. Biol. Chem.* 281:501–507.
- Cooper G.M. (2002) *La cellula*, Zanichelli.
- D'Alessandro M, Turina P, Melandri BA.(2008) *Biochim Biophys Acta.* 1777:1518-27.
- Davenport J.W., McCarty R.E. (1981) *J. Biol. Chem.* 256:8947–8954.
- Davies J.M., Hunt I., Sanders D. (1994) *Proc. Natl. Acad. Sci.* 91:8547–8551.
- Dimroth P, Kaim G, Matthey U.(2000) *J Exp Biol.* Jan;203(Pt 1):51-59.
- Drobinskaya I.Y., Kozlov I.A., Murataliev M.B., Vulfson E.N., *FEBS Lett.* 182 (1985) 419–424.
- Duncan TM, Bulygin VV, Zhou Y, Hutcheon ML, Cross RL. (1995) *Proc Natl Acad Sci U S A.* 92:10964-8.
- Duncan TM, Zhou Y, Bulygin VV, Hutcheon ML, Cross RL. (1995) *Biochem Soc Trans.* 23:736-41.
- Dunn SD. (1986) *Anal Biochem.* 157:144-53.
- Dunn SD. (1986) *Anal Biochem.* 159:35-42.
- Dunn S.D. (1995) *Nat. Struct. Biol.* 2:915–918.
- Dunn S.D., McLachlin D.T., Revington M. (2000) *Biochim Biophys Acta.* 1458:356-363.

- Dunn SD, Tozer RG, Antczak DF, Heppel LA. (1985) *J Biol Chem.* 260:10418-25.
- Dunn S.D., Zadorozny V.D., Tozer R.G., Orr L.E. (1987) *Biochemistry* 26:4488–4493.
- Duvezin-Caubet S., Caron M., Giraud M.F., Velours J., di Rago J.P. (2003) *Proc. Natl. Acad. Sci. U. S. A.* 100:13235–13240.
- Dykhhoorn DM, St Pierre R, Linn T. (1996) *Gene.* 177:133-6.
- Evron Y., Johnson E.A., McCarty R.E. (2000) *J. Bioenerg. Biomembr.* 32:501–506.
- Feniouk B.A., Suzuki T., Yoshida M. (2006) *Biochim. Biophys. Acta* 1757:326–338.
- Feniouk B.A., Suzuki T., Yoshida M. (2007) *J. Biol. Chem.* 282:764–772.
- Fillingame R.H., Girvin M.E., Jiang W., Valiyaveetil F., Hermolin J. (1998) *Acta Physiol Scand Suppl.* 643:163-168.
- Fillingame R.H., Jiang W., Dmitriev O.Y. (2000) *J. Exp. Biol.* 203:9–17.
- Fillingame RH, Jiang W, Dmitriev OY, Jones PC.(2000) *Biochim Biophys Acta.* 1458:387-403.
- Fischer S., Gräber P., Turina P. (2000) *J. Biol. Chem.* 275:30157–30162.
- Ganti S., Vik SB. (2007) *J Bioenerg Biomembr.* 39:99-107.
- Gao Y.Q., Yang W., Karplus M. (2005) *Cell* 123:195–205.
- Gardner J.L., Cain B.D. (1999) *Arch. Biochem. Biophys.* 361:302–308.
- Gibbons C., Montgomery M.G., Leslie A.G., Walker J.E. (2000) *Nat. Struct. Biol.* 7:1055–1061.
- Girvin M.E., Rastogi V.K., Abildgaard F., Markley J.L., Fillingame R.H. (1998) *Biochemistry*, 37:8817-8824.
- Greene MD, Frasch WD. (2003) *J Biol Chem.* 278:51594-8.
- Groth G.& Pohl E. (2001) *J.Biol.Chem.* 276(2):1345-1352.
- Hausrath A.C., Capaldi R.A., Matthews B.W. (2001) *J.Biol.Chem.* 276:47227-47232.
- Hausrath AC, Grüber G, Matthews BW, Capaldi RA. (1999) *Proc Natl Acad Sci U S A.* 96:13697-702.
- Hess HH, Derr JE. (1975) *Anal Biochem.* 63:607-13.

- Hinkle P., (1974) *Biochem Biophys Res Commun* 58:178-184.
- Hirono-Hara Y., Ishizuka K., Kinoshita Jr. K., Yoshida M., Noji H. (2005) *Proc. Natl. Acad. Sci. U. S. A.* 102:4288–42893.
- Holloway PW. (1973) *Anal Biochem.*53:304-8.
- Hyndman D.J., Milgrom Y.M., Bramhall E.A., Cross R.L. (1994) *J.Biol.Chem.* 269: 28871-28877.
- Iida T., Inatomi K., Kamagata Y., Maruyama T. (2002) *Extremophiles* 6:369-375
Ingledew WS & Poole RK (1984) *Microbiol Rev.* 48:222-271.
- Jiang W, Hermolin J, Fillingame RH. (2001) *Proc Natl Acad Sci U S A.* 98:4966-71.
- Junge W., Lill H., Engelbrecht S., (1997) *Trends Biochem Sci.* 22:420-423.
- Kabaleeswaran V, Puri N, Walker JE, Leslie AG, Mueller DM. (2006) *EMBO J.* 25(22):5433-42.
- Kadenbach B. (2003) *Biochim. Biophys. Acta* 1604:77–94.
- Kagawa R, Montgomery MG, Braig K, Leslie AG, Walker JE. (2004) *EMBO J.* 23:2734-44.
- Kato-Yamada, Y., Bald, D., Koike, M., Motohashi, K., Hisabori, T., and Yoshida, M.(1999) *J. Biol. Chem.* 274:33991–33994.
- Kato-Yamada Y., Noji H., Yasuda R., Kinoshita K. Jr, Yoshida M. (1998) *J.Biol.Chem.* 273:19375-19377.
- Kayalar C, Rosing J, Boyer PD. (1977) *J Biol Chem.* 252:2486-91.
- Kinoshita Jr. K., Adachi K., Itoh H. (2004) *Annu. Rev. Biophys. Biomol. Struct.* 33:245–268.
- Kozlov I.A., Vulfson E.N. (1985) *FEBS Lett.* 182:425–428.
- Kuki M., Noumi T., Maeda M., Amemura A., Futai M. (1988) *J.Biol. Chem.* 263:17437-17442.
- Lanzetta P.A., Alvarez L.J., Reinach P.S., Candia O.A. (1979) *Anal. Biochem.* 100:95–97.
Lederberg J. & Tatum E. L. (1946) *Nature* 158:558.
- Lin E. C. C., and D. R Kuritzkes (1987) *American society for microbiology, Washington DC* 1: 244-284.

- Löbau S., Weber J., Senior A.E. (1998) *Biochemistry* 37:10846–10853.
- Löbau S., Weber J., Senior A.E. (1998) *Biochemistry* 37:10846–10853.
- Lowry, O. H., Rosebrough, N. J., Farr, A. L., and Randall, R. J. (1951) *J. Biol. Chem.* 193:265–275.
- M. Nishimura[27], Ito T., Chance B. (1962) *Biochim. Biophys. Acta* 59:177–182.
- Mcquate J.T., Utter M.F. (1959) *J. Biol. Chem.* 234:2151–2157.
- Melandri B.A. (1993) *L'energia dei viventi*, La Nuova Italia Scientifica.
- Mendel-Hartvig J., Capaldi R.A. (1991) *Biochemistry* 30:1278–1284.
- Menz, R. I., Walker, J. E. & Leslie, A. G. W. (2001) *Cell* 106, 331–341.
- Miki, J., Maeda, M., Mukohata, Y., and Futai, M. (1988) *FEBS Lett.* 232:221–226.
- Mills, J. D., Mitchell, P., and Schürmann, P. (1980) *FEBS Lett.* 112:173–177.
- Mitchell P. (1966) *Biol Rev Camb Philos Soc.* 41:445-502.
- Moriyama Y., Nelson N. (1988) *Prog. Clin. Biol. Res.* 273:387–394.
- Mosher M.E., White L.K., Hermolin J., Fillingame R.H. (1985) *J. Biol. Chem.* 260: 4807–4814.
- Müller M.L., Jensen M., Taiz L. (1999) *J. Biol. Chem.* 274:10706–10716.
- Muneyuki E., Yoshida M., Bullough D.A., Allison W.S. (1991) *Biochim. Biophys. Acta* 1058:304–311.
- Nagle J.F., Wiener M.C., (1988) *Biochim. Biophys. Acta* 942:1-10.
- Nalin, C. M., and McCarty, R. E. (1984) *J. Biol. Chem.* 259:7275–7280.
- Nicholls D.G., Ferguson S.J. (1982) *Bioenergetics 2*, Academic Press, London.
- Nishimura M., Ito T., Chance B. (1962) *Biochim Biophys Acta.* 59:177-182.
- Noji H., Yasuda R., Yoshida M., Kinoshita K. Jr. (1997) *Nature* 386:299-302.
- Nowak, K. F., and McCarty, R. E. (2004) *Biochemistry* 43:3273–3279.
- Ogilvie I, Wilkens S, Rodgers AJ, Aggeler R, Capaldi RA. (1998) *Acta Physiol Scand Suppl.*643:169-75.

- Ohnishi T, Kaback H.R. (1987) *Biochemistry* 26:7732-7737.
- Olsson K., Keis S., Morgan H.W., Dimroth P., Cook G.M. (2003) *J. Bacteriol.* 185:461–465.
- Penefsky H.S. (2005) *FEBS Lett.* 579:2250–2252.
- Peskova Y.B., Nakamoto R.K. (2000) *Biochemistry* 39:11830–11836.
- Pick U., Weiss M. (1988) *Eur. J. Biochem.* 173:623–628.
- Poole, R.K. & Ingledew, W.J. (1987) F.C. Neidhardt ed., American Society for Microbiology, Washington, DC. pp170-200.
- Rastogi V.K., Girvin M.E. (1999) *Nature* 402:263-268.
- Rodgers AJ, Capaldi RA. (1998) *J Biol Chem.* 273:29406-10.
- Rodgers A.J., Wilce M.C. (2000) *Nat. Struct. Biol.* 11:1051–1054.
- Rondelez Y., Tresset G., Nakashima T., Kato-Yamada Y., Fujita H., Takeuchi S., Noji H. (2005) *Nature* 433: 773–777.
- Rosing J, Harris DA, Kemp A Jr, Slater EC., *Biochim Biophys Acta.* 1975 Jan 31;376(1):13-26.
- Sabbert D., Engelbrecht S., Junge W. (1996) *Nature* 381:623-5.
- Sambrook, J., Fritsh, E. F., and Maniatis, T. (1989) *Molecular Cloning: A Laboratory Manual*, 2nd Ed., Cold Spring Harbor Laboratory, Cold Spring Harbor, NY.
- Schägger H, Aquila H, Von Jagow G. (1988) *Anal Biochem.* 173:201-5.
- Schmidt R.A., Qu J., Williams J.R., Brusilow W.S. (1998) *J. Bacteriol.* 180:3205–3208.
Schmidt G., Gräber P.(1985) *Biochim. Biophys. Acta*, 808:46-51.
- Schuldiner S., Rottenberg H., Avron M. (1972) *Eur. J. Biochem.* 25:64–70.
- Seelert H., Poetsch A., Dencher N.A. Engel A., Stahlberg H., Muller D.J. (2000) *Nature* 405:418-419.
- Segel I.H., 1975, *Enzyme Kinetics*. New York, John Wiley & Sons, pp109-111.
- Shimabukuro K, Yasuda R, Muneyuki E, Hara KY, Kinoshita K Jr, Yoshida M.(2003) *Proc Natl Acad Sci U S A.*100:14731-6.
- Shoshan V., Strotmann H. (1980) *J. Biol. Chem.* 255:996–999.

- Singh S., Turina P., Bustamante C.J., Keller D.J., Capaldi R. (1996) FEBS Lett. 397:30-34.
- Steigmiller S, Turina P, Gräber P. (2008) Proc Natl Acad Sci U S A. 105:3745-50.
- Stock D., Leslie A.G., Walker J.E. (1999) Science 286(5445):1700-1705.
- Stryer L. (1996), Biochimica, Zanichelli.
- Suzuki T., Murakami T., Iino R., Suzuki J., Ono S., Shirakihara Y., Yoshida M. (2003) J. Biol. Chem. 278: 46840–46846.
- Tsunoda S.P., Aggeler R., Noji H., Kinoshita K. Jr, Yoshida M., Capaldi R.A. (2000) FEBS Lett. 470:244-248.
- Tsunoda S.P., Rodgers A.J., Aggeler R., Wilce M.C., Yoshida M., Capaldi R.A. (2001) Proc. Natl. Acad. Sci. 98:6560–6564.
- Turina M.P., Venturoli G., Melandri B.A. (1990) Eur. J. Biochem. 192:39–47.
- Turina P. (2000) J. Bioenerg. Biomembr. 32:373–381.
- Turina P. (2000) J. Bioenerg. Biomembr. 32:373-381.
- Turina P., Giovannini D., Gubellini F., Melandri B.A. (2004) Biochemistry 43:11126–11134.
- Turina P., Rebecchi A., D'Alessandro M., Anefors S., Melandri B.A. (2006) Biochim. Biophys. Acta 1757: 320–325.
- Ueoka-Nakanishi H, Nakanishi Y, Konno H, Motohashi K, Bald D, Hisabori T.J (2004) Biol Chem. 279:16272-7.
- Uhlir U, Cox GB, Guss JM. (1997) Structure 5:1219-1230.
- Van Walraven H.S., Scholts M.J., Lill H., Matthijs H.C., Dilley R.A., Kraayenhof R. (2002) J. Bioenerg. Biomembr. 34:445–454.
- Vieira J, Messing J. 1982 Gene. 19:259-68.
- Vik, S.B. (2000) J. Bioenerg. Biomembranes 32:485–491.
- Weber J, Senior AE. (2003) FEBS Lett. 545:61-70.
- Wilkens S. (2005) Adv. Protein Chem. 71:345–382.

-
- Wilkins S., Dahlquist F.W., McIntosh L.P., Donaldson L.W., Capaldi R.A. (1995) *Nat Struct Biol.* 2:961-967.
- Wilkins S., Capaldi R.A. (1998) *Biochim Biophys Acta* 1365:93-97.
- Wilkins S., Rodgers A., Ogilvie I, Capaldi RA (1997) *Biophys Chem.* 68:95-102.
- Wilkins S., Zhou J., Nakayama R., Dunn SD., Capaldi RA. (2000) *J Mol Biol.* 295:387-391.
- Xiao, Y., Metzler, M., and Mueller, D. M. (2000) *J. Biol. Chem.* 275:6963–6968.
- Xie D., Lill H., Hauska G., Maeda M., Futai M., Nelson N., (1993) *Biochim. Biophys. Acta* 1172: 267-273.
- Xiong, H., Zhang, D., and Vik, S. B. (1998) *Biochemistry* 37:16423–16429.
- Yang W, Gao YQ, Cui Q, Ma J, Karplus M. (2003) *Proc Natl Acad Sci U S A.* 100:874-9.
- Yasuda R., Noji H., Yoshida M., Kinoshita K. Jr. Itoh H. (2001) *Nature* 410:898-904.
- Yoshida M., Muneyuki E., Hisabori T. (2001) *Nat. Rev., Mol. Cell Biol.* 2:669–677.
- Zhang Y., Fillingame R.H. (1995) *J. Biol. Chem.* 270:24609–24614.
- Zharova T.V., Vinogradov A.D. (2006) *Biochemistry* 45:14552–14558.
- Zharova T.V., Vinogradov A.D. (2006) *Biochim. Biophys. Acta* 1757:304–310.
- Zimmermann B, Diez M, Zarrabi N, Gräber P, Börsch M. (2005) *EMBO J.* 24:2053-63.